

In presenting this thesis in partial fulfillment of the requirements for an advanced degree at Idaho State University, I agree that the Library shall make it freely available for inspection. I further state that permission for extensive copying of my thesis for scholarly purposes may be granted by the Dean of the Graduate School, Dean of my academic division, or by the University Librarian. It is understood that any copying or publication of this thesis for financial gain shall not be allowed without my written permission.

Signature _____

Date _____

Spatial Structure, Temporal Patterns, and Drivers of Stream Drying
In the Gibson Jack Watershed, Bannock County, Idaho

by

Thane Kindred

A thesis

Submitted in partial fulfilment

Of the requirements for the degree of

Masters of Science in the Department of Geological Sciences

Idaho State University

Summer 2022

To the Graduate Faculty:

The members of the committee appointed to examine the thesis of Thane Kindred find it satisfactory and recommend that it be accepted

Sarah Godsey

Major Advisor

Di Wu

Committee Member

Rebecca Hale

Graduate Faculty Representative

Acknowledgements

In the completion of my thesis, I would like to take a moment to thank the many people who helped me along the way:

First, I want to publicly thank everyone who helped me with fieldwork. That list includes Sarah Newcomb, Austin Bowmen, Kevin Gauthier, Daniel Vega, Heidi Funnell, Leonie Kiewiet, Brandon Yokely, Riley Landfear, Trever Hanks, Stuart Rex, Justin Miller, Tiffany Jeske, Arya Legg, Michael Ferraro, and Adam Arbon for help deploying STICs, retrieving STICs, and characterizing STIC sites. I want to give special thanks to Kathleen Van Wesenbeek, Alyssa Farnes, and Alyssa DeSmit for the extensive fieldwork they helped me with in both 2020 and 2021. I could not have done my research without their help.

I want to give a special thanks to Cami Christensen and CoSE IT for help with the lab computers. I also want to thank those who participated in the writing workshop and thus helped me improve my writing: Xavier Jenkins, Brenlee Shipps, Nirajan Bhattarai, Micaela Wilson, Talissa Cota, and Jill McDonald. My experience at ISU would have been very different without these people.

I also want to thank the professors at ISU for the classes they taught and the mentoring they provided for me. Specifically, I would like to thank those who served on my committee: Sarah Godsey, Di Wu, and Rebecca Hale for their support and guidance.

Finally, I want to thank my family for their support. Of special mention is my wife Lynn Kindred who supported me financially and emotionally through grad school. She is my motivation and support. I owe my success to her.

From the bottom of my heart, thank you.

Thane Kindred

Table of Contents

List of Figures	ix
List of Tables.....	xii
List of Abbreviations.....	xiii
Abstract.....	xiv
Chapter I: Current State of Non-perennial Stream Research	1
1.1. Overview	1
1.2. Stream drying, water quality, and its legal protections	4
1.2A. Protecting non-perennial streams	4
1.2B. Stream drying and biogeochemistry	7
1.3. Metrics used to quantify drying in non-perennial streams.....	8
1.4. Modeling patterns of stream drying	12
1.4.1. Current models predicting drying patterns	12
1.4.2. Spatial autocorrelation, semivariograms, and toregrams	16
1.5. Drivers of intermittency	20
1.5.1. Meteorological variables	21
1.5.2. Physiographic variables	22
1.5.3. Land cover variables.....	23
1.5.4. Meteorology, physiography and land cover in Gibson Jack.....	25
1.6. Conclusion	27
1.7. Figures	28
1.8. Tables	34
1.9. References	35
Chapter 2. Spatial Patterns of Stream Drying in a Semi-arid Mountainous Headwater Stream: Structure and Drivers.....	42
2.1. Introduction.....	42
2.2. Site Description.....	44
2.3. Methods	45
2.3.1. Field Methods	46
2.3.2. Interpretation of STIC Data.....	47
2.3.3. Modeling	49
2.4. Results	51
2.5. Discussion	54

2.5.1A. What spatial structures exist in stream drying at or below the watershed scale?	54
2.5.1B. What are the benefits of torgegrams vs.semivariograms when modeling autocorrelation in stream drying?	55
2.5.2. How accurately can we predict the metrics of intermittency by taking autocorrelation into account in our models?.....	56
2.5.4. Where in a stream network should we place sensors to improve the efficiency of our monitoring campaign?	60
2.6. Conclusion.....	61
2.7. Figures	63
2.8. Tables.....	73
2.9. Works Cited.....	76
Chapter 3: Temporal Patterns: Drying, Wetting, and Cycling	80
3.1. Introduction.....	80
3.2. Site description	82
3.3. Methods	83
3.3.1. Field Methods	84
3.3.2. Interpretation.....	85
3.3.3. Analysis of Patterns	86
3.4. Results	87
3.5. Discussion	89
3.5.1A. How variable is stream drying across seasonal and sub-seasonal temporal scales throughout a watershed?	89
3.5.1 B. How might the variability in stream drying help us differentiate between intermittent and ephemeral streams?	91
3.5.2. How synchronous are the patterns of wetting and drying across the watershed?.....	92
5.3. What physical characteristics may drive the temporal patterns we see?	94
3.6. Conclusion.....	95
3.7. Figures	97
3.8. Tables.....	105
3.9. References	106
Chapter 4. Questions for Future Work	109
4.1. Introduction.....	109
4.2. What <i>nested</i> spatial structures exist in stream drying?	109
4.3. What are the hierarchical drivers of stream drying <i>within</i> a watershed?	110
4.4. Suggested Technical Improvements	111

4.4.1. The Future of STARS and SSN	112
4.4.2. Accurate Channel Network Maps	113
4.4.3. STIC Threshold Determination and Challenges	113
4.4. Conclusions	114
4.5. Figures	115
4.6. References.....	116
Appendix 1: Detailed Methods	117
A1.1. Introduction	117
A1.2. Field Work	117
A1.3. Random Forest.....	118
A1.4. Confusion Matrices, ROCs, and AUCs	120
A1.5. Kruskal-Wallis Test.....	121
A1.7 Figures.....	123
A1.6. Tables	128
A1.7. References.....	129
Appendix 2: Detailed Results	130
A2.1. Introduction	130
A2.2. 2020 STIC data	130
A2.3. Field data from 2021	130
A2.4. Thresholds	130
A2.5. Models	131
A2.6. Cluster Analysis	131
A2.7 Figures.....	132
A2.8 Tables	138
Appendix 3: How to Create a .ssn object using STARS	187
A3.1. Introduction	187
A.3.2. Part 1: Software Requirements and Installation	187
A3.3. Part 2: Getting Started in ArcMap	189
A3.4. Part 3: Build a Landscape Network.....	191
A3.5. Part 4: Incorporating points in the LSN	195
A3.6. Part 5: Creating Reach Contributing Areas	197
A3.7. Part 6: Calculating Watershed Attributes	203
A3.8. Part 7: Calculating Spatial Variables	212

A3.9. Conclusion	218
A.3.10 Figures.....	220
Appendix 4: Advice for Future Grad Students	224
A4.1. Congratulations and Introduction	224
A4.2. Make Time for What You Value.....	224
A4.3. Make the small things count.....	226
A4. Move Forward to Better Days.....	227
A.5. Parting Words	228
A.6. References.....	229

List of Figures

Figure 1.1: Charts showing the most important controls on different spatial (A) and temporal (B) scales. Bold text indicates variables that we will address in later chapters. Charts were modified from Costigan et al. (2019). 28

Figure 1.2: Scatter plots showing the spatial and temporal resolution used by all stream drying studies in the last decade. The labels on graph points correspond to the studies listed in Table 1.1. Note that the majority of studies either used small spatial scales. 29

Figure 1.3: Example of a stream length duration curve or SLDC (A). A particular point on the curve such as (t, L) shows the percent of a season (t) that the length of the stream matches or exceeds that length (L). Examples of possible drying patterns within a watershed are also shown (B and C). Though the SLDC is a good way of characterizing changes in the instantaneous network extent, it gives us little spatial information beyond that. For example, the SLDC by itself cannot indicate connectivity. Clea 30

Figure 1.4: Conceptual models showing how physical and probabilistic space relate to each other after Botter and Durigetto (2019). After assigning each point a probability of flow, where 1 means perennial and 0 means always dry, we order the points from most likely dry to most likely wet. When determining how much of the stream is wet, we start from the bottom of the probabilistic model and work up until we reach our instantaneous flowing network extent for a particular time. 31

Figure 1.5: Example plots of a semivariogram (A), covariance function (B), and torgegram (C). Important features, such as the nugget, sill, and range, are identified in both the semivariogram and the torgegram. Additionally, a conceptual stream map is shown (D) indicating methods of calculating distances between points. The orange arrows in D correspond with the semivariogram and covariance function in A and B. Similarly, the blue arrow corresponds to the connected semivariogram (blue curve in C) for point-pairs where water flows from the upstream point to the downstream point whereas the green arrow corresponds to the unconnected semivariogram (green curve in C) for point-pairs that span multiple tributaries. 32

Figure 1.6: Torgegram created from data collected by Gendaszek et al. (2020). Notice the clear range and nugget exhibited in this torgegram despite the high nugget. In this thesis, we seek data to quantify a similarly shaped torgegram, but with a much smaller nugget. 33

Figure 2.1: Map of the Gibson Jack watershed located in southwestern Idaho. The map shows the locations of the STICs deployed from August 2020 to October 2020 as circles and STICs deployed from May 2021 to October 2021 as triangles. Some symbols appear filled because of dense placement of nests. 63

Figure 2.2: Histograms showing the distribution of seasonal streamflow permanence values in 2020 (A) and 2021 (B). Because the data from both years was bimodal, all subsequent analyses assume binomial data (wet > 0.5 and dry < 0.5). 64

Figure 2.3: (A) Map showing the sites where STICs were deployed in both 2020 and 2021. The accompanying charts (B-E) summarize data collected from the 2021 sites. At most sites, STICs reported mostly wet or dry conditions over the course of the study. For this reason, we interpreted our seasonal streamflow permanence as either predominantly wet (1) or dry (0). The 2020 data can be found in Appendix 2. 68

Figure 2. 4: Empirical torgogram of combined 2020 and 2021 data. The empirical torgogram shows three plateaus in grey: one at a range of ~100 m, one at a range of ~500 m, and a final one at a range of ~1,000 m. This was modeled as shown in black using an exponential tail-up model. These three plateaus may drive the variety of ranges across the different models.69

Figure 2. 5: Empirical semivariogram of combined 2020 and 2021 data (A) and the semivariogram produced by the best model in black (B). The best Cartesian spatial model, which used an exponential shape and elevation as an explanatory variable reveals a range of ~400 m, very similar to the range produced by the best tail-up stream-network spatial model. .69

Figure 2. 6: Predictions of seasonal streamflow permanence made by comparing our best models with field observations made Aug 29-30, 2020. The combined model (A) accurately predicted flow presence for 76% of all mapped sites on these days. Conversely, the 2020 model (B) accurately predicted flow presence for 78% of all mapped sites on these days.70

Figure 2. 7: Results from the random forest analysis reveal that drainage area, metasedimentary rocks, loam, and tree cover are the most important variables driving stream drying. Omission of any of these variables leads to a mean decrease in accuracy of the model prediction of over 30%. Variables are colored based on whether they predominantly reflect physiographic (brown) or land-cover (green) conditions.71

Figure 2. 8: Torgogram calculated from the work of Gendaszek et al. (2020) indicating an intermediate nugget of 7,208 m. This roughly matches the maximum range that our models calculated.....72

Figure 3. 1: Map of the Gibson Jack watershed located in southwest Idaho. The map shows the locations of the STICs deployed from May 2021 to October 2021..... 97

Figure 3. 2: The distribution of mid-season wetting events lasting less than 24 hours is extremely right-skewed. 98

Figure 3. 3: Map showing the sites where we deployed STICs (A). Categories of stream drying appear in every tributary without an obvious pattern..... 99

Figure 3. 4: Time series showing the presence (blue) or absence (orange) of water at each site shown in Figure 3.3 grouped by class (excluding sites that were only wet or dry). Class 2 has the vast majority of short-duration wetting/drying cycles. 101

Figure 3. 5: Map showing when a site first experienced a no-flow event. Note that the majority of sites dried for the first time before the end of May..... 102

Figure 3. 6: Plots showing the amount of precipitation during the 2021 field season (A), the number of wet sites each day (B) and the daily change in the number of wet sites (C) throughout the watershed. 103

Figure 3. 7: Clock plots showing the number of STICs wet on the wettest days (A), the driest days (B), and the change in the percentage of wet STICs on the wettest days (C) and the driest days (D). 104

Figure 4. 1: Empirical torgogram of combined 2020 and 2021 data. The empirical torgogram shows three plateaus in grey: one at a range of ~100 m, one at a range of ~500 m, and a final one at a range of ~1,000 m. This was modeled as shown in black using an exponential tail-up model. These three plateaus may drive the variety of ranges across the different models. 115

Figure A1. 1: Example of a decision tree with three layers. The data run through this tree will be split into two groups based on a first randomly selected variable. The groups will then be split into wet and dry groups based on a second randomly selected variable..... 123

Figure A1. 2: Results from the first round of a random forest analysis. From these results, we chose to discard upstream distance and elevation because they are correlated with drainage area. Similarly, we decided to discard silt loam because it is correlated with loam, and both colluvium and carbonates because they are correlated with metaseds. 124

Figure A1. 3: A plot of the error rates as we add additional trees. The red line indicates the error rate of dry sites, the blue line indicates the error rate when classifying wet sites, and the green line indicates the overall out-of-bag error rate. We chose to include only 3,000 trees because the error rate does not change with more trees. 125

Figure A1. 4: Empirical torgegrams for each of the 17 candidate variables for the Kruskal-Wallis test. Ten of the torgegrams (A) indicated that autocorrelation was present, so statistical analysis, such as the Kruskal-Wallis test and calculating a mean, would produce biased results. We chose to only run the test on the seven variables that demonstrated no autocorrelation (B) to ensure that we met the assumptions of the test. 127

Figure A2 1: Plot indicating presence/absence of water at 92 sites throughout the 2020 season (A) and map showing predictions of binary seasonal streamflow permanence across the watershed compared to observations made on Aug 29-30 (B). These predictions were made using a tailup model with the Mariah shape that used elevation as an explanatory variable. Note that this map is identical to Figure 2.6B because all 2020 sites had seasonal stream permanence values that matched the recording made on Aug 29-30 of that year. 134

Figure A2 2: Semivariograms and torgegrams created from 2020 data. The empirical semivariogram (A) and torgegram (B) are shown. Additionally both the semivariogram from the best cartesian model (C) and the torgegram from the best tail-up model (D) are shown. The best cartesian model was spherical in shape and used silt loam as an explanatory variable. The best tail-up model had a Mariah shape and used elevation as an explanatory variable. 135

Figure A2 3: Semivariograms and Torgegrams created from 2021 data. The empirical semivariogram (A) and torgegram (B) are shown. Additionally the semivariogram from the best cartesian model is shown (C). We do not show the torgegram from the best tail-up model because the empirical torgegram revealed a pure nugget. 136

Figure A2 4: A graph of the WSS elbow method (A) and of the three classes identified by the cluster analysis (B)..... 137

Figure A3. 1: Example of what a completed RCA raster should look like when the edges are displayed above them. Note that each RCA corresponds to one, and only one, edge..... 220

Figure A3. 2: Conceptual diagram of calculating segment proportional influence. Note that water flows from top to bottom in this diagram. The proportional influence is calculated for the bottom of each edge feature and included in the edges attribute table. 221

Figure A3. 3: Conceptual diagram for calculating Additive Function Value. Once the value has been calculated for an edge, all points along that edge have the same AFV. 222

List of Tables

Table 1.1. Summary of scales used in stream drying literature	34
Table 2.1. Summary of literature on hierarchical drivers of stream drying	73
Table 2.2. Variables used in the random Forest Analysis	74
Table 2.3. Sample models generated using both years of data	75
Table 3.1 Variables used in the Kruskal-Wallis Test	105
Table 3.2 Results from the Kruskal-Wallis Test	105
Table A1.1 Variables used in the Random Forest Analysis	128
Table A2.1 Pebble count results in centimeters	139
Table A2.2 Canopy cover measured with a densiometer	157
Table A2.3 2021 site characterization used in random forest analysis	160
Table A2.4 Calibration curves selected thresholds for every STIC used in Gibson Jack	169
Table A2.5 Spatial models created from 2020 data	172
Table A2.6 Spatial models created from 2021 data	178
Table A2.7 Spatial models created from 2020 and 2021 data	181
Table A2.8 Summary of kriging models	186

List of Abbreviations

AFV	Additive function value
AUC	Area under the curve
CWA	Clean water act
DEM	Digital elevation model
IQRPC	Inter quartile range of a pebble count
ISU	Idaho State University
IT	Internal technical
LSN	Landscape network
MPC	Mean of a pebble count
NWPR	Navigable water protection rule
PC	Principle component
PCA	Principle components analysis
PI	Proportional influence
PROSPER	Probability of streamflow permanence
RCA	Reach contributing area
ROC	Receiver operating characteristic
SLDC	Stream length duration curve
SSN	Stream statistical network
STIC	Stream temperature, intermittency, and conductivity

Abstract

Current models of stream drying require extensive data and drying predictions could be improved if we understood (1) the spatial scales of autocorrelation in stream drying, (2) its drivers, and (3) the synchrony of wetting and drying. We measured relative electrical conductivity, a proxy for the absence or presence of water, at 92 (2020) and 121 (2021) locations across the ~16.8-km² Gibson Jack watershed (Idaho, USA). We then calculated seasonal streamflow permanence at each location, developed a predictive kriging model, and calculated the number of wet sites each day. We found that (1) seasonal streamflow permanence is autocorrelated on scales of ~400 m, (2) topographic, lithologic, and pedologic variables were the top three drivers of stream drying, and (3) drying largely occurred asynchronously whereas rewetting occurred synchronously. These results suggest that the hierarchy of drivers of stream drying may be dynamic and scale-dependent in both space and time.

Keywords: Autocorrelation, Intermittency, Gibson Jack

Chapter I: Current State of Non-perennial Stream Research

1.1. Overview

In hydrology, even apparently simple characteristics, such as the presence or absence of water in a streambed, can vary throughout a watershed and over the course of a season. As our use of water resources increases and the world's climate changes, the percentage of streams that experience drying will likely increase throughout most of the world (Rupp et al., 2008). Indeed, metrics indicating the severity of stream drying indicate that non-perennial conditions are increasing throughout most of the United States (Zipper et al., 2021), making our understanding of these streams increasingly important.

These drying streams have a variety of names, including 'arid' (Hay et al., 2018), 'temporary' (Botter and Durrigetto, 2020), 'dry' (Steward et al., 2011), and 'seasonal' (Keller et al., 2019). Two of the most common terms include 'intermittent', referring to a stream that dries seasonally, and 'ephemeral', referring to a stream that is only wet after a storm event (Busch et al., 2020). Collectively, these streams are classified as 'non-perennial' (Busch et al., 2020; Shanafield et al., 2020), or intermittent rivers and ephemeral streams (IRES; Allen et al., 2020). Following recommendations from Busch et al. (2020), after their extensive study of these terms, we will use 'non-perennial', 'intermittent', and 'ephemeral' in this paper to avoid confusion between common terms used by different disciplines.

Regardless of the name used to describe them, the most conservative estimates claim that ~30% of streams worldwide are non-perennial (Tooth, 2000), though more recent estimates suggest that the majority of streams worldwide are non-perennial (51-60%; Messenger et al., 2021). Like their perennial counterparts, non-perennial streams play an important role as municipal water sources (Brown et al., 2008, Robinne et al., 2019, Ruhi et al., 2018), wildlife habitat (Darty et al., 2014; Katz et al. 2012; Stubbington et al. 2017), and transporters of soil, sediment, and nutrients (Belmont et al., 2011; Shumilova et al., 2019). However, unlike perennial streams, the role that non-perennial streams play depends largely on their drying patterns. For example, because non-perennial streams go through wet and dry phases, they have a higher biodiversity than perennial streams (Datry et al., 2014; Allen et al, 2013). Additionally, drying patterns in non-perennial streams affect water chemistry and habitat quality (Datry et al., 2014; Pisani et al., 2016; Jaeger et al., 2014) in both the non-perennial stream and in downstream perennial waters (Hale and Godsey, 2019).

To aid policy and research decisions, scientists have developed models that predict stream drying. In the last decade, these models have increased from ~50% accuracy (Fritz et al., 2013) up to ~80% accuracy (Jaeger et al., 2019) in some places. However, these new models typically require extensive data and/or monitoring campaigns (e.g., Botter and Durighetto, 2020; Jaeger et al., 2019; Ward et al., 2018). Furthermore, we lack an understanding of the spatial scales on which monitoring needs to take place. If we measure on scales that are too large, we risk missing important small-scale variations. Conversely, if we measure on small scales, we risk spending resources to collect data that is not independent. Put a different way, model

development could be more efficient if we better understood the spatiotemporal scales at which stream drying varies. We can characterize these scales of variation as the degree to which points are related to each other across different distances or timescales, known as autocorrelation. By properly accounting for autocorrelation, we can improve the efficiency of our data collection by measuring on appropriate spatiotemporal scales. This ensures that sampling locations are independent of each other and that we use statistical methods that account for any lack of independence (Isaak et al., 2014).

Most studies that seek to improve our predictions of stream drying focus on identifying the most important drivers of stream drying (Costigan et al., 2016; Dohman et al., 2021; Hammond et al. 2021; Jaeger et al., 2019; Pate et al., 2020; Warix et al., 2021). Despite these efforts, we still lack consensus on the most important driver or even the number of drivers. This problem results, at least in part, from the different scales used by different studies, which emphasize different controls (Figure 1.1; Costigan et al., 2016).

In this chapter, we review four key aspects of continued research on non-perennial streams. First, we explore the implications of stream drying for both water protection in the United States and our understanding of biogeochemical processes. Second, we characterize the debate over which spatiotemporal metrics we should use to characterize stream drying. Third, we detail the improvements to non-perennial predictive models needed to retain predictive power as climate changes. Specifically, we address the need to incorporate spatial structure into these models. Finally, despite a large number of studies focused on the drivers of stream drying, we explore why there

still remains a lack of consensus on their hierarchy. Underlying all of these aspects of this review is our belief that a better understanding of non-perennial streams will improve our ability to manage and study these important resources.

1.2. Stream drying, water quality, and its legal protections

1.2A. Protecting non-perennial streams

The United States government has long acknowledged the importance of perennial streams. In 1972, the US Congress created the Clean Water Act (CWA) to protect “Waters of the United States” (WOTUS). However, the law only vaguely defined WOTUS as traditionally navigable bodies of water and all of their tributaries. Consequently, policymakers and policy enforcers have debated whether non-perennial streams should receive protection or not (Walsh and Ward, 2019). In 1986, the Environmental Protection Agency (EPA) defined WOTUS as any body of water that had a bed, banks, and evidence of flow (USDOD, 1986). Wetlands within 500 ft of either WOTUS or a 100-yr floodplain also received protection (USDOD, 1986). In 2006, the extent of CWA protection was challenged by John Rapanos, who wanted to fill in three wetland areas on his property. The EPA warned Rapanos that the wetland areas were protected by the CWA, and when Rapanos ignored their warnings, the EPA brought a civil suit against him that was eventually heard by the US Supreme Court. Of the nine justices, four ruled that wetlands adjacent to navigable waters or their tributaries were protected. Another four ruled that adjacent wetlands were not protected unless there was a clear surface connection between the wetlands and the nearby navigable waters.

The deciding opinion, offered by Justice Anthony Kennedy, stated that simply being adjacent to navigable waters and their tributaries does not warrant protection, however, a test of significant nexus can justify protection even without surface connection (Rapanos v. United States, 2006). In the years that followed this court case, a significant nexus test became required for all wetlands that were not explicitly protected (Walsh and Ward, 2019).

In an attempt to decrease the number of wetlands that required a significant nexus test, the Clean Water Rule (CWR), adopted in 2015, changed the definition of protected wetlands to anything within 100 ft of jurisdictional waters, 1,500 ft of jurisdictional waters and the 100-year floodplain, or 1,500 ft of traditionally navigable waters. Under the CWR, any wetland beyond 1,500 ft from navigable waters, but closer than 4,000 ft required a significant nexus test (USDOD and USEPA, 2015).

In 2020, the Navigable Water Protection Rule (NWPR; USDOD, 2020) redefined the jurisdiction of the CWA to all intermittent and perennial streams, deliberately excluding ephemeral streams. It further redefined protected wetlands as everything with a clear surface connection to a jurisdictional stream. This redefinition eliminated the need for the significant nexus test, but it decreased the total amount of protected wetlands. For example, a study in the Wabash River Basin (Indiana) conducted in 2019 before the NWPR became official, showed that a maximum of 3% of the watershed was not protected by the 2015 CWR with another ~20% requiring a significant nexus test. By contrast, the 2020 NWPR left almost 40% of the watershed unprotected with 0% of the watershed requiring a significant nexus test (Walsh and Ward, 2019).

Upon taking office in 2021, the Biden administration ordered a review of CWR policy from any relevant agency (Executive Office of the President, 2021). This action resulted in a temporary return to 2015 CWR regulations. Later, in November 2021, the Biden administration proposed a rule that would return to pre-2015 regulations. This proposed rule is closed for comment and was implemented on February 7, 2022 (USDOD, 2021). This return to older regulations means that WOTUS is once again defined as any body of water that has a bed, banks, and evidence of flow, with wetlands not explicitly protected, but requiring a significant nexus test.

Given the recent intermittency of US water protection law, we should consider the ramifications of recent policy. Some interpretations of the CWA rely heavily on our ability to accurately characterize streams as perennial, intermittent, or ephemeral. However, current models focus more on distinguishing perennial from non-perennial streams (e.g., Jaeger et al., 2019). Additionally, scientific and legal communities have not yet come to a consensus on the distinction between ephemeral and intermittent streams (Walsh and Ward, 2019), despite efforts by some to do so (Busch et al. 2020). Furthermore, while some areas have fairly accurate maps of perennial/non-perennial streams (e.g., Jaeger et al., 2019), these are not available across the entire United States. To date, a nationwide repository of non-perennial streams does not exist (Jaeger et al., 2021).

As we work to create a nationwide repository of non-perennial streams, we need to consider the resolution (i.e. smallest spatial scale) at which the inventory for this repository needs to be conducted. Such resolution needs to be small enough to satisfy all concerned parties, but large enough to be feasible. For example, a resolution of 30 m

(e.g., Jaeger et al., 2019) would likely be small enough that landowners and environmentalists would not object, but such an effort may not be feasible across the entire United States. A study, such as this one, that explicitly explores scales of autocorrelation in non-perennial streams can help us justify our choice in spatial resolution.

1.2B. Stream drying and biogeochemistry

The temporary nature of non-perennial streams affects every aspect of in-stream processes at both the reach and network scale (Hale and Godsey, 2019). Despite this fact, many stream scientists have ignored non-perennial streams in favor of their perennial counterparts (Allen et al. 2020). Here we explore how a better understanding of non-perennial streams could improve our understanding of in-stream biogeochemical processes.

First and foremost, the wet/dry cycles characteristic of non-perennial streams can lead to higher concentrations of nutrients than their perennial counterparts when the stream is wet. Dry periods allow organic material, such as leaves and sticks, to build up in the streambed (Acuña et al., 2007) and this accumulation of organic material positively correlates with both photosynthesis and respiration rates (Acuña et al, 2015). Upon rewetting, there is an increase in dissolved material (Shumilova et al., 2019), especially dissolved organic carbon (von Schiller et al., 2015), associated with the mobilization and processing of the accumulated material.

Flowing stream networks have a unique potential for biogeochemical communication (i.e. chemical concentrations from one site are related to chemical concentrations at another site) via the stream network despite vast distances between sites (Hale and Godsey, 2019). We characterize the relationship between points in the stream network as connectivity (Larsen et al., 2020). Even though connectivity between a point and the stream network above it plays a critical role in controlling biogeochemistry (e.g. DOC concentrations; Vannote et al., 1980; Bertuzzo et al, 2017), connectivity still needs to be explicitly incorporated into biogeochemical models (Hale and Godsey, 2019).

1.3. Metrics used to quantify drying in non-perennial streams

Management and policy decisions, including where to monitor water quality, depend on our ability to accurately characterize non-perennial streams. However, the lack of consistent ways to quantify stream drying makes it difficult to compare stream drying patterns between various studies. Here we review more than a dozen spatial, temporal, and spatiotemporal metrics of stream drying and why one might choose to use each metric. We also briefly discuss the field methods used to collect data on stream drying.

The *presence/absence of water* at a particular point and time serves as a foundational metric and is often used to define metrics at other spatial or temporal scales. If presence/absence is defined at one location over time, then we can use temporal metrics to represent the change (or stability) in stream drying at a point.

Streamflow permanence is calculated as the percent or proportion of time that a site has surface water on daily, monthly, or seasonal scales (Warix et al., 2021; Hale and Godsey, 2019). This can be useful in characterizing general trends over the chosen period of time. Conversely, we can calculate *no-flow fraction* as the number of days a site is dry over the number of days in a year (e.g., Hammond et al., 2021). Other temporal metrics include “*first no-flow*” (Hammond et al., 2021) or “*first day dry*” (Warix et al., 2021) which is defined as the number of days from the beginning of the water year until a particular site has no flow or the date/time that a site first experiences drying, respectively. These metrics are useful in determining how long flow sources that may vary among seasons or years, such as spring snowmelt or seasonal monsoons, can sustain surface flow.

While some metrics rely solely upon absence/presence observations, other temporal metrics summarize additional information about site drying characteristics. *Peak-to-no-flow duration*, which describes the number of days from peak discharge to no-flow observations at a point (Hammond et al., 2021) and the *time between maximum wet proportion and peak runoff* (Jensen et al. 2019) require flow data from a stream gauge to determine the timing of peak flow. Similarly, the *time to respond to a rainfall event* (Goulsbra et al. 2007) requires precipitation data to determine when rainfall events occur. Similar to first-no-flow, these metrics are useful for determining how long an event, such as a storm, can sustain surface flow at a particular site.

If “snapshot” data from multiple locations at a single moment are available, then we can calculate spatial metrics. *Instantaneous flowing network extent* can be calculated as the percent of the mapped network, or the number of sensor locations,

with flowing water at a particular time (Warix et al., 2021; Paillex et al., 2020). Flowing network extent is sometimes known as *wetted network length* when it is expressed as a length instead of as a percent (Botter & Durigetto, 2020). This metric is good at characterizing the spatial extent of a stream at a moment of interest which we can compare to other moments. Other spatial metrics include *flowing stream drainage density*, which is defined as the length of flowing stream per area (Goulsbra et al., 2014). This metric is good for comparing drainage efficiency of non-perennial systems across different watersheds at various times.

The spatial metrics discussed above describe observations at individual points in a watershed, but under some circumstances, we want to know which points in a watershed are connected via surface flow, a property sometimes referred to as *connectivity* (Larsen et al., 2012). Here *flowing network connectivity* is quantified as the percent of surface-connected upstream length that is flowing, or the number of sites above a point that are flowing without surface interruptions (Hale and Godsey, 2019) at a given moment. Disconnected sites may have negligible or delayed impacts on downstream biogeochemistry whereas connected sites may dominate downstream biogeochemical responses.

To explore both spatial and temporal changes, most studies use a variety of the metrics described above; however, sometimes it is important to integrate over both space and time. For example, Warix et al. (2021) and Paillex et al. (2020) independently propose inversely related spatiotemporal metrics. Warix et al. (2021) propose the *seasonal flowing network extent*, which integrates the percent of sensors flowing across the season. In practice, this metric describes the proportion of the stream that contains

perennial flow. Conversely, Paillex et al. (2020) propose *the percent of sensors that go dry at any point in the season* as a spatiotemporal metric, or the proportion of the stream that contains non-perennial flow.

To calculate the spatiotemporal metrics discussed above, hydrologists have two options: they can map the stream by walking its length, or they can deploy sensors that indicate presence/absence over time. Mapping allows researchers to record the absence and presence of water at (approximately) a single moment leading to the accurate quantification of spatial metrics. However, mapping requires vast amounts of time and therefore is often collected at coarse temporal resolutions – often just once or twice per season (Figure 1.2; Table 1.1).

Alternatively, researchers can use sensors that indicate the presence/absence of water at a particular location throughout the season. These sensors can take many forms, such as conductivity and/or temperature sensors, in-stream wells, or stream gages. Regardless of the type of sensor, the data they collect allows us to interpret the absence or presence of water. For example, zero flow at a stream gage can sometimes indicate stream drying at that location (Zimmer et al., 2020). Similarly, a high electrical conductivity can indicate the presence of water, while a low electrical conductivity typically indicates the absence of water (Chapin et al., 2014). Unlike walking the length of the stream, sensors offer very fine temporal resolution but are often deployed sparsely in space due to the limitations on the number of sensors available for a particular study (Figure 1.2; Table 1.1).

Irrespective of how the data is collected, having quantifiable metrics allows us to map stream drying across space and time and predict stream drying in watersheds. However, the lack of consistent metrics makes it difficult to identify similarities between different metrics used in various studies. A more uniform use of non-perennial metrics would benefit hydrologists, policy makers/enforcers, and other researchers interested in non-perennial streams. As we will do throughout this thesis, we recommend that researchers adopt the following terms/metrics whenever possible to avoid confusion: “absence/presence”, “streamflow permanence”, “instantaneous wetted network extent”, and “seasonal flowing network extent” because they focus on the amount of time water is present rather than the amount of time water is absent. Additionally, we will use “first no-flow” because it more explicitly allows a timestamp in the metric whereas “first day dry” implies only a date, and sub-daily variations may be important, as we will explore in Chapter 3.

1.4. Modeling patterns of stream drying

1.4.1. Current models predicting drying patterns

Because monitoring campaigns require many resources, researchers have developed models of stream drying that allow us to make predictions with limited observations. The most accurate of these models has achieved ~80% accuracy in some places (Jaeger et al., 2019). If these models are to replace more direct methods of observation, they need to be even more accurate than they currently are. Additionally, these models need to be more universally applicable and ideally should require less

intensive field campaigns. Here we review three of the most accurate models of stream drying that are currently available.

To date, the PRObability of Streamflow Permanence (PROSPER) model boasts an 80% accuracy rate (Jaeger et al., 2019), a feat achieved by predicting the absence/presence of water using a random forest classification method (Breiman, 2001). The method uses approximately two-thirds of the available 3,878 observations of presence/absence data from 1977 to 2016 across the Pacific Northwest region (defined as all of Washington, most of Oregon and Idaho, and parts of Montana, Wyoming, Utah, and Nevada) at a spatial resolution of 30 m to predict the annual probability of flow. The remaining observations are used to validate the predictions. This bootstrapping method was run 500 times to calculate the probability that a site was wet, or the proportion of model runs in which a site was classified as perennial, a metric that Jaeger et al. (2019) called *stream permanence probability*. This metric is similar to streamflow permanence, but adds a probability associated with the bootstrapping technique to reflect both prediction uncertainty and dynamics over multiple years of record. If this probability at a stream pixel was over 0.5, then the site was classified as wet, otherwise, it was dry. The pixels were further classified by confidence level, a number between 1 (low) and 5 (high) that expresses the difference between the stream permanence probability and 0.5, and thus the likelihood that a site actually is wet or dry. The confidence values assigned to a site are (1) 0%, (2) 70%, (3) 80%, (4) 90%, and (5) 95%. When stream permanence probability is combined with confidence level, the result is one of 10 integer values between -5, meaning dry with a 95% confidence level, and +5, meaning wet with 95% confidence level. Intermediate steps indicate the corresponding confidence level

(e.g. -3 indicates dry with an 80% confidence level whereas 2 indicates wet with a 70% confidence level). The model had a global out-of-bag error rate (i.e., the number of misclassified observations divided by the total number of observations) of 19.55% with regional error rates ranging from 17.68% to 21.90% (Jaeger et al., 2019).

Though this model is a vast improvement over similar previous models that have error rates of ~50% (e.g., Fritz et al., 2013), Jaeger et al. (2019) claim that this tool is not meant to replace on-the-ground local knowledge. Rather it helps us understand regional hydrology as it is affected by changing climatic conditions. At present, the PROSPER model does not attempt to separate ephemeral and intermittent streams.

Another accurate model developed in recent years is the reduced-complexity mechanistic model of Ward et al. (2018). The model boasts minimal data requirements – a DEM (Digital Elevation Model), a mapped stream, and estimates of several hydrologic variables. Some of these hydrologic variables can be derived from the DEM and mapped stream, but others, like hydraulic conductivity, porosity, and Manning's roughness coefficient, may still be difficult to estimate in watersheds where little research has been conducted. For example, the model requires a reach-scale solute transport test to calibrate the hydrological model as well as estimates of instantaneous flowing network extent to calibrate the estimated absence/presence values throughout the watershed.

To validate the reduced-complexity model, Ward et al. (2018) used a combination of field observations and measurements of stream stage. The model performed well when predicting the instantaneous flowing network extent, but it

struggled to accurately predict connectivity, meaning that it gives a good overview of a watershed at a particular time, but it struggles to characterize the connections between points that may be important. The real advantage of this model is that once it is calibrated at a site, it is easy to apply to different years. For example, at the H. J. Andrews Experimental Forest in Oregon, Ward et al. (2020) explored changes in stream hydrology over the last 60 years using data from stream gauges to drive the model.

Finally, the third modeling approach for understanding stream drying is the Stream Length Duration Curve (SLDC), a statistical tool used to predict instantaneous and seasonal flowing network extent, which shows the amount of time throughout the season that an instantaneous flowing network extent is met or exceeded (Figure 1.3; Botter and Durighetto, 2020). We can use this tool to measure instantaneous flowing network extent at any given moment, reported as either stream length or percent of the total network. A steep duration curve indicates rapid changes in flowing extent with time while a shallow curve indicates more gradual changes.

To determine the locations of wetting in a watershed, stream length duration curves operate in probabilistic space (Figure 1.4). Unlike physical models, probabilistic models organize locations based on the seasonal streamflow permanence, with the driest sites on the top and the wettest sites on the bottom. By relating probabilistic space to physical space, the location of wet streambeds can be predicted based on the wetted length provided by the duration curve (Botter and Durighetto, 2020).

Applying this model to the Valfredda catchment in Italy required visual absence/presence observations at each of 504 locations at ~30 m separation during 10

fortnightly surveys. These surveys provided the data needed to calculate the streamflow permanence at each of the locations. Implicit in this campaign is the assumption that each observation point represents the ~15 m of stream length directly above and below it. This hefty set of observations was also used to validate the SLDC. The validation indicated that in a 16.8 km stream network, the model never classified more than 1 km incorrectly.

Though the SLDC considers correlation between streamflow permanence at observation points, they fail to consider how these correlations may or may not be associated with spatial separation between observation points. As such, it is unclear how accurately this model would perform with input data collected at different scales or observations at different spatiotemporal resolutions. What is certain is that a better understanding of spatial autocorrelation in stream drying would help us better implement the SLDC by clarifying the spatiotemporal resolutions of both observations and modeling that are required.

1.4.2. Spatial autocorrelation, semivariograms, and torgograms

In chapter 2 of this thesis, we improve upon previous non-perennial models by using a statistical method known as kriging. Kriging uses a spatial linear model and spatial autocorrelation to make predictions that are interpolated across space. To make these interpolations, kriging uses a metric known as semivariance. Semivariance is the average difference between data separated by a specified separation distance. When semivariance is plotted against separation distance, the plot is known as a

semivariogram (Figure 1.5A). Semivariograms are useful because they tell us the spatial scales at which autocorrelation can explain variations in the data.

We can characterize semivariograms with three parameters: the nugget, sill, and range. The nugget is the semivariance at a separation distance of zero. A large nugget indicates that either sampling separation was too large, or sampling equipment was not sensitive enough to observe autocorrelation on the smallest spatiotemporal scales. The nugget can help researchers know the smallest gap between measurements required in a monitoring campaign. The sill is the part of the graph where the slope is zero and the graph appears to form a horizontal asymptote. From the magnitude of semivariance at the sill, we learn the maximum average difference in values between points in our data set. The range is the separation distance where the sill begins to form. The range shows us the maximum separation at which autocorrelation is observed. When generating models, the range is important because it indicates the maximum distance at which autocorrelation can affect predictions.

We use the semivariogram because it allows us to visually assess the nugget, sill, and range. However, to perform the mathematics of kriging, we rely on the covariance function (Figure 1.5B) which is related to the semivariogram in that the x-axis reflects the separation distance between points, but differs because covariance is plotted on the y axis. Whereas semivariance reflects the difference between points, covariance reflects the similarities between points.

To interpolate values at predicted points, we use the equation $\mathbf{C}\mathbf{w} = \mathbf{D}$ where \mathbf{C} is a matrix derived from the covariance function, \mathbf{w} is a matrix of weights used to calculate

the value at an unknown point, and \mathbf{D} is a matrix that represents the spatial relationships between data points and a single prediction point. We can calculate \mathbf{C} and \mathbf{D} from empirical data, but solving for \mathbf{w} requires an invertible \mathbf{C} matrix. An invertible \mathbf{C} matrix is unlikely to result from empirical data, so we often use modeled covariance rather than empirical. Solving the equation above for \mathbf{w} , resulting in $\mathbf{w} = \mathbf{D}\mathbf{C}^{-1}$, allows us to interpolate values at each of our prediction points using the calculated weights, \mathbf{w} .

Kriging methods that rely on semivariograms are useful where points are related to each other over Cartesian distances (orange arrow in Figure 1.5D). In streams, however, points are connected via the stream network, which is likely not a straight line and only allows for points to be related up and downstream rather than in all directions. As such, points that are close to each other in Cartesian space may not be closely connected via the stream network. For this reason, stream hydrologists use a torgegram rather than a semivariogram (Figure 1.5C; Zimmerman and Ver Hoef, 2017). A torgegram consists of two semivariograms, each with its own range, nugget, and sill. The connected torgegram plots the relationships among connected points, meaning that the points are sequential along flow direction (blue arrow in Figure 1.5D), and the unconnected torgegram plots points that would never flow into each other, such as points in separate tributaries (green arrow in Figure 1.5D). Crucially, each of these semivariograms calculates distances based on the stream network rather than on Cartesian space. As with ordinary kriging in Cartesian space, we can create a covariance function using stream distance and use it for interpolation. The creation and use of a torgegram and its associated covariance function is facilitated by the Stream Statistical Network (SSN) package for R (Ver Hoef et al, 2014).

For non-perennial data, we weight data above a prediction point more than data below a prediction point because we expect water above the point in a stream network to flow down. This kind of weighting when using a toregram is called tail-up. Conversely, a tail-down weighting assumes that predicted values are influenced more by sites downstream of them. A mnemonic to remember the difference between tail-up and tail-down weighting is that a fish (or a bit of information) swimming to a point of interest has its tail facing up if it came from upstream and down if it came from downstream.

To our knowledge, only one study so far has attempted kriging to predict stream drying in a stream network (Gendaszek et al. 2020). Many studies cannot use kriging techniques due to a common rule of thumb that requires at least 25 pairs of points at lags less than half the maximum for high-quality semivariance estimates (Journel and Huijbregts, 1978). To abide by this rule of thumb, Gendaszek et al. (2020) chose to combine two watersheds to create a toregram. In combining two watersheds, they assumed that the two watersheds have the same spatial autocorrelation.

The data from the two combined watersheds, both larger than 500 km², have separation distances between sensors ranging from 400 m to 48,600 m. Such large separation distances risk producing a pure nugget, but the toregram produced by Gendaszek et al. (2020) has a shape that shows both a clear sill and a defined range despite a relatively large nugget of ~1 (Figure 1.6).

The models produced from data obtained by Gendaszek et al. (2020) generated a model quality metric (Area Under the Curve or AUC; see Appendix 1 for more details)

between 85 percent and 91 percent. Despite their high accuracy rates, they do not report metrics such as the range and sill, which would clarify the spatial structure of stream drying in these watersheds. We hope to expand upon their work by explicitly exploring the spatial structure of stream drying and by focusing our efforts in just one watershed that has been studied in detail.

1.5. Drivers of intermittency

In addition to autocorrelation, we can use non-spatial variables to improve our predictive models (Costigan et al. 2016). Despite the work done to understand non-spatial drivers of stream drying (Costigan et al., 2016; Dohman et al., 2021; Hammond et al., 2021; Jaeger et al., 2019; Pate et al., 2020; Ward et al., 2018; Warix et al., 2021), we still lack consensus on the most important driver or even the number of significant drivers. In this chapter, we give a brief overview of these drivers using the three categories established by Costigan et al. (2016): meteorological, physiographic, and land use.

In our brief overview of these drivers, we will refer to four spatial scales over which these drivers may vary: watershed, stream segment, reach, and meter, which we define here. The watershed scale refers to a length of stream, starting from the highest tributaries, greater than a kilometer (Frissel et al., 1986). The watershed is made up of several stream segments and reaches. A stream segment is defined as a ~100 m length of stream while a stream reach is defined as ~10 m (Frissel et al., 1986). The smallest spatial scale that we will explore is the meter scale.

Our brief overview of drivers will also include multiple temporal scales. Specifically, we will focus on the seasonal and daily scales. Though we will mention temporal scales larger than a year because of their importance to other studies on non-perennial streams, they are not the focus of this overview because the studies presented in later chapters of this thesis only include two field campaigns; one in the summer of 2020 and a second in the summer of 2021. We define a season as a period of time when temperatures, precipitation, and duration of sunlight are relatively consistent. Daily scales refer to ~24-hour periods that typically represent a full day/night cycle.

1.5.1. Meteorological variables

We will start by exploring meteorological variables that drive stream drying. On the watershed scale and above, energy inputs (often represented by temperature) and precipitation are emphasized as primary drivers of stream drying (Hammond et al., 2021; Snelder et al., 2013; Levick et al., 2008). This is because the quantity of surface water has a clear relationship with both the amount of evapotranspiration (ET) and precipitation (Konrad, 2006; Doering et al., 2007). If precipitation exceeds energy inputs, streams are more likely to be perennial. Conversely, if energy inputs exceed precipitation, we find more non-perennial streams (Snelder et al., 2013; Levick et al., 2008). On sub-watershed scales (i.e. the reach and meter scales), energy inputs are still the primary drivers, but the amount of sunlight or wind over a stream are emphasized more than temperature because variations in radiation and wind are more likely at these small spatial scales (Costigan et al., 2016).

Energy inputs and precipitation can vary on temporal scales as well as spatial scales. On daily scales, individual precipitation events often cause non-perennial streams to wet up in the short term (Jaeger and Olden, 2012), especially if an event is intense. The pattern of increased wetting can be extended to longer temporal scales if events are frequent over the course of a season or a year (Costigan et al., 2016). Conversely, the lack of precipitation events over seasonal and yearly scales, a phenomenon known as hydrologic drought (Bazrafshan et al., 2015) can lead to more stream drying.

1.5.2. Physiographic variables

Physiographic variables include topography, lithology, and regolith. On the watershed scale, lithology is emphasized as a major driver (Costigan et al., 2016). For example, permeable soils and bedrock allow water to quickly move between the surface and subsurface (Doering et al., 2007). Thus, groundwater sources can recharge streams during drier periods (Jencso and McGlynn, 2011), which can buffer against stream drying.

Topographic variables are emphasized on the watershed, stream segment, and reach scale. On the watershed scale, elongated basin shapes have fewer perennial streams due to the rapid pace at which they deliver water to streams (Snelder et al., 2013). On the stream segment and reach scales, streams that have slopes steeper than the groundwater table slope tend to have higher streamflow permanence values (Konrad, 2006). Conversely, on the stream segment and reach scales, streams that

have elevations higher than the water table have lower streamflow permanence values due to the loss of water from the surface to the water table (Konrad, 2006).

On the smallest spatial scales, streambed permeability, not necessarily lithologic permeability of the underlying bedrock, is a driver of stream drying. This corresponds with work conducted by Pate et al. (2020) that found a relationship between stream drying and streambed grain size on the reach scale. However, in southeastern Idaho, semivariograms of shallow surface Ksat showed a range on the single-meter scale (Ferraro, 2021), below the reach-scale, which may explain why median grain size was not a strong predictor of stream drying in Gibson Jack. This may indicate that streambed grain size and shallow surface permeability drives stream drying in some locations, but not others, depending on the scales at which it varies.

Changes in physiography can change the amount of stream drying. For example, a small landslide may control drying patterns over small scales (i.e., sub-yearly scales) if it is small, or on large scales (i.e., over a year), if it requires extensive erosion to remove (Wu et al., 2019). Other physiographic controls that may vary over sub-annual timescales include freeze-thaw cycles (Musa et al., 2016) and clay expansion (McKinstry, 1965). Despite the abundance of research on both freeze-thaw cycles and clay expansion, we are not aware of any studies that relate these phenomena to non-perennial streams.

1.5.3. Land cover variables

The final category is land cover or the non-regolith material that covers Earth's surface due to meteorological, geologic, ecologic, and anthropogenic activity (Costigan et al., 2016). On the watershed scale, biome is emphasized as a major driver of stream drying. Though we observe non-perennial streams in all terrestrial biomes (Shanafield et al., 2021), drier biomes, such as deserts, grasslands, and tundras, tend to have more non-perennial streams and lower stream permanence values (Dodds, 1997; Poff, 1996). It is important to note that even though Costigan et al. (2016) classifies biome as a landcover variable, biome is related to both climate and topography, meaning that any studies that explore biome as a driver of stream drying need to consider correlated explanatory variables.

On reach scales, anthropogenic disturbances such as urbanization are emphasized as important drivers. Anthropogenic development, such as construction of infrastructure, decreases infiltration rates and reduces groundwater recharge resulting in more non-perennial streams and flashy hydrographs (Rheinhardt et al., 2009). Similarly, on reach scales, groundwater extraction can decrease stream permanence values by depleting aquifers (Costigan et al., 2016; Falke et al., 2011) as can any sort of water diversion structure, such as dams, weirs, and irrigation systems (Steward et al., 2011; Caruso and Hanes, 2011). However, if water release from a dam is regular, stream permanence can increase on the reach scale (Steward et al., 2011; Hassan and Egozi, 2001). Similarly, consistent wastewater discharge can create artificial perennial streams (Luthy et al., 2015). On the meter scale, vegetation cover can change abruptly. The quantity and type of plants directly relate to transpiration rates (Schreiber and

Riederer, 1996). Conversely, canopy cover can decrease sunlight on a stream and reduce the evaporation that occurs.

Land cover can also change over time and lead to changes in stream drying patterns. For example, many biomes experience multiple seasonal changes within each year that affect both plant and animal behavior. In many places, temperature and precipitation change drastically from month to month, leading to changes in vegetation cover throughout the year. On longer temporal scales, biomes may change due to climate change or anthropogenic activity over the course of several years (Beck et al., 2011). Similarly, land cover can temporarily change due to events such as fire, shifting both as plants are burned and as new growth is established in burn scars (Eva and Lambin, 2001).

1.5.4. Meteorology, physiography and land cover in Gibson Jack

We conducted this thesis research in Gibson Jack, a watershed located in southeastern Idaho that drains an area of ~25.5 km² into the Portneuf River. We chose this site because it exhibits a wide range of drying patterns, from always wet to almost always dry. Additionally, many of the physiographic, land cover, and meteorological variables identified as potential drivers of stream drying (Figure 1.1; Costigan et al., 2016; Dohman et al., 2021; Hammond et al., 2021; Jaeger et al., 2019; Pate et al., 2020; Ward et al., 2018; Warix et al., 2021) have been mapped extensively in this watershed. On a practical note, Gibson Jack is close to Idaho State University in Pocatello, Idaho (~10 km away), allowing us to visit it regularly even during a global pandemic.

Over space, physiographic and land cover variables vary throughout the watershed. Metasedimentary rocks, such as quartzite, largely underlie the northern half of the watershed and carbonates largely underlie the south (Rodgers and Othberg, 1999). Gibson Jack includes steep slopes (mean $\sim 20^\circ$) with maximum elevations reaching $\sim 2,200$ m with the outlet located at $\sim 1,500$ m. On the reach scale, soils in Gibson Jack are primarily characterized as silty loams and fine sandy clay loams, many of which contain gravel (Davidson, 1977).

Land cover variables mapped throughout the watershed include vegetative cover, land management, grazing, and recreation. Vegetative cover in the watershed varies from Douglas fir on the north-facing slopes to sagebrush, grasses, and juniper on the south-facing slopes (Evenden et al., 2001). On the reach scale, recreational activity is largely limited to the constructed trails, with more activity lower in the watershed. Grazing occurs most intensely in the north fork.

Temporally, meteorological and land cover variables change throughout the year. A weather station in Gibson Jack recorded temperatures during water year 2020 (Oct 2019-Sep 2020) ranging from 18.8°C to -6.7°C with an average of 5.4°C . Precipitation ranges from 0.38 m/yr in dry years to 0.76 m/yr in wet years in the form of both rain and snow (Welhan, 2006).

The intensity of land use changes seasonally in Gibson Jack. Grazing is restricted during the winter months due to the snow that covers most of the watershed. As the snow melts and temperatures rise in the spring, cattle graze in parts of the

watershed. The type of recreation by local residents also changes drastically from season to season.

1.6. Conclusion

Our understanding of non-perennial streams plays a critical role in policy and research decisions. These decisions include choices about what streams to protect on the federal level and what models accurately represent biogeochemical concentrations in streams. We can aid in these decisions by accurately characterizing non-perennial streams and developing models to predict stream drying where direct observation is not possible. Though predictive models have improved in recent years, we can further improve them by identifying the scales of autocorrelation and applying them to model development. Additionally, we can improve our models by better understanding the variables that drive stream drying. As we address gaps in our understanding of non-perennial streams, we will better inform management decisions that rely upon accurate characterizations of surface water and improve sampling designs for biogeochemical and hydrological research in non-perennial systems.

1.7. Figures

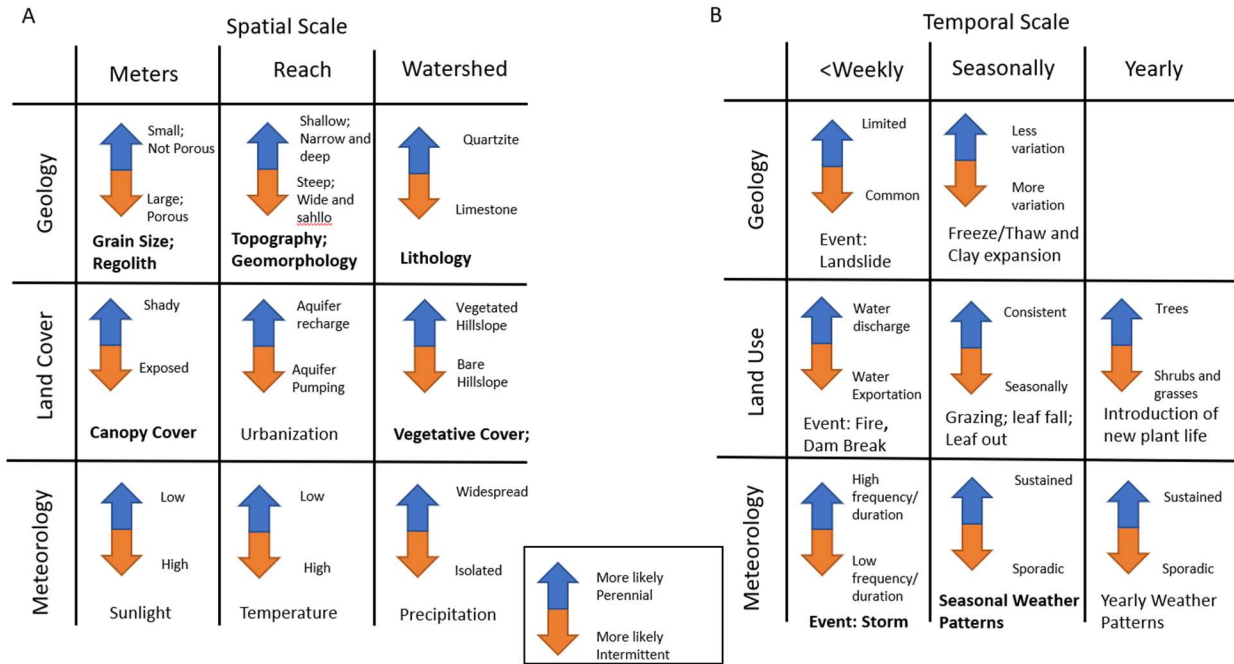


Figure 1.1: Charts showing the most important controls on different spatial (A) and temporal (B) scales. Bold text indicates variables that we will address in later chapters. Charts were modified from Costigan et al. (2019).

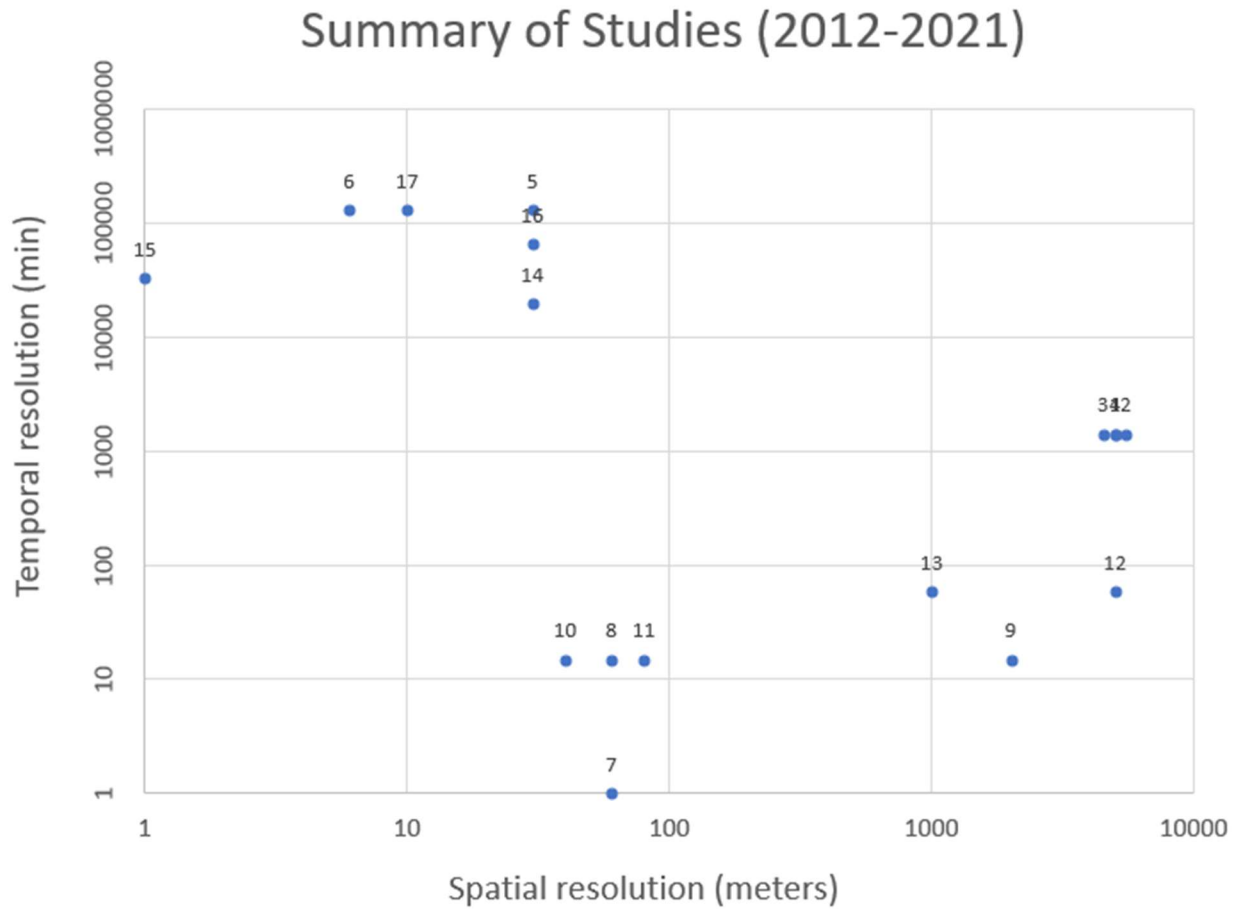


Figure 1. 2: Scatter plots showing the spatial and temporal resolution used by all stream drying studies in the last decade. The labels on graph points correspond to the studies listed in Table 1.1. Note that the majority of studies either used small spatial scales.

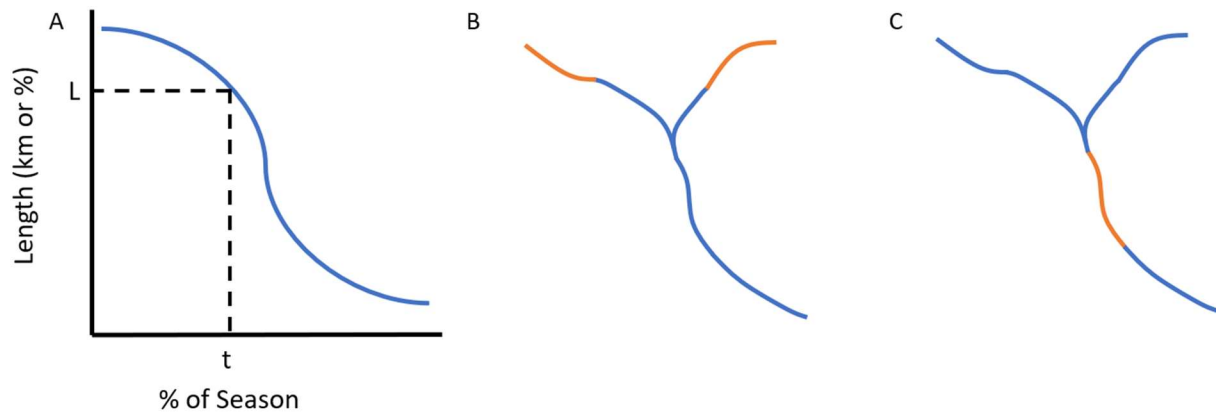


Figure 1. 3: Example of a stream length duration curve or SLDC (A). A particular point on the curve such as (t, L) shows the percent of a season (t) that the length of the stream matches or exceeds that length (L). Examples of possible drying patterns within a watershed are also shown (B and C). Though the SLDC is a good way of characterizing changes in the instantaneous network extent, it gives us little spatial information beyond that. For example, the SLDC by itself cannot indicate connectivity.

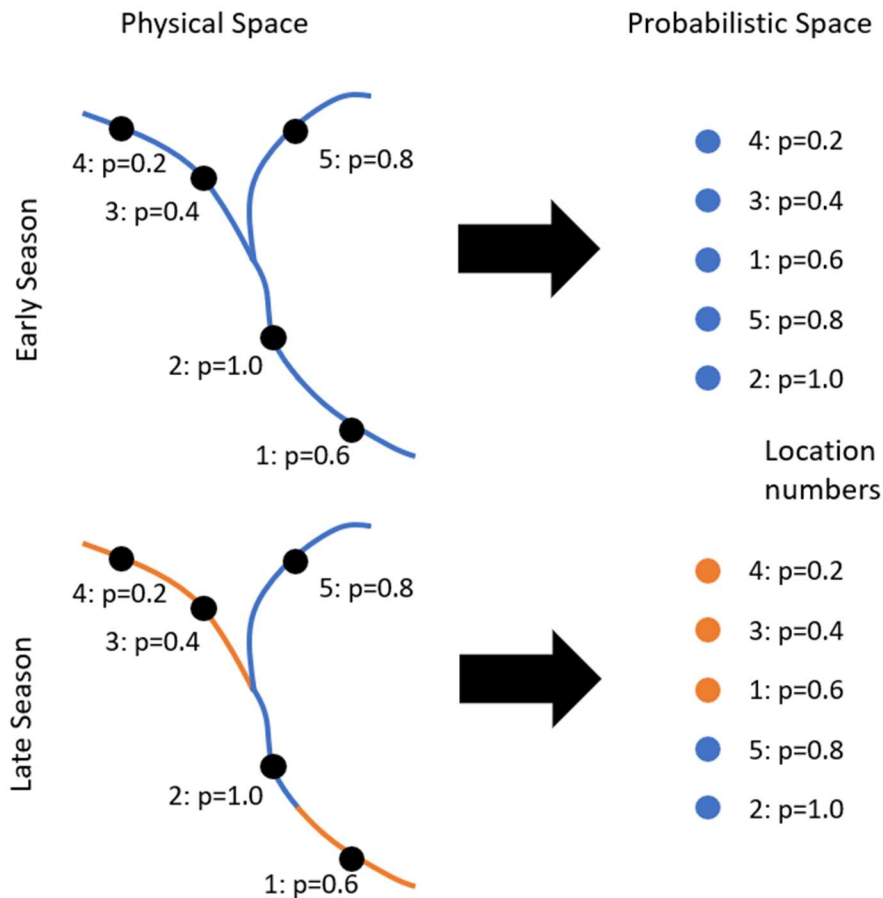


Figure 1. 4: Conceptual models showing how physical and probabilistic space relate to each other after Botter and Durighetto (2019). After assigning each point a probability of flow, where 1 means perennial and 0 means always dry, we order the points from most likely dry to most likely wet. When determining how much of the stream is wet, we start from the bottom of the probabilistic model and work up until we reach our instantaneous flowing network extent for a particular time.

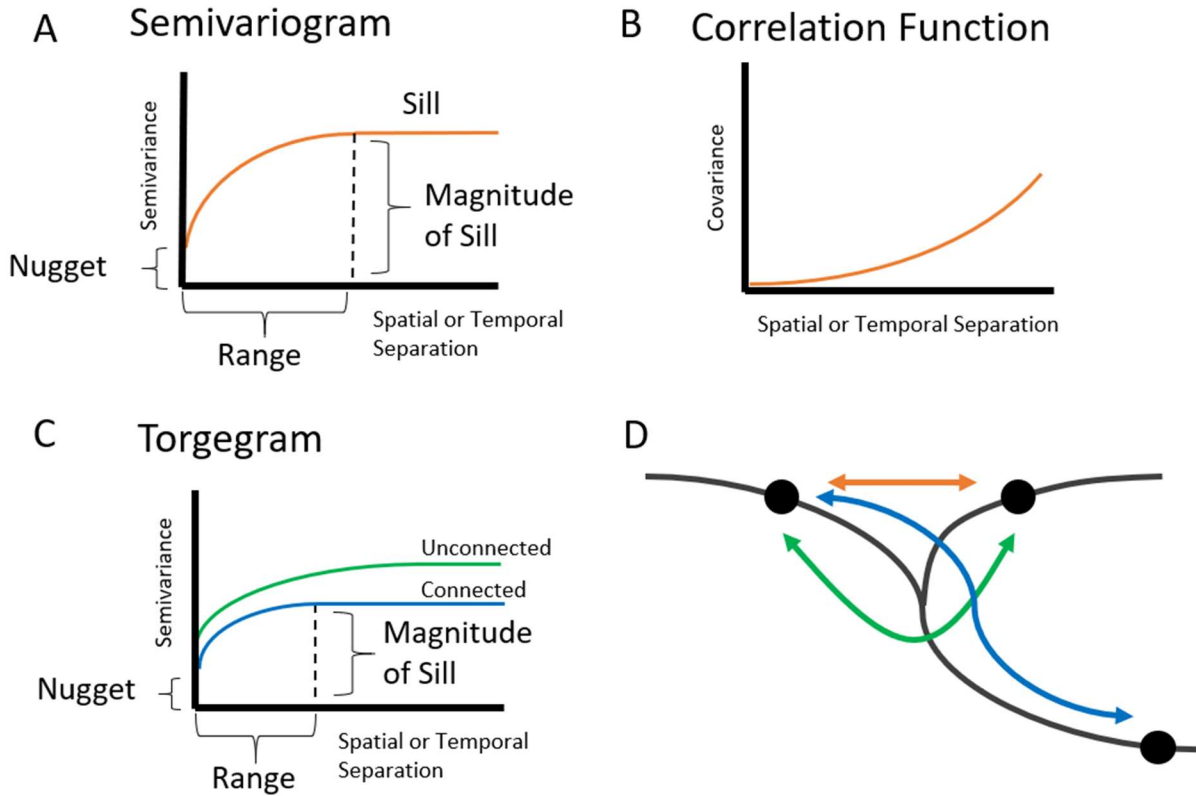


Figure 1. 5: Example plots of a semivariogram (A), covariance function (B), and torgegram (C). Important features, such as the nugget, sill, and range, are identified in both the semivariogram and the torgegram. Additionally, a conceptual stream map is shown (D) indicating methods of calculating distances between points. The orange arrows in D correspond with the semivariogram and covariance function in A and B. Similarly, the blue arrow corresponds to the connected semivariogram (blue curve in C) for point-pairs where water flows from the upstream point to the downstream point whereas the green arrow corresponds to the unconnected semivariogram (green curve in C) for point-pairs that span multiple tributaries.

Empirical Torgegram of Binary Intermittency

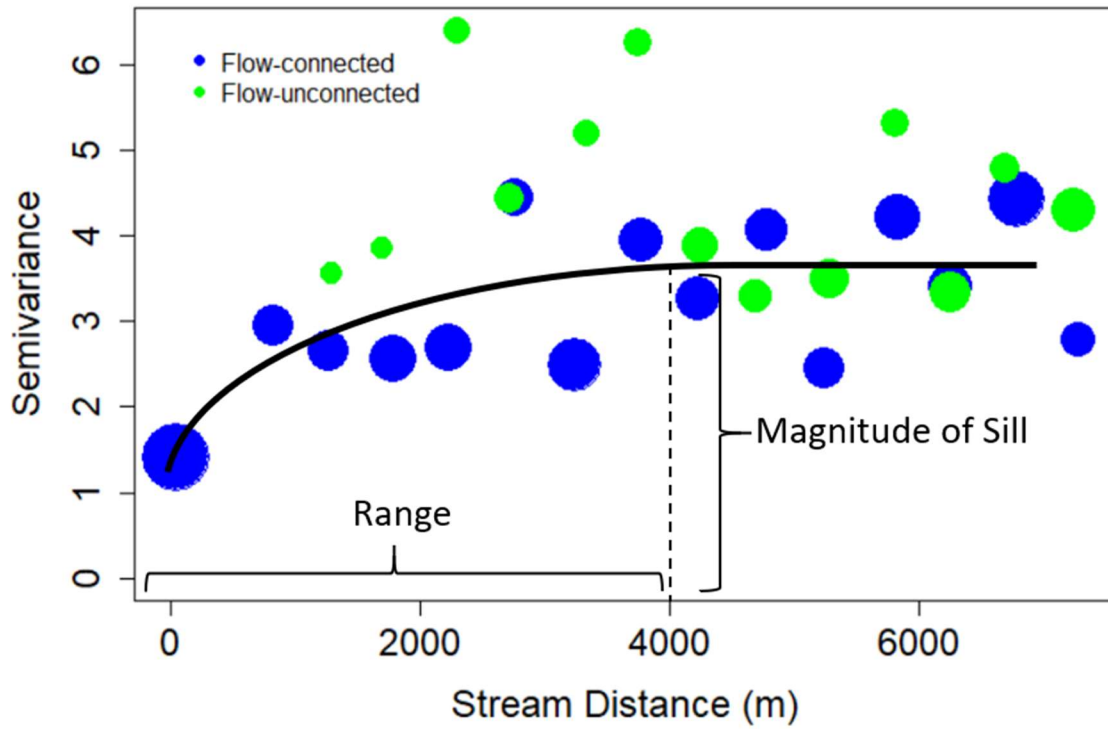


Figure 1. 6: Torgegram created from data collected by Gendaszek et al. (2020). Notice the clear range and nugget exhibited in this torgegram despite the high nugget. In this thesis, we seek data to quantify a similarly shaped torgegram, but with a much smaller nugget.

1.8. Tables

Table 1.1. Summary of scales used in stream drying literature				
Citation #	Author(s)	Year	Spatial Resolution (m)	Temporal Resolution (min)
1	Hammond et al.	2021	5000	1440
2	Zipper et al.	2020	5500	1440
3	Price et al.	2020	4500	1440
4	Hammond et al.	2021	5000	1440
5	Jaeger et al.	2019	30	131400
6	Pate et al.	2020	6	131400
7	Goulsbra et al.	2014	60	1
8	Dohman et al.	2021	60	15
9	Jaeger and Olden	2012	2000	15
10	Jensen et al.	2019	40	15
11	Warix et al.	2021	80	15
12	Gendaszek et al.	2020	5000	60
13	Paillex et al.	2020	1000	60
14	Botter & Durighetto	2020	30	20160
15	Ward et al.	2018	1	32850
16	Fritz et al.	2013	30	65700
17	Hale and Godsey	2019	10	131400

1.9. References

- Acuña, V., Casellas, M., Corcoll, N., Timoner, X., and Sabater, S., 2015, Increasing extent of periods of no flow in intermittent waterways promotes heterotrophy: *Freshwater Biology*, v. 60, p. 1810–1823, doi:[10.1111/fwb.12612](https://doi.org/10.1111/fwb.12612).
- Acuña, V., Giorgi, A., Muñoz, I., Sabater, F., and Sabater, S., 2007, Meteorological and riparian influences on organic matter dynamics in a forested Mediterranean stream: *Journal of the North American Benthological Society*, v. 26, p. 54–69, doi:[10.1899/0887-3593\(2007\)26\[54:MARIOO\]2.0.CO;2](https://doi.org/10.1899/0887-3593(2007)26[54:MARIOO]2.0.CO;2).
- Allen, D.C. et al., 2020, River ecosystem conceptual models and non-perennial rivers: A critical review: *WIREs Water*, v. 7, doi:[10.1002/wat2.1473](https://doi.org/10.1002/wat2.1473).
- Allen, D.C., Galbraith, H.S., Vaughn, C.C., and Spooner, D.E., 2013, A Tale of Two Rivers: Implications of Water Management Practices for Mussel Biodiversity Outcomes During Droughts: *AMBIO*, v. 42, p. 881–891, doi:[10.1007/s13280-013-0420-8](https://doi.org/10.1007/s13280-013-0420-8).
- Bazrafshan, J., Nadi, M., and Ghorbani, K., 2015, Comparison of empirical copula-based joint deficit Index (JDI) and multivariate standardized precipitation Index (MSPI) for drought monitoring in Iran: *Water Resources Management*, v. 29, p. 2027–2044, doi:[10.1007/s11269-015-0926-x](https://doi.org/10.1007/s11269-015-0926-x).
- Beck, P.S.A., Juday, G.P., Alix, C., Barber, V.A., Winslow, S.E., Sousa, E.E., Heiser, P., Herriges, J.D., and Goetz, S.J., 2011, Changes in forest productivity across Alaska consistent with biome shift: *Ecology Letters*, v. 14, p. 373–379, doi:[10.1111/j.1461-0248.2011.01598.x](https://doi.org/10.1111/j.1461-0248.2011.01598.x).
- Belmont, P. et al., 2011, Large Shift in Source of Fine Sediment in the Upper Mississippi River: *Environmental Science & Technology*, v. 45, p. 8804–8810, doi:[10.1021/es2019109](https://doi.org/10.1021/es2019109).
- Bertuzzo, E., Helton, A.M., Hall, R.O., and Battin, T.J., 2017, Scaling of dissolved organic carbon removal in river networks: *Advances in Water Resources*, v. 110, p. 136–146, doi:[10.1016/j.advwatres.2017.10.009](https://doi.org/10.1016/j.advwatres.2017.10.009).
- Botter, G., and Durigetto, N., 2020, The stream length duration curve: A tool for characterizing the time variability of the flowing stream length: *Water Resources Research*, v. 56, doi:[10.1029/2020WR027282](https://doi.org/10.1029/2020WR027282).
- Breiman, L., 2001, Random forests: *Machine learning*, v. 45, p. 5–32.
- Brown, T.C., Hobbins, M.T., and Ramirez, J.A., 2008, Spatial distribution of water supply in the coterminous united states: *JAWRA Journal of the American Water Resources Association*, v. 44, p. 1474–1487, doi:[10.1111/j.1752-1688.2008.00252.x](https://doi.org/10.1111/j.1752-1688.2008.00252.x).
- Busch, M.H. et al., 2020, What's in a name? Patterns, trends, and suggestions for defining non-perennial rivers and streams: *Water*, v. 12, p. 1980, doi:[10.3390/w12071980](https://doi.org/10.3390/w12071980).

- Caruso, B.S., and Haynes, J., 2011, Biophysical-regulatory classification and profiling of streams across management units and ecoregions: *JAWRA Journal of the American Water Resources Association*, v. 47, p. 386–407, doi:[10.1111/j.1752-1688.2010.00522.x](https://doi.org/10.1111/j.1752-1688.2010.00522.x).
- Chapin, T.P., Todd, A.S., and Zeigler, M.P., 2014, Robust, low-cost data loggers for stream temperature, flow intermittency, and relative conductivity monitoring: *Water Resources Research*, v. 50, p. 6542–6548, doi:[10.1002/2013WR015158](https://doi.org/10.1002/2013WR015158).
- Costigan, K.H., Jaeger, K.L., Goss, C.W., Fritz, K.M., and Goebel, P.C., 2016, Understanding controls on flow permanence in intermittent rivers to aid ecological research: integrating meteorology, geology and land cover: *Integrating science to understand flow Intermittence: Ecohydrology*, v. 9, p. 1141–1153, doi:[10.1002/eco.1712](https://doi.org/10.1002/eco.1712).
- Datry, T., Larned, S.T., and Tockner, K., 2014, Intermittent rivers: A challenge for freshwater ecology: *BioScience*, v. 64, p. 229–235, doi:[10.1093/biosci/bit027](https://doi.org/10.1093/biosci/bit027).
- Davidson, 1977, Soils and geology of the west fork mink Creek and Gibson Jack creeks: Caribou national forest open-file report 2540:
- Dodds, W.K., 1997, Distribution of Runoff and Rivers Related to Vegetative Characteristics, Latitude, and Slope: A Global Perspective: *Journal of the North American Benthological Society*, v. 16, p. 162–168, doi:[10.2307/1468248](https://doi.org/10.2307/1468248).
- Doering, M., Uehlinger, U., Rotach, A., Schlaepfer, D.R., and Tockner, K., 2007, Ecosystem expansion and contraction dynamics along a large Alpine alluvial corridor (Tagliamento River, Northeast Italy): *Earth Surface Processes and Landforms*, v. 32, p. 1693–1704, doi:[10.1002/esp.1594](https://doi.org/10.1002/esp.1594).
- Dohman, J.M., Godsey, S.E., and Hale, R.L., 2021, Three-dimensional subsurface flow path controls on flow permanence: *Water Resources Research*, v. 57, p. 10.
- Eva, H., and Lambin, E.F., 2000, Fires and land-cover change in the tropics: a remote sensing analysis at the landscape scale: *Journal of Biogeography*, v. 27, p. 765–776.
- Evenden, A.G., Moeur, M., Shelly, J.S., Kimball, S.F., and Wellner, C.A., 2001, Research natural areas on national forest system lands in Idaho, Montana, Nevada, Utah, and Western Wyoming: A guidebook for scientists, managers, and educators: U.S. Department of Agriculture, Forest Service, Rocky Mountain Research Station RMRS-GTR-69, RMRS-GTR-69 p., doi:[10.2737/RMRS-GTR-69](https://doi.org/10.2737/RMRS-GTR-69).
- Executive Office of the President, 2021, Protecting public health and the environment and restoring science to tackle the climate crisis: *Federal Register*, v. 86, p. 7037–7043.
- Falke, J.A., Fausch, K.D., Magelky, R., Aldred, A., Durnford, D.S., Riley, L.K., and Oad, R., 2011, The role of groundwater pumping and drought in shaping ecological futures for

- stream fishes in a dryland river basin of the western great plains, USA: *Ecohydrology*, v. 4, p. 682–697, doi:[10.1002/eco.158](https://doi.org/10.1002/eco.158).
- Ferraro, M.J., 2021, Patterns in Headwater Stream in the Northern Rocky Mountains, Idaho, USA [MS thesis]: Idaho State university, 205 p.
- Frissell, C.A., Liss, W.J., Warren, C.E., and Hurley, M.D., 1986, A hierarchical framework for stream habitat classification: Viewing streams in a watershed context: *Environmental Management*, v. 10, p. 199–214, doi:[10.1007/BF01867358](https://doi.org/10.1007/BF01867358).
- Fritz, K.M., Hagenbuch, E., D'Amico, E., Reif, M., Wigington, P.J., Leibowitz, S.G., Comeleo, R.L., Ebersole, J.L., and Nadeau, T.-L., 2013, Comparing the extent and permanence of headwater streams from two field surveys to values from hydrographic databases and maps: *JAWRA Journal of the American Water Resources Association*, v. 49, p. 867–882, doi:[10.1111/jawr.12040](https://doi.org/10.1111/jawr.12040).
- Gendaszek, A.S., Dunham, J.B., Torgersen, C.E., Hockman-Wert, D.P., Heck, M.P., Thorson, J., Mintz, J., and Allai, T., 2020, Land-Cover and Climatic Controls on Water Temperature, Flow Permanence, and Fragmentation of Great Basin Stream Networks: *Water*, v. 12, p. 1962, doi:[10.3390/w12071962](https://doi.org/10.3390/w12071962).
- Goulsbra, C., Evans, M., and Lindsay, J., 2014, Temporary streams in a peatland catchment: pattern, timing, and controls on stream network expansion and contraction: *Earth Surface Processes and Landforms*, v. 39, p. 790–803, doi:[10.1002/esp.3533](https://doi.org/10.1002/esp.3533).
- Hale, R.L., and Godsey, S.E., 2019, Dynamic stream network intermittence explains emergent dissolved organic carbon chemostasis in headwaters: *Hydrological Processes*, p. hyp.13455, doi:[10.1002/hyp.13455](https://doi.org/10.1002/hyp.13455).
- Hammond, J.C. et al., 2021, Spatial patterns and drivers of nonperennial flow regimes in the contiguous United States: *Geophysical Research Letters*, v. 48, doi:[10.1029/2020GL090794](https://doi.org/10.1029/2020GL090794).
- Hassan, M.A., and Egozi, R., 2001, Impact of wastewater discharge on the channel morphology of ephemeral streams: *Earth Surface Processes and Landforms*, v. 26, p. 1285–1302, doi:[10.1002/esp.273](https://doi.org/10.1002/esp.273).
- Hay, S.E., Jenkins, K.M., and Kingsford, R.T., 2018, Diverse invertebrate fauna using dry sediment as a refuge in semi-arid and temperate Australian rivers: *Hydrobiologia*, v. 806, p. 95–109, doi:[10.1007/s10750-017-3343-8](https://doi.org/10.1007/s10750-017-3343-8).
- Isaak, D.J. et al., 2014, Applications of spatial statistical network models to stream data: Spatial statistical network models for stream data: *Wiley Interdisciplinary Reviews: Water*, v. 1, p. 277–294, doi:[10.1002/wat2.1023](https://doi.org/10.1002/wat2.1023).
- Jaeger, K.L., and Olden, J.D., 2012, Electrical resistance sensor arrays as a means to quantify longitudinal connectivity of rivers: Using sensors to quantify longitudinal

- connectivity in rivers: *River Research and Applications*, v. 28, p. 1843–1852, doi:[10.1002/rra.1554](https://doi.org/10.1002/rra.1554).
- Jaeger, K.L., Olden, J.D., and Pelland, N.A., 2014, Climate change poised to threaten hydrologic connectivity and endemic fishes in dryland streams: *Proceedings of the National Academy of Sciences*, v. 111, p. 13894–13899, doi:[10.1073/pnas.1320890111](https://doi.org/10.1073/pnas.1320890111).
- Jencso, K.G., and McGlynn, B.L., 2011, Hierarchical controls on runoff generation: Topographically driven hydrologic connectivity, geology, and vegetation: *Water Resources Research*, v. 47, doi:[10.1029/2011WR010666](https://doi.org/10.1029/2011WR010666).
- Jensen, C.K., McGuire, K.J., McLaughlin, D.L., and Scott, D.T., 2019, Quantifying spatiotemporal variation in headwater stream length using flow intermittency sensors: *Environmental Monitoring and Assessment*, v. 191, p. 226, doi:[10.1007/s10661-019-7373-8](https://doi.org/10.1007/s10661-019-7373-8).
- Journel, A.G., 1978, *Mining Geostatistics*: London, Academic Press.
- Katz, G.L., Denslow, M.W., and Stromberg, J.C., 2012, The Goldilocks effect: intermittent streams sustain more plant species than those with perennial or ephemeral flow: *Desert riparian diversity: Freshwater Biology*, v. 57, p. 467–480, doi:[10.1111/j.1365-2427.2011.02714.x](https://doi.org/10.1111/j.1365-2427.2011.02714.x).
- Keller, K. et al., 2019, Dry season habitat use of fishes in an Australian tropical river: *Scientific Reports*, v. 9, p. 5677, doi:[10.1038/s41598-019-41287-x](https://doi.org/10.1038/s41598-019-41287-x).
- Konrad, C.P., 2006, Location and timing of river-aquifer exchanges in six tributaries to the Columbia River in the Pacific Northwest of the United States: *Journal of Hydrology*, v. 329, p. 444–470, doi:[10.1016/j.jhydrol.2006.02.028](https://doi.org/10.1016/j.jhydrol.2006.02.028).
- Larsen, L.G., Choi, J., Nungesser, M.K., and Harvey, J.W., 2012, Directional connectivity in hydrology and ecology: *Ecological Applications*, v. 22, p. 2204–2220, doi:[10.1890/11-1948.1](https://doi.org/10.1890/11-1948.1).
- Levick, L.R. et al., 2008, *The Ecological and Hydrological Significance of Ephemeral and Intermittent Streams in the Arid and Semi-arid American Southwest*: Washington, D.C., U.S. Environmental Protection Agency and USDA/ARS Southwest Watershed Research Center, 116 p.
- Luthy, R.G., Sedlak, D.L., Plumlee, M.H., Austin, D., and Resh, V.H., 2015, Wastewater-effluent-dominated streams as ecosystem-management tools in a drier climate: *Innovations in the Face of Climate Change*, v. 13, p. 477–485, doi:[10.1890/150038](https://doi.org/10.1890/150038).
- McKinstry, H.A., 1965, Thermal expansion of clay minerals: *The American Mineralogist*, v. 50, p. 11.

- Messenger, M.L., Lehner, B., Cockburn, C., Lamouroux, N., Pella, H., Snelder, T., Tockner, K., Trautmann, T., Watt, C., and Datry, T., 2021, Global prevalence of non-perennial rivers and streams: *Nature*, v. 594, p. 391–397, doi:[10.1038/s41586-021-03565-5](https://doi.org/10.1038/s41586-021-03565-5).
- Musa, A., Ya, L., Anzhi, W., and Cunyang, N., 2016, Characteristics of soil freeze–thaw cycles and their effects on water enrichment in the rhizosphere: *Geoderma*, v. 264, p. 132–139, doi:[10.1016/j.geoderma.2015.10.008](https://doi.org/10.1016/j.geoderma.2015.10.008).
- Paillex, A., Siebers, A.R., Ebi, C., Mesman, J., and Robinson, C.T., 2020, High stream intermittency in an alpine fluvial network: Val Roseg, Switzerland: *Limnology and Oceanography*, v. 65, p. 557–568, doi:[10.1002/lno.11324](https://doi.org/10.1002/lno.11324).
- Pate, A.A., Segura, C., and Bladon, K.D., 2020, Streamflow permanence in headwater streams across four geomorphic provinces in Northern California: *Hydrological Processes*, p. hyp.13889, doi:[10.1002/hyp.13889](https://doi.org/10.1002/hyp.13889).
- Pisani, O., Dodds, W.K., and Jaffé, R., 2016, Characterizing organic matter inputs to sediments of small, intermittent, prairie streams: a molecular marker and stable isotope approach: *Aquatic Sciences*, v. 78, p. 343–354, doi:[10.1007/s00027-015-0435-2](https://doi.org/10.1007/s00027-015-0435-2).
- Poff, N., 1996, A hydrogeography of unregulated streams in the United States and an examination of scale-dependence in some hydrological descriptors: *Freshwater Biology*, v. 36, p. 71–79, doi:[10.1046/j.1365-2427.1996.00073.x](https://doi.org/10.1046/j.1365-2427.1996.00073.x).
- Rapanos v. United States (2006). 547 US 715.
- Rheinhardt, R.D., McKenney-Easterling, M., Brinson, M.M., Masina-Rubbo, J., Brooks, R.P., Whigham, D.F., O'Brien, D., Hite, J.T., and Armstrong, B.K., 2009, Canopy composition and forest structure provide restoration targets for low-order riparian ecosystems: *Restoration Ecology*, v. 17, p. 51–59, doi:[10.1111/j.1526-100X.2007.00333.x](https://doi.org/10.1111/j.1526-100X.2007.00333.x).
- Robinne, F.-N., Bladon, K.D., Silins, U., Emelko, M.B., Flannigan, M.D., Parisien, M.-A., Wang, X., Kienzle, S.W., and Dupont, D.P., 2019, A regional-scale index for assessing the exposure of drinking-water sources to wildfires: *Forests*, v. 10, p. 384, doi:[10.3390/f10050384](https://doi.org/10.3390/f10050384).
- Rodgers, D.W., and Othberg, K.L., 1999, Geologic map of the Pocatello south quadrangle, Bannock and Power counties, Idaho: Idaho Geologic Survey Geologic map.
- Ruhi, A., Messenger, M.L., and Olden, J.D., 2018, Tracking the pulse of the Earth's fresh waters: *Nature Sustainability*, v. 1, p. 198–203, doi:[10.1038/s41893-018-0047-7](https://doi.org/10.1038/s41893-018-0047-7).
- Rupp, D.E., Larned, S.T., Arscott, D.B., and Schmidt, J., 2008, Reconstruction of a daily flow record along a hydrologically complex alluvial river: *Journal of Hydrology*, v. 359, p. 88–104, doi:[10.1016/j.jhydrol.2008.06.019](https://doi.org/10.1016/j.jhydrol.2008.06.019).
- von Schiller, D., Graeber, D., Ribot, M., Timoner, X., Acuña, V., Martí, E., Sabater, S., and Tockner, K., 2015, Hydrological transitions drive dissolved organic matter quantity and

- composition in a temporary Mediterranean stream: *Biogeochemistry*, v. 123, p. 429–446, doi:[10.1007/s10533-015-0077-4](https://doi.org/10.1007/s10533-015-0077-4).
- Schreiber, L., and Riederer, M., 1996, Ecophysiology of cuticular transpiration: comparative investigation of cuticular water permeability of plant species from different habitats: *Oecologia*, v. 107, p. 426–432, doi:[10.1007/BF00333931](https://doi.org/10.1007/BF00333931).
- Shanafield, M., Bourke, S.A., Zimmer, M.A., and Costigan, K.H., 2021, An overview of the hydrology of non-perennial rivers and streams: *WIREs Water*, v. 8, doi:[10.1002/wat2.1504](https://doi.org/10.1002/wat2.1504).
- Shumilova, O. et al., 2019, Simulating rewetting events in intermittent rivers and ephemeral streams: A global analysis of leached nutrients and organic matter: *Global Change Biology*, v. 25, p. 1591–1611, doi:[10.1111/gcb.14537](https://doi.org/10.1111/gcb.14537).
- Snelder, T.H., Datry, T., Lamouroux, N., Larned, S.T., Sauquet, E., Pella, H., and Catalogne, C., 2013, Regionalization of patterns of flow intermittence from gauging station records: *Hydrology and Earth System Sciences*, v. 17, p. 2685–2699, doi:[10.5194/hess-17-2685-2013](https://doi.org/10.5194/hess-17-2685-2013).
- Steward, A.L., Marshall, J.C., Sheldon, F., Harch, B., Choy, S., Bunn, S.E., and Tockner, K., 2011, Terrestrial invertebrates of dry river beds are not simply subsets of riparian assemblages: *Aquatic Sciences*, v. 73, p. 551–566, doi:[10.1007/s00027-011-0217-4](https://doi.org/10.1007/s00027-011-0217-4).
- Stubbington, R., England, J., Wood, P.J., and Sefton, C.E.M., 2017, Temporary streams in temperate zones: recognizing, monitoring and restoring transitional aquatic-terrestrial ecosystems: *Temporary streams in temperate zones: Wiley Interdisciplinary Reviews: Water*, v. 4, p. e1223, doi:[10.1002/wat2.1223](https://doi.org/10.1002/wat2.1223).
- Tooth, S., 2000, Process, form and change in dryland rivers: a review of recent research: *Earth-Science Reviews*, v. 51, p. 67–107, doi:[10.1016/S0012-8252\(00\)00014-3](https://doi.org/10.1016/S0012-8252(00)00014-3).
- USDOD, 1986, Final rule for regulatory programs of the corps of engineers: *Federal Register*, v. 51, p. 41206–41260.
- USDOD, 2020, Navigable water protection rule: “Definition of waters of the United States”: *Federal Register*, v. 85, p. 22250–22342.
- USDOD, 2021, Revised definition of “waters of the United States”: *Federal Register*, v. 86, p. 69372–69450.
- USDOD, and USEPA, 2015, Clean water rule: definition of “waters of the United States”: *Federal Register*, v. 80, p. 37054–37127.
- Vannote, R.L., Cummins, K.W., Minshall, G.W., Sedell, J.R., and Cedell, J.R., 1980, The River Continuum Concept: *Canadian Journal of Fisheries and Aquatic Science*, v. 37, p. 130–137.

- Ver Hoef, J.M., Peterson, E.E., Clifford, D., and Shah, R., 2014, SSN: An R package for spatial statistical modeling on stream networks: *Journal of Statistical Software*, v. 56, p. 45.
- Walsh, R., and Ward, A.S., 2019, Redefining clean water regulations reduces protections for wetlands and jurisdictional uncertainty: *Frontiers in Water*, v. 1, p. 1, doi:[10.3389/frwa.2019.00001](https://doi.org/10.3389/frwa.2019.00001).
- Ward, A.S., 2020, Climate Change Causes River Network Contraction and Disconnection in the H.J. Andrews Experimental Forest, Oregon, USA: v. 2, p. 10.
- Ward, A.S., Schmadel, N.M., and Wondzell, S.M., 2018, Simulation of dynamic expansion, contraction, and connectivity in a mountain stream network: *Advances in Water Resources*, v. 114, p. 64–82, doi:[10.1016/j.advwatres.2018.01.018](https://doi.org/10.1016/j.advwatres.2018.01.018).
- Warix, S.R., Godsey, S.E., Lohse, K.A., and Hale, R.L., 2021, Influence of groundwater and topography on stream drying in semi-arid headwater streams: *Hydrological Processes*, doi:[10.1002/hyp.14185](https://doi.org/10.1002/hyp.14185).
- Welhan, J.A., 2006, Water balance and pumping capacity of the lower portneuf river valley aquifer, Bannock County, Idaho: , p. 36.
- Wu, L.Z., Deng, H., Huang, R.Q., Zhang, L.M., Guo, X.G., and Zhou, Y., 2019, Evolution of lakes created by landslide dams and the role of dam erosion: A case study of the Jiajun landslide on the Dadu River, China: *Quaternary International*, v. 503, p. 41–50, doi:[10.1016/j.quaint.2018.08.001](https://doi.org/10.1016/j.quaint.2018.08.001).
- Zimmer, M.A. et al., 2020, Zero or not? Causes and consequences of zero-flow stream gage readings: *WIREs Water*, v. 7, doi:[10.1002/wat2.1436](https://doi.org/10.1002/wat2.1436).
- Zimmerman, D.L., and Ver Hoef, J.M., 2017, The Torgegram for Fluvial Variography: Characterizing Spatial Dependence on Stream Networks: *Journal of Computational and Graphical Statistics*, v. 26, p. 253–264, doi:[10.1080/10618600.2016.1247006](https://doi.org/10.1080/10618600.2016.1247006).
- Zipper, S.C. et al., 2021, Pervasive changes in stream intermittency across the United States: *Environmental Research Letters*, v. 16, p. 084033, doi:[10.1088/1748-9326/ac14ec](https://doi.org/10.1088/1748-9326/ac14ec).

Chapter 2. Spatial Patterns of Stream Drying in a Semi-arid Mountainous Headwater Stream: Structure and Drivers

2.1. Introduction

Streams that dry for at least part of the year are classified as non-perennial and comprise more than half of streams worldwide (Messenger et al., 2021). Like their perennial counterparts, intermittent streams play an important role as municipal water sources (Brown et al., 2008, Robinne et al., 2019, Ruhi et al., 2018), wildlife habitat (Datry et al., 2014; Katz et al. 2012; Stubbington et al. 2017), and transporters of soil, sediment, and nutrients (Belmont et al., 2011; Shumilova et al., 2019). However, unlike perennial streams, the spatial and temporal drying patterns exhibited by non-perennial streams make their corresponding environmental problems more complex. For example, the amount of dissolved organic carbon in the stream is related to the degree to which a stream dries (Hale and Godsey, 2019). Similarly, though most perennial streams are unambiguously protected by the Environmental Protection Act of 1972, the protection of non-perennial streams is much less clear (Walsh and Ward, 2019). As such, our understanding of stream processes and our ability to manage water resources depends heavily on our understanding of non-perennial streams and our ability to predict when and where streams will dry.

Models that predict stream drying have improved significantly in the last several years despite challenges such as the lack of consistency in the scales of monitoring and

the lack of consensus on the hierarchical drivers of stream drying. For example, models that predict stream permanence have increased from ~50% accuracy (Fritz et al., 2013) up to ~80% accuracy (Jaeger et al., 2019) in some places. However, these new models typically require extensive field campaigns (Botter and Durighetto, 2020; Jaeger et al., 2019; Jensen et al., 2019; Ward et al., 2018). These field campaigns could be more efficient if we better understood the spatial scales at which stream drying varies – that is, the degree to which monitoring locations are related to each other – also known as autocorrelation. Ignoring autocorrelation can lead to inappropriate statistical methods (Isaak et al., 2014), resulting in biased models that poorly predict spatial patterns in natural systems (Dale and Fortin, 2009). Additionally, an improved understanding of autocorrelation could help constrain the hierarchy of the controls of stream drying.

Despite the large number of studies that focus on the controls of stream drying (Costigan et al., 2016; Dohman et al., 2021; Hammond et al. 2021; Jaeger et al., 2019; Pate et al., 2020; Ward et al., 2018; Warix et al., 2021), we still lack consensus on the most important driver or even the number of drivers. This lack of consensus results, at least in part, from the different scales used by different studies, emphasizing different controls (Table 2.1; Costigan et al., 2016). These drivers include meteorological, land cover, and physiographic drivers that may vary in importance depending on the scale of the study.

In this study, we seek to answer the following questions: (1A) What are the spatial structures of watershed and subwatershed-scale stream drying?; (1B) What are the benefits of torsegrams vs semivariograms when modeling autocorrelation in stream drying?; (2) How accurately can we predict steam drying by taking spatial

autocorrelation into account in our models?; (3) What are the hierarchical drivers of stream drying within a watershed?; and (4) Where in a stream network should we place sensors to improve the efficiency of our characterization of stream drying? By answering these questions, we will improve our ability to efficiently monitor and accurately predict stream drying.

2.2. Site Description

We conducted this research in Gibson Jack, a watershed located in the northern Rocky Mountains in southeastern Idaho that drains an area of ~25.5 km² into the Portneuf River. We chose this site because it exhibits a wide range of drying patterns, from perennial to almost always dry. Additionally, many of the physiographic, land cover, and meteorological variables identified as potential drivers of stream drying (Costigan et al., 2016; Dohman et al., 2021; Hammond et al., 2021; Jaeger et al., 2019; Pate et al., 2020; Ward et al., 2018; Warix et al., 2021) have been mapped extensively in Gibson Jack, allowing us to use them in our models.

The elevation ranges from ~2,200 m at the highest peaks to ~1,500 m at the outlet, with steep slopes (mean ~20°) draining to the streams. Metasedimentary rocks, such as quartzite, largely underlie the northern half of the watershed and carbonates largely underlie the southern half (Rodgers and Othberg, 1999). Soils in Gibson Jack are primarily characterized as silty loams and fine sandy clay loams, many of which contain gravel (Davidson, 1977).

Vegetative cover varies with aspect: Douglas fir dominates the north-facing slopes and sagebrush, grasses, and juniper cover the south-facing slopes (Evenden et

al., 2001). The US Forest Service manages most of the north fork as a Research Natural Area, meaning that it is a quality environmental area that is managed for minimal human impact (Evenden et al., 2001). Grazing and recreation, common throughout much of the watershed, occur more in the summer than in the winter.

Typically, precipitation in Gibson Jack is limited during the summer months, when seasonal drying occurs in parts of the stream network (Hale and Godsey, 2019; Dohman et al. 2021). Winter air temperatures average below zero and snowpacks accumulate from October or November through the spring snowmelt period (typically Feb through Jun), with streams freezing at the surface or to the bed in most years (Dohman et al. 2021).

2.3. Methods

To explore spatial structure in stream drying and improve non-perennial predictive models, we deployed Stream Temperature, Intermittency, and Conductivity sensors (STICs; following Chapin et al. 2014) in Gibson Jack during two field seasons (Aug-Oct 2020 and May-Oct 2021) as described in detail in section 3.1. The sensors recorded temperature and relative electrical conductivity, the latter of which we interpreted as wet or dry observations based on differences in how well air and water can conduct electricity; the details of this interpretation are described in section 3.2. Finally, we used this data to explore spatial structure via semivariograms and torgegrams and to determine a hierarchy of steam drying drivers via random forest analysis, as described in section 3.3.

2.3.1. Field Methods

During both the 2020 and 2021 field seasons, we used Onset HOBO Pendant waterproof temperature and light sensors (Model UA-002-64) with modifications that repurpose the light-sensing capabilities to measure the relative electrical conductivity in units of lux. Our modifications follow Chapin et al. (2014) except that conductivity is measured at the bottom of the STIC rather than at the top, allowing our STICs to detect even small amounts of water in the stream bed. The ability of the sensor to collect temperature data was unchanged. Relative electrical conductivity is significantly higher in water than in air, allowing us to identify a threshold (detailed in section 3.2) such that we interpret higher values as wet and lower values as dry.

In 2020, we deployed 92 STIC sensors in Gibson Jack (Figure 2.1). We chose to use an unbalanced sampling design to ensure that we had sufficiently small spatial separation while still collecting data throughout the watershed. In each tributary, we deployed a STIC at the highest location that we thought experienced wetting in the spring of 2020 and might rewet in the fall based on three key field observations: channelization, an armored layer, and vegetation depressed in a unilateral direction (following Ferraro, 2021). We placed additional STICs at 12.5 m, 25 m, 37.5 m, 50 m, and 100 m downstream of the first STIC, so that each nest included six STICs within 100 m of one another. We then deployed additional nests of STICs 1,000 m below the 0 m location, followed by the same nested spacing pattern. Where tributary junctions resulted in overlapping downstream nests, we retained just one nest due to limitations in our total number of sensors (Figure 2.1). All STICs recorded relative electrical

conductivity at 15-minute intervals from 19 August 2020 (or earlier, in a few cases) through 17 October 2020, when we retrieved them to avoid them being encased in ice over winter.

In 2021, we placed the STICs in different locations to capture the most temporal variability in the network, based on results from 2020 and mapping by Hale and Godsey (2019). Because we again sought to capture the smallest scales of autocorrelation, we again deployed nests of STICs with spacing similar to the pattern used in 2020 except that instead of nests clustered near the top of each tributary, all nests were centered in reaches that had been observed to be both wet and dry during past observations. Again, STICs recorded relative electrical conductivity at 15-minute intervals from no later than 17 May 2021 through 16 October 2021, when we retrieved them. We added an additional 29 STICs in 2021 for a total of 121 STICs deployed throughout the watershed.

We also field mapped the absence/presence of water using 10 m resolution on August 29-30, 2020, and used these spatially continuous observations as validation of our best models. For more details about these comparisons, see section 3.3 below.

2.3.2. Interpretation of STIC Data

To interpret the relative electrical conductivity as wet or dry observations, we calibrated each STIC using four calibration standards: 84 $\mu\text{S}/\text{cm}$, 447 $\mu\text{S}/\text{cm}$, and 1,413 $\mu\text{S}/\text{cm}$, and air (assumed to be 0 $\mu\text{S}/\text{cm}$). We then fit a linear relationship between the values measured by each STIC and the calibration standards and interpreted the y-

intercept of this relationship as the threshold between wet and dry. To validate this interpretation, we compared all STIC-based inferences of wet and dry conditions to observations recorded in the field. Most of the inferred flow conditions matched our field observations (87% in 2020 and 63% in 2021); for example, if we observed a site as wet on May 17, 2021, our interpretation of STIC data also indicated the site was wet. We believe that the 2021 sites were more difficult to interpret because they transitioned between wet and dry more often than the 2020 sites did. To interpret data from the sites where flow status was incorrectly inferred at least once based on the y-intercept threshold, we examined data from each STIC individually and selected a different threshold that (A) was within one standard error of the linear calibration intercept and (B) matched the field observations. In the five cases where these criteria did not result in a clear threshold (for example, a wide range of thresholds remained acceptable or multiple thresholds were required to match field observations), we chose 1 or 2 thresholds that permitted rewetting only during storm events, but not at other times. Storm events were defined by independent precipitation data from a nearby weather station. A full list of the thresholds applied to each STIC sensor is provided in appendix 2.

We then calculated seasonal streamflow permanence at each location by dividing the number of wet measurements by the total number of measurements for the overlapping period of record for all STICs in each season (i.e., Aug-Oct 2020 and May-Oct 2021). We chose to use seasonal streamflow permanence because it represents broad drying across the season rather than focusing on specific times that may or may not represent general temporal trends. Because 94% (2020) and 59% (2021) of the

seasonal streamflow permanence values at each site were >0.9 or <0.1 (Figure 2.2), for all subsequent analyses, we treat the seasonal flow permanence data as binary. We interpreted values at or above 0.5 as 1 or “wet”, and any value less than 0.5 as 0 or “dry”.

2.3.3. Modeling

To generate predictive models of stream drying that incorporated autocorrelation, we employed the SSN package in R (Ver Hoef, 2014). In doing this, we kriged using both Cartesian and tail-up models to predict binary seasonal streamflow permanence. In the empirical toregram, we looked for two problematic characteristics: the flow-connected toregram crossing its flow-unconnected counterpart and a curve that increases without bound (Zimmerman and Ver Hoef, 2017). If observed, these characteristics would suggest that the assumption of stationarity was violated, likely because the seasonal streamflow permanence varied with other spatially distributed variables in the watershed. To correct for this potential issue, we used a variety of physiographic and land cover variables as explanatory variables in our models.

Because we were modeling binary data, we evaluated our models using confusion matrices and receiver operating characteristic (ROC) curves. We assumed the best model would have a high area under the curve (AUC) and would include only significant explanatory variables. We then compared the predictions made by our best model with field observations made throughout the watershed on August 29 and 30 of 2020.

We modeled both years' STIC data independently, and also found that the STIC locations that were wet in 2020 remained wet even under the driest conditions in 2021. With this in mind, we combined the two years of data, assuming that all 2020 sites remained either wet or dry respectively in 2021. This combined dataset allowed us to fully predict patterns throughout the watershed and enabled more accurate kriging in the most dynamic portions of the watershed. Those combined results are presented below for all analyses except for the random forest because the detailed site characterization required for this analysis was only completed in 2021.

We then compared the results from our models to the field mapping we performed on Aug 29-30, 2020. We did this twice: first with the best model using data from both years and then with a model that used only data collected on the days we had mapped the stream. In this way, we hoped to both test the accuracy of our seasonal model and give the most accurate predictions we could with the data we collected.

Finally, we assessed the hierarchical drivers of stream drying by using a classification random forest analysis (Breiman, 2001). We focused on the 2021 data set to develop the random forest due to the extensive field data collected during that year. In total, we used 17 variables in our random forest models (Table 2.2). Not all of these variables are independent of each other. Drainage area, elevation, and upstream distance are all correlated in Gibson Jack due to the mountainous nature of the watershed. Lithological variables (i.e. carbonates, colluvium, and metasedimentary rocks) are also correlated with each other, as are the soil variables (i.e. silt loam and loam). For this reason, we ran the random forest twice. The first time, we ran it with all the variables regardless of how correlated they were. After determining this preliminary

hierarchy of variables, we removed all but the most important variable in each of the correlated sets (e.g., we only used drainage area and omitted elevation and upstream distance because drainage area was the most important predictor in that group of correlated predictor variables; see Appendix 1).

2.4. Results

The seasonal streamflow permanence calculated for both years was extremely bimodal. Even in the 2021 field season, when we deployed STICs targeting the most dynamic locations, most sites were mostly wet or mostly dry. In fact, of the 121 sites studied in 2021, only 15 had streamflow permanence values between 0.25 and 0.75 (Figure 2.2) and in 2020, no sites had streamflow permanence values within this range. The observed bimodality led to challenges with kriging each year's data set individually: we found that models based only on the 2020 data struggled to classify the most dynamic reaches (Figure A2.1B). Conversely, the 2021 data produced a pure nugget, indicating that stream drying was so variable that kriging could not characterize anything beyond the areas immediately surrounding STIC locations (see appendix 2). The combined dataset avoided these problems by increasing the observations at short and moderate separation distances while still maintaining coverage throughout most of the network.

Most nests of sensors exhibited similar wet/dry behavior over the season (Figure 2.3A-C) with some notable exceptions, especially when short-term variations are considered (e.g., Figure 2.3D-E). We evaluated non-spatial as well as spatial models in both Cartesian and flow-network framework after combining the two years of data as

described in section 3.3. We first summarize the non-spatial models and then compare the two categories of spatial models. Thirteen of the models included a significant explanatory variable, but no spatial component. The best of these non-spatial models had an AUC of 85.16%, and the average AUC was only 63.99% (Table A2.8). In contrast, the spatial models all performed significantly better, with tail-up models having an average AUC of 96.65% (Table A2.8). The average AUC of spatial models was ~33% higher than the average of all non-spatial models.

The empirical torgegram clearly shows a small nugget (Figure 2.4), but the range and sill remained more difficult to accurately constrain. The flow-connected torgegram appears to plateau at a separation distance of ~200 m before continuing to rise at a separation distance of ~500 m. After another short plateau, the curve again appears to rise until ~1,000 meters at which it reaches a final plateau. Of the 83 models that included an explanatory variable intended to correct for the multiple plateaus, only 15 included variables that were significant at an alpha of 0.05. However, all but 3 of these models were non-spatial. The average nugget produced by our tail-up models was 0.005 with a standard deviation of 0.030. The average partial sill produced by these models was 1.25 with a standard deviation of 0.30. The range produced by the these models had a mean of 1,447 m, with a standard deviation of 2,388 m. Range values ranged from as low as 87 m and as high as 7,354 m (Table A2.7). We determined that our best tail-up model was the exponential model that had no explanatory variables. Though several models that included explanatory variables had higher AUCs, the explanatory variables were not significant in these models, so we excluded them. The Mariah model with no explanatory variables had a slightly higher AUC, but the range

calculated by this model did not match a visual examination of the toreggram (Figure 2.4).

Finally, we determined that the best Cartesian spatial model was the exponential model that included elevation as an explanatory variable (Figure 2.5). It included a nugget of 1.24×10^{-8} , a sill of 1.05, and range of 410 m. Like the tail-up flow-network-based exponential model, the exponential Cartesian-based model did not have the highest AUC, but those models with higher AUCs either included insignificant explanatory variables, or had ranges that did not visually match the semivariogram (Figure 2.5).

When compared to field observations made on August 29 and 30, 2020, the combined exponential tail-up flow-network-based spatial model accurately predicted 76% of all prediction locations (Figure 2.6). Mismatches mainly occurred lower in the watershed with incorrect dry predictions dominating lower in the watershed and incorrect wet predictions dominating in the tributaries. The model based only on the August observations had fairly similar overall performance, accurately predicting 78% of all prediction points. In contrast to the combined model, mismatches in August mainly occurred at intermediate locations in the watershed between the high dry STIC nests and the lower wet STIC nests.

The random forest analysis revealed that drainage area is the most important non-spatial variable for predicting stream drying with a 50% decrease in accuracy if the variable was removed (Figure 2.7). The area underlain by metasedimentary rocks and loam as well as by trees were also important variables: a ~40% decrease in accuracy

was observed if each were removed. The interquartile range of the pebble counts, geomorphic depth of the stream, and slope were the least important variables in the model; each would lead to a <5% decrease in accuracy if removed.

2.5. Discussion

To interpret our results and explore their implications, we will explore our research questions shifting from observing and modeling spatial patterns to characterizing drivers of those patterns:

2.5.1A. What spatial structures exist in stream drying at or below the watershed scale?

The flow-connected tolograms from the combined datasets had remarkably consistent nuggets and sills, regardless of shape and explanatory variable (see Table A2.7). The very small nugget indicates that we adequately measured stream drying at small enough spatial scales to characterize the spatial structure. By comparison, data from Gendaszek et al. (2020; Figure 2.8) indicated a nugget of 0.259 in their best model, a value ~50x the average nugget of 0.005 that we observed. Note that these values are unitless, but comparable because they are comparing binary flow permanence values of either 0 or 1. Similarly, the partial sill that we calculated was internally consistent among our models (Table A2.7). Our sill is also similar to the 0.898 calculated from data by Gendaszek et al. (2020; Figure 2.8).

In contrast to the consistent nugget and sill estimated by all tologram models, the estimated ranges in our models varied widely from <200 m to over 7 km (Table A2.7). Autocorrelation is thus likely at separation distances <100 meters within a stream

network whereas at larger separation distances, any autocorrelation is more complex. The variety of estimated ranges in Gibson Jack likely reflects the complex shape of the empirical torgogram (Figure 2.4). As a point of comparison, Gendaszek et al. (2020; Figure 2.6) estimated ranges of 176 m, 7,208 m, and 97,538 m, from smallest to largest, using a complex set of models. The smallest of our ranges roughly matches the smallest range found by Gendaszek et al. (2020), while the largest of our ranges roughly matched their intermediate range. Their largest range estimate reflects their decision to combine data from multiple watersheds into one stream network model; we only worked within one watershed. Future research on stream spatial structures would benefit from incorporating complex torgogram shapes into modeling packages such as the SSN R package to better identify nested ranges of stream drying. Multiple plateaus have also been observed in water quality (McGuire et al. 2014).

The scales of autocorrelation that we found suggest that policymakers and enforcers can monitor streams on the scale of 100 to 200 m. This is a conservative separation distance because it may produce data with some autocorrelation, but even our models with the smallest ranges suggest that this separation distance will capture the full spatial variability in the data.

2.5.1B. What are the benefits of torgograms vs. semivariograms when modeling autocorrelation in stream drying?

The best Cartesian and tail-up models performed very similarly to each other. Specifically, the best models produced ranges that are almost identical to each other. We hypothesize that elevation, which is an explanatory variable in the best Cartesian

model, but not in the best tail-up model, can act as a proxy for stream distance in a semivariogram..

The observed equivalence between the Cartesian and tail-up models in a mountainous watershed such as Gibson Jack may not be transferable to other watersheds where physical site characteristics may not serve as a strong proxy for stream distance like they do in Gibson Jack. For example, watersheds with a higher drainage density in Cartesian space may find tail-up models more useful than their Cartesian counterparts. Future research will need to be done in different watersheds to explore the differences between these two model types.

2.5.2. How accurately can we predict the metrics of intermittency by taking autocorrelation into account in our models?

The spatial models were a vast improvement over their nonspatial counterparts, suggesting that there is indeed spatial structure in stream drying that should guide monitoring and predictions of flow absence/presence. However, our predictions leave room for improvement: we noticed that some of our prediction errors resulted from a surprising mismatch between the DEM-derived geomorphic channel network and the actual channel network. We corrected the network in a few locations where STICs were located. However, at some tributary junctions, we noticed that expected tributaries were subtle or did not appear to have incised geomorphic channels at all. During the mapping on 29-30 August, there was no observed flow in these tributaries, and because the goal of that effort was not to map the geomorphic network extent, we did not carefully assess whether these tributaries should be considered part of the channel network at all. Thus,

we believe that we could improve our model by manually mapping the extent of the channel network rather than relying on DEM-derived network calculations. This high-accuracy channel mapping effort would be difficult, but valuable. In general, we believe that work that relies solely on DEM-derived channels, especially in carbonate terrain, should be carefully reviewed.

We also want to discuss a possibly confusing modeling result. Most sites were either flowing or dry >90% of the time and our overall model performed well (AUC>95% with 80-100% accuracy of predictions at STIC locations). However, when comparing seasonal flow predictions against observations on 29-30 Aug 2020, our model accuracy decreased to ~76%. When we used data from only the days on which we made the mapping observations, our model improved slightly to ~78% because 23 (10%) of the sites exhibited different behavior on those dates than during the full season. This increase in accuracy was mostly seen lower in the watershed along the mainstem. The accuracy of our spatial models roughly matches that of the PROSPER model (Jaeger et al., 2019), and requires only flow observation data at some locations to generate accurate flow maps throughout a watershed, potentially simplifying the model development process and allowing policymakers/enforcers to implement it easier. A large part of the inaccuracy of the Aug 2020 model (Figure 2.6B) is due to false wet predictions in tributaries that have never been observed to be flowing during the entire field campaign; as we noted above, these tributaries deserve careful geomorphic channel mapping to ensure that they are accurately represented rather than assuming the DEM-derived channel network is correct

2.5.3. What are the hierarchical drivers of stream drying within a watershed?

The results from our random forest analysis differ from others' findings (e.g., Hammond et al, 2021, Price et al., 2020, and Jaeger et al, 2019; Table 2.1) that suggest land cover variables such as vegetation type are more important than physiographic variables such as topography and lithology. Curiously, our hierarchy of drivers of drying in Gibson Jack is somewhat similar to the hierarchy of drivers of regional trends in drying (Zipper et al., 2020): they reported that topography was the second most important driver of trends in stream drying after meteorological variables. Although Pate et al. (2020) also found that topography was an important driver of drying, some of their top drivers were unimportant at Gibson Jack. We did not have data to explore all of the drivers in Gibson Jack that have been identified as important in other studies (e.g., we did not have a model of winter precipitation at all STIC locations), but we still included most of them. We also note that Costigan et al. (2016) suggest a variety of drivers that we were unable to explore in this study, including many meteorological variables. Like many others, we assumed that these meteorological variables would not vary widely at the relatively small spatial scales of a watershed, but future models could potentially explicitly test this assumption by incorporating these variables.

We hypothesize that the differences between these studies result from two major differences relating to the scale of observation and the questions being asked. First, different spatial and temporal scales seem to emphasize different controls. At larger scales, especially larger spatial extents, studies generally emphasize differences

between watersheds whereas the study we performed in Gibson Jack focused exclusively on variations within a watershed. This dependence on scale seems to apply to temporal scales as well. Thus, studies comparing results at different time scales (at the same sites) can produce different hierarchies of controls. The apparently nested torgegram that we produced (Figure 2.4) suggests distinct relationships at different spatial scales: each plateau may reflect a different dominant driver, though more research is needed to confirm this hypothesis and to confirm the dominant driver at each plateau. Furthermore, stream drying on the subwatershed scale may not have a uniform hierarchy of drivers. For example, implicit in the work of Pate et al. (2020) is the assumption that four watersheds in northern California would have similar hierarchies. If this assumption is false, then drivers may reflect differences between watersheds rather than differences between perennial and non-perennial streams. In this study, we made a similar assumption that the hierarchy was consistent across the watershed. If hierarchies vary with scale, including within relatively small spatial extents, then further improvements in predictions of stream drying may rely largely on thoughtful sample design: deciding when, where, and how to make presence/absence observations is non-trivial, and we devote section 5.4 to our recommendations on that front.

The second major reason that these studies may identify different dominant drivers of drying is that different studies ask different questions that rely on different metrics. For example, Zipper et al. (2021) were interested in changes in stream drying patterns over decades, so they used a random forest to predict *trends* in seasonal streamflow permanence rather than seasonal streamflow permanence itself like Hammond et al. (2021) uses. Similarly, both of these studies were interested in trends

across the entire United States, while Pate et al. (2020) and Jaeger et al. (2019) were only interested in regions of the United States. The spatial extent chosen by each of these studies reflects the questions they were asking.

2.5.4. Where in a stream network should we place sensors to improve the efficiency of our monitoring campaign?

The locations of sensors undoubtedly affected the results of this study and others like it. Although the unbalanced sampling design that we employed allowed us to create a toregogram in 2020, the data we collected that year greatly underutilized the potential that STICs have to provide near-continuous temporal data. Instead, we collected extremely consistent “wet” or “dry” data from perennial or ephemeral sites, respectively. In 2021, we sought to better leverage the sensors by deploying STICs only in locations where we had previously observed both wet and dry conditions with the intention of observing the most dynamic changes in streamflow permanence throughout the network. However, perhaps in part because Gibson Jack experienced extreme drought in 2021, many of the sites that we instrumented still remained dry for much of the season. Furthermore, the data from these most dynamic reaches did not represent the watershed as a whole. By combining our 2020 and 2021 data, we essentially created a stratified sampling design where we focused on the driest sites, the wettest sites, and the most dynamic sites. We recommend that future studies combine STICs with carefully timed manual flow mapping that includes both high- and low-flow conditions. In this way, researchers can prioritize STIC placement in the most dynamic locations, where more frequent observations would complement periodic field mapping efforts during both wet and dry conditions. Though predicting the most dynamic locations

before a field season is difficult, failing to do so will result in inefficient sampling, which should be avoided when possible. To avoid missing the most dynamic locations, we also recommend that researchers deploy additional sensors some distance above and below the predicted dynamic locations. If mapping is not possible prior to STIC deployment, then separation distances of ~15-200 m with coverage throughout a watershed may lead to the most efficient sensor deployment if the network extent is not too large. Our STIC data reveals that repeated mapping may lead to pseudoreplication errors: mapping may appear to generate independent observations, but if conditions are stable, such observations may just be repeated mapping of the same flow condition.

2.6. Conclusion

In this study, we found that unbalanced sampling designs enable us to create a torgegram of stream drying which we used to explore the spatial structure of stream drying in Gibson Jack, a catchment in the northern Rockies, USA. We found that a variety of models resulted in similar values for the nugget and sill, but that the range varied by up to several kilometers based on shape of the model and the explanatory variable included in the model. The best-fit model suggested that autocorrelation was likely at separation distances of ~400 m. Overall, we found that spatial models predicted stream drying much better than their non-spatial counterparts, improving predictions by more than 30%. This suggests that autocorrelation is an important quality to consider when monitoring and predicting stream drying.

A random forest analysis performed on our data found that topography, lithology, vegetation, and soil type were the most important variables in predicting stream drying.

Future studies could improve the accuracy of these predictions by including additional variables, specifically meteorological variables, and by conducting field mapping of the river corridor rather than using a DEM to calculate it.

2.7. Figures

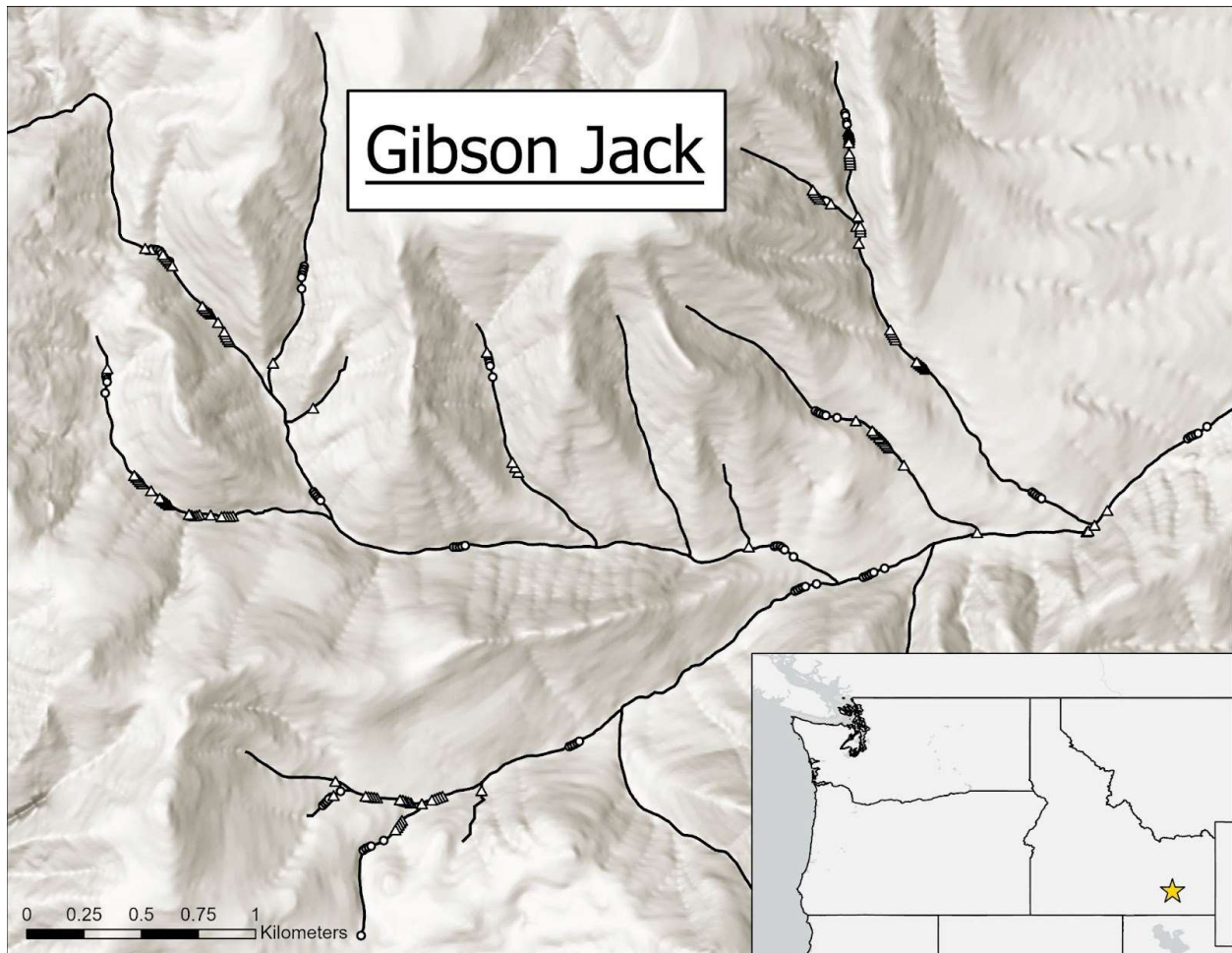


Figure 2. 1: Map of the Gibson Jack watershed located in southwestern Idaho. The map shows the locations of the STICs deployed from August 2020 to October 2020 as circles and STICs deployed from May 2021 to October 2021 as triangles. Some symbols appear filled because of dense placement of nests.

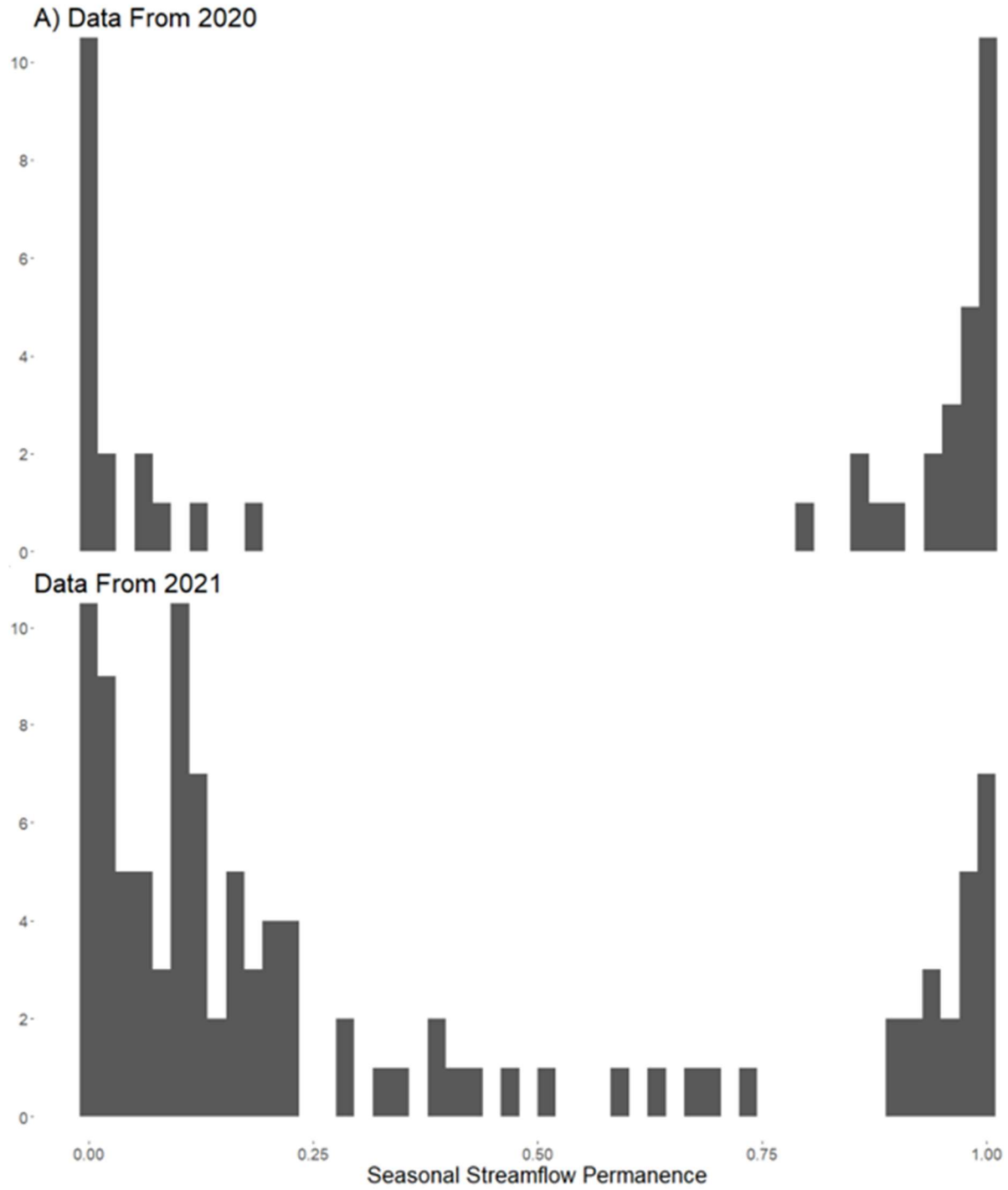
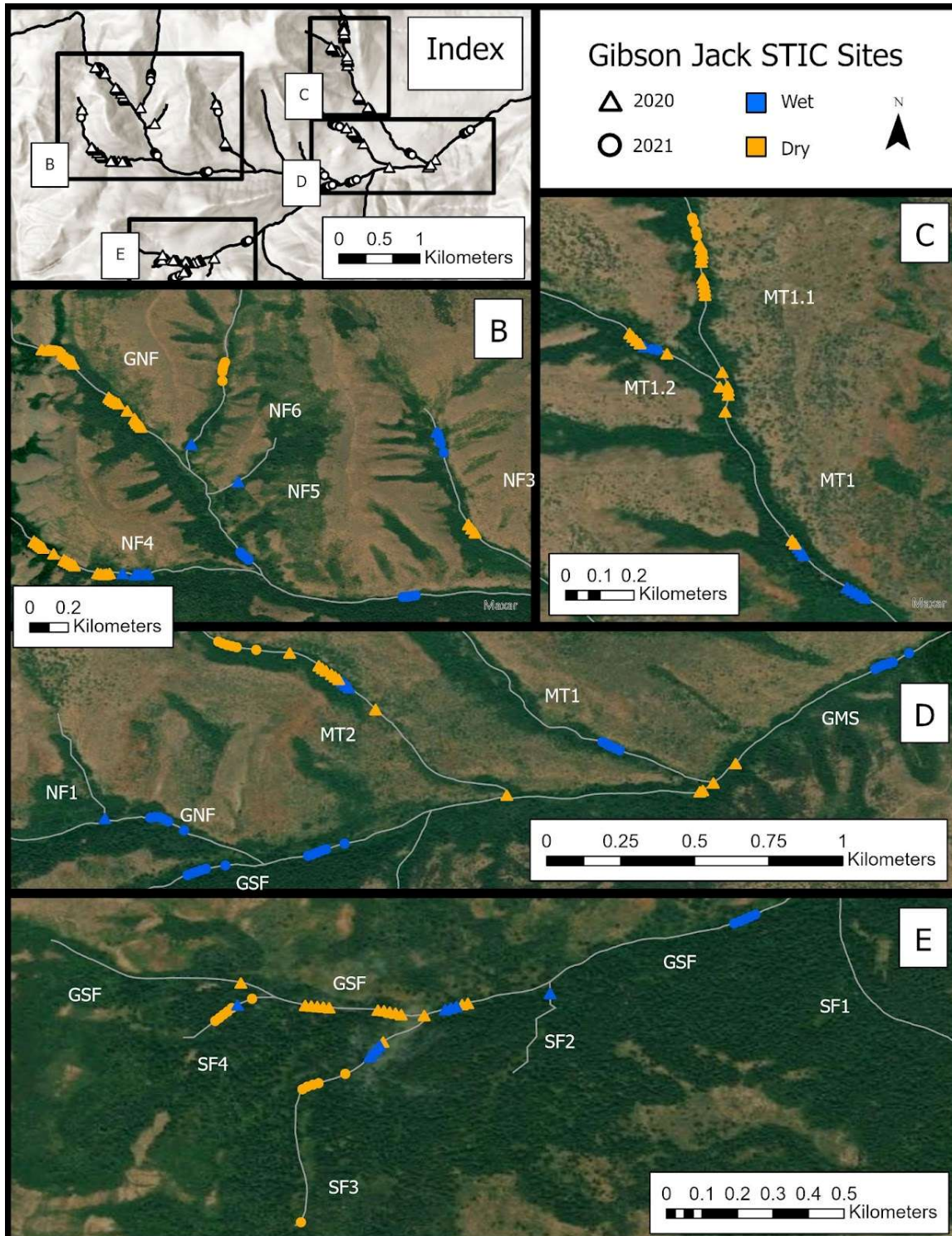
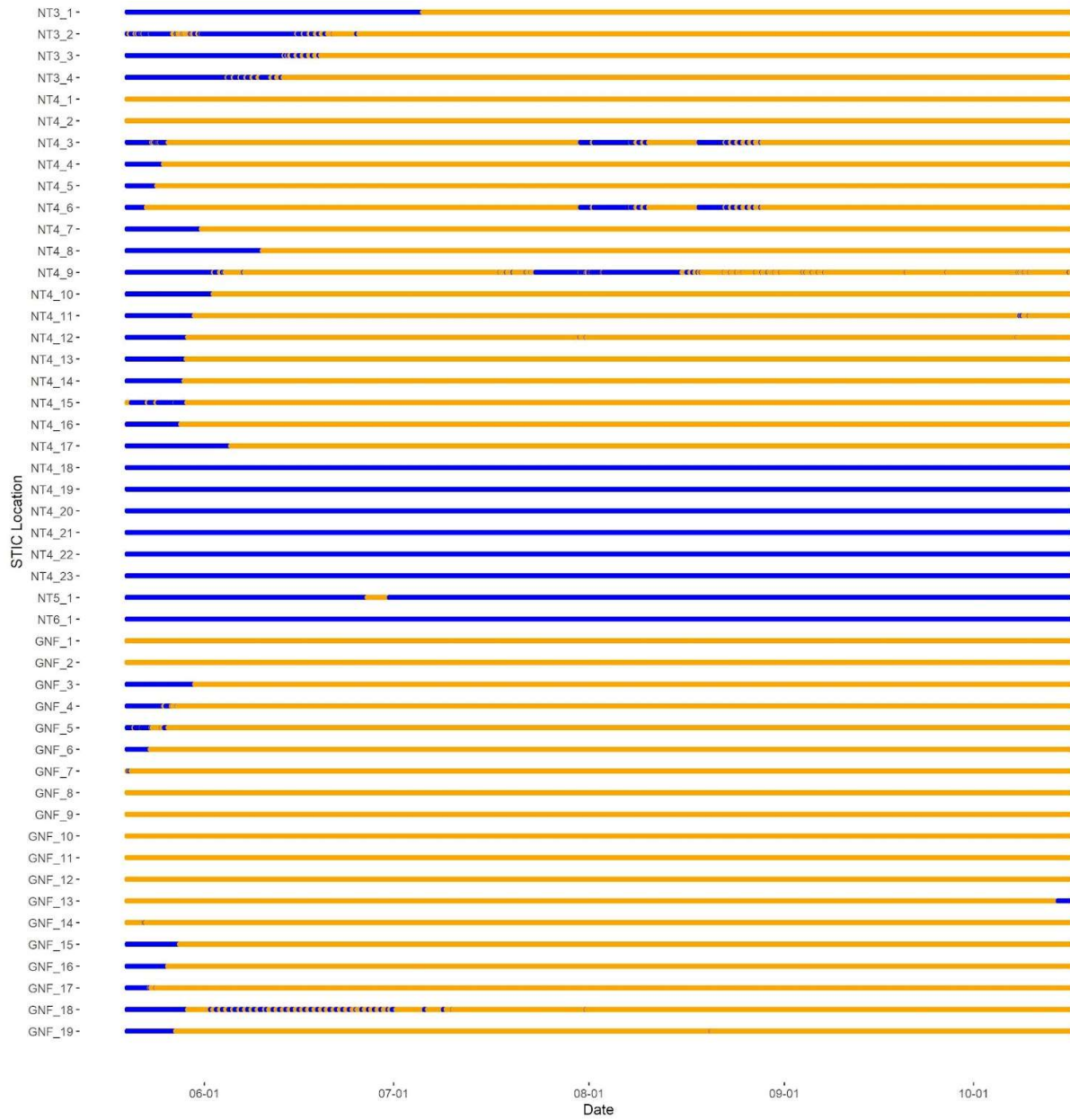


Figure 2. 2: Histograms showing the distribution of seasonal streamflow permanence values in 2020 (A) and 2021 (B). Because the data from both years was bimodal, all subsequent analyses assume binomial data (wet > 0.5 and dry < 0.5).

A



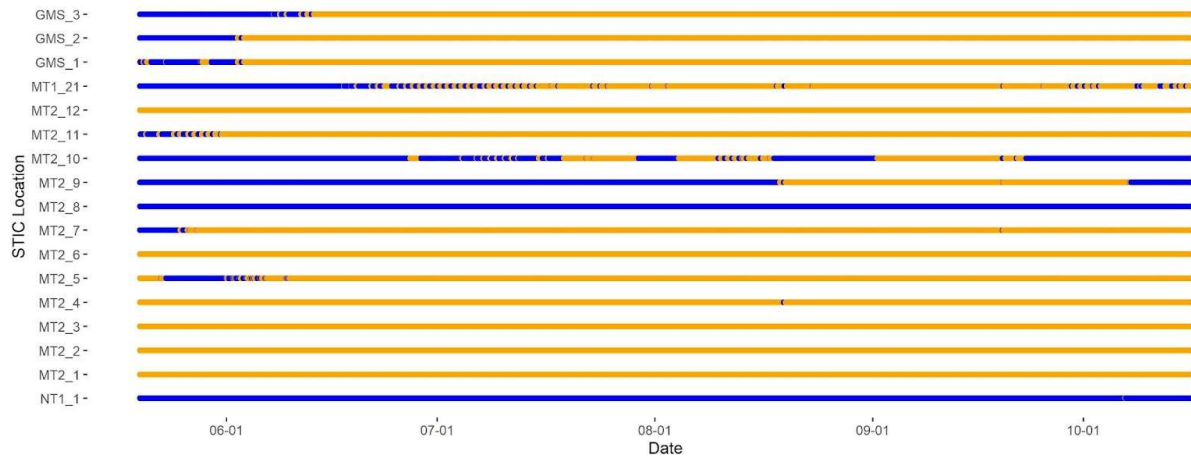
B



C



D



E

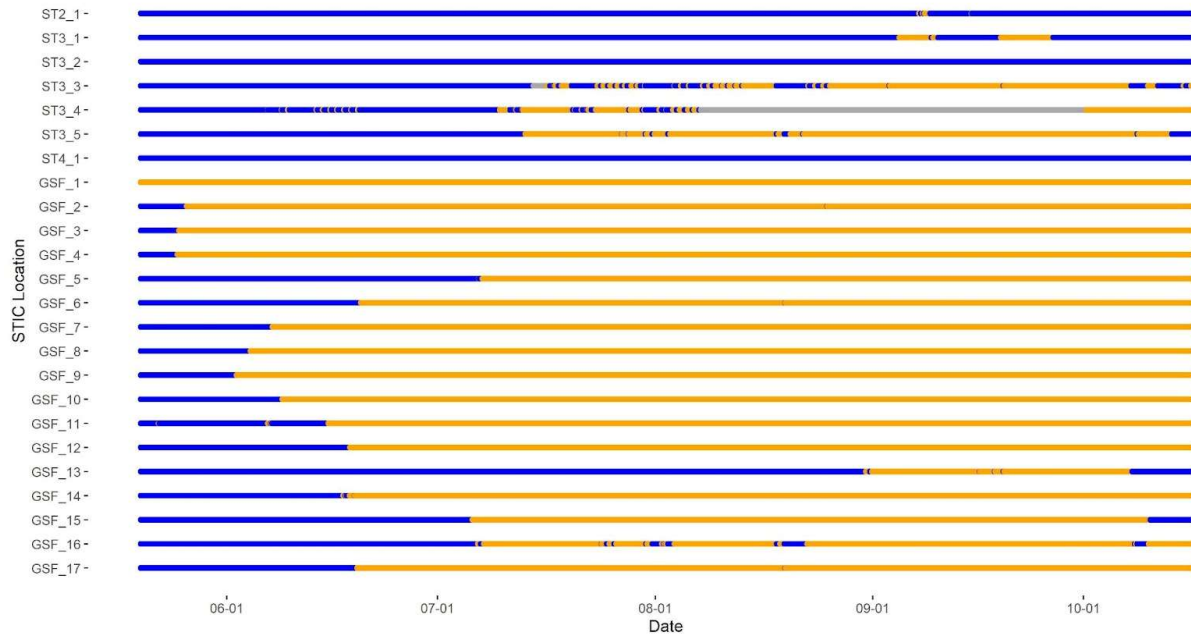


Figure 2. 3: (A) Map showing the sites where STICs were deployed in both 2020 and 2021. The accompanying charts (B-E) summarize data collected from the 2021 sites. At most sites, STICs reported mostly wet or dry conditions over the course of the study. For this reason, we interpreted our seasonal streamflow permanence as either predominantly wet (1) or dry (0). The 2020 data can be found in Appendix 2.

Empirical Torgegram of Binary Stream Drying

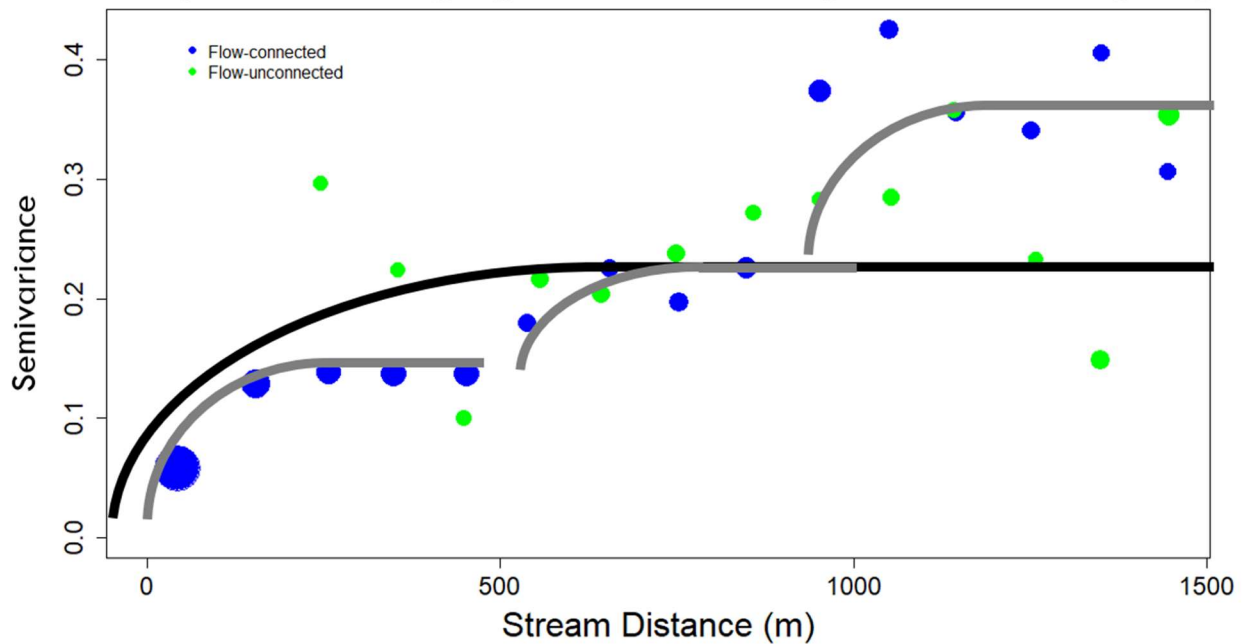


Figure 2. 4: Empirical torgegram of combined 2020 and 2021 data. The empirical torgegram shows three plateaus in grey: one at a range of ~100 m, one at a range of ~500 m, and a final one at a range of ~1,000 m. This was modeled as shown in black using an exponential tail-up model. These three plateaus may drive the variety of ranges across the different models.

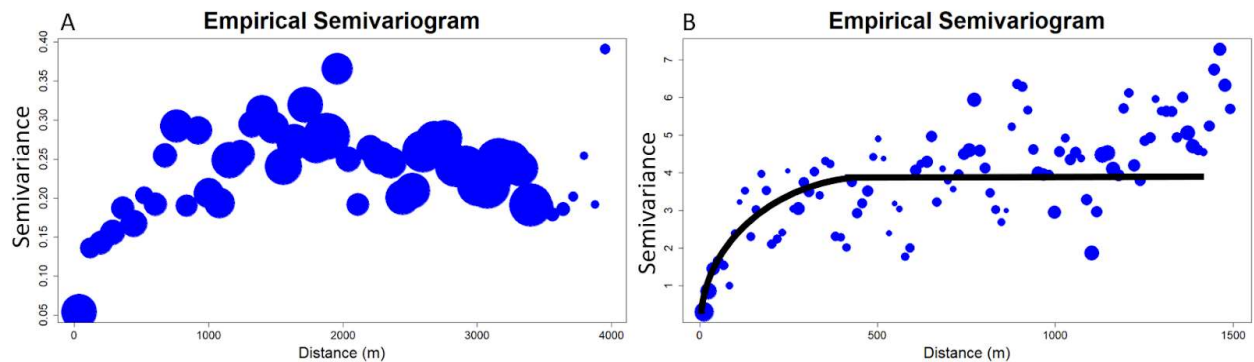


Figure 2. 5: Empirical semivariogram of combined 2020 and 2021 data (A) and the semivariogram produced by the best model in black (B). The best Cartesian spatial model, which used an exponential shape and elevation as an explanatory variable reveals a range of ~400 m, very similar to the range produced by the best tail-up stream-network spatial model.

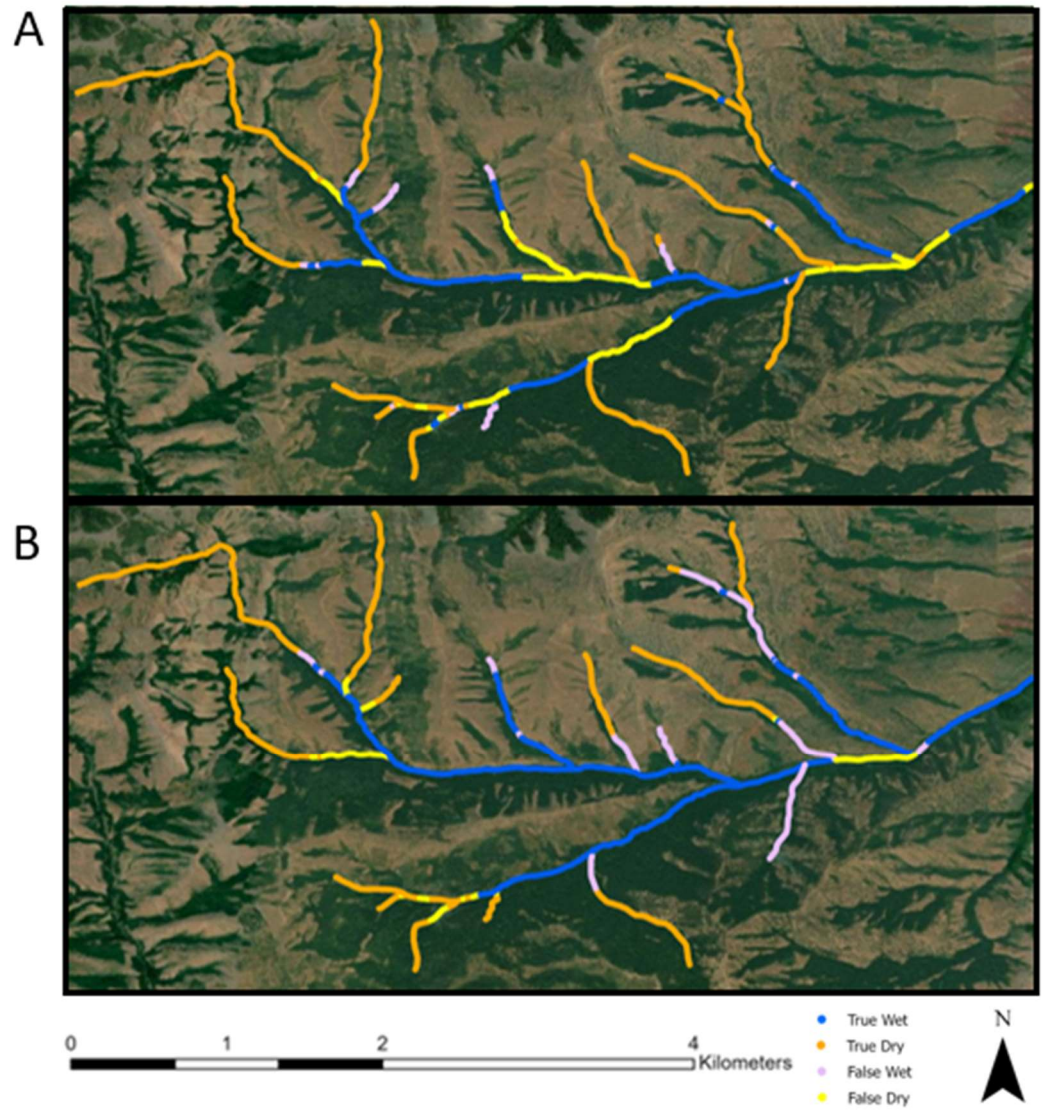


Figure 2. 6: Predictions of seasonal streamflow permanence made by comparing our best models with field observations made Aug 29-30, 2020. The combined model (A) accurately predicted flow presence for 76% of all mapped sites on these days. Conversely, the 2020 model (B) accurately predicted flow presence for 78% of all mapped sites on these days.

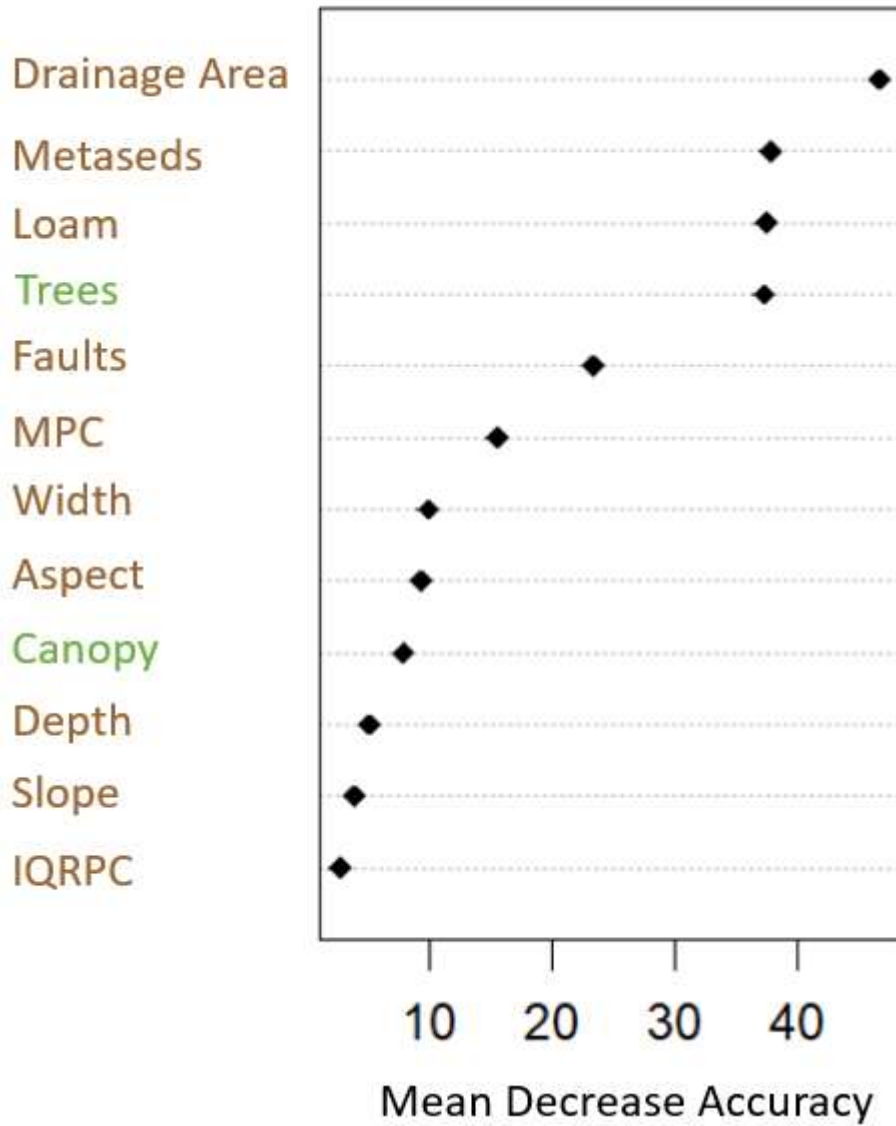


Figure 2. 7: Results from the random forest analysis reveal that drainage area, metasedimentary rocks, loam, and tree cover are the most important variables driving stream drying. Omission of any of these variables leads to a mean decrease in accuracy of the model prediction of over 30%. Variables are colored based on whether they predominantly reflect physiographic (brown) or land-cover (green) conditions.

Empirical Torgegram of Binary Stream Drying

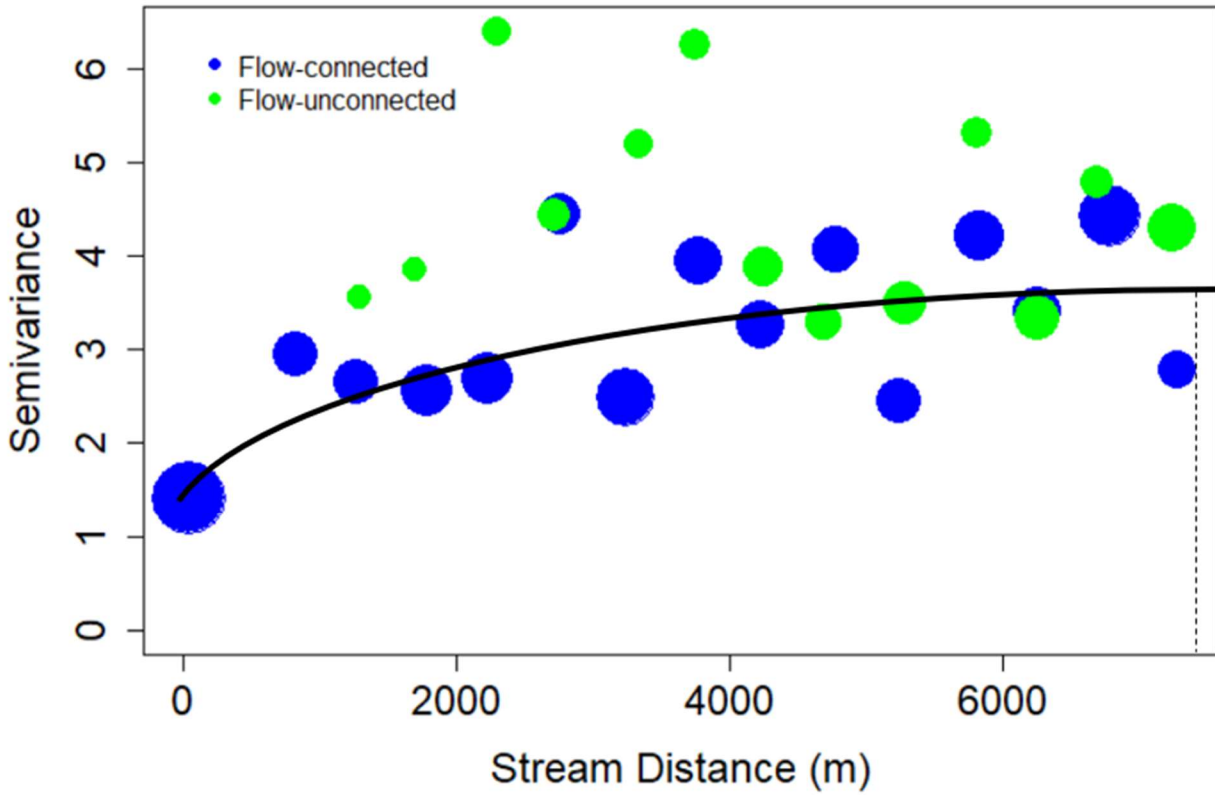


Figure 2. 8: Torgegram calculated from the work of Gendaszek et al. (2020) indicating an intermediate nugget of 7,208 m. This roughly matches the maximum range that our models calculated.

2.8. Tables

Table 2.1: Summary of literature on hierarchical drivers of stream drying. Colors correspond to the groups of variables established by Costigan et al. (2016): blue for meteorological, green for land cover, and brown for physiographic.

Metric predicted by Random	Streamflow Permanence	Streamflow Permanence Trends	Drying Classification*	Streamflow Permanence	Stream Permanence Probability	Absence/ Presence observation
Spatial Extent	Continent	Continent	Continent	Mountain West Region	Pacific NW Region	Four Watersheds
Spatial Grain	Watershed	Watershed	Watershed	Watershed	Reach (30m)	Reach (6m)
Temporal Extent	>10 years	>20 years	>10 years	>10 years	1977-2016	Jun-Sep 2018
Temporal Resolution	Daily	Daily	Daily	Daily	15 min	1+ per season
Question	What drives stream drying across the US?	What drives changes in stream drying across the US?	What stream drying characteristics differentiate watersheds?	What drives stream drying in the mountain west?	How well can we predict stream drying in the Pacific Northwest?	What drives stream drying in four watersheds in mountainous California?
Sample Size	540 stream gauges	540 stream gauges	894 stream gauges	40 stream gauges	24316 observations	101 stream; 10 sites per stream
1st	Aridity**	Previous Year's Aridity**	Grassland	Forest***	Precipitation	Grain size: 50th percentile
2nd	Impervious***	Drainage Area	Wetland	Human Water Use	Minimum Temperature	Winter Precipitation
3rd	Cultivated***	Current Year's Aridity**	Elevation	Snow and Ice	Forest***	Drainage Area
4th	Seasonal Precipitation	Bedrock Depth	Percent Snow	Slope	Percent Baseflow in flow	Grain size: 16th percentile
Study	Hammond et al., 2021	Zipper et al., 2020	Price et al., 2020	Hammond et al., 2021	Jaeger et al., 2019	Pate et al., 2020

*Classifications based on peak-to-no-flow duration, drying rate, no flow duration, and antecedent peak quantile.

**Aridity is defined as Precipitation/Potential Evapotranspiration.

***As percent of drainage area.

Table 2.2. Variables used in the random forest analysis.

Name	Units	Alias
Drainage Area	m ²	Drainage Area
Carbonates	percent	Carbonates
Colluvium	percent	Colluvium
Metasedimentary Rocks	percent	Metaseds
Loamy Soils	percent	Loam
Silt Loam Soils	percent	Silt Loam
Tree Cover	percent	Trees
Slope	degrees	Slope
Aspect	degrees	Aspect
Elevation	ft	Elevation
Upstream Distance	m	Upstream Distance
Median of Pebble Count	cm	MPC
Interquartile Range of Pebble Count	cm	IQRPC
Geomorphic Depth	cm	Depth
Geomorphic Width	cm	Width
Percent Canopy Cover	percent	Canopy Cover
Faults Crossing the Stream	count	Faults

Explanatory Variable	Shape	AUC	False Positive	False Negative	Partial Sill	Range (m)	Nugget	Sig of 1 st Variable	Sig of 2 nd Variable
Metaseds	Exponential	98.01	8	6	1.10	469	6.86E-09	0.139	NA
Trees	Exponential	97.82	8	6	1.10	455	1.82E-08	0.123	NA
Metaseds	Mariah	97.54	7	9	1.12	6460	6.21E-09	0.759	NA
Trees	Mariah	97.47	7	8	1.13	6479	1.86E-08	0.600	NA
1	Spherical	97.43	11	4	13.27	3089	1.82E-02	NA	NA
1	Cauchy	97.33	8	6	0.84	116	5.25E-02	NA	NA
Elevation	Exponential	97.23	9	6	1.05	410	1.24E-08	0.044	NA
1	Mariah	97.21	7	9	1.10	6231	1.10E-08	NA	NA
1	Exponential	97.03	8	7	1.02	431	1.30E-08	NA	NA
Elevation	Mariah	96.97	8	6	1.16	6145	3.96E-08	0.056	NA
Elevation	NULL	77.80	19	38	1.02	NA	NA	0.000	NA
Trees	NULL	57.60	9	64	1.01	NA	NA	0.003	NA
Metaseds	NULL	52.61	0	83	1.01	NA	NA	0.031	NA

Notes: Colors correspond with model type: Orange for Cartesian, blue for tail up, and grey for non-spatial. NA indicates not applicable.

2.9. Works Cited

- Belmont, P. et al., 2011, Large Shift in Source of Fine Sediment in the Upper Mississippi River: *Environmental Science & Technology*, v. 45, p. 8804–8810, doi:[10.1021/es2019109](https://doi.org/10.1021/es2019109).
- Botter, G., and Durighetto, N., 2020, The stream length duration curve: A tool for characterizing the time variability of the flowing stream length: *Water Resources Research*, v. 56, doi:[10.1029/2020WR027282](https://doi.org/10.1029/2020WR027282).
- Breiman, L., 2001, Random forests: *Machine learning*, v. 45, p. 5–32.
- Brown, T.C., Hobbins, M.T., and Ramirez, J.A., 2008, Spatial distribution of water supply in the coterminous united states: *JAWRA Journal of the American Water Resources Association*, v. 44, p. 1474–1487, doi:[10.1111/j.1752-1688.2008.00252.x](https://doi.org/10.1111/j.1752-1688.2008.00252.x).
- Chapin, T.P., Todd, A.S., and Zeigler, M.P., 2014, Robust, low-cost data loggers for stream temperature, flow intermittency, and relative conductivity monitoring: *Water Resources Research*, v. 50, p. 6542–6548, doi:[10.1002/2013WR015158](https://doi.org/10.1002/2013WR015158).
- Costigan, K.H., Jaeger, K.L., Goss, C.W., Fritz, K.M., and Goebel, P.C., 2016, Understanding controls on flow permanence in intermittent rivers to aid ecological research: integrating meteorology, geology and land cover: *Integrating science to understand flow Intermittence: Ecohydrology*, v. 9, p. 1141–1153, doi:[10.1002/eco.1712](https://doi.org/10.1002/eco.1712).
- Dale, M.R.T., and Fortin, M.-J., 2009, Spatial autocorrelation and statistical tests: Some solutions: *Journal of Agricultural, Biological, and Environmental Statistics*, v. 14, p. 188–206, doi:[10.1198/jabes.2009.0012](https://doi.org/10.1198/jabes.2009.0012).
- Datry, T., Larned, S.T., and Tockner, K., 2014, Intermittent rivers: A challenge for freshwater ecology: *BioScience*, v. 64, p. 229–235, doi:[10.1093/biosci/bit027](https://doi.org/10.1093/biosci/bit027).
- Davidson, 1977, Soils and geology of the west fork mink Creek and Gibson Jack creeks: Caribou national forest open-file report 2540:
- Dohman, J.M., Godsey, S.E., and Hale, R.L., 2021, Three-dimensional subsurface flow path controls on flow permanence: *Water Resources Research*, v. 57, p. 10.
- Evenden, A.G., Moeur, M., Shelly, J.S., Kimball, S.F., and Wellner, C.A., 2001, Research natural areas on national forest system lands in Idaho, Montana, Nevada, Utah, and Western Wyoming: A guidebook for scientists, managers, and educators: U.S. Department of Agriculture, Forest Service, Rocky Mountain Research Station RMRS-GTR-69, RMRS-GTR-69 p., doi:[10.2737/RMRS-GTR-69](https://doi.org/10.2737/RMRS-GTR-69).
- Ferraro, M.J., 2021, Patterns in Headwater Stream in the Northern Rocky Mountains, Idaho, USA [MS thesis]: Idaho State university, 205 p.

- Fritz, K.M., Hagenbuch, E., D'Amico, E., Reif, M., Wigington, P.J., Leibowitz, S.G., Comeleo, R.L., Ebersole, J.L., and Nadeau, T.-L., 2013, Comparing the extent and permanence of headwater streams from two field surveys to values from hydrographic databases and maps: *JAWRA Journal of the American Water Resources Association*, v. 49, p. 867–882, doi:[10.1111/jawr.12040](https://doi.org/10.1111/jawr.12040).
- Gendaszek, A.S., Dunham, J.B., Torgersen, C.E., Hockman-Wert, D.P., Heck, M.P., Thorson, J., Mintz, J., and Allai, T., 2020, Land-Cover and Climatic Controls on Water Temperature, Flow Permanence, and Fragmentation of Great Basin Stream Networks: *Water*, v. 12, p. 1962, doi:[10.3390/w12071962](https://doi.org/10.3390/w12071962).
- Hale, R.L., and Godsey, S.E., 2019, Dynamic stream network intermittence explains emergent dissolved organic carbon chemostasis in headwaters: *Hydrological Processes*, p. hyp.13455, doi:[10.1002/hyp.13455](https://doi.org/10.1002/hyp.13455).
- Hammond, J.C. et al., 2021, Spatial patterns and drivers of nonperennial flow regimes in the contiguous United States: *Geophysical Research Letters*, v. 48, doi:[10.1029/2020GL090794](https://doi.org/10.1029/2020GL090794).
- Isaak, D.J. et al., 2014, Applications of spatial statistical network models to stream data: *Spatial statistical network models for stream data: Wiley Interdisciplinary Reviews: Water*, v. 1, p. 277–294, doi:[10.1002/wat2.1023](https://doi.org/10.1002/wat2.1023).
- Jaeger, K.L., Sando, R., McShane, R.R., Dunham, J.B., Hockman-Wert, D.P., Kaiser, K.E., Hafen, K., Risley, J.C., and Blasch, K.W., 2019, PRObability of Streamflow PERmanence Model (PROSPER): A spatially continuous model of annual streamflow permanence throughout the Pacific Northwest: *Journal of Hydrology X*, v. 2, p. 100005, doi:[10.1016/j.hydroa.2018.100005](https://doi.org/10.1016/j.hydroa.2018.100005).
- Jensen, C.K., McGuire, K.J., McLaughlin, D.L., and Scott, D.T., 2019, Quantifying spatiotemporal variation in headwater stream length using flow intermittency sensors: *Environmental Monitoring and Assessment*, v. 191, p. 226, doi:[10.1007/s10661-019-7373-8](https://doi.org/10.1007/s10661-019-7373-8).
- Katz, G.L., Denslow, M.W., and Stromberg, J.C., 2012, The Goldilocks effect: intermittent streams sustain more plant species than those with perennial or ephemeral flow: *Desert riparian diversity: Freshwater Biology*, v. 57, p. 467–480, doi:[10.1111/j.1365-2427.2011.02714.x](https://doi.org/10.1111/j.1365-2427.2011.02714.x).
- McGuire, K.J., Torgersen, C.E., Likens, G.E., Buso, D.C., Lowe, W.H., and Bailey, S.W., 2014, Network analysis reveals multiscale controls on streamwater chemistry: *Proceedings of the National Academy of Sciences*, v. 111, p. 7030–7035, doi:[10.1073/pnas.1404820111](https://doi.org/10.1073/pnas.1404820111).
- Messenger, M.L., Lehner, B., Cockburn, C., Lamouroux, N., Pella, H., Snelder, T., Tockner, K., Trautmann, T., Watt, C., and Datry, T., 2021, Global prevalence of non-perennial rivers and streams: *Nature*, v. 594, p. 391–397, doi:[10.1038/s41586-021-03565-5](https://doi.org/10.1038/s41586-021-03565-5).

- Pate, A.A., Segura, C., and Bladon, K.D., 2020, Streamflow permanence in headwater streams across four geomorphic provinces in Northern California: *Hydrological Processes*, p. hyp.13889, doi:[10.1002/hyp.13889](https://doi.org/10.1002/hyp.13889).
- Price, A.N., Jones, C.N., Hammond, J.C., Zimmer, M.A., and Zipper, S.C., 2021, The drying regimes of non-perennial rivers and streams: *Geophysical Research Letters*, v. 48.
- Robinne, F.-N., Bladon, K.D., Silins, U., Emelko, M.B., Flannigan, M.D., Parisien, M.-A., Wang, X., Kienzle, S.W., and Dupont, D.P., 2019, A regional-scale index for assessing the exposure of drinking-water sources to wildfires: *Forests*, v. 10, p. 384, doi:[10.3390/f10050384](https://doi.org/10.3390/f10050384).
- Rodgers, D.W., and Othberg, K.L., 1999, Geologic map of the Pocatello south quadrangle, Bannock and Power counties, Idaho: Idaho Geologic Survey Geologic map.
- Ruhi, A., Messenger, M.L., and Olden, J.D., 2018, Tracking the pulse of the Earth's fresh waters: *Nature Sustainability*, v. 1, p. 198–203, doi:[10.1038/s41893-018-0047-7](https://doi.org/10.1038/s41893-018-0047-7).
- Shumilova, O. et al., 2019, Simulating rewetting events in intermittent rivers and ephemeral streams: A global analysis of leached nutrients and organic matter: *Global Change Biology*, v. 25, p. 1591–1611, doi:[10.1111/gcb.14537](https://doi.org/10.1111/gcb.14537).
- Stubbington, R., England, J., Wood, P.J., and Sefton, C.E.M., 2017, Temporary streams in temperate zones: recognizing, monitoring and restoring transitional aquatic-terrestrial ecosystems: *Temporary streams in temperate zones: Wiley Interdisciplinary Reviews: Water*, v. 4, p. e1223, doi:[10.1002/wat2.1223](https://doi.org/10.1002/wat2.1223).
- Ver Hoef, J.M., Peterson, E.E., Clifford, D., and Shah, R., 2014, SSN: An R package for spatial statistical modeling on stream networks: *Journal of Statistical Software*, v. 56, p. 45.
- Walsh, R., and Ward, A.S., 2019, Redefining clean water regulations reduces protections for wetlands and jurisdictional uncertainty: *Frontiers in Water*, v. 1, p. 1, doi:[10.3389/frwa.2019.00001](https://doi.org/10.3389/frwa.2019.00001).
- Ward, A.S., Schmadel, N.M., and Wondzell, S.M., 2018, Simulation of dynamic expansion, contraction, and connectivity in a mountain stream network: *Advances in Water Resources*, v. 114, p. 64–82, doi:[10.1016/j.advwatres.2018.01.018](https://doi.org/10.1016/j.advwatres.2018.01.018).
- Warix, S.R., Godsey, S.E., Lohse, K.A., and Hale, R.L., 2021, Influence of groundwater and topography on stream drying in semi-arid headwater streams: *Hydrological Processes*, doi:[10.1002/hyp.14185](https://doi.org/10.1002/hyp.14185).
- Zimmerman, D.L., and Ver Hoef, J.M., 2017, The Torgegram for Fluvial Variography: Characterizing Spatial Dependence on Stream Networks: *Journal of Computational and Graphical Statistics*, v. 26, p. 253–264, doi:[10.1080/10618600.2016.1247006](https://doi.org/10.1080/10618600.2016.1247006).

Zipper, S.C. et al., 2021, Pervasive changes in stream intermittency across the United States: Environmental Research Letters, v. 16, p. 084033, doi:[10.1088/1748-9326/ac14ec](https://doi.org/10.1088/1748-9326/ac14ec).

Chapter 3: Temporal Patterns: Drying, Wetting, and Cycling

3.1. Introduction

Given enough time, even characteristics that we take for granted can change drastically. One such characteristic is the presence or absence of water in a streambed, which can vary over surprisingly short periods of time. Streams that dry up for at least part of the year are classified as non-perennial and comprise more than half of streams worldwide (Messenger et al., 2021). Though drying is ubiquitous, studies of its duration and frequency typically rely on compilations of daily flow (e.g., Hammond et al. 2020; Price et al. 2020) that can be used to understand seasonal and multi-year drying. In addition, a handful of studies use observations of sub-daily drying and rewetting (e.g., Warix et al. 2020).

Drying and rewetting of non-perennial streams across multiple temporal scales can influence municipal water sources (Brown et al., 2008, Robinne et al., 2019, Ruhi et al., 2018), wildlife habitats (Darty et al., 2014; Katz et al. 2012; Stubbington et al. 2017), and soil, sediment, and nutrient transport (Belmont et al., 2011; Shumilova et al., 2019). For example, non-perennial streams exhibit higher biodiversity than their perennial counterparts because they go through wet and dry phases (Darty et al., 2014; Allen et al., 2013). This is especially true for microbial communities that may be able to establish themselves in a matter of days and then persist until conditions change again (Battin et al., 2003).

The wet/dry cycles characteristic of non-perennial streams can lead to higher concentrations of nutrients than their perennial counterparts. Dry periods allow organic material to build up in the streambed (Acuña et al., 2007), increasing with both photosynthesis and respiration (Acuña et al., 2015). When rewetting occurs, this accumulation results in an increase in dissolved material, especially dissolved organic carbon (Shumilova et al., 2019; von Schiller et al., 2015).

Although water quality of perennial streams has long been protected, protections for non-perennial streams have been both more limited and more complicated. For example, the US Congress created the Clean Water Act (CWA) in 1972 to protect “Waters of the United States” (WOTUS); however, the jurisdictional definition of WOTUS is fiercely debated to this day (Walsh and Ward, 2020). Recent developments in definitions of WOTUS rely heavily on our ability to accurately characterize streams as perennial, intermittent, or ephemeral (USDOD and USEPA, 2020). However, current models focus more on distinguishing perennial from non-perennial streams (e.g., Jaeger et al., 2019). This results, in part, due to the lack of consensus in scientific and legal communities on the distinction between ephemeral and intermittent streams (Walsh and Ward, 2019), despite efforts by some to standardize these definitions (Busch et al. 2020). Additionally, while some areas have accurate maps of perennial/non-perennial streams (e.g., Jaeger et al., 2019), these are not available across the entire United States. To date, a nationwide repository of non-perennial streams does not exist (Jaeger et al., 2021).

Though many studies characterize seasonal drying patterns (e.g., Hammond et al., 2021; Hale and Godsey, 2019; Pate et al. 2020; Jaeger et al., 2019; Warix et al.,

2021), few studies focus on short-term drying patterns. One such study (Jensen et al., 2019) found that instantaneous wetted network extent increased by 50% shortly after storm events, but subsequently dropped back to antecedent conditions after a few hours. However, we know of only one study that focuses on short-term drying during periods of little or no precipitation (Warix et al., 2021). They present data from a small number of sensors as well as modeling work that suggests that evapotranspiration can drive short-term drying and rewetting, but only when conditions are primed for seasonal drying. We build off this work by deploying more sensors with a focus on dynamic locations because understanding the potential synchrony of drying across sites and temporal scales remains unexplored.

In this chapter, we seek to answer the following questions: (1A) How variable is stream drying across seasonal and sub-seasonal temporal scales throughout a watershed?; (1B) How might the variability of stream drying help us differentiate between intermittent and ephemeral streams?; (2) How synchronous are the patterns of wetting and drying at the most dynamic sites in a watershed?; and (3) What physical characteristics may drive the temporal patterns of drying and rewetting?

3.2. Site description

We conducted this work in Gibson Jack, a tributary of the Portneuf River in southeastern Idaho that drains an area of ~25.5 km². We chose this site because it exhibits a wide range of drying patterns, from perennial to almost always dry.

The elevation ranges from ~2,200 m at the highest peaks to ~1,500 m at the outlet, with steep slopes (mean ~20°) draining to the streams. Metasedimentary rocks, such as quartzite, largely underlie the northern half of the watershed and carbonates largely underlie the southern half (Rodgers and Othberg, 1999). Soils in Gibson Jack are primarily characterized as silty loams and fine sandy clay loams, many of which contain gravel (Davidson, 1977).

Vegetative cover varies with aspect: Douglas fir dominates the north-facing slopes and sagebrush, grasses, and juniper cover the south-facing slopes (Evenden et al., 2001). The US Forest Service manages most of the north fork as a Research Natural Area, meaning that it is a quality environmental area that is managed for minimal human impact (Evenden et al., 2001). Grazing and recreation, common throughout much of the watershed, occur more in the summer than in the winter.

A weather station in Gibson Jack recorded temperatures ranging from 31.78 °C to –16.67 °C with an average of 6.14°C in water year 2020. Precipitation during the year was 0.455 m in the form of both rain and snow (Welhan, 2006).

The intensity of land use changes seasonally in Gibson Jack. Grazing is restricted during the winter months due to the snow that covers the watershed. As the snow melts and temperatures rise in the spring, cattle graze in parts of the watershed. Recreation by local residents also increases during the summer months.

3.3. Methods

To explore temporal patterns of drying, we deployed Stream Temperature, Intermittency, and Conductivity sensors (STICs) in Gibson Jack during the summer of 2021 (May-Oct) as described in section 3.1, and interpreted the conductivity data as “wet” or “dry” with a threshold approach described in section 3.2. We calculated the number of wet sites and how that number changed with time to explore synchrony between sites. Finally, we performed a cluster analysis to differentiate between groups of similar sites as described in section 3.3.

3.3.1. Field Methods

We used modified Onset HOBO Pendant waterproof temperature and light sensors (Model UA-002-64) that repurpose the light-sensing capabilities (STICs) to measure relative electrical conductivity in units of lux. Our modifications follow Chapin et al. (2014) except that conductivity is measured at the bottom of the STIC rather than at the top, allowing our STICs to detect even small amounts of water in the stream bed. The ability of the sensor to collect temperature data was unchanged. Relative electrical conductivity is significantly higher in water than in air, allowing us to identify a threshold (detailed in section 3.2) such that we interpret higher values as wet, and lower values as dry.

In 2021, we deployed 122 STICs in different locations to capture the most temporal variability in the network (Figure 3.1) based on mapping by Hale and Godsey (2019) and an initial survey that we conducted in 2020 (see chapter 2). Because we sought to capture scales of autocorrelation as well as temporal patterns, we deployed nests of STICs at intervals as closely spaced as 12.5 m to as far apart as 1,000 m (see

chapter 2). All nests were centered in reaches that had been observed to be both wet and dry during past site visits. The STICs recorded relative electrical conductivity at 15-minute intervals from no later than 17 May through 16 October 2021, when we retrieved them.

3.3.2. Interpretation

To interpret the relative electrical conductivity as wet or dry observations, we calibrated each STIC using four calibration standards: 84 $\mu\text{S}/\text{cm}$, 447 $\mu\text{S}/\text{cm}$, and 1413 $\mu\text{S}/\text{cm}$, and air (assumed to be 0 $\mu\text{S}/\text{cm}$). We then modeled a linear relationship between the values measured by each STIC and the calibration standards and assumed the y-intercept from this relationship represented the threshold between wet and dry. To validate this interpretation, we compared all STIC-based inferences of wet and dry conditions to observations recorded in the field. 63% of the inferred flow conditions, based on the y-intercept threshold, matched the field observations we had (e.g. if we observed a site as wet on May 17, 2021, our interpretation of STIC data also indicated the site was wet). To interpret data from the sites where flow status was incorrectly inferred at least once, we examined each data set individually and selected a threshold that (A) matched our field observations and (B) was within the standard error of our linear calibration intercept. In the 5 cases where these criteria did not result in a clear threshold, we chose 1-2 thresholds that allowed short wetting during storm events, as indicated by precipitation data, but not at other times. A full list of thresholds is provided in the appendix.

3.3.3. Analysis of Patterns

We first calculated seasonal streamflow permanence by summing the number of wet measurements and dividing by the total number of measurements at each site. To classify sites, we first assumed that all sites with a seasonal streamflow permanence greater than 0.99 (or less than 0.01) as always wet (or always dry). For all other sites, we classified them using a k-means cluster analysis (Frades and Matthiesen, 2010) based on the following metrics, which we calculated for each site: (1) seasonal streamflow permanence, (2) first no-flow event (measured from day of deployment, with a value of 0 indicating the sensor was dry when the STIC was deployed), (3) the number of drying events during the season, (4) the average duration of drying events, and (5) the interquartile range of drying event duration. We chose these metrics because they represented (1) seasonal trends in stream drying, (2) the ability for spring runoff to sustain surface flow, and (3) the short-term drying/rewetting cycles that occurred at many sites. The number of classes used in the k-means cluster analysis was determined using the elbow method (see Appendix 1). Finally, to determine what physical characteristics may drive the temporal differences between classes, we performed a Kruskal-Wallis test on seven physical variables that were shown to have no autocorrelation (Figure A1.4; see Appendix 1).

To explore synchrony on the seasonal scale at the most dynamic sites, we calculated the mean number of sites wet for each day, and then plotted those values against time. Taking the derivative of this plot allowed us to quantify the change in the number of wet STICs over time. To explore what physical characteristics may drive

synchrony, we divided the data into five groups based on first no-flow events: dry on deployment, dried in May after deployment, dried in June, dried between July 1st and October 16, and never dried. We then performed a Kruskal-Wallis test using the same variables we used before for these five categories of first no-flow.

To explore synchrony on sub-daily scales, we created “clock plots.” To create the clock plots, we selected only the locations where we observed wet-dry cycles on sub-daily scales. For each site, we then selected the wettest day with wet-dry cycles and recorded the time at which the site dried and rewetted. We then repeated this process selecting for the driest days of the season for each sensor rather than the wettest. We then plotted the number of sites that experienced sub-daily wet-dry cycles that were wet or dry at a given time on their wettest and driest day. We chose to plot this number on a circular rose plot to visualize the cyclical nature of daily wetting and drying patterns.

3.4. Results

Even though we deployed STICs to target places that we expected to vary between wet and dry status, seasonal streamflow permanence had a bimodal distribution, with more than half of sites (59%) having a seasonal streamflow permanence of higher than 0.9 or less than 0.1 (16% and 43% of all sites, respectively).

Across the 121 sites, we observed almost 1,200 wetting events: their durations ranged from 15 min to more than two months. The distribution of durations is severely

right-skewed, with 1,129 wetting events lasting 24 hours or less. These short-term rewetting events occur in every tributary in the watershed (Figure 3.2).

Approximately 40% of sites were classified as consistently wet or dry (13% or 27%, respectively). The k-means cluster analysis then revealed three different site clusters (Figure 3.3). The first cluster consisted of approximately 9% of all sites. It was characterized by early first no-flow events, low seasonal streamflow permanence, and only a handful of wetting events. The second cluster consisted of approximately 17% of all sites. It was characterized by late first no-flow events, high seasonal streamflow permanence, and many short drying events. The third and final cluster consisted of approximately 34% of all sites. It was characterized by early first no-flow events, low seasonal streamflow permanence, and only a few short drying events. The Kruskal-Wallis test revealed that colluvium, median of a pebble count, and trees also distinguished the five classes from each other (Table 3.2).

Most sites dried over the course of the first two months of the season (May and June; Figure 3.4) with the drying rate reaching seasonal lows on May 27 and May 29 with approximately five sites drying on each of those days. STICs within the same nest often dried at nearly the same time, with upstream sites drying slightly earlier than sites downstream within the same nest. However, there were some exceptions to this pattern: in some tributaries (e.g., SF3 and MT1), downstream sites dried earlier than upstream sites. Rewetting rates, on the other hand, peaked on July 30, Aug 18, and Oct 10 with three or four sites wetting on those days (Figure 3.5). The best-fit rewetting rate was negative until mid-August showing that drying dominated through the spring and

summer. After dividing the data into five groups based on the date of first-day-dry, the Kruskal-Wallis test revealed that colluvium, loam, and trees can distinguish the five groups from each other (Table 3.2).

On the wettest day of the season for each site, many sites rewet in the morning before drying again in the evening. The most common drying time, with four or five sites drying in an hour, occurred at 14:00 (Figure 3.6C). Another common drying time, with two or three sites drying within an hour, occurred at 03:00. Rewetting events mainly occurred at 05:00 and 20:00 with wetting of two to four sites/hour.

On the driest day of the season for each site, sites exhibit similar patterns to the wettest days, though both wetting and drying happened earlier than they did on the wettest days and were less synchronous than on the wettest days of wet-dry cycling. This shift to slightly less synchronous drying is reflected by a drying rate of only one and two sites per hour. One exception was up to three sites that dried around 17:00. Rewetting of one to three sites per hour occurred at 05:00 and 20:00.

3.5. Discussion

To interpret our results and explore their implications, we will explore each research question individually.

3.5.1A. How variable is stream drying across seasonal and sub-seasonal temporal scales throughout a watershed?

The bimodal distribution of seasonal streamflow permanence suggests that during a year of severe drought, there is little variability in flow permanence at any given

site. This finding surprised us because our preliminary investigations (i.e. our 2020 deployment and Hale and Godsey, 2019) indicated that our 2021 field sites had the best chance to exhibit intermediate seasonal streamflow permanence values.

It is likely that if we had selected different sites we would have gotten different results. What is unclear is how different those results would have been, and how much those results would represent the most dynamic reaches of the stream network. In some tributaries, we chose sites lower in the tributaries that never dried (e.g. NF4 and MT1). This suggests that, at least in those tributaries, we measured stream drying at the perennial/non-perennial transition point. If we had additional STICs, it would have been wise to place them just below STICs in tributaries where we did not capture perennial sites (e.g. GSF and GNF) so that we could ensure that we had measured the perennial/non-perennial transition point.

The large number of drying/wetting cycles that we observed suggests that, at some sites, stream drying is highly dynamic, even from one hour to the next. This may indicate a variable shallow water table that may be driven by evapotranspiration. These short-duration drying events could have important implications for biogeochemistry and microbiology. For example, consistently short drying events would make it difficult for a microbial community to establish itself before a rewetting event occurs (Battin et al., 2003). Similarly, short drying events would preclude the build-up of coarse organic material, which may in turn limit changes to biogeochemical concentrations normally associated with rewetting events (Acuña et al, 2015; Shumilova et al., 2019)

In performing the cluster analysis, we chose five metrics that we thought would best represent the temporal patterns we observed. Other temporal metrics, such as *no-flow fraction* (Hammond et al., 2020), would be correlated with metrics we included and thus would not greatly influence our results. The hydrologic literature also includes a set of metrics that require stream discharge or rain gage data, such as *Peak-to-no-flow* duration (Hammond et al., 2020) or the *time to respond to a rainfall event* (Goulsbra et al., 2007). These metrics would provide interesting results related to the duration that a water source can retain flow, but we did not have those kinds of data available to us at each STIC, and so could not address these questions.

3.5.1 B. How might the variability in stream drying help us differentiate between intermittent and ephemeral streams?

The key difference between ephemeral and intermittent streams is the dependence of a stream on precipitation for surface flow, with ephemeral streams solely relying on precipitation and intermittent streams having other sources of flow (Busch et al., 2020). Thus, during a drought year, we expect ephemeral streams to have low seasonal streamflow permanence and few, if any, drying/rewetting events. This corresponds with classes 1 and 3 identified in our cluster analysis. Conversely, we would expect intermittent streams to have a higher streamflow permanence and the ability to rewet after drying events even without the aid of precipitation. This corresponds with class 2 identified in our cluster analysis.

This classification of ephemeral and intermittent streams could be confirmed by repeating the cluster analysis on data obtained from the same sites but in a wetter year. In a wetter year, we would expect ephemeral sites (i.e. classes 1 and 3) to have a lower

seasonal streamflow permanence, but more drying/rewetting events corresponding to precipitation. Conversely, we would expect intermittent sites (i.e. class 2) to have a higher streamflow permanence and fewer drying/rewetting events because of the dual flow sources of precipitation and groundwater. If these patterns persist and if the classifications remain stable, government agencies could adopt a method similar to the one used in this chapter to distinguish ephemeral and intermittent sites from each other.

3.5.2. How synchronous are the patterns of wetting and drying across the watershed?

Synchrony appears to differ between wetting and drying events in the Gibson Jack watershed. The consistent drying observed through most of the season (see the best-fit line in Figure 3.5) suggests that drying is often asynchronous, possibly reflecting a range of drivers that play important roles in stream drying. A range of drivers could potentially lead to sites drying at different times as different sources of flow last for varying amounts of time throughout a watershed. This conclusion would be consistent with the work done by Jaeger et al. (2019) who concluded from a random forest analysis that 27 of their 29 explanatory variables had a mean decrease accuracy of over 10%. Despite the general asynchronous drying trend, a few dips observed in the graph (Figure 3.5) suggest that drying can occasionally synchronize under drought conditions. This may result from the lack of precipitation during a period when flow transitions from snowmelt driven to rain driven.

On the other hand, rewetting appears to be more synchronous than drying. Only a few days throughout the season saw more than two STICs wet up on the same day,

suggesting that wetting occurs synchronously or not at all. This pattern, combined with the drought experienced by Gibson Jack in 2021, may indicate that rewetting is primarily driven by precipitation patterns, which were sparse.

On sub-daily scales, we see clear temporal patterns at sites where cycling was observed. As evapotranspiration is a major process that varies over the course of a day, the cycles we observed are likely driven by it. Indeed, White (1932) developed a method for predicting shallow groundwater reserves by measuring transpiration. Conversely, Fahle and Dietrich (2013) were able to predict evapotranspiration using fluctuations in groundwater levels. Given the documented relationship between groundwater levels and evapotranspiration, we hypothesize that during the day when evapotranspiration increases, shallow subsurface water reserves decrease until they finally empty as the sun sets. Groundwater reserves then replenish throughout the night until rewetting occurs sometime in the morning. We observe this on both the wettest days of the season and the driest days of the season, though both rewetting and drying occurs earlier on the driest days.

The wettest days of the season had significant periods of gradual, asynchronous rewetting, but only one major synchronous drying event. This differs from the seasonal pattern of synchronous wetting and asynchronous drying that we observed, suggesting that different processes are driving seasonal drying patterns compared to diel drying patterns on the wettest day.

The asynchronous drying and synchronous rewetting at sub-daily scales exhibited on the driest days suggests that the process that drives synchrony on the

wettest days has a threshold, below which it has no effect on daily stream drying cycles. This is similar to what we observed across seasonal scales suggesting that they may share the same drivers.

5.3. What physical characteristics may drive the temporal patterns we see?

Both the classes identified by the clustering analysis, and the first-no-flow event groups were differentiated by colluvium, trees, and soil characteristics. This suggests that the cluster analysis and the first-no-flow groupings are more correlated than was initially thought. It suggests that the cluster analysis either relied heavily on the first-no-flow metric, or that the first-no-flow metric is related to the other metrics such as seasonal streamflow permanence.

Both Jaeger et al. (2019) and Hammond et al. (2021) claimed that forest cover was the most important non-meteorological variable in predicting stream drying. This corresponds with our Kruskal-Wallis test that suggests forest cover can differentiate between classes and groups. However, lithology is not identified as an important variable in most studies.

Future studies may be able to use trees, colluvium, and pebble counts to distinguish between the classes. This may be beneficial because lithology and soil has been mapped across much of the United States, allowing analysis to be conducted with minimal field work. Similarly, lidar, which is available for much of the country, may allow for differentiation between tree cover and other plant cover with minimal field work. Additionally, tree height is a variable that may be useful for forest health, giving us

multiple reasons to calculate that variable. Conversely, pebble counts are time-consuming and may not be the most practical way to differentiate between sites, especially when other, less time-intensive methods are available.

3.6. Conclusion

To explore the variability of stream drying on sub-seasonal scales, we measured the absence/presence of flow at 15-minute intervals at 121 locations throughout the Gibson Jack watershed. We conclude that even the most dynamic sites had a bimodal distribution of seasonal streamflow permanence values. We also observed many drying/rewetting cycles, the overwhelming majority of which were shorter than 24 hours in length. This work characterizes stream drying on scales that are often overlooked in hydrologic literature. The sub-seasonal characterization also allowed us to quantifiably discern between intermittent and ephemeral streams using a cluster analysis. Policy makers and enforcers may use this method of classifying ephemeral and intermittent streams in the future to answer legal questions about the jurisdiction of the CWA.

On seasonal scales, drying occurred asynchronously, although the majority of sites first dried sometime in May. Conversely, any rewetting that occurred happened synchronously. For the wettest day of the season at sites that experience short-duration drying/rewetting cycles, we observed the reverse trend (i.e. drying was synchronous and wetting was asynchronous) reflecting different controls on wetting and drying at different temporal scales. However, the driest day of the season at these same sites showed trends similar to the seasonal trends (i.e. drying was asynchronous and wetting was synchronous). By better understanding the synchrony of wetting and drying

patterns across a watershed, we can better determine how the biogeochemical processes at one site are related to the biogeochemical processes at other sites.

3.7. Figures

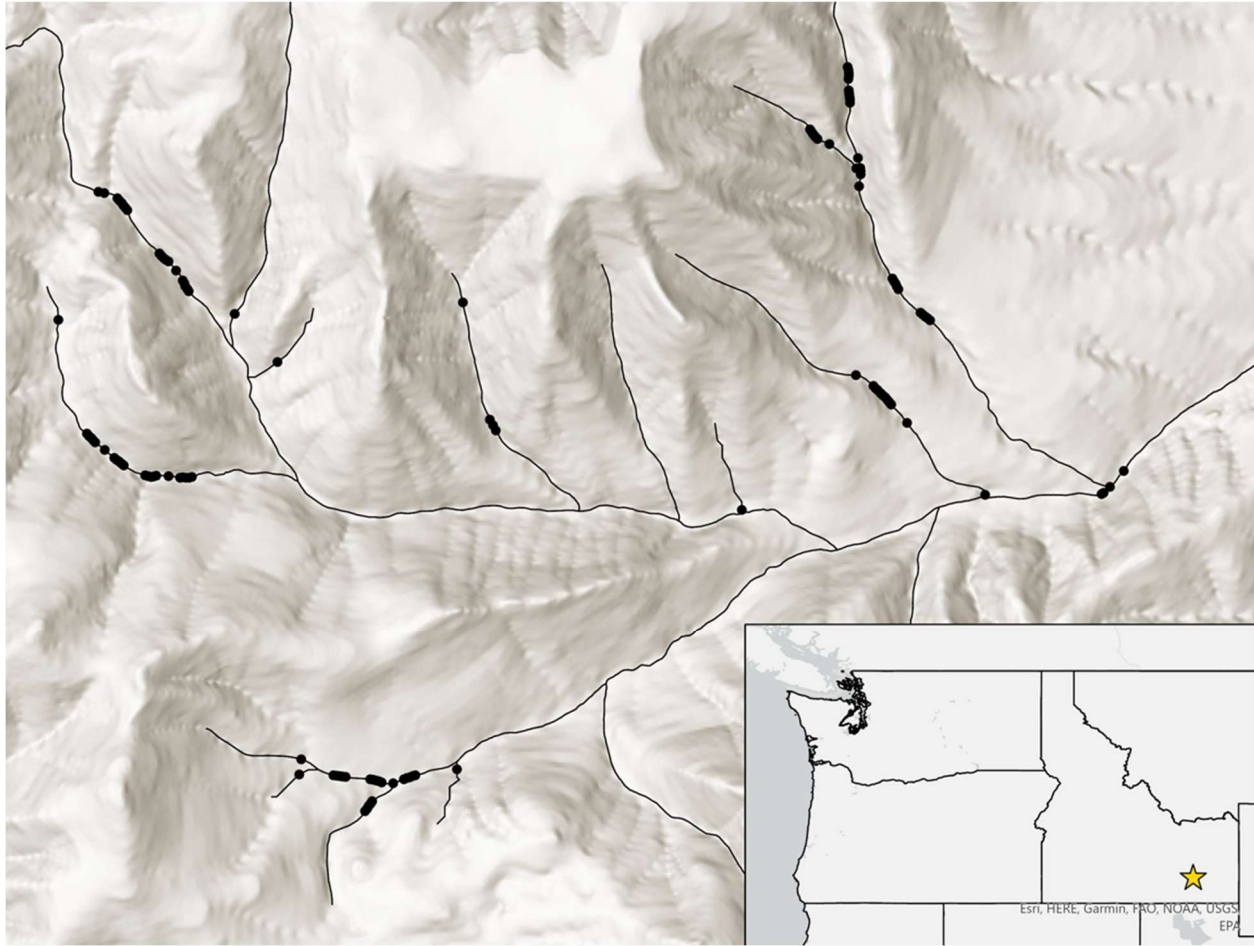


Figure 3. 1: Map of the Gibson Jack watershed located in southwest Idaho. The map shows the locations of the STICs deployed from May 2021 to October 2021.

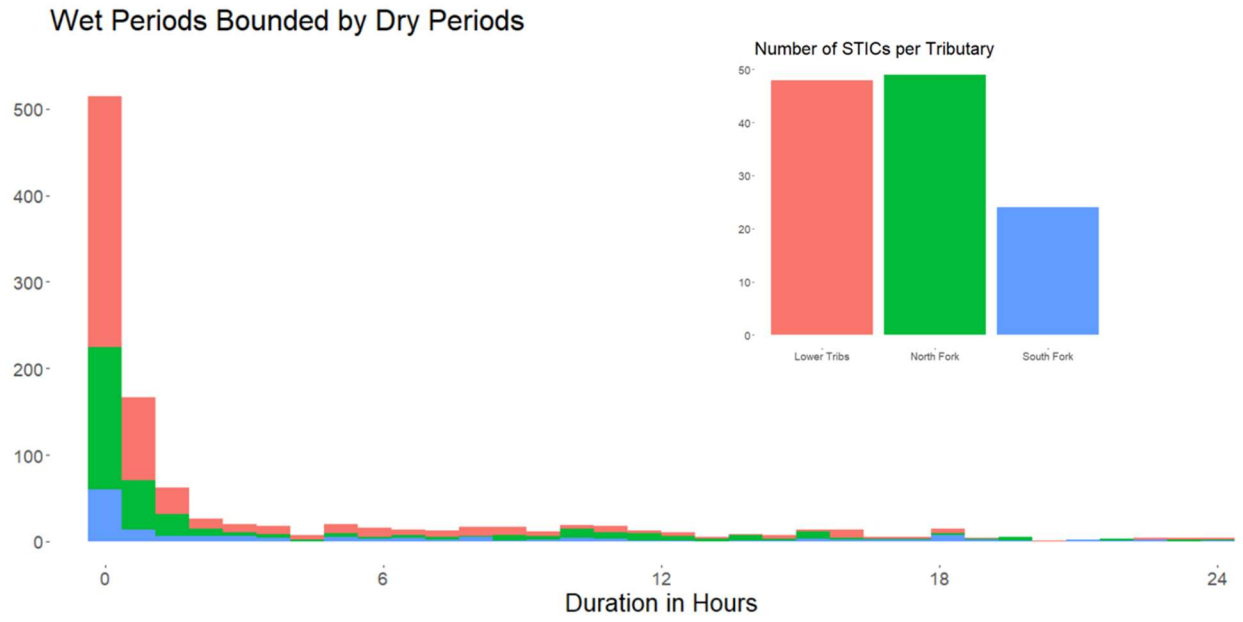


Figure 3. 2: The distribution of mid-season wetting events lasting less than 24 hours is extremely right-skewed.

A

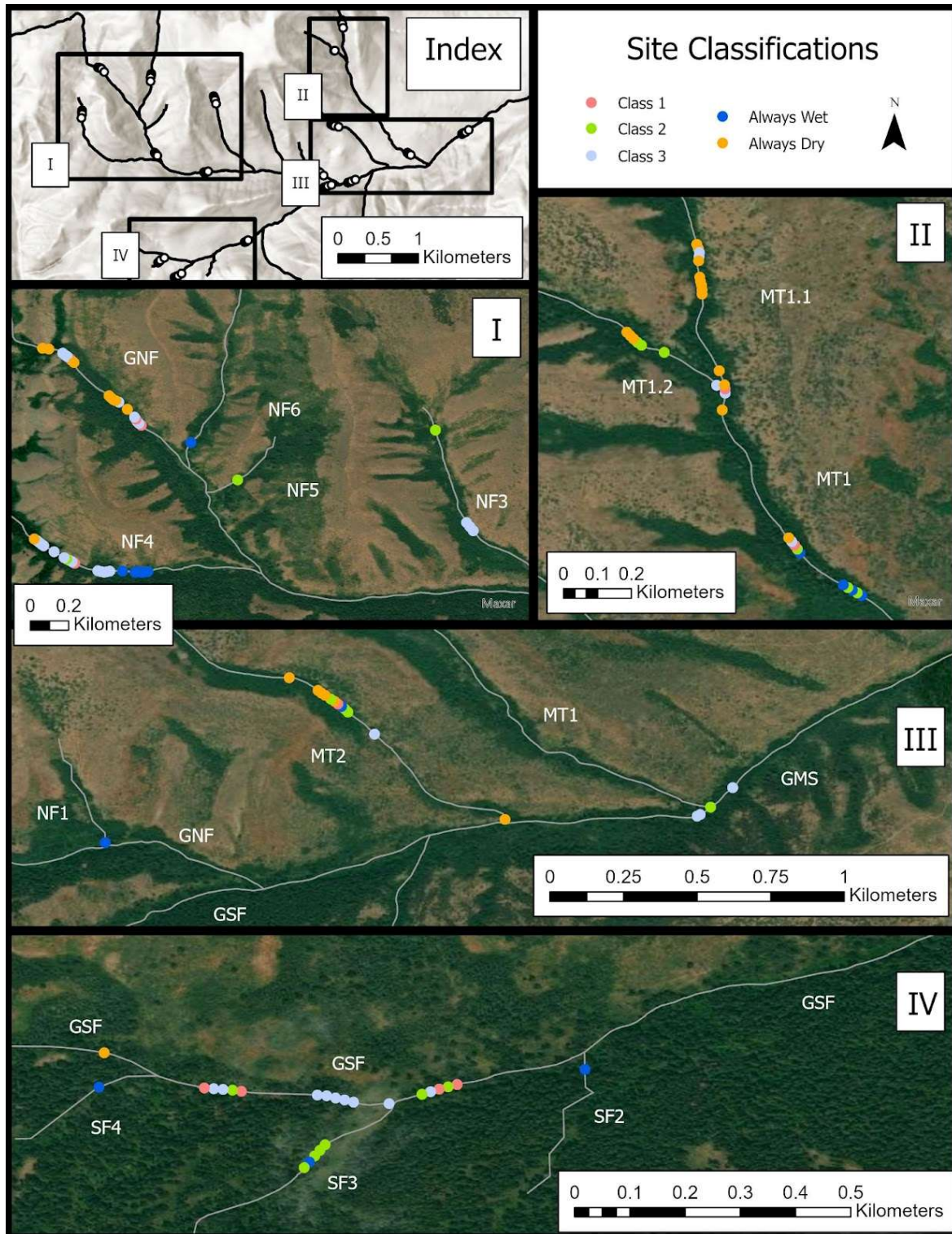
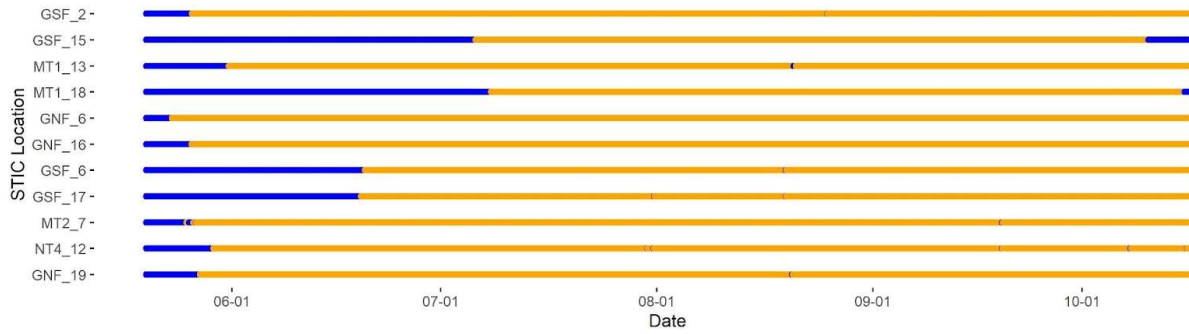


Figure 3.3: Map showing the sites where we deployed STICs (A). Categories of stream drying appear in every tributary without an obvious pattern.

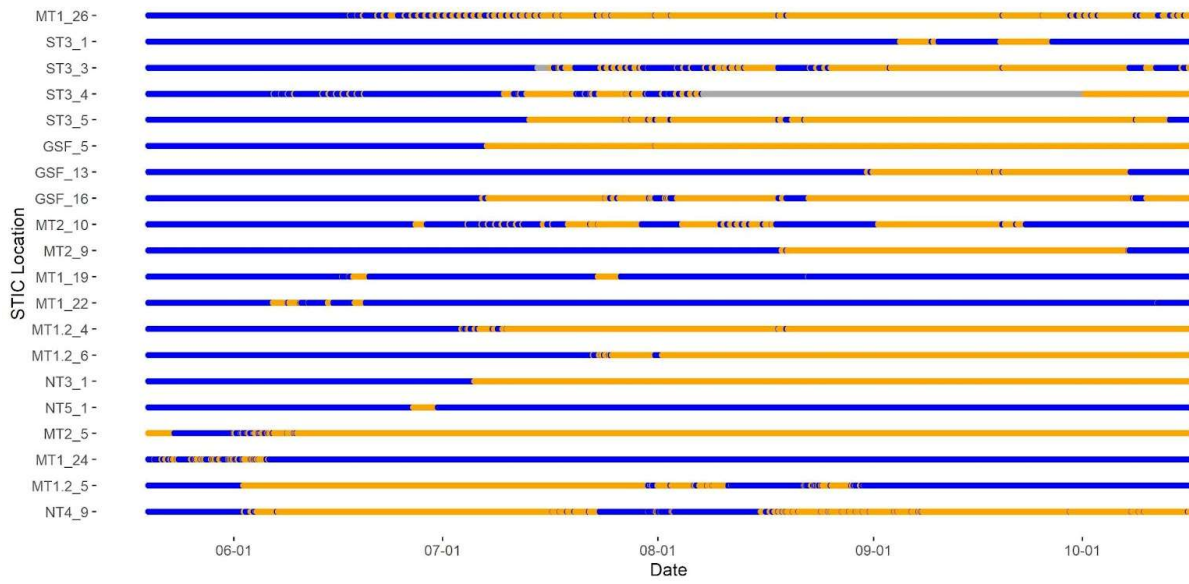
A

Class 1



B

Class 2



C

Class 3

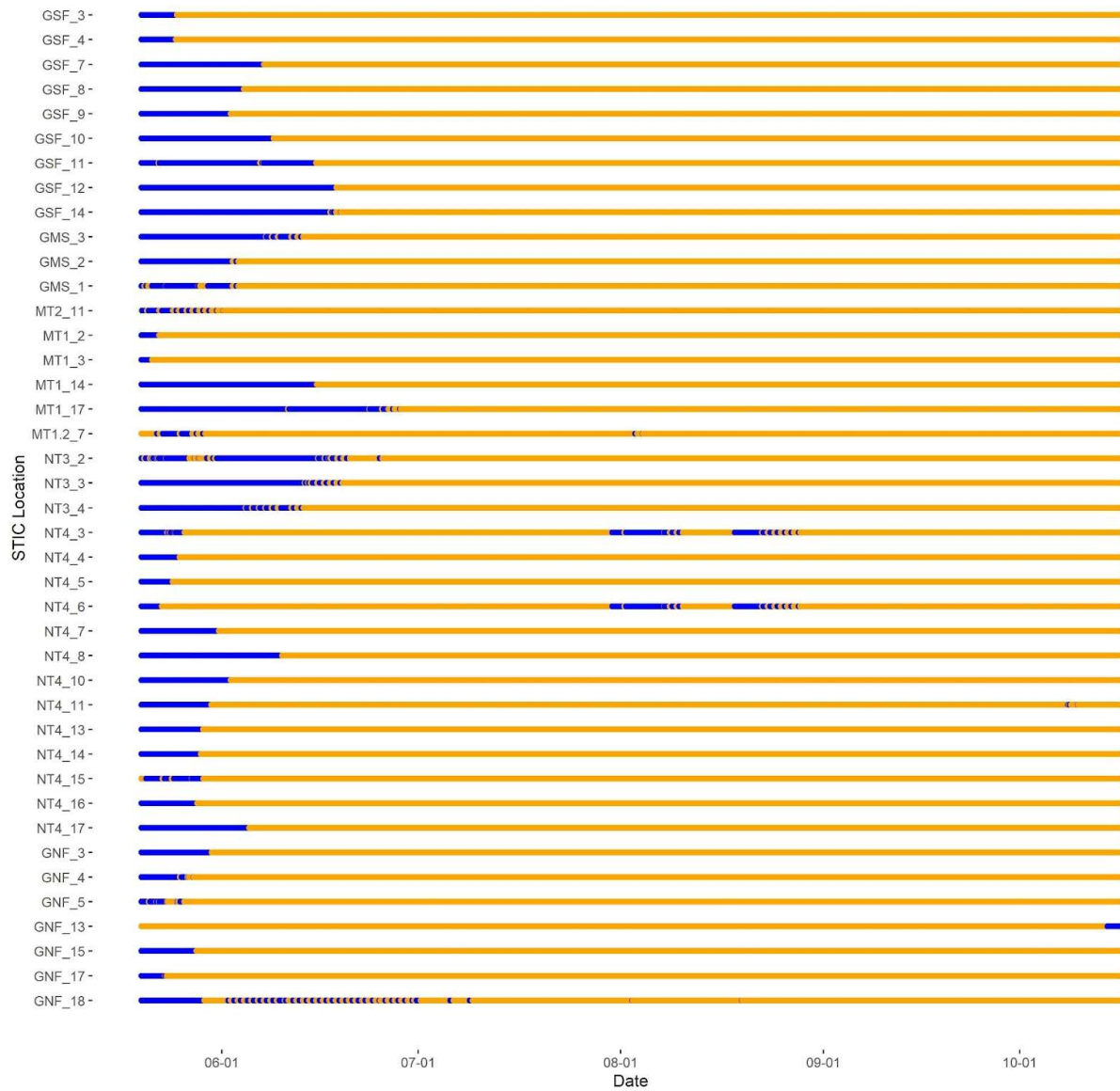


Figure 3. 4: Time series showing the presence (blue) or absence (orange) of water at each site shown in Figure 3.3 grouped by class (excluding sites that were only wet or dry). Class 2 has the vast majority of short-duration wetting/drying cycles.

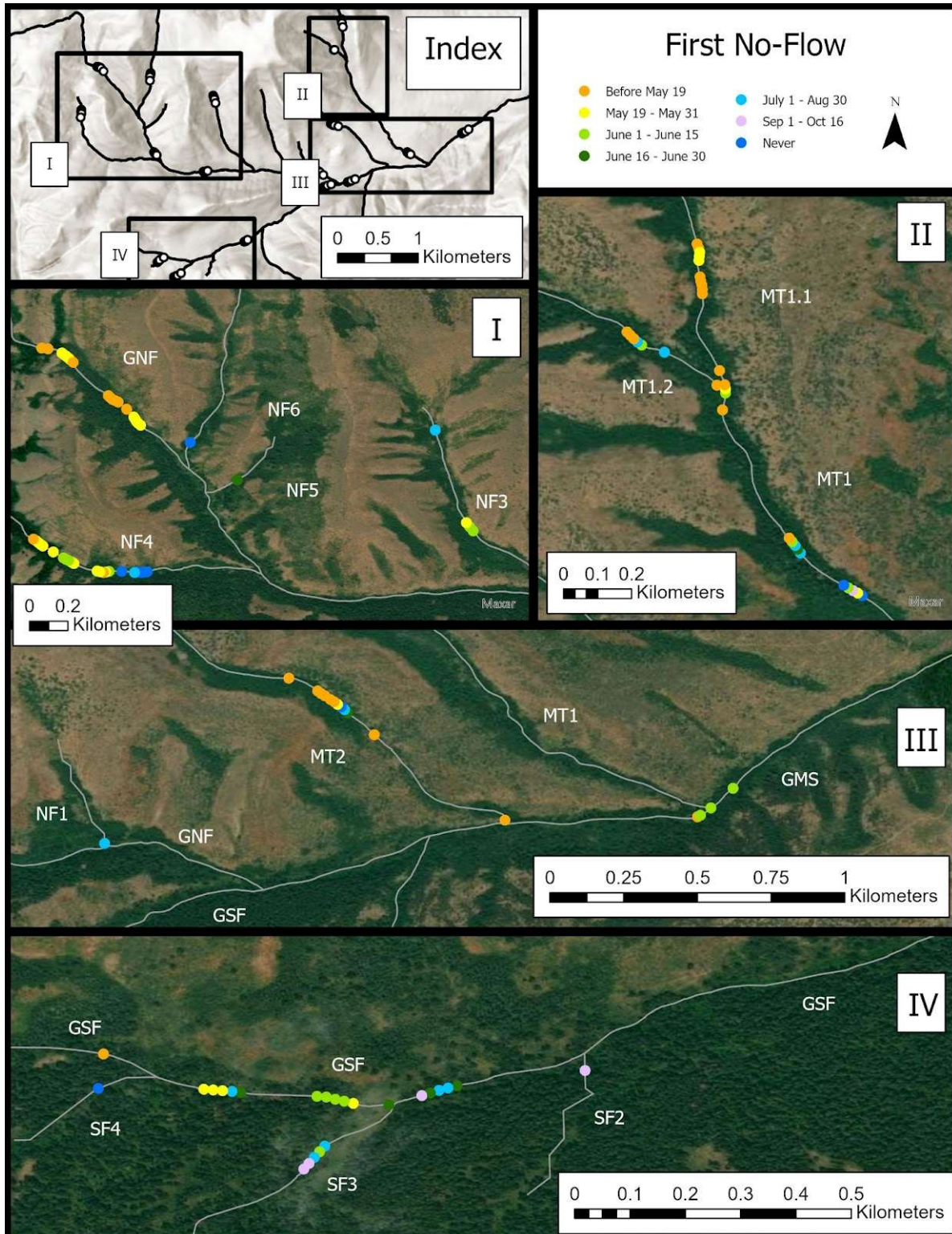


Figure 3. 5: Map showing when a site first experienced a no-flow event. Note that the majority of sites dried for the first time before the end of May.

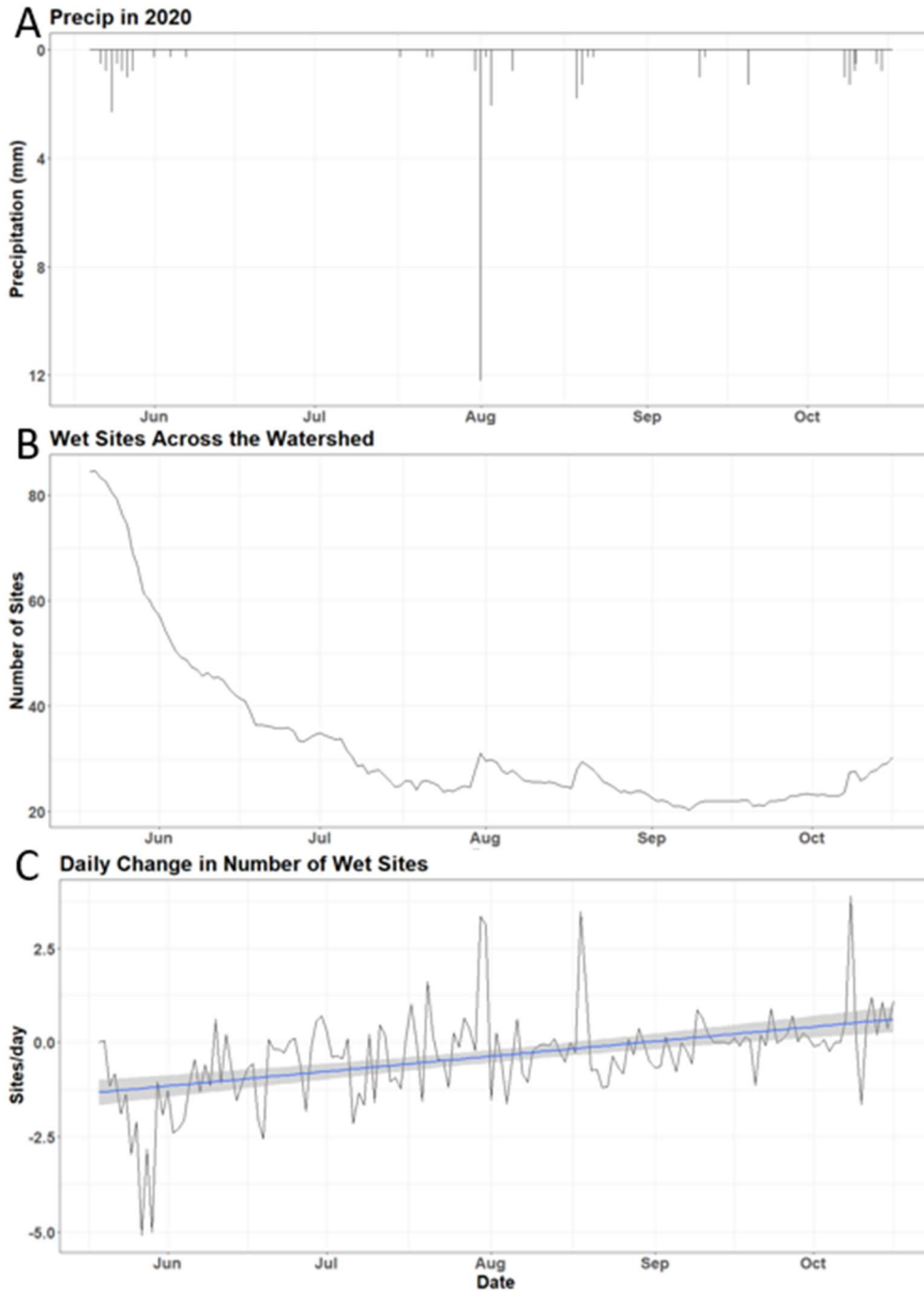


Figure 3. 6: Plots showing the amount of precipitation during the 2021 field season (A), the number of wet sites each day (B) and the daily change in the number of wet sites (C) throughout the watershed.

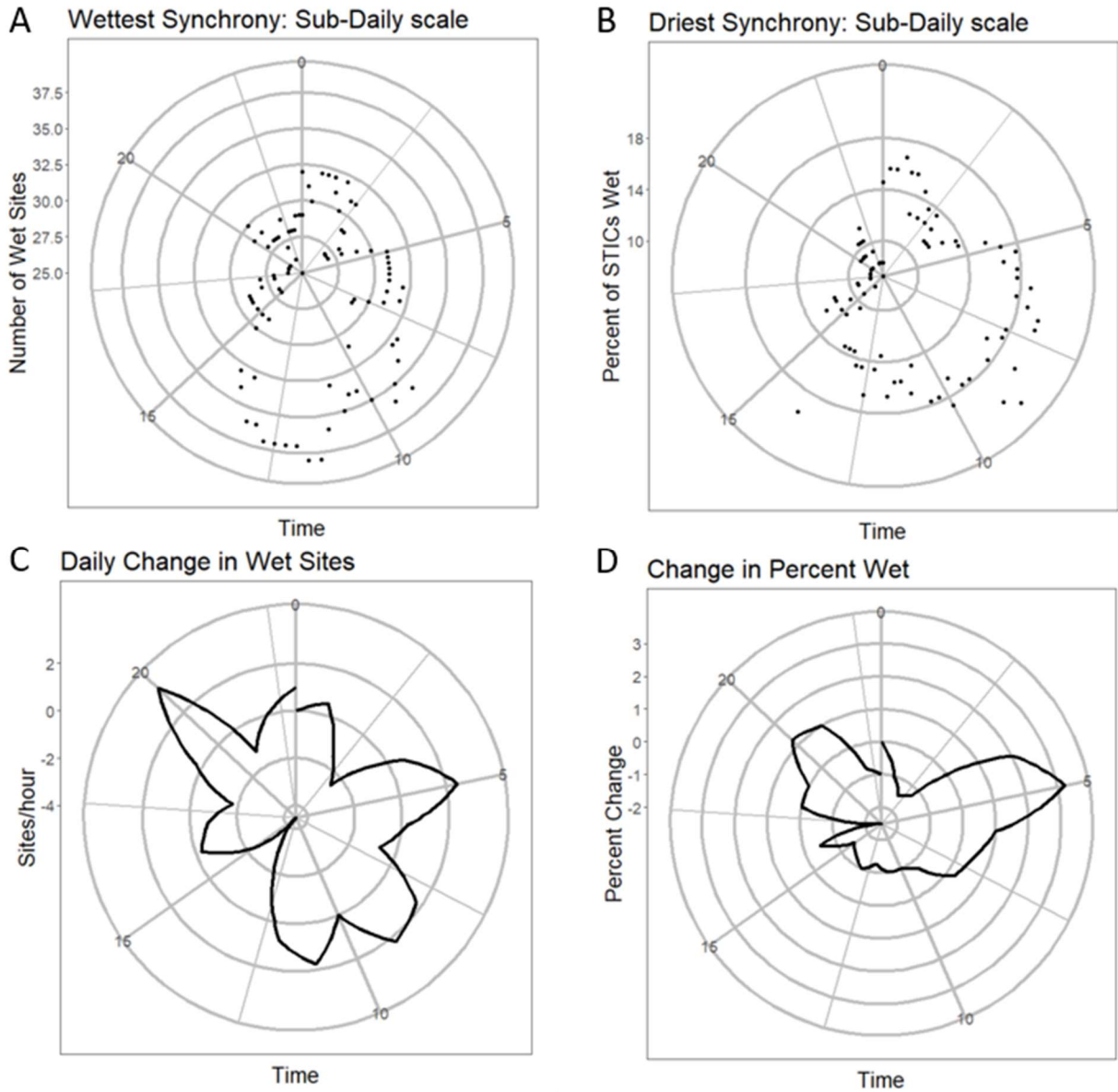


Figure 3. 7: Clock plots showing the number of STICs wet on the wettest days (A), the driest days (B), and the change in the percentage of wet STICs on the wettest days (C) and the driest days (D).

3.8. Tables

Table 3.1. Variables used in the Kruskal-Wallis Test.

Name	Units	Alias
Drainage Area	m ²	Drainage Area
Colluvium	percent	Colluvium
Loamy Soils	percent	Loam
Tree Cover	percent	Trees
Slope	degrees	Slope
Median of Pebble Count	cm	MPC
Percent Canopy Cover	percent	Canopy Cover

Table 3.2. Results from Kruskal-Wallis Test

Variable	Classes Identified by Cluster Analysis	First-No-Flow Event Groups
Colluvium	0.0094	0.0296
Slope	0.1011	0.3809
Loam	0.1036	0.0062
Silt Loam	0.2506	0.0876
PCM	0.0061	0.0502
Canopy	0.0628	0.2059
Trees	0.0001	0.0022

Values highlighted in blue can differentiate between classes.

3.9. References

- Acuña, V., Casellas, M., Corcoll, N., Timoner, X., and Sabater, S., 2015, Increasing extent of periods of no flow in intermittent waterways promotes heterotrophy: *Freshwater Biology*, v. 60, p. 1810–1823, doi:[10.1111/fwb.12612](https://doi.org/10.1111/fwb.12612).
- Acuña, V., Giorgi, A., Muñoz, I., Sabater, F., and Sabater, S., 2007, Meteorological and riparian influences on organic matter dynamics in a forested Mediterranean stream: *Journal of the North American Benthological Society*, v. 26, p. 54–69, doi:[10.1899/0887-3593\(2007\)26\[54:MARIOO\]2.0.CO;2](https://doi.org/10.1899/0887-3593(2007)26[54:MARIOO]2.0.CO;2).
- Allen, D.C., Galbraith, H.S., Vaughn, C.C., and Spooner, D.E., 2013, A Tale of Two Rivers: Implications of Water Management Practices for Mussel Biodiversity Outcomes During Droughts: *AMBIO*, v. 42, p. 881–891, doi:[10.1007/s13280-013-0420-8](https://doi.org/10.1007/s13280-013-0420-8).
- Battin, T.J., Kaplan, L.A., Newbold, J.D., Cheng, X., and Hansen, C., 2003, Effects of Current Velocity on the Nascent Architecture of Stream Microbial Biofilms: *Applied and Environmental Microbiology*, v. 69, p. 5443–5452, doi:[10.1128/AEM.69.9.5443-5452.2003](https://doi.org/10.1128/AEM.69.9.5443-5452.2003).
- Belmont, P. et al., 2011, Large Shift in Source of Fine Sediment in the Upper Mississippi River: *Environmental Science & Technology*, v. 45, p. 8804–8810, doi:[10.1021/es2019109](https://doi.org/10.1021/es2019109).
- Brown, T.C., Hobbins, M.T., and Ramirez, J.A., 2008, Spatial distribution of water supply in the coterminous united states: *JAWRA Journal of the American Water Resources Association*, v. 44, p. 1474–1487, doi:[10.1111/j.1752-1688.2008.00252.x](https://doi.org/10.1111/j.1752-1688.2008.00252.x).
- Busch, M.H. et al., 2020, What's in a name? Patterns, trends, and suggestions for defining non-perennial rivers and streams: *Water*, v. 12, p. 1980, doi:[10.3390/w12071980](https://doi.org/10.3390/w12071980).
- Chapin, T.P., Todd, A.S., and Zeigler, M.P., 2014, Robust, low-cost data loggers for stream temperature, flow intermittency, and relative conductivity monitoring: *Water Resources Research*, v. 50, p. 6542–6548, doi:[10.1002/2013WR015158](https://doi.org/10.1002/2013WR015158).
- Datry, T., Larned, S.T., and Tockner, K., 2014, Intermittent rivers: A challenge for freshwater ecology: *BioScience*, v. 64, p. 229–235, doi:[10.1093/biosci/bit027](https://doi.org/10.1093/biosci/bit027).
- Davidson, 1977, Soils and geology of the west fork mink Creek and Gibson Jack creeks: Caribou national forest open-file report 2540:
- Evenden, A.G., Moeur, M., Shelly, J.S., Kimball, S.F., and Wellner, C.A., 2001, Research natural areas on national forest system lands in Idaho, Montana, Nevada, Utah, and Western Wyoming: A guidebook for scientists, managers, and educators: U.S. Department of Agriculture, Forest Service, Rocky Mountain Research Station RMRS-GTR-69, RMRS-GTR-69 p., doi:[10.2737/RMRS-GTR-69](https://doi.org/10.2737/RMRS-GTR-69).

- Fahle, M., and Dietrich, O., 2014, Estimation of evapotranspiration using diurnal groundwater level fluctuations: *Water Resources Research*, v. 50, p. 273–286, doi:[10.1002/2013WR014472](https://doi.org/10.1002/2013WR014472).
- Frades, I., and Matthiesen, R., 2010, Overview on Techniques in Cluster Analysis, *in* Matthiesen, R. ed., *Bioinformatics Methods in Clinical Research*, Totowa, NJ, Humana Press, *Methods in Molecular Biology*, v. 593, p. 81–107, doi:[10.1007/978-1-60327-194-3_5](https://doi.org/10.1007/978-1-60327-194-3_5).
- Goulsbra, C., Evans, M., and Lindsay, J., 2014, Temporary streams in a peatland catchment: pattern, timing, and controls on stream network expansion and contraction: *Earth Surface Processes and Landforms*, v. 39, p. 790–803, doi:[10.1002/esp.3533](https://doi.org/10.1002/esp.3533).
- Hale, R.L., and Godsey, S.E., 2019, Dynamic stream network intermittence explains emergent dissolved organic carbon chemostasis in headwaters: *Hydrological Processes*, p. hyp.13455, doi:[10.1002/hyp.13455](https://doi.org/10.1002/hyp.13455).
- Hammond, J.C. et al., 2021, Spatial patterns and drivers of nonperennial flow regimes in the contiguous United States: *Geophysical Research Letters*, v. 48, doi:[10.1029/2020GL090794](https://doi.org/10.1029/2020GL090794).
- Jaeger, K.L., Sando, R., McShane, R.R., Dunham, J.B., Hockman-Wert, D.P., Kaiser, K.E., Hafen, K., Risley, J.C., and Blasch, K.W., 2019, PRObability of Streamflow PERmanence Model (PROSPER): A spatially continuous model of annual streamflow permanence throughout the Pacific Northwest: *Journal of Hydrology X*, v. 2, p. 100005, doi:[10.1016/j.hydroa.2018.100005](https://doi.org/10.1016/j.hydroa.2018.100005).
- Jensen, C.K., McGuire, K.J., McLaughlin, D.L., and Scott, D.T., 2019, Quantifying spatiotemporal variation in headwater stream length using flow intermittency sensors: *Environmental Monitoring and Assessment*, v. 191, p. 226, doi:[10.1007/s10661-019-7373-8](https://doi.org/10.1007/s10661-019-7373-8).
- Katz, G.L., Denslow, M.W., and Stromberg, J.C., 2012, The Goldilocks effect: intermittent streams sustain more plant species than those with perennial or ephemeral flow: *Desert riparian diversity: Freshwater Biology*, v. 57, p. 467–480, doi:[10.1111/j.1365-2427.2011.02714.x](https://doi.org/10.1111/j.1365-2427.2011.02714.x).
- Messenger, M.L., Lehner, B., Cockburn, C., Lamouroux, N., Pella, H., Snelder, T., Tockner, K., Trautmann, T., Watt, C., and Datry, T., 2021, Global prevalence of non-perennial rivers and streams: *Nature*, v. 594, p. 391–397, doi:[10.1038/s41586-021-03565-5](https://doi.org/10.1038/s41586-021-03565-5).
- Pate, A.A., Segura, C., and Bladon, K.D., 2020, Streamflow permanence in headwater streams across four geomorphic provinces in Northern California: *Hydrological Processes*, p. hyp.13889, doi:[10.1002/hyp.13889](https://doi.org/10.1002/hyp.13889).
- Robinne, F.-N., Bladon, K.D., Silins, U., Emelko, M.B., Flannigan, M.D., Parisien, M.-A., Wang, X., Kienzle, S.W., and Dupont, D.P., 2019, A regional-scale index for assessing

the exposure of drinking-water sources to wildfires: *Forests*, v. 10, p. 384, doi:[10.3390/f10050384](https://doi.org/10.3390/f10050384).

Rodgers, D.W., and Othberg, K.L., 1999, Geologic map of the Pocatello south quadrangle, Bannock and Power counties, Idaho: Idaho Geologic Survey Geologic map.

Ruhi, A., Messenger, M.L., and Olden, J.D., 2018, Tracking the pulse of the Earth's fresh waters: *Nature Sustainability*, v. 1, p. 198–203, doi:[10.1038/s41893-018-0047-7](https://doi.org/10.1038/s41893-018-0047-7).

von Schiller, D., Graeber, D., Ribot, M., Timoner, X., Acuña, V., Martí, E., Sabater, S., and Tockner, K., 2015, Hydrological transitions drive dissolved organic matter quantity and composition in a temporary Mediterranean stream: *Biogeochemistry*, v. 123, p. 429–446, doi:[10.1007/s10533-015-0077-4](https://doi.org/10.1007/s10533-015-0077-4).

Shumilova, O. et al., 2019, Simulating rewetting events in intermittent rivers and ephemeral streams: A global analysis of leached nutrients and organic matter: *Global Change Biology*, v. 25, p. 1591–1611, doi:[10.1111/gcb.14537](https://doi.org/10.1111/gcb.14537).

Stubbington, R., England, J., Wood, P.J., and Sefton, C.E.M., 2017, Temporary streams in temperate zones: recognizing, monitoring and restoring transitional aquatic-terrestrial ecosystems: *Temporary streams in temperate zones: Wiley Interdisciplinary Reviews: Water*, v. 4, p. e1223, doi:[10.1002/wat2.1223](https://doi.org/10.1002/wat2.1223).

USDOD, and USEPA, 2015, Clean water rule: definition of "waters of the United States: *Federal Register*, v. 80, p. 37054–37127.

Walsh, R., and Ward, A.S., 2019, Redefining clean water regulations reduces protections for wetlands and jurisdictional uncertainty: *Frontiers in Water*, v. 1, p. 1, doi:[10.3389/frwa.2019.00001](https://doi.org/10.3389/frwa.2019.00001).

Warix, S.R., Godsey, S.E., Lohse, K.A., and Hale, R.L., 2021, Influence of groundwater and topography on stream drying in semi-arid headwater streams: *Hydrological Processes*, doi:[10.1002/hyp.14185](https://doi.org/10.1002/hyp.14185).

Welhan, J.A., 2006, Water balance and pumping capacity of the lower portneuf river valley aquifer, Bannock County, Idaho: , p. 36.

White, W.N., 2013, A Method of Estimating Ground-water Supplies Based on Discharge by Plants and Evaporation from Soil: , p. 133.

Chapter 4. Questions for Future Work

4.1. Introduction

In the previous chapters of this thesis, we have tried to answer several questions relating to spatial and temporal patterns of stream drying. However, a single thesis can only answer so many questions. Here we explore two questions that we believe need more work to fully answer: What *nested* spatial structures exist in patterns of stream drying? and What are the hierarchical drivers of stream drying *within* a watershed? We also explore some of the technical improvements that are needed for the field to move forward.

4.2. What *nested* spatial structures exist in stream drying?

Mathematically, the spatial models we created in chapter 2 have ranges as small as 87 m to as large as 7,354 m. We hypothesize that this observed variability in the estimated ranges is a result of the multiple sills and ranges exhibited by the empirical toregram (Figure 4.1). These observations suggest that there may be nested spatial structures within our stream drying data that may be the result of multiple drivers, each driving stream drying on a different scale.

Nested spatial structures are not new to hydrology. A recent study on geochemical patterns revealed that several chemical concentrations exhibited nested spatial structures suggesting that both fine-scale patchiness and broad-scale trends existed in the watershed (McGuire et al., 2014). Similarly, Gendaszek et al. (2020)

produced a torgegram with three nested spatial structures, and thus three ranges when kriging for stream drying.

The SSN package, which we used to perform the intense mathematics involved in making a torgegram, allows for nested models as long as the nested models in question are of different types (e.g. we can use one tail-up model and one tail-down model, but not two tail-up models). Because stream drying can take place only in the stream, and water in Gibson Jack Creek flows downstream, not upstream, we believe a tail-down model would not reflect the physical spatial structure of stream drying. We hypothesize that a model with multiple tail-up shapes, or a model with multiple Cartesian shapes would best model the empirical torgegram. Thus, further research on the spatial structures of stream drying can be more easily facilitated if we prioritize the inclusion of nested tail-up models in the SSN package. If nested models were more completely implemented in the SSN package, we could test our hypothesis by comparing results using models that use both tail-up and Cartesian distances with models that use only tail-up or only Cartesian distances.

4.3. What are the hierarchical drivers of stream drying *within* a watershed?

To define the hierarchical drivers of stream drying on watershed and subwatershed scales, we make two suggestions. First, we need to more thoroughly explore the possibility that meteorological variables vary at fine spatial scales. Like many studies, we assumed that meteorological variables were relatively homogeneous throughout the Gibson Jack watershed despite it spanning ~500 m in elevation and

despite experiencing storms that only affected part of the watershed during the course of this thesis work. This could be remedied by using sensors to measure light intensity at fine scales, rain gauges to measure precipitation variability within a watershed, and remote sensing to measure variability in snow depth, as just three possible examples. With this data, we might be able to explain more of the spatial stream drying patterns that this thesis was unable to explore, and that is often assumed to be negligible at subwatershed scales.

Secondly, we need more fine-scale studies, like this one, in a variety of watersheds. One of the hazards presented by characterizing small-scale drivers is that they may not be uniformly important, meaning that small-scale drivers in one watershed may not be important drivers in another watershed. Hammond et al. (2021) acknowledged this hazard when shifting from continental to regional scales by identifying important variables for each separate ecoregion. Indeed, the lack of a uniform hierarchy of subwatershed drivers may be the reason for the difference in findings between small-scale studies. By performing more small-scale studies, like this one, in a variety of watersheds, we may be better able to identify how drivers vary across regions and within watersheds. We may even find that the ecoregions Hammond et al. (2021) used do not adequately separate watersheds for the purpose of determining drivers of stream drying.

4.4. Suggested Technical Improvements

In addition to tackling these two scientific questions, we have identified three critical technical limitations to the study of spatial patterns of stream drying that we

highlight below, including the future of the STARS and SSN software, the accurate delineation of the geomorphic channel network, and the accurate determination of thresholds for interpreting wet or dry conditions using STIC sensors.

4.4.1. The Future of STARS and SSN

The use of the SSN package requires a .ssn (“dot-S-S-N”) object that can be created using the Spatial Tools for the Analysis of River Systems (STARS) toolbox available for ArcMap versions 6 and later. The methods for using STARS are provided in appendix 3 of this thesis. Though this process worked for us, STARS is quickly becoming obsolete as the ESRI community moves to more advanced versions of ArcPro.

One possible solution to this risk of obsolescence is to convert the STARS scripts from Python 2 to Python 3, potentially enabling the scripts to run in ArcPro. The hazard with this option is the large time commitment involved as well as the potential compatibility issues between some of the required supporting software for STARS such as PythonWin. Converting the script may require advanced programming skills as well as a deep understanding of how ArcPro operates and was beyond the scope of this thesis.

Another possible solution is the continued development of the OpenSTARS R package (Kattwinkel et al, 2020). Unfortunately, the package did not work for us when we tried it in early 2021, but recent revisions may make the package a viable option for future studies involving toregrams.

4.4.2. Accurate Channel Network Maps

In our statistical analysis, we relied heavily upon a channel network developed from a digital elevation model (DEM). However, this channel network did not perfectly match our field observations. This created two problems for us. First, the GPS points we had taken for each of our STICs occasionally indicated a location that was not located within the stream corridor. This was particularly a problem for the 2020 location ST3-1 (for which the derived channel network did not extend far enough up the watershed) and the 2021 location MT2-11 (for which the derived tributary outlet did not align with the observed one). Second, the digital channel network identified multiple tributaries where there were none observed in the field. These theoretical tributaries were sometimes predicted as wet by the stream models, which artificially decreased the accuracy of our models.

Field validation of the channel network would improve this accuracy without requiring additional dynamic flow data. As future work is planned for Gibson Jack, we recommend that GPS data is collected along the channel network to digitize it, rather than deriving it using a DEM. Doing so will require a substantial effort, but we believe that the accuracy provided by such a map would make it worthwhile. Further, these limitations are unlikely to be limited to the Gibson Jack watershed, and especially in watersheds underlain by carbonates, a field validation of the geomorphic channel network ought to be conducted.

4.4.3. STIC Threshold Determination and Challenges

In the creation of this thesis, we developed a method for determining STIC thresholds that we believe is defensible, but it relies heavily on the assumption that the

STIC threshold for a given sensor is consistent over time. This assumption is not always true and may have led to occasional misinterpretations. Additionally, 13% of 2020 STICs and 37% of 2021 STICs could not be consistently interpreted using our simple threshold methods, in which case we relied upon field observations to validate our choices. If field observations are limited, this could limit the interpretation or reliability of future STIC-based stream drying data.

We recommend that future studies that use STICs record frequent field observations as that is sometimes the only way to interpret data from STICs. We also recommend that researchers consistently calibrate STICs both before and after deployment. When calibrating the STICs, it may be helpful to use more than four calibration standards to constrain the model fit and decrease the standard error in the intercept calculation that is presented in this thesis.

4.4. Conclusions

The questions we proposed in sections 4.2 and 4.3 build upon the work presented in chapters 2 and 3 of this thesis and answer questions that we were unable to tackle in the past two years. We have also identified technical issues in section 4.3 that deserve to be addressed in the coming years to advance research on the spatial patterns of stream drying. We believe that progressing in these scientific and technical directions will further our understanding of stream drying and thus advance our ability to understand and solve future environmental problems.

4.5. Figures

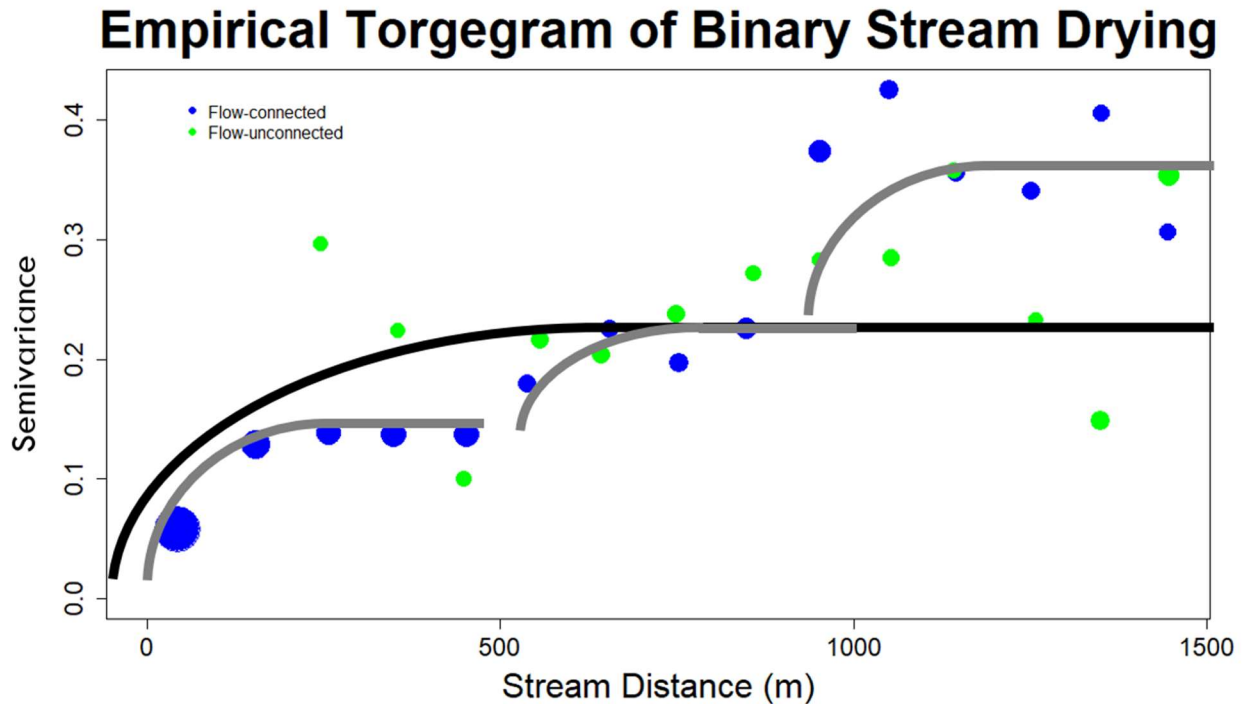


Figure 4. 1: Empirical torgegram of combined 2020 and 2021 data. The empirical torgegram shows three plateaus in grey: one at a range of ~100 m, one at a range of ~500 m, and a final one at a range of ~1,000 m. This was modeled as shown in black using an exponential tail-up model. These three plateaus may drive the variety of ranges across the different models.

4.6. References

- Gendaszek, A.S., Dunham, J.B., Torgersen, C.E., Hockman-Wert, D.P., Heck, M.P., Thorson, J., Mintz, J., and Allai, T., 2020, Land-Cover and Climatic Controls on Water Temperature, Flow Permanence, and Fragmentation of Great Basin Stream Networks: *Water*, v. 12, p. 1962, doi:[10.3390/w12071962](https://doi.org/10.3390/w12071962).
- Hammond, J.C. et al., 2021, Spatial patterns and drivers of nonperennial flow regimes in the contiguous United States: *Geophysical Research Letters*, v. 48, doi:[10.1029/2020GL090794](https://doi.org/10.1029/2020GL090794).
- Kattwinkel, M., Szöcs, E., Peterson, E., and Schäfer, R.B., 2020, Preparing GIS data for analysis of stream monitoring data: The R package openSTARS (S. Nedkov, Ed.): *PLOS ONE*, v. 15, p. e0239237, doi:[10.1371/journal.pone.0239237](https://doi.org/10.1371/journal.pone.0239237).
- McGuire, K.J., Torgersen, C.E., Likens, G.E., Buso, D.C., Lowe, W.H., and Bailey, S.W., 2014, Network analysis reveals multiscale controls on streamwater chemistry: *Proceedings of the National Academy of Sciences*, v. 111, p. 7030–7035, doi:[10.1073/pnas.1404820111](https://doi.org/10.1073/pnas.1404820111).

Appendix 1: Detailed Methods

A1.1. Introduction

In writing this thesis, we found methods that needed a detailed explanation. However, including the full explanation in the body of each chapter created impediments and confusion for the reader. To remedy the problem, we created this appendix. Here, the reader will find the detailed methods for our 2021 fieldwork, random forest analysis, receiver operating curves (ROCs), clustering analysis, and the Kruskal-Wallis test. Note that code for Rstudio is not provided in this appendix, but current versions can be found at https://github.com/CodeRThane/Kindred_Thesis_2022.

A1.2. Field Work

At each of our 2021 sites, we completed three in situ site assessments: we performed a pebble count, took geomorphic measurements, and estimated canopy cover. The pebble counts were conducted by first grabbing a pebble at random within arm's length of the STIC. We then measured the intermediate axis of the pebble and then discarded it away from the STIC to ensure it was not measured twice. This process was repeated 100 times at each site.

Additionally, we measured the geomorphic width and depth of the channel as defined by the presence of banks and vegetation. We also estimated canopy cover using a concave densitometer. We took four readings, one in each cardinal direction, then took an average of those readings. Because each canopy cover count was

measured out of a total of 96, we multiplied the average by 1.04 to get a percentage of canopy cover.

A1.3. Random Forest

Random forest models combine the simplicity of a decision tree with accuracy. Though random forests can be used to predict numerical values, we chose to focus on the classification capabilities of random forests. Decision trees, such as the one shown in Figure A1.1, classify data based on a series of yes or no questions. To build these trees, an algorithm performs bootstrapping, which is a process of randomly selecting data from a dataset. Importantly, bootstrapping allows for duplicate or repeated selections and typically relies on approximately two-thirds of the data given to it. The data that is not used to create a decision tree is sometimes referred to as the out-of-bag data, which is important when we assess the error of our model. From the bootstrapped data, the algorithm randomly selects a variable to divide the data, thus creating a branch or layer in the decision tree. The algorithm then randomly selects another variable that guides the second branch or layer of the decision tree. The algorithm randomly selects variables to create additional layers of the decision tree until the tree has a specified number of layers. In R, we specify this number with the “mtry” argument.

The algorithm generates decision trees by repeating the process above until it creates a “forest” of a specified size. In R, we specify this number with the “ntree” argument. Once the forest is created, the trees can be used to classify the out-of-bag data. When classifying the out-of-bag data, each sample is run through every tree created by the algorithm that did not use that sample to create the tree. Like a

democratic body, each tree indicates the appropriate classification, and the classification that receives the most “votes” is reported as the outcome of the analysis. By generating and using several decision trees, the random forest method ensures that a single inaccurate tree does not ruin the classification method. We can then calculate an error rate for the out-of-bag samples as the number of incorrectly classified samples divided by the total number of out-of-bag samples.

We used 17 variables in our random forest analysis (see Table A1.1). Not all of these variables are independent of each other. Drainage area, elevation, and upstream distance are all correlated in Gibson Jack due to the mountainous nature of the watershed. Lithological variables (i.e., carbonates, colluvium, and metasedimentary rocks) are also correlated with each other, as are the soil variables (e.g., silt loam and loam). For this reason, we ran the random forest twice. The first time, we ran it with all the variables regardless of how correlated they were (Figure A1.2). After determining a hierarchy of variables, we removed all but the most important variable in each of the correlated sets (e.g., we only used drainage area because it was more important to our random forest than elevation and upstream distance).

We used a forest containing 3,000 trees. We chose to use that many trees by running a random forest analysis using 5,000 trees and calculated the out-of-bag error rate after each tree was added. We then plotted the out-of-bag error rate associated with each additional tree and found that the error rate stabilized before 3,000 (Figure A1.3) indicating that we did not need a larger forest. Each decision tree used 3 variables. This number was determined by running the random forest analysis 10 times on the dataset that did not include correlated data, using a different number of variables

each time. We found that using three variables resulted in a model with the smallest out-of-bag error rate.

A1.4. Confusion Matrices, ROCs, and AUCs

A confusion matrix and a receiver operating curve (ROC) can reveal the accuracy of binary spatial models. Confusion matrices use a leave-one-out cross-validation method to evaluate the number of correct predictions a particular model produces. However, predictive models, such as kriging, often depend heavily upon thresholds that differentiate one category (e.g. wet) from another (e.g. dry). As the choice in threshold greatly impacts the confusion matrix, we can generate many confusion matrices, each with a different threshold, to fully explore the success of a model. To summarize all of these confusion matrices, we use the ROC which plots *sensitivity*, or the proportion of accurate wet predictions, on the y-axis and *specificity*, or the proportion of dry predictions that are accurately predicted, on the x-axis ([Altman and Bland, 1994](#)). The curve represents the number of points predicted correctly using a particular threshold. We can quantify the success of several thresholds using the percent Area Under the Curve (AUC).

Cluster Analysis

A cluster analysis seeks to divide a dataset into a set number of groups, determined by the user, based on the graphical distance between the data points. The algorithm performs a three-step process to form these groups. First, it places a set number of points at random locations on the graph. In step 2, the algorithm groups the data points based on which ones are closest to the random points set in step one. In

step three, the algorithm calculates the middle (average) of each group. The algorithm then repeats steps two and three using the average points rather than randomly placed points created in step one. The cluster analysis is complete if the groups remain unchanged after this iteration, otherwise, the algorithm continues to repeat steps two and three until a steady-state is achieved. We can automate this process using the *kmeans* function in R. When doing this, we specify the number of randomly generated points, and thus the number of clusters, using the “centers” argument.

In some cases, such as ours, where we use more than just two variables to classify data, a cluster analysis begins with a principal components analysis (PCA). A PCA allows us to plot data with more than three variables by creating a series of principal components (PC) composed of some combination of the variables in the data. By plotting wet and dry points on a graph with PC1 on the x-axis and PC2 on the y-axis, we can see which PC, and thus which drivers best predict stream drying.

A1.5. Kruskal-Wallis Test

This is a method that tests the null hypothesis that there is no difference between the data in different groups. The test starts by assigning rank values to the data with the smallest value getting a one and the largest value getting the number of observations, N. The test then sums the rank values (R) in each group and then calculates the Kruskal-Wallis statistic, sometimes referred to as H:

$$H = \frac{12}{N(N+1)} \sum R^2 - 3(N+1)$$

If H is less than a threshold value (α ; often 0.05), then we reject the null hypothesis. In practical terms, this means that we infer that the groups differ from one another.

In applying this method, we tried using all 17 variables that we used for the random forest analysis. However, many of them violated the assumption of independent data points, that is, many of the variables were autocorrelated with each other. We chose to only use this method for each variable that exhibited a pure nugget in its empirical variogram, indicating that no autocorrelation was present (Figure A1.4). This left only the following variables for the analysis: colluvium, slope, loam, silt loam, pebble count median, canopy, and trees.

A1.7 Figures

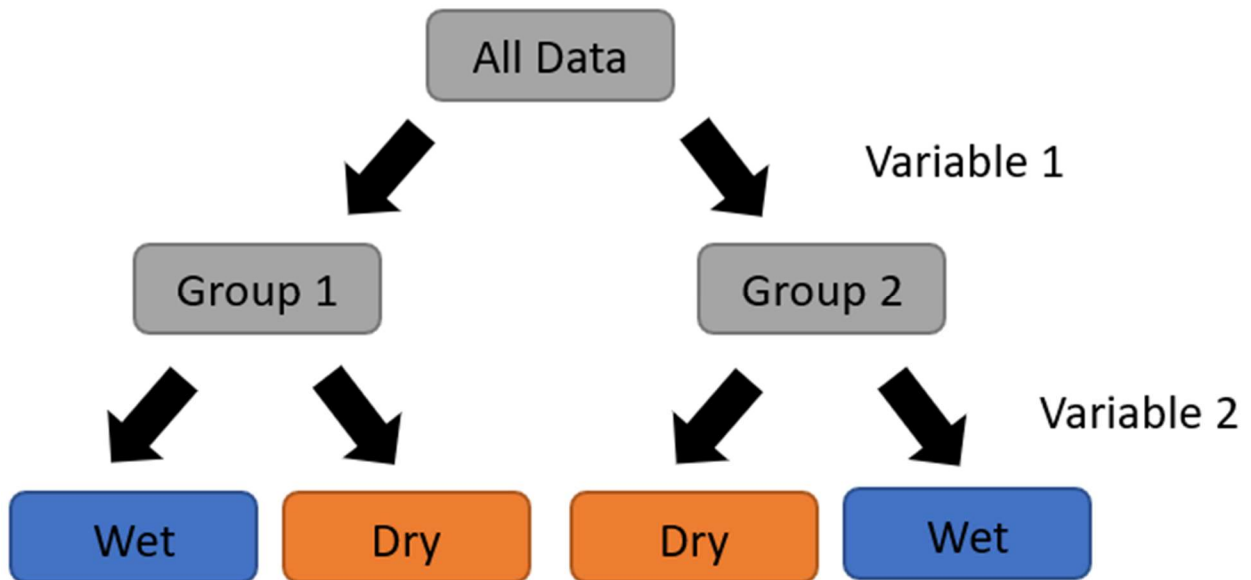


Figure A1. 1: Example of a decision tree with three layers. The data run through this tree will be split into two groups based on a first randomly selected variable. The groups will then be split into wet and dry groups based on a second randomly selected variable.

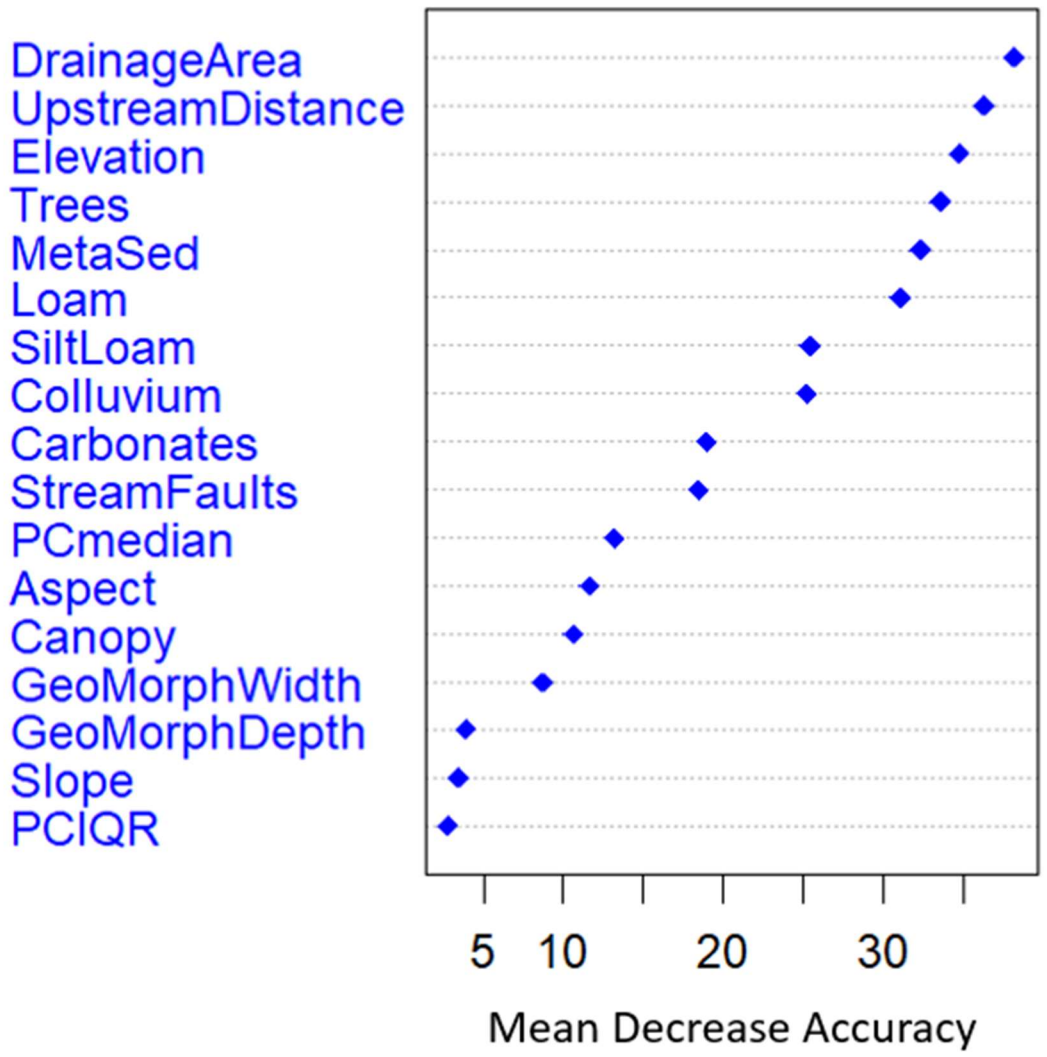


Figure A1. 2: Results from the first round of a random forest analysis. From these results, we chose to discard upstream distance and elevation because they are correlated with drainage area. Similarly, we decided to discard silt loam because it is correlated with loam, and both colluvium and carbonates because they are correlated with metaseds.

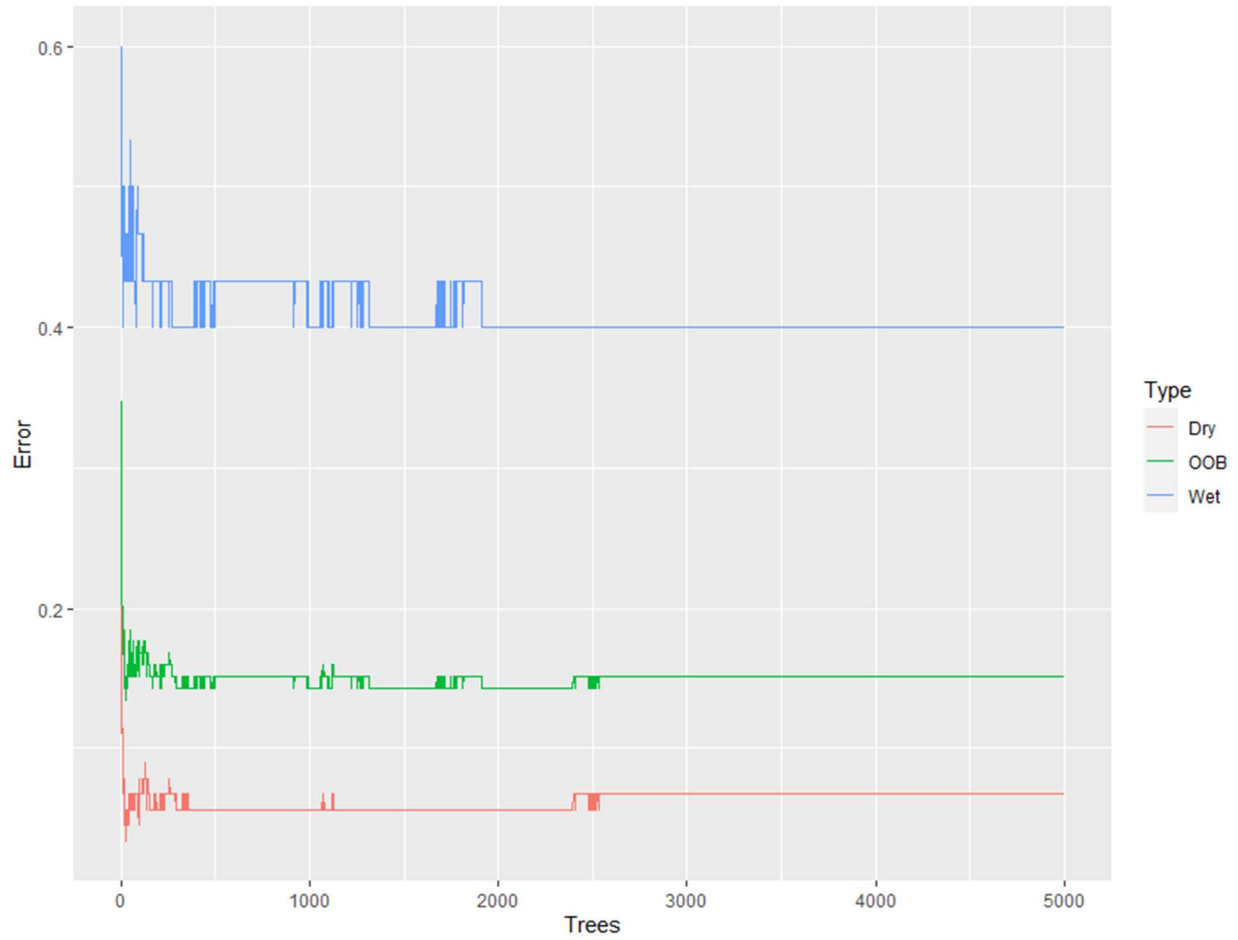
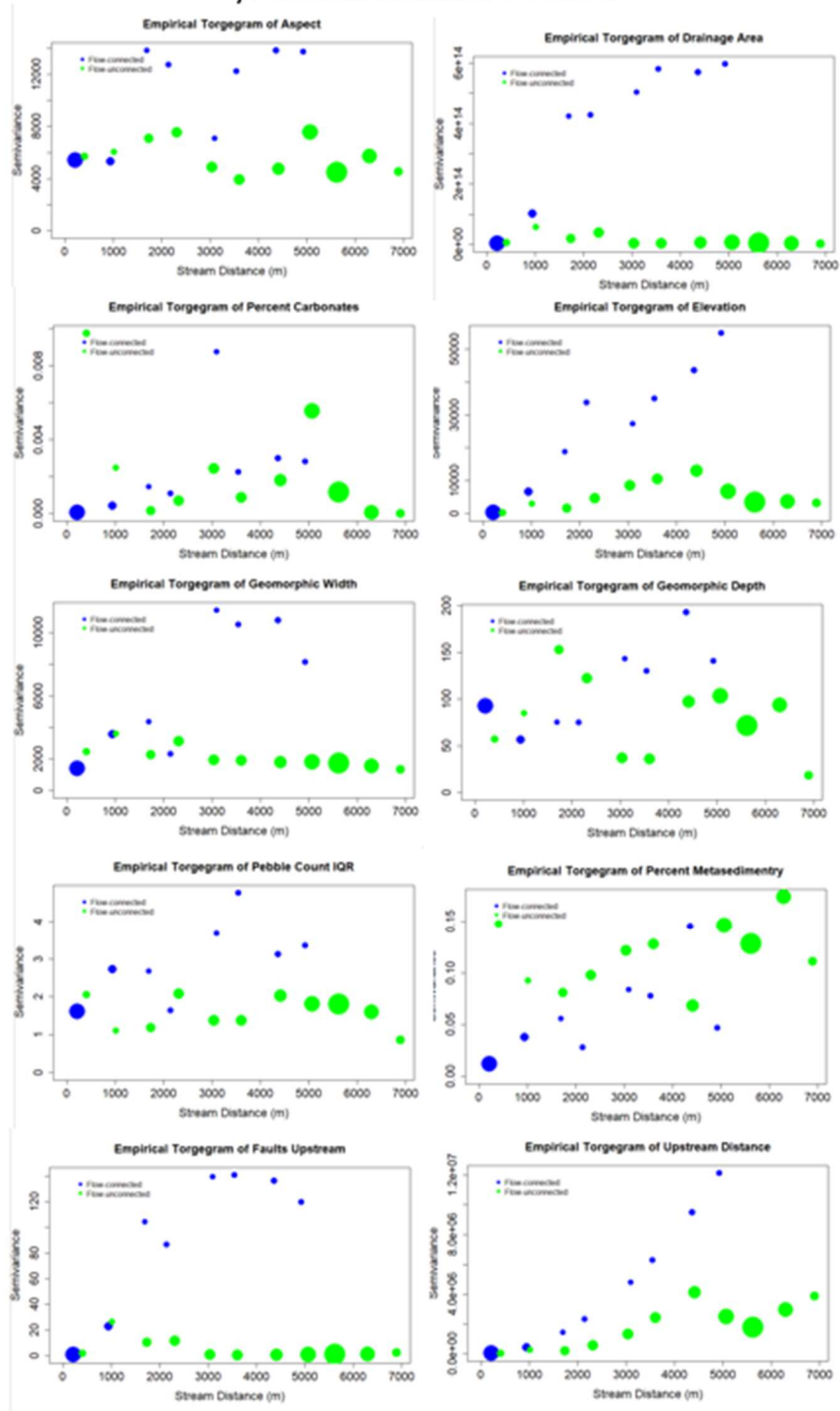


Figure A1. 3: A plot of the error rates as we add additional trees. The red line indicates the error rate of dry sites, the blue line indicates the error rate when classifying wet sites, and the green line indicates the overall out-of-bag error rate. We chose to include only 3,000 trees because the error rate does not change with more trees.

A) Autocorrelation Present



B) No Autocorrelation

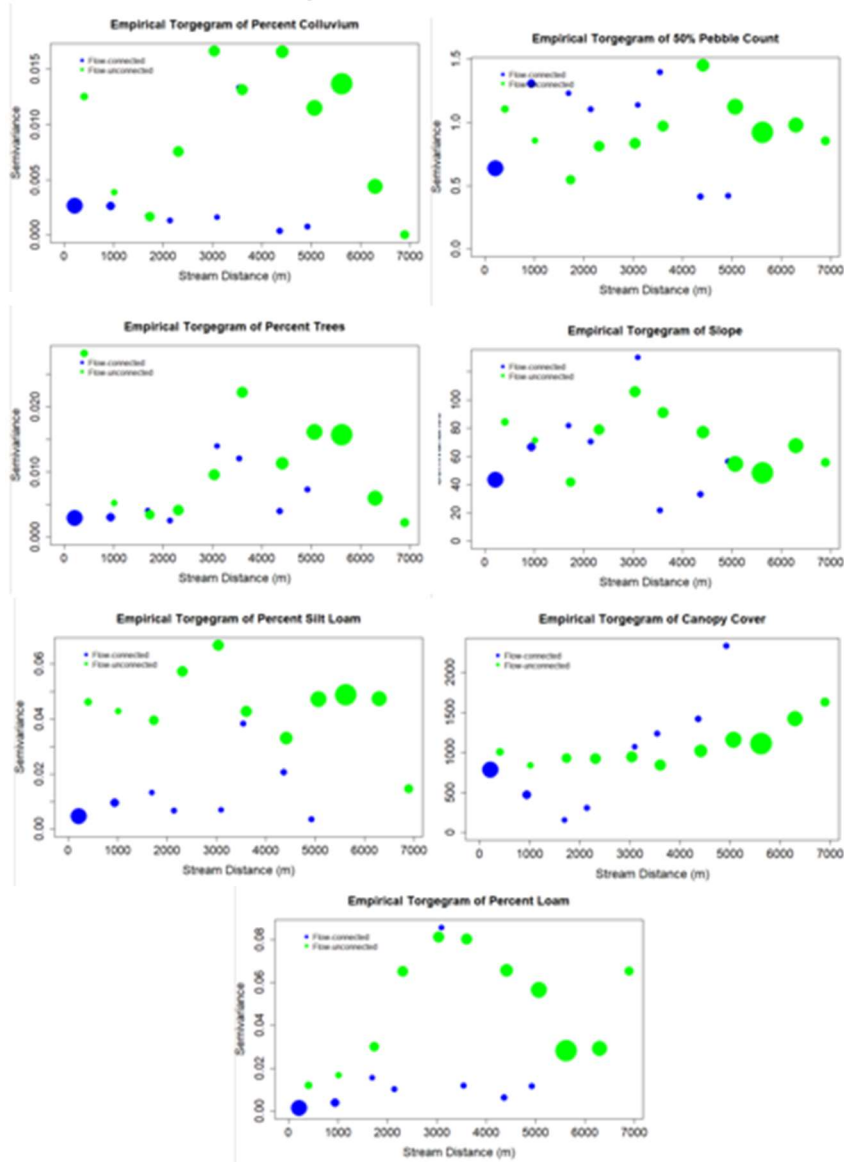


Figure A1. 4: Empirical torgegrams for each of the 17 candidate variables for the Kruskal-Wallis test. Ten of the torgegrams (A) indicated that autocorrelation was present, so statistical analysis, such as the Kruskal-Wallis test and calculating a mean, would produce biased results. We chose to only run the test on the seven variables that demonstrated no autocorrelation (B) to ensure that we met the assumptions of the test.

A1.6. Tables

Table A1.1. Variables used in the random forest analysis.		
Name	Units	Alias
Drainage Area	m ²	Drainage Area
Carbonates	percent	Carbonates
Colluvium	percent	Colluvium
Metasedimentary Rocks	percent	Metaseds
Loamy Soils	percent	Loam
Silt Loam Soils	percent	Silt Loam
Tree Cover	percent	Trees
Slope	degrees	Slope
Aspect	degrees	Aspect
Elevation	ft	Elevation
Upstream Distance	m	Upstream Distance
Median of Pebble Count	cm	MPC
Interquartile Range of Pebble Count	cm	IQRPC
Geomorphic Depth	cm	Depth
Geomorphic Width	cm	Width
Percent Canopy Cover	percent	Canopy Cover
Faults Crossing the Stream	count	Faults

A1.7. References

- Altman, D.G., and Bland, J.M., 1994, Statistics Notes: Diagnostic tests 3: receiver operating characteristic plots: *BMJ*, v. 309, p. 188–188, doi:[10.1136/bmj.309.6948.188](https://doi.org/10.1136/bmj.309.6948.188).
- Breiman, L., 2001, Random forests: Machine learning, v. 45, p. 5–32.
- Frades, I., and Matthiesen, R., 2010, Overview on Techniques in Cluster Analysis, *in* Matthiesen, R. ed., *Bioinformatics Methods in Clinical Research*, Totowa, NJ, Humana Press, *Methods in Molecular Biology*, v. 593, p. 81–107, doi:[10.1007/978-1-60327-194-3_5](https://doi.org/10.1007/978-1-60327-194-3_5).

Appendix 2: Detailed Results

A2.1. Introduction

In writing this thesis, we have collected more data, and run more analyses than we could include in the body of the thesis. To remedy the problem, and publish our data, we created this appendix. Here, the reader will find 2020 STIC data, our 2021 site characterization data; the thresholds we used to interpret STIC measurements; the kriging models we generated from 2020, 2021, and combined datasets; and the cluster analysis we performed on 2021 data.

A2.2. 2020 STIC data

The presence/absence charts from 2020 and the predictions across the watershed are included here in Figure A2.1.

A2.3. Field data from 2021

The results from the summer 2021 field season, and from site characterization in GIS are presented here in Tables A2.1-3).

A2.4. Thresholds

The lux thresholds chosen for each STIC are included here in Table A2.4.

A2.5. Models

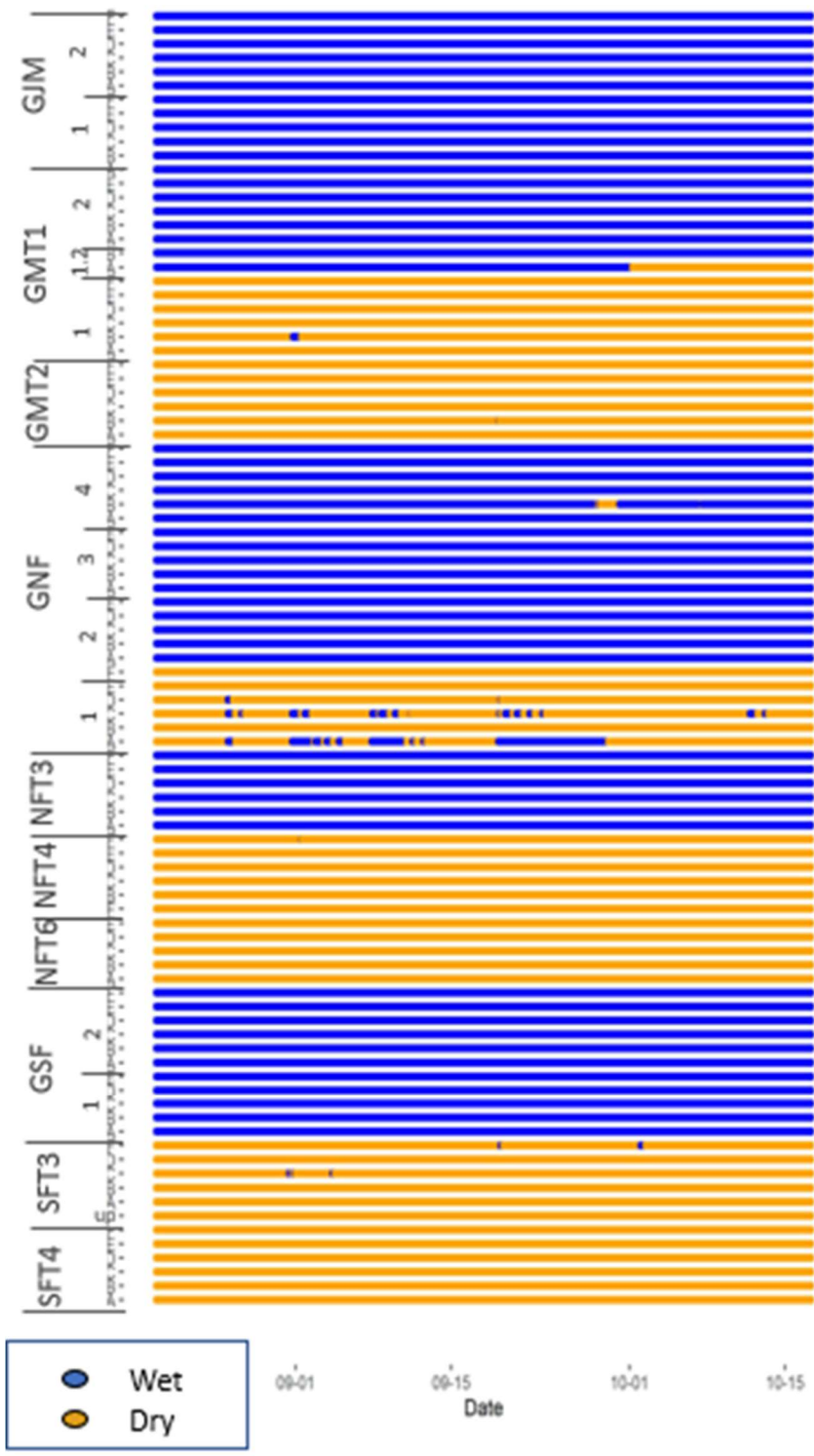
Included in this appendix are tables containing every model we generated (Tables A2.5-7) and a summary of said models (Table A2.8). Additionally, semivariograms and toregrams from both empirical data and the best models are included here (Figures A2.2 and A2.3).

In 2020, the best Cartesian model and the best tail-up model performed similarly with both having high AUCs and similar ranges despite the differences in shape and explanatory variables. In 2021, the empirical semivariogram and empirical toregram were quite different from each other with the semivariogram showing a need for detrending and the toregram showing a pure nugget. This thesis is more focused on the differences between semivariograms and toregrams that use both the 2020 and 2021 data, but future work might further explore our data from individual years.

A2.6. Cluster Analysis

Based on the elbow method, we chose to separate our data into 3 classes. A graph showing the three clusters is available in this appendix (Figure A2.4).

A2.7 Figures



B

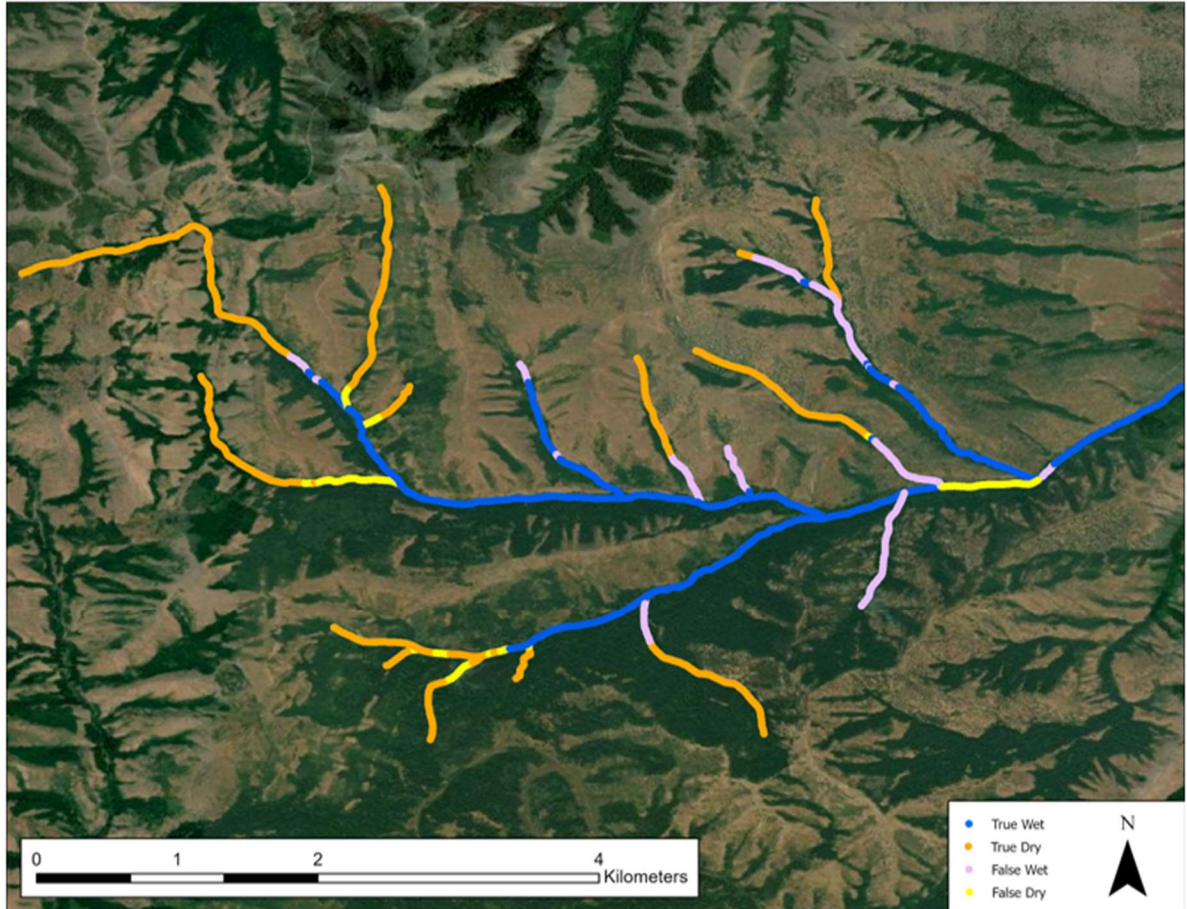


Figure A2 1: Plot indicating presence/absence of water at 92 sites throughout the 2020 season (A) and map showing predictions of binary seasonal streamflow permanence across the watershed compared to observations made on Aug 29-30 (B). These predictions were made using a tailup model with the Mariah shape that used elevation as an explanatory variable. Note that this map is identical to Figure 2.6B because all 2020 sites had seasonal stream permanence values that matched the recording made on Aug 29-30 of that year.

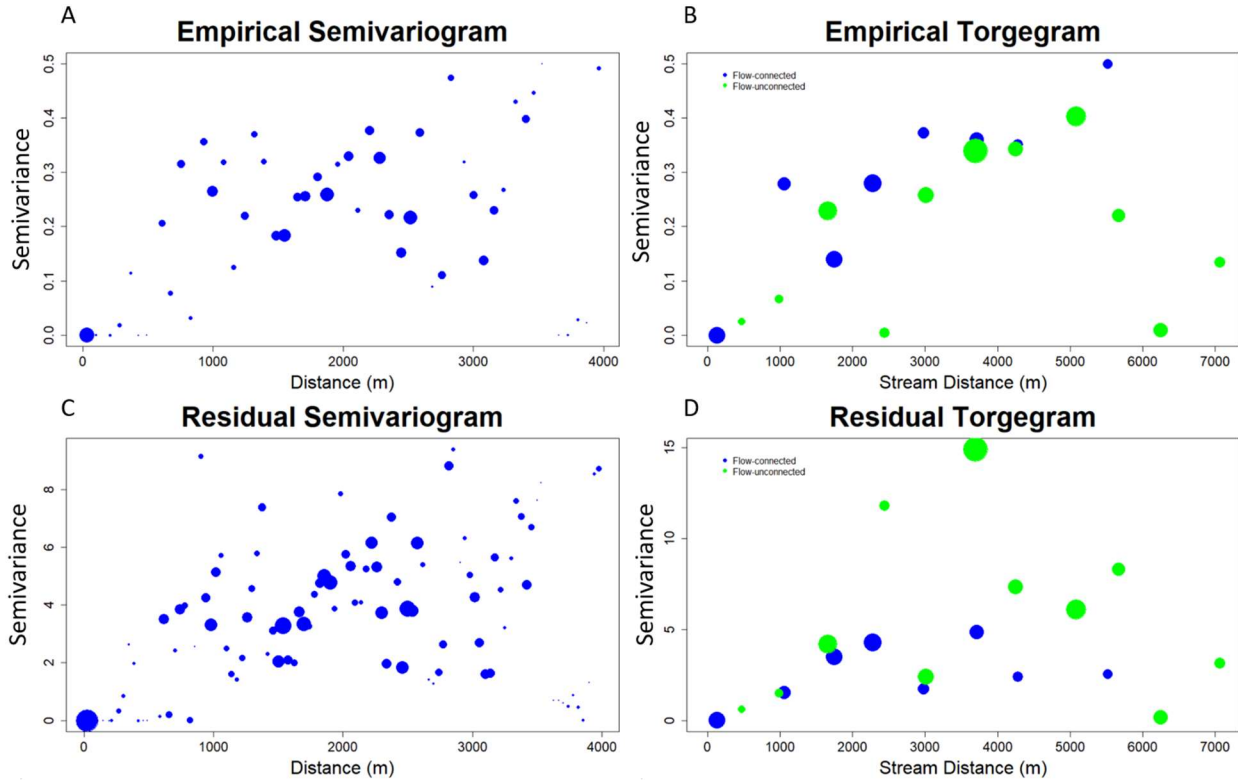


Figure A2 2: Semivariograms and torgograms created from 2020 data. The empirical semivariogram (A) and torgogram (B) are shown. Additionally both the semivariogram from the best cartesian model (C) and the torgogram from the best tail-up model (D) are shown. The best cartesian model was spherical in shape and used silt loam as an explanatory variable. The best tail-up model had a Mariah shape and used elevation as an explanatory variable.

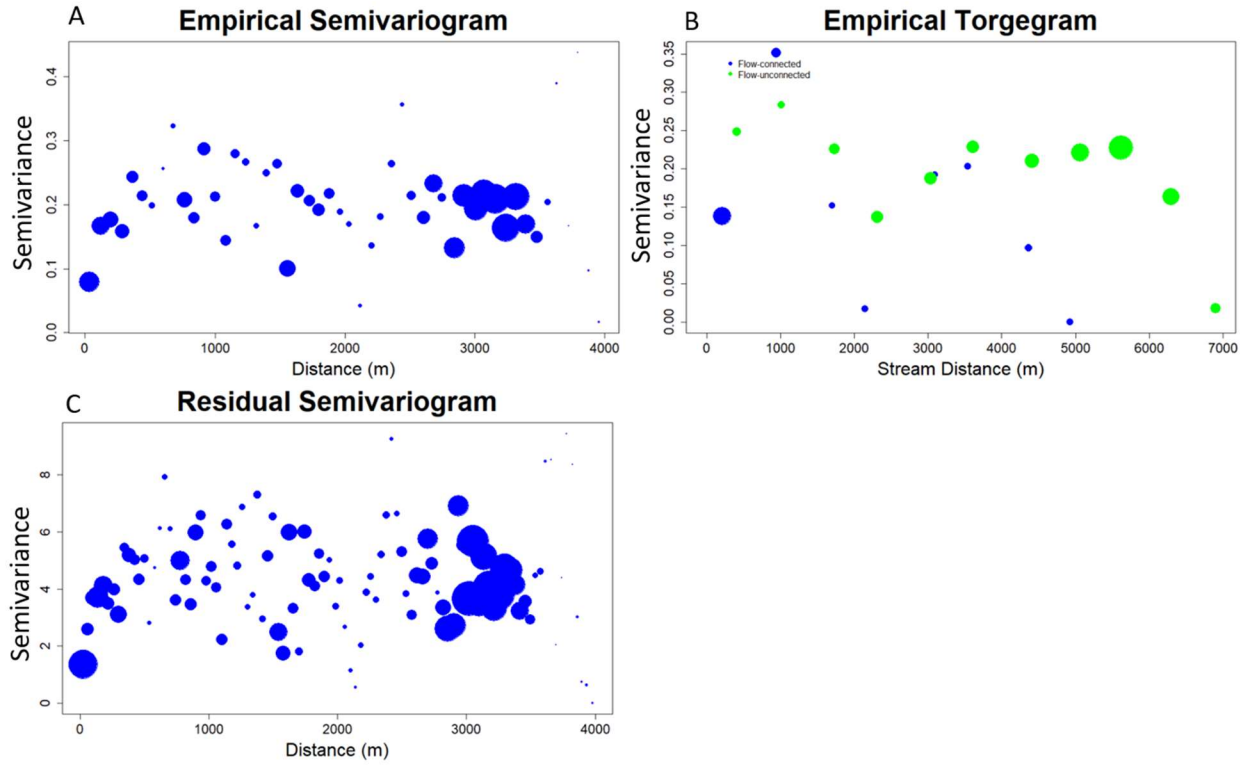


Figure A2 3: Semivariograms and Torgegrams created from 2021 data. The empirical semivariogram (A) and torgegram (B) are shown. Additionally the semivariogram from the best cartesian model is shown (C). We do not show the torgegram from the best tail-up model because the empirical torgegram revealed a pure nugget.

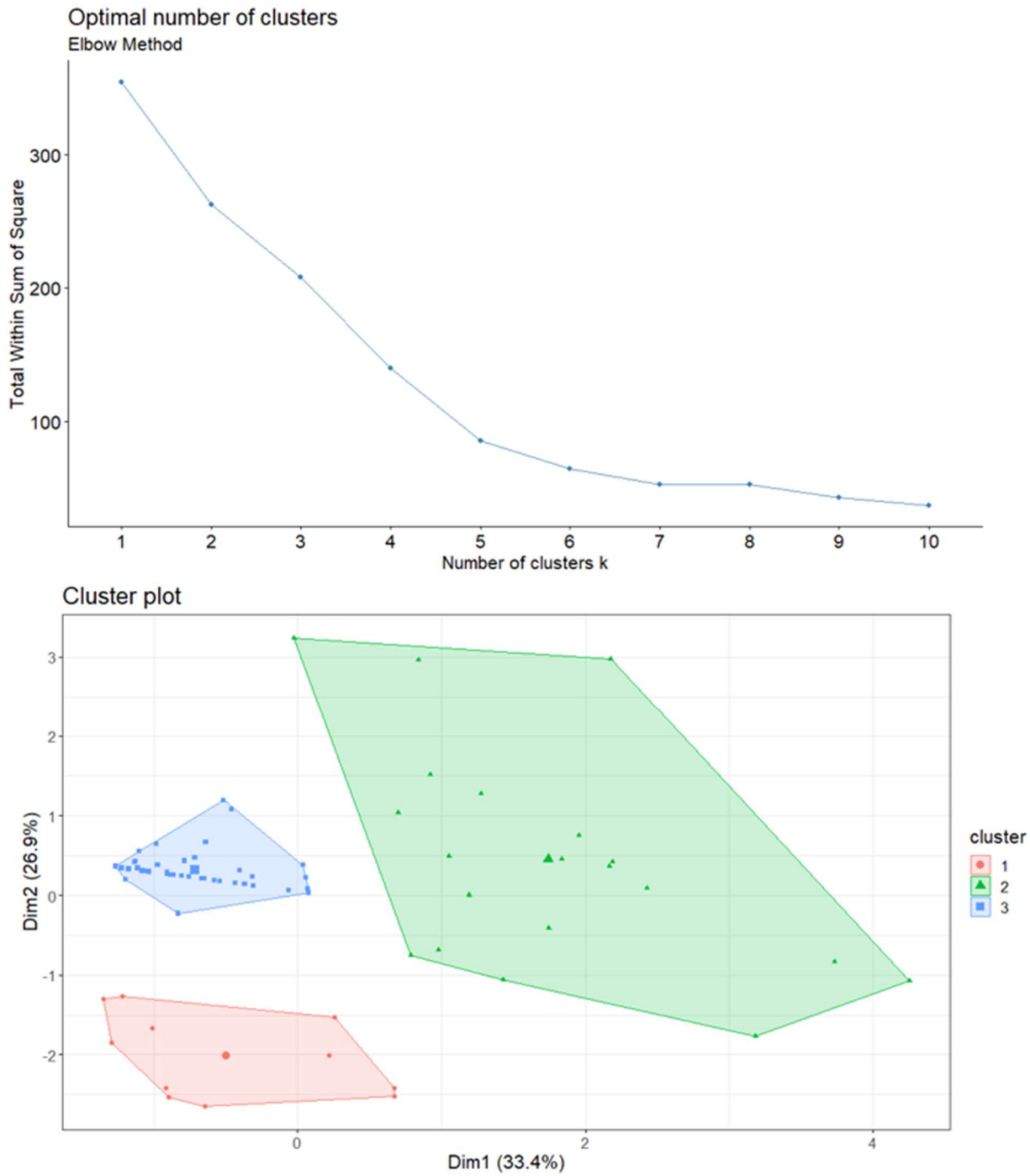


Figure A2 4: A graph of the WSS elbow method (A) and of the three classes identified by the cluster analysis (B).

A2.8 Tables

Table A2.1. Pebble count results in centimeters.

Site																		
NF01	<0.1	<0.1	0.6	<0.1	1.4	<0.1	1.9	3.5	<0.1	0.7	<0.1	<0.1	1.6	<0.1	0.8	<0.1	<0.1	
NF02	1.9	<0.1	1.2	1.1	3.2	<0.1	0.9	3.2	<0.1	1.4	<0.1	0.4	0.7	1.1	2	1.7	2.1	
NF03	0.4	<0.1	<0.1	0.8	1.4	<0.1	<0.1	<0.1	2	<0.1	<0.1	<0.1	2.3	<0.1	<0.1	2.1	<0.1	
NF04	1.5	3.8	2.8	11.7	0.5	1	1.6	0.8	0.6	1.5	0.3	0.6	3.7	1	0.9	1.8	<0.1	
NF05	0.1	0.5	8.5	25.5	7.3	2.5	3.4	0.5	2.4	2.6	3.3	0.2	2	10.8	2.5	3.5	14	
NF06	<0.1	4	8.6	1.3	1.3	0.2	3.7	17	9	>30	0.4	6.4	2.3	2.3	3.5	1.4	1.4	
NF07	0.4	4.8	3.3	2	0.6	1.5	1.3	1.2	2.8	0.8	3.6	1.9	1.1	2.1	0.4	1.3	<0.1	
NF08	4.2	7.3	9.2	6.8	1.5	2.4	12.6	5.2	>30	>30	5.2	3.3	2.3	11	3.6	5	10.6	
NF09	1.3	1.2	1.1	2.2	0.6	1.2	2.3	1.3	1	0.8	1.1	1.1	1.6	0.7	1.7	1.2	1	
NF10	2.4	0.9	0.5	0.7	11.6	0.9	10.6	0.9	0.9	4.7	2.1	0.8	1.3	2.2	3.1	1.8	1.5	
NF11	1.6	4.3	2.8	4.8	1.3	1.6	2.2	3.3	3.4	4.1	7.6	1.2	1	1.3	1.9	2.2	1.1	
NF12	27.4	7.3	27.5	17.5	1.6	2.8	0.6	8.2	0.5	2.3	3.1	3	1.1	0.9	3.3	8.3	1	
NF13	13.9	16.7	7.9	3.9	4.4	10.5	9.7	3	4.2	2.1	9.6	3.4	2.2	4	12.9	2.3	11.1	
NF14	9.3	14.8	10.3	10.5	8.9	11.4	3.8	10.1	4	3.9	10.4	4	3	3	2.9	5.1	3	
NF15	2.1	2.1	2.1	1.9	1.8	3.2	2.8	2	1.7	2.3	2.4	2.1	4.9	1.8	2.4	1.7	2.8	
NF16	0.9	3.9	5.1	4.1	6.6	2.3	1.3	2.6	0.8	2.8	<0.1	1.7	2.8	3.4	4.5	1	<0.1	
NF17	7.5	5.4	1.7	7.1	0.7	0.5	1.5	3.6	11.3	2.7	1.5	2	17.1	1.7	1.8	3	3	
NF18	3.3	3.3	2.8	4.1	2.5	0.6	1.3	1.2	1.9	3.6	4.6	2.1	0.6	1.1	8.1	1.7	2.9	
NF19	1.7	1.5	1.7	3.2	2.6	2.5	<0.1	8	2.1	2.3	1.2	5.4	2.3	<0.1	3.8	2.9	2.7	
NF20	<0.1	3	1.7	<0.1	1.9	4.9	4	<0.1	2.9	<0.1	2.1	1.9	2.7	3.3	3.1	5.6	2.4	
NF21	1.8	2.7	4.6	2	3	2.1	8.9	4.4	4.7	1.1	13.1	4.7	0.9	3.8	4.5	2.7	2.9	
NF22	3.6	0.9	3.9	2.3	1.6	0.9	7.2	2.6	0.7	1.2	2.3	0.8	2.9	4.1	4.3	1.3	3.5	
NF23	>30	2.9	9.9	2.6	10.9	3	2.3	1.9	2	2	5.4	1.7	19.3	1.9	1.8	11	1.1	
NF24	2.4	2.1	2.3	2.4	4.1	1.6	1.1	1.3	2.2	1.9	2	3.1	2.4	2	2.3	1.9	0.9	
NF25	3.5	<0.1	0.3	1.3	1.4	4	8	3.2	1.4	1.6	2	3	3.3	2.4	1.4	2.5	2.2	
NF26	3.4	3	4.1	2.9	3.4	1.8	1.5	0.9	2.1	1.1	2.6	3	2.6	2	2.1	4	2.8	
NF27	3.1	2.1	1.9	1.2	3.5	7.6	5.8	3.8	1.1	1.2	0.4	1.2	1.1	0.9	1.2	0.4	0.6	
NF28	13	10.2	2.3	0.9	1.2	1.2	4.8	1.6	2.2	1.1	1.2	1.1	1.4	0.8	0.8	0.7	2.2	
MS29	<0.1	<0.1	<0.1	<0.1	<0.1	<0.1	<0.1	<0.1	0.8	<0.1	1.9	<0.1	<0.1	<0.1	<0.1	<0.1	0.8	
MS30	4.7	<0.1	<0.1	1.3	2.1	<0.1	0.5	0.3	1.3	1.7	1.1	1.8	0.2	1.6	<0.1	1.3	0.6	
MS31	0.1	<0.1	1.2	0.1	0.1	16.1	0.2	<0.1	<0.1	0.7	5	<0.1	0.8	0.1	8.3	<0.1	0.4	
MS32	<0.1	3.7	0.8	<0.1	<0.1	<0.1	0.6	1.3	1.1	3	<0.1	3.5	1.2	1.3	2	1.2	0.9	
MS33	8.5	<0.1	5.9	<0.1	<0.1	1.1	1.6	9.9	<0.1	1.3	<0.1	3.2	7.3	<0.1	<0.1	0.6	0.8	
MS34	<0.1	<0.1	<0.1	<0.1	<0.1	<0.1	<0.1	<0.1	<0.1	<0.1	<0.1	<0.1	<0.1	<0.1	<0.1	<0.1	<0.1	
MS35	<0.1	<0.1	<0.1	<0.1	<0.1	<0.1	<0.1	<0.1	<0.1	<0.1	<0.1	<0.1	<0.1	<0.1	<0.1	<0.1	<0.1	
MS36	<0.1	<0.1	<0.1	<0.1	<0.1	<0.1	<0.1	<0.1	<0.1	<0.1	<0.1	<0.1	<0.1	<0.1	<0.1	<0.1	<0.1	
MS37	<0.1	<0.1	<0.1	<0.1	<0.1	<0.1	<0.1	2	5.1	0.9	0.6	<0.1	<0.1	<0.1	<0.1	1.8	<0.1	
MS38	1.7	2.9	<0.1	2.3	<0.1	<0.1	<0.1	<0.1	<0.1	1.7	<0.1	0.3	0.7	1.1	0.8	<0.1	3.5	
MS39	<0.1	1.6	<0.1	5.9	<0.1	<0.1	<0.1	<0.1	0.8	<0.1	1.5	<0.1	0.7	<0.1	<0.1	2.3	<0.1	
MS40	<0.1	<0.1	<0.1	<0.1	<0.1	3.9	<0.1	<0.1	<0.1	<0.1	1.2	<0.1	<0.1	<0.1	0.6	<0.1	<0.1	
MS41	2.3	6.6	3.8	4.3	2.1	4.8	5.5	1.5	6	5.5	4.1	3.2	1.3	2.3	4.5	2.7	4.4	
MS42	1.2	>30	5.3	2	3.2	7.4	7.5	2	2.3	5.7	3.5	2.1	8.4	16.2	3.3	2	2.2	
MS43	3.7	6.9	5.8	5.8	4	1.4	1.2	11.9	1.8	17.3	3.6	2.1	2.5	3.7	1	0.1	1.8	
MS44	22.3	2.4	7	1.1	0.4	6.3	12.3	4.9	1.5	2.2	27	7.4	0.2	1.4	9.2	14.5	8.7	
MS45	2.5	5.4	5.5	16.6	12.5	0.5	10.2	0.8	13	3.3	<0.1	2.4	2.5	1.7	2.8	17.4	2.7	

Table A2.1. (Cont.) Pebble count results in centimeters.																	
Site																	
NF01	<0.1	<0.1	<0.1	<0.1	2.7	1.4	<0.1	<0.1	3.1	<0.1	2.1	2.3	1.4	2.3	<0.1	1.4	<0.1
NF02	<0.1	<0.1	1.6	<0.1	<0.1	0.1	<0.1	2.6	2	0.6	1.9	1.7	1.2	1.1	0.7	0.6	<0.1
NF03	1.7	<0.1	<0.1	1	0.9	1.4	<0.1	0.8	<0.1	1.3	1.4	<0.1	<0.1	1.5	0.6	2.4	1.3
NF04	0.7	3.7	0.3	<0.1	0.1	2.9	3.5	0.4	0.9	2	7.1	0.2	10.1	8.4	0.9	2.6	2.7
NF05	1.3	0.5	<0.1	0.3	<0.1	1.4	0.2	1.8	8.9	3.3	0.7	0.4	3.1	4.2	1.4	<0.1	0.8
NF06	5.2	10	3.8	1.5	5.5	5	4	7	3.3	5.2	2.7	8.3	4.1	3.8	1.9	2.1	2.2
NF07	1	1.8	3.2	1.9	0.9	0.5	0.6	3.8	<0.1	1.7	2.5	2.1	<0.1	1.3	<0.1	<0.1	1.9
NF08	1.1	2.4	4	7.5	1.2	6.3	12.2	3.2	0.6	7.2	3.3	0.7	7.1	1.5	7.2	12.6	2.9
NF09	0.9	1	2.2	1.1	1.1	3.2	0.5	2.6	0.8	2.2	0.6	1.1	1.2	2.1	0.6	1.2	1.1
NF10	1.3	2.3	0.4	0.6	1	2.1	4.1	0.2	0.5	2.3	1.5	<0.1	5.3	1	8.5	8.3	<0.1
NF11	11.3	14.7	0.7	0.1	1.2	1.7	1.6	17.8	2.6	3.9	2.4	2.6	2.1	5	0.8	3.3	0.6
NF12	3.1	2.8	2.4	13.3	0.5	0.6	4.1	2.9	6	5.7	3.7	3.1	2.7	0.8	11.9	<0.1	12.1
NF13	3.7	18.7	3.4	4.7	19.5	3.1	1	2.5	0.6	0.8	1.7	3.9	2.9	3.6	2.5	4	2.7
NF14	5.2	11.2	2.1	1.4	3	4	2.8	1.1	12.4	3.6	3.6	1.1	3	2.6	1.8	2.1	6.7
NF15	2.8	1.6	5	1.1	0.8	<0.1	2.8	1	2.9	2.8	4	2.2	1.9	2.4	1.3	1.4	0.8
NF16	3.5	2.8	1.5	0.8	1.4	2.3	0.8	2.2	1.9	1.9	<0.1	3.4	1.6	4.3	1.8	2.6	0.8
NF17	1.7	2.2	2.1	3.1	1.8	1.1	3.2	2.8	1.7	<0.1	6	2.6	3	2.7	1.6	2.1	1.8
NF18	3.4	1.7	1.7	17.8	17.5	1.23.2	2.6	0.9	7.3	1.7	0.4	0.8	0.6	9.1	0.2	1.9	1.2
NF19	2.6	3.5	2.5	3.3	16.1	0.6	2.6	3.4	4.1	1.9	2.4	1.9	3.5	0.3	1.6	1.1	1.4
NF20	3.1	0.7	<0.1	1.5	2	4.1	<0.1	1.8	<0.1	1.4	1.3	0.5	0.8	3.8	3.5	<0.1	7.3
NF21	0.7	4.7	1.7	2.7	3.9	0.2	1.8	1.9	1.3	1.3	3.1	2.5	3.1	1.4	2.1	1.1	0.5
NF22	5.3	4.6	0.8	1.9	3.1	4.1	3.7	1.9	1.4	2.5	6.3	3	2.8	4.4	4.1	6.5	2.3
NF23	25.9	5.7	7.9	5.3	4.6	3.1	1.6	1	5.1	3.7	6.5	4.1	2.2	8	1.7	3.1	7.2
NF24	1.3	0.8	0.7	1	2.1	1.6	1.9	1.6	1.1	1.1	2	1	2.1	2.3	1.7	0.8	0.7
NF25	3.3	3.2	2.1	2.7	4.4	2.6	2.5	2.8	<0.1	<0.1	<0.1	3.2	2.4	1.8	5	2.7	3.1
NF26	2.7	2.7	1.6	1.6	2.4	2.9	2.3	2.5	1.1	1.9	1.8	0.8	3	0.8	0.7	1.5	2.4
NF27	0.5	0.6	0.9	0.9	0.6	0.6	0.7	0.8	0.3	0.4	0.7	0.2	1.8	2.2	2.1	2.2	2
NF28	2.2	3.4	6.8	3.6	3.1	2.8	2.2	2.4	1.6	1.6	2.2	2.3	1.4	1.2	1.3	1.9	1.4
MS29	<0.1	<0.1	<0.1	<0.1	<0.1	<0.1	<0.1	1.1	<0.1	<0.1	<0.1	<0.1	<0.1	<0.1	<0.1	<0.1	<0.1
MS30	0.1	1.1	2.4	3.6	3.3	2	1.4	2.4	0.4	2.5	1.4	2.3	2.2	0.2	2	<0.1	1.3
MS31	12.6	0.3	<0.1	2.3	0.2	<0.1	1.5	<0.1	9.9	<0.1	<0.1	6.6	2.6	0.3	<0.1	2.1	0.8
MS32	0.8	<0.1	1	2.8	0.9	<0.1	<0.1	0.3	<0.1	3.2	<0.1	1.1	2.7	0.5	12.9	1.1	1.3
MS33	<0.1	1.4	<0.1	<0.1	5	<0.1	<0.1	2.2	0.9	<0.1	<0.1	1.9	<0.1	1.2	4.2	<0.1	0.6
MS34	<0.1	<0.1	<0.1	<0.1	<0.1	<0.1	<0.1	<0.1	<0.1	<0.1	<0.1	<0.1	<0.1	<0.1	<0.1	<0.1	<0.1
MS35	<0.1	<0.1	<0.1	<0.1	<0.1	<0.1	<0.1	<0.1	<0.1	<0.1	<0.1	<0.1	<0.1	<0.1	<0.1	<0.1	<0.1
MS36	<0.1	<0.1	<0.1	1.3	2.4	3.3	3.4	10.5	0.2	<0.1	1.4	<0.1	<0.1	<0.1	1.3	13.6	<0.1
MS37	0.5	1.2	0.5	<0.1	1.2	1.5	<0.1	<0.1	3.4	<0.1	1.9	<0.1	2.8	0.9	0.5	<0.1	<0.1
MS38	0.6	0.9	0.5	<0.1	0.3	<0.1	<0.1	1.7	3.8	2	<0.1	1.1	<0.1	<0.1	1.6	0.8	3.1
MS39	0.9	1.1	2	<0.1	<0.1	<0.1	1.7	<0.1	12.2	<0.1	3.6	<0.1	1	<0.1	<0.1	<0.1	0.7
MS40	3.6	1	<0.1	2.1	0.7	0.6	<0.1	<0.1	<0.1	2.5	1.2	<0.1	1.7	0.9	<0.1	<0.1	1
MS41	3.5	3.3	3.7	2.5	0.6	1.5	3.6	1.5	4.4	1.6	3.4	3.2	1.6	3.4	2.1	1.4	2.9
MS42	1.7	4.3	2.1	1.6	1	2.8	10.1	2.5	1.4	3.6	8.3	1.3	2.9	3.7	1.6	5.2	1.1
MS43	3	1.4	0.5	1	2.9	19.2	10.1	0.7	0.4	2.3	5.9	0.7	2.3	5.2	<0.1	6	2.5
MS44	17.9	2.6	11.5	1.3	3	4.4	13.8	17.9	19.6	0.1	5	7.9	3.6	2	2.7	1.2	<0.1
MS45	>30	6.8	16.5	2	2	1.3	1.1	17.4	10.6	13.6	<0.1	4	3.9	1.4	2.4	11.9	3.6

Table A2.1. (Cont.) Pebble count results in centimeters.

Site																		
NF01	1.8	1.2	1.7	<0.1	<0.1	<0.1	<0.1	1.9	<0.1	<0.1	<0.1	<0.1	<0.1	<0.1	<0.1	<0.1	<0.1	1.9
NF02	0.2	0.2	<0.1	<0.1	1.4	1.6	0.3	0.6	<0.1	1.3	<0.1	2.2	0.1	1.4	<0.1	1.2	0.4	
NF03	1	1.3	<0.1	1.7	1.1	<0.1	1.4	1.2	<0.1	0.4	2.7	<0.1	1.3	<0.1	1.5	0.8	<0.1	
NF04	3.2	0.4	0.5	2.3	0.4	15.5	5.7	3.4	1.8	0.7	1.2	0.3	<0.1	0.7	2.8	1.4	0.4	
NF05	3.5	0.6	1.7	1.9	3	1.1	2	2.3	1.3	0.7	4.1	0.7	2.7	0.7	2.4	1.2	1.2	
NF06	0.3	16.4	4.6	5	0.9	5.7	2.9	1.7	2.9	14.8	2.1	3.1	18.5	3	5.5	0.7	4.1	
NF07	0.9	0.3	<0.1	3.5	0.9	1.4	<0.1	1	0.8	<0.1	2.3	<0.1	2.1	1	<0.1	1.5	<0.1	
NF08	1.9	<0.1	1.4	1.4	5.8	<0.1	4.2	0.4	8.9	1.1	3.4	2.6	0.4	6	5	0.8	<0.1	
NF09	3.2	2.3	2.1	2.2	1.2	2.9	0.6	0.6	1.2	1.1	1.8	1	1.3	1.3	1.1	1.2	1.1	
NF10	1	0.4	0.2	1.2	2.6	<0.1	0.6	3.5	3.8	1.5	0.7	1.2	3.2	3.4	0.3	3.4	2.9	
NF11	3.9	3	6.9	2.1	1.1	2.1	17.6	2.8	1.8	1.1	5	0.7	2.3	3.3	2.8	2.3	0.3	
NF12	2.6	0.7	9	1.7	5.1	0.7	2.9	2.9	2.9	3.4	5.3	2.3	2.5	1.5	<0.1	3.9	2	
NF13	0.7	2.2	1.7	3.3	4.6	4.6	6	2.9	4.6	3.6	0.2	2.4	2.4	1	1.6	8.3	0.9	
NF14	<0.1	0.4	1.2	3.6	6.1	1.6	1.1	2.1	2.2	2.1	2.3	1.9	2.1	1.4	1.6	2.1	4.3	
NF15	1.1	0.1	0.2	0.4	0.1	0.1	0.1	0.1	0.4	0.3	0.2	0.3	2.2	2.4	<0.1	3.2	1.4	
NF16	1.8	2.5	3.3	4.8	4.1	5.1	17.3	1	3.7	2.9	2.4	2.3	5.6	3.2	0.5	1.4	2.2	
NF17	1.6	3.3	<0.1	2.4	1.8	4.1	2.6	1.1	<0.1	2.6	3.7	2.7	0.9	3.6	1.6	2.3	2.9	
NF18	2.5	4.2	1.3	1.3	2.5	5.6	3.8	2.2	3.5	6.9	2.1	0.6	0.9	0.7	1	2.5	2.2	
NF19	1.6	1.2	0.9	1.7	0.7	3.6	10.7	3.3	1.6	2.6	1	5.4	5.1	2.6	2.1	1.4	2.7	
NF20	5.4	<0.1	<0.1	0.6	3.1	3.8	3.8	4	<0.1	3	8.1	2.1	2.3	3	<0.1	1.7	2.9	
NF21	1.1	12.8	4.2	1.4	2.7	0.6	5.4	4.2	2.2	2.1	5.9	1.2	2	1.8	5.6	0.6	3.8	
NF22	1.6	1.4	1.7	3.6	4.1	1.1	1.1	1.6	1.5	1.5	2.8	2.1	2.6	2.6	0.4	1	0.4	
NF23	2.3	0.5	<0.1	1.3	2.3	<0.1	0.4	5.5	0.4	1.9	0.7	2.4	0.6	1.3	0.8	1.9	2.7	
NF24	0.7	2	0.4	0.6	0.4	0.9	2.1	2.1	2.9	3.1	0.6	1.2	2.4	1.7	3	2.1	3	
NF25	2.5	1.7	8.1	2	0.9	1.1	2	4.6	3.1	2.9	1.4	10.4	3	1.8	2.2	8.2	2.1	
NF26	0.4	1.9	1.1	2.2	2.1	2.8	1.7	2.1	2.3	0.6	1.1	0.8	<0.1	1.4	2	1.6	2.3	
NF27	2.8	3	3.1	4	2.6	2.6	1.7	2.6	3.6	4	2.3	1.2	3.6	3.2	4.1	2	6.1	
NF28	1.1	0.8	2.2	1.9	0.8	0.7	0.4	2.1	1	2.1	1.5	1.1	0.9	0.3	0.2	0.1	0.1	
MS29	<0.1	<0.1	<0.1	0.6	<0.1	<0.1	<0.1	2	1.2	3.5	<0.1	<0.1	<0.1	<0.1	0.4	0.6	<0.1	
MS30	1.7	0.5	2.4	<0.1	1.8	2.1	11.9	0.7	0.9	1.8	<0.1	0.3	0.5	0.4	1.4	2.2	<0.1	
MS31	1.6	<0.1	<0.1	0.6	<0.1	<0.1	<0.1	5.6	0.6	0.1	<0.1	0.4	0.9	9.7	0.8	<0.1	8.2	
MS32	0.6	0.7	<0.1	3.3	<0.1	<0.1	2.2	1	1.7	1.5	1.5	3.5	1.3	0.2	5	1.1	1	
MS33	2.2	<0.1	0.4	<0.1	8.5	4.7	1.2	13.9	<0.1	3	8.3	2.2	<0.1	<0.1	3.4	0.4	<0.1	
MS34	<0.1	<0.1	<0.1	<0.1	<0.1	<0.1	<0.1	<0.1	<0.1	<0.1	<0.1	<0.1	<0.1	<0.1	<0.1	<0.1	<0.1	
MS35	<0.1	<0.1	<0.1	<0.1	<0.1	<0.1	<0.1	<0.1	<0.1	<0.1	<0.1	<0.1	<0.1	<0.1	<0.1	<0.1	<0.1	
MS36	0.5	<0.1	<0.1	1.6	1.2	<0.1	<0.1	1.1	1.1	<0.1	1	<0.1	<0.1	1.6	3.5	<0.1	<0.1	
MS37	<0.1	2	<0.1	<0.1	4	3.7	1.3	<0.1	1.3	0.8	<0.1	<0.1	<0.1	0.9	<0.1	0.7	1.1	
MS38	3	<0.1	1.1	<0.1	1.1	0.7	2.8	2	0.4	1.4	1.3	<0.1	0.8	<0.1	1.7	1.2	2.6	
MS39	<0.1	<0.1	<0.1	<0.1	<0.1	1.5	2.2	1.5	<0.1	<0.1	0.7	1.7	2	1.1	<0.1	<0.1	1.6	
MS40	<0.1	<0.1	1	1.5	3.8	<0.1	0.7	<0.1	<0.1	1	0.9	<0.1	0.8	0.7	<0.1	<0.1	1	
MS41	2.9	5.7	1.1	0.9	1.6	3.3	1.9	1.8	1.4	2.8	2.1	2.9	2.3	1	1.8	2.1	1.2	
MS42	3.1	0.9	8.5	2.6	2.4	2.1	0.8	1.8	<0.1	5.8	1.5	1.1	0.9	2.3	24.4	1.3	0.6	
MS43	4.3	2	3.2	3.2	2.1	9.3	0.7	<0.1	2.5	<0.1	4.8	7	2.1	6.2	3.9	2.3	0.8	
MS44	1.2	11.1	18.9	1	10.8	0.2	0.9	2.9	1.3	1.5	0.6	3.2	3.7	2.1	2.1	7.1	3	
MS45	0.4	9.9	6	1.3	<0.1	1.6	1.9	0.6	2.4	1.5	1.8	<0.1	8.7	0.7	4.2	9.8	17.8	

Table A2.1. (Cont.) Pebble count results in centimeters.

Site																		
NF01	1.3	1.4	<0.1	<0.1	1.5	<0.1	2.1	<0.1	1.7	1.1	0.8	<0.1	0.9	<0.1	<0.1	1.8	0.8	
NF02	0.3	0.8	0.6	0.5	0.4	0.6	0.9	0.5	0.2	0.8	0.8	0.1	1.9	1.2	0.9	0.2	<0.1	
NF03	2.5	2.1	<0.1	0.9	1.3	<0.1	<0.1	1.3	<0.1	<0.1	<0.1	1.5	1.5	2.1	<0.1	<0.1	2.3	
NF04	1.5	4.4	<0.1	3.9	6.6	2	1.5	4.1	3.2	3.1	1.5	2.7	2.7	1.7	1.4	1.4	1	
NF05	0.6	0.2	0.6	0.8	0.4	0.3	5.3	<0.1	2.2	4	1.9	2.1	0.1	8.8	3.5	0.4	1.4	
NF06	0.4	5.2	27.2	2.7	21.4	1.7	4	6.6	4.7	1.5	1.5	3.1	1.1	0.6	13.6	2.3	2.9	
NF07	<0.1	1.6	<0.1	0.9	0.8	0.8	1	1.9	<0.1	1.8	0.6	0.7	0.1	0.4	<0.1	<0.1	1.6	
NF08	0.5	0.9	1.6	1	0.4	1	5.3	7.9	8.5	5.3	3.6	6.4	1.8	6.7	15.3	0.3	2.5	
NF09	1.5	1.5	1.3	0.6	1.4	1	1.2	15.3	0.7	2	1.8	2.5	1.9	1.8	1	0.5	0.8	
NF10	1.1	1.9	4.1	8.3	6.5	1	0.6	0.7	3.9	18.7	3	1.1	0.1	1.8	11.2	5.6	0.1	
NF11	3.6	>30	2.8	4.7	1	5.4	2.2	2.3	0.6	11	0.6	5.1	1.9	2.3	12.3	8.2	0.7	
NF12	2.9	<0.1	7.8	<0.1	2.3	<0.1	2.7	4.8	2.1	<0.1	<0.1	3.4	5.1	0.3	1.3	0.7	<0.1	
NF13	1.8	0.5	3.2	1.7	9.9	1.2	0.6	0.8	3	3.7	4.3	2.8	1.9	2.5	2.3	1.9	3.9	
NF14	1.6	2.4	1.8	2.3	2.1	2.1	1.7	0.9	0.6	1.3	4.2	3.6	4.4	<0.1	<0.1	2.1	1.8	
NF15	2	<0.1	<0.1	<0.1	0.6	3.6	<0.1	<0.1	0.9	2.6	2.9	<0.1	<0.1	<0.1	<0.1	<0.1	<0.1	
NF16	<0.1	0.7	2.7	0.7	0.9	1.1	1.9	3.8	0.4	12.1	3.4	4.8	3.8	1.5	1	0.9	0.7	
NF17	6.8	2.9	1.4	2.9	4.3	1.8	1.1	3.3	2.9	2.6	1.7	6.6	<0.1	2.2	1.1	1.2	2.3	
NF18	2	1.9	2.6	4.2	5.1	16.6	0.9	3.8	2.4	1.4	1.7	10.2	2.4	1.3	2.8	3.3	4.8	
NF19	2.1	1.5	3.2	1.1	9.3	4.9	8.5	3.4	2	15.7	2.9	0.5	1.1	2.1	4.6	6.9	<0.1	
NF20	2.3	3.6	2.8	2.4	2	2.5	2.9	9.6	2.4	2	1.9	3.7	1.2	1.5	3	3.1	2.8	
NF21	2.9	1.9	3.1	1.1	2.4	2.3	1.8	3.1	2.5	3.6	1.1	2.1	1.8	3.9	1.9	1.1	1.6	
NF22	2	2.2	1.5	1.9	2.2	3.4	0.6	5.6	1.3	1	2.2	3	2	2.5	1.5	0.3	3.5	
NF23	4.1	2.6	2	4.3	9.7	3	6.4	3.3	2.8	8.9	<0.1	1.7	2.5	1.6	0.7	0.9	2.4	
NF24	1.1	1.8	1.9	2	1.6	1.5	1.2	2.4	1.8	1.5	1.7	0.9	0.6	1.2	2.1	0.5	1.2	
NF25	0.4	0.6	1.1	3.2	<0.1	1.4	1.1	<0.1	<0.1	1.9	2.1	1.3	3.9	2.3	3.8	1.3	3.4	
NF26	3	2.7	2.6	2.1	2.8	2.8	0.9	0.8	0.9	1.4	1.8	1.8	1.9	2.1	1.3	1.8	1.6	
NF27	2.2	2.1	2.2	2.1	3	3	1.9	2.2	4.2	1.8	1.6	1.1	1.2	2.7	3.6	3.1	15.6	
NF28	18	2	11.1	2.8	4.3	4.4	3.3	2.2	3	4	2.1	2.5	2.2	2.5	3	1.2	3.3	
MS29	<0.1	<0.1	<0.1	<0.1	<0.1	<0.1	<0.1	<0.1	<0.1	0.8	3.3	<0.1	<0.1	<0.1	<0.1	<0.1	<0.1	
MS30	1.4	2.8	1	1.5	2.2	<0.1	<0.1	<0.1	0.6	1.5	3.2	1.5	2	1	5.4	1.2	2.2	
MS31	<0.1	0.1	<0.1	3	<0.1	1.2	1	0.1	<0.1	<0.1	0.2	2.5	<0.1	<0.1	0.8	0.2	1.2	
MS32	0.9	0.9	2	1.5	<0.1	0.4	5.8	2	1.2	<0.1	<0.1	3.3	2	0.6	1.5	0.5	0.9	
MS33	3.6	7.2	<0.1	<0.1	<0.1	<0.1	<0.1	<0.1	<0.1	14.1	0.3	<0.1	<0.1	6.3	6.9	3.4	0.8	
MS34	<0.1	<0.1	<0.1	<0.1	<0.1	<0.1	<0.1	<0.1	<0.1	<0.1	<0.1	<0.1	<0.1	<0.1	<0.1	<0.1	<0.1	
MS35	<0.1	<0.1	<0.1	<0.1	<0.1	<0.1	1.1	<0.1	<0.1	<0.1	0.9	<0.1	<0.1	<0.1	<0.1	<0.1	<0.1	
MS36	<0.1	2.2	<0.1	1.2	2.5	<0.1	<0.1	<0.1	<0.1	1.7	<0.1	<0.1	<0.1	2.4	<0.1	<0.1	<0.1	
MS37	1	0.6	1.6	<0.1	<0.1	<0.1	<0.1	<0.1	<0.1	<0.1	<0.1	<0.1	1.3	<0.1	<0.1	1.8	<0.1	
MS38	<0.1	<0.1	1.3	1.2	4.4	0.1	0.5	<0.1	1.1	1.1	<0.1	<0.1	0.6	<0.1	0.9	<0.1	2.9	
MS39	<0.1	2	<0.1	1.1	<0.1	<0.1	<0.1	<0.1	1.4	<0.1	<0.1	<0.1	<0.1	3.2	<0.1	0.5	0.7	
MS40	0.8	<0.1	<0.1	<0.1	1.4	<0.1	<0.1	0.9	<0.1	<0.1	<0.1	0.8	0.2	<0.1	<0.1	<0.1	<0.1	
MS41	2.6	5.8	3.9	4	1.4	1	1.3	3.1	1.7	2.3	2.5	3.6	1.3	1.4	2.6	2.2	4	
MS42	1.7	0.5	9.9	2.2	1.2	0.7	0.9	3.8	2.1	3.4	5	0.8	0.9	0.8	4.5	1.9	1.6	
MS43	2.1	5.1	1.7	0.3	0.9	3.4	1.3	1.1	<0.1	3.5	0.8	1	0.5	0.8	2.9	6.2	0.6	
MS44	1.7	3	0.6	3.7	1.1	5.6	3.1	0.6	5.8	4.6	1.9	2.8	1.7	1.6	1.7	0.3	0.2	
MS45	6.5	0.1	22.8	2.4	3.2	2.1	8.7	4.8	1	1.6	11.4	11	6.8	3.3	1	0.9	0.6	

Table A2.1. (Cont.) Pebble count results in centimeters.

Site																		
NF01	<0.1	2	1.8	1.5	<0.1	1.1	<0.1	<0.1	0.9	<0.1	<0.1	0.6	<0.1	<0.1	0.7	1	<0.1	
NF02	0.7	0.5	2.3	1	0.6	0.8	0.5	0.9	1.1	0.4	2	0.4	0.9	0.6	0.8	0.6	0.7	
NF03	1.7	1.4	1.3	<0.1	1.6	<0.1	1.9	<0.1	<0.1	0.9	<0.1	<0.1	<0.1	1.4	<0.1	1.9	<0.1	
NF04	0.6	2.2	10.8	1	0.6	1.5	0.8	3.7	1.4	1.8	0.8	4	2.5	2.6	1	<0.1	1.7	
NF05	<0.1	0.1	0.4	<0.1	10.3	1.6	0.2	5.4	0.3	0.4	0.8	1.3	0.6	9.8	9.8	1.9	0.1	
NF06	0.9	1.5	1.7	<0.1	5.5	1.3	0.5	0.4	<0.1	3.8	5.2	0.9	19	6.5	2	1	1.2	
NF07	<0.1	<0.1	1.3	<0.1	1.6	1.7	0.1	1.4	0.1	2.6	<0.1	0.6	1.7	1.6	1.4	1.5	0.9	
NF08	1.7	3.3	5.4	1.1	3.7	6.6	7.6	2.2	2.7	4	7	8.4	1	12.9	4.7	22.2	13.4	
NF09	2.1	1.6	1.9	1.7	0.7	1.6	1.7	1.8	1.1	2	2.8	1.8	2.5	1.5	2.5	0.6	0.7	
NF10	0.7	0.6	2.5	1.2	4.5	2	2.1	7.5	6.3	2.1	4.4	2.5	0.6	1.2	2.9	1.9	1.5	
NF11	2.9	0.5	9.2	7.2	6.3	26.1	0.9	1.7	1.3	2.5	1.9	1.2	4.3	2.1	0.8	0.8	1.1	
NF12	2.2	7.3	0.7	<0.1	<0.1	0.7	5.7	7.6	4.5	3.6	8.3	2.1	0.2	<0.1	<0.1	<0.1	<0.1	
NF13	2.5	1.6	0.8	1.6	2.1	1.9	3.6	2.5	1.7	1.2	1.5	3.1	14.7	1.6	2.7	1.5	0.8	
NF14	0.8	1.1	<0.1	1.9	2.2	0.8	1.2	2.2	2.8	2.1	1.9	1.9	2.6	1.8	1.9	1.1	0.9	
NF15	<0.1	<0.1	<0.1	<0.1	<0.1	2	4.6	<0.1	<0.1	2.3	1.4	0.9	2.3	0.6	0.4	1.4	0.6	
NF16	2.3	0.5	4.3	3	1.6	2.1	1.3	1.2	2.6	2.3	1.8	2.6	3.2	0.9	1.7	2.8	3.9	
NF17	4.1	2.1	1.7	4.6	1.6	3.9	2.8	9.6	3.1	1.2	1.8	11.6	1.7	2.1	5.6	2.6	1.2	
NF18	1.3	4.3	3.1	2.8	1.1	4.6	2.1	2.6	3.1	0.6	2.1	1.9	2.4	2.6	1.3	2.6	2.6	
NF19	0.8	0.9	13.7	10.8	11.8	<0.1	3.3	0.5	1.8	10.7	1.8	0.9	5.5	3.4	1.9	1.1	1.4	
NF20	<0.1	2.4	1.5	1.1	1.3	1.7	3.1	1	2.6	1.4	0.9	1.6	2.2	2.7	3.3	3	2.1	
NF21	4.2	1.2	1.3	3.3	2.8	2.9	4.1	1.3	1.4	4.6	2.9	2.3	8.1	6.6	7.3	17.3	4.2	
NF22	0.9	2.4	2	2.4	2.9	1.8	1.2	1.5	3.3	3.6	3.2	0.3	2.5	1.6	1.8	1.1	3	
NF23	6.9	6.3	0.5	2.4	2.9	2.2	3.8	3.1	2.1	1.9	5.8	3.9	2.9	3.8	6.6	2.4	1.6	
NF24	1.1	0.8	1.3	0.6	1.8	1.6	1.6	1.8	2.2	1.3	1.9	1.9	1.9	4.6	2.2	1.4	2.5	
NF25	0.1	<0.1	0.6	1.3	2.3	0.8	0.1	0.8	1.3	1.6	3.1	1.7	1.3	0.8	2.8	0.1	0.1	
NF26	1.8	1.1	1.6	0.8	1.1	0.3	1.6	2.2	1	1	1.7	1.3	1.4	1.3	1.2	3.2	2.2	
NF27	4.2	0.6	2.1	0.2	0.2	0.4	1.9	1.7	0.7	0.4	0.5	0.6	0.2	0.2	0.1	0.4	0.7	
NF28	3.1	2.3	1.9	2.2	2.8	1.6	2	2.4	4.1	2.2	1.9	1.1	2.1	1.8	1.3	1.3	1.8	
MS29	<0.1	<0.1	<0.1	0.4	1.4	0.8	<0.1	0.9	2	1.3	1	2.5	0.6	0.8	<0.1	<0.1	0.6	
MS30	2.2	1.3	2.5	1	0.6	0.2	0.3	0.7	2.4	0.7	0.8	0.7	0.2	2.6	1	3.4	<0.1	
MS31	<0.1	<0.1	<0.1	<0.1	<0.1	1.3	<0.1	<0.1	0.5	0.5	<0.1	0.5	0.3	0.8	6.9	<0.1	<0.1	
MS32	1.2	0.8	2.4	0.6	1.4	0.6	2.5	1.9	1.3	1.3	2.7	<0.1	1.8	1.2	4	2.1	5.6	
MS33	<0.1	<0.1	<0.1	<0.1	7.6	<0.1	<0.1	3.5	0.4	<0.1	1.2	0.6	<0.1	<0.1	0.7	2.9	<0.1	
MS34	<0.1	<0.1	<0.1	<0.1	<0.1	<0.1	<0.1	<0.1	<0.1	<0.1	<0.1	<0.1	<0.1	<0.1	<0.1	<0.1	<0.1	
MS35	<0.1	4.1	<0.1	<0.1	<0.1	<0.1	<0.1	<0.1	<0.1	<0.1	<0.1	<0.1	<0.1	<0.1	<0.1	<0.1	<0.1	
MS36	<0.1	8.6	1.8	0.2	0.9	<0.1	<0.1	<0.1	<0.1	0.5	<0.1	<0.1	<0.1	0.7	<0.1	<0.1	<0.1	
MS37	11.4	0.5	0.7	<0.1	<0.1	<0.1	1.5	<0.1	<0.1	<0.1	2.1	<0.1	<0.1	<0.1	<0.1	<0.1	<0.1	
MS38	2.2	3.2	2.8	3.1	<0.1	0.8	<0.1	<0.1	1.2	0.5	<0.1	<0.1	<0.1	<0.1	<0.1	3.9	0.3	
MS39	<0.1	3.1	0.6	<0.1	2.1	<0.1	<0.1	1.1	1.4	<0.1	2.7	<0.1	<0.1	<0.1	<0.1	1	1	
MS40	<0.1	<0.1	<0.1	<0.1	1.9	<0.1	<0.1	<0.1	1.2	4.6	0.4	<0.1	1.8	<0.1	2.9	1	1.2	
MS41	0.9	2.8	5.1	3.9	1.4	2.9	4.2	1.3	4.2	4	1.3	2.3	2.2	1.1	2.5	0.8	3.4	
MS42	7	0.6	0.5	1.2	2.7	1.3	1.4	1.2	1.9	1.9	8.4	1.4	1.4	1.3	1.4	1.9	0.9	
MS43	2.6	<0.1	6.3	9.5	7.3	5.5	2.1	0.8	1.8	5.3	<0.1	0.1	0.7	0.7	0.8	1.6	4.8	
MS44	4.6	1	3.7	0.3	2	1.2	5.8	8.6	0.5	1.3	3.2	7.8	0.9	8	0.9	5.1	0.1	
MS45	6.4	2.9	3.3	1.8	4	0.7	3	1.8	2.4	1	1.6	0.7	1.8	0.7	16.1	11.5	4.2	

Table A2.1. (Cont.) Pebble count results in centimeters.

Site																		
NF01	<0.1	2	1.8	1.5	<0.1	1.1	<0.1	<0.1	0.9	<0.1	<0.1	0.6	<0.1	<0.1	0.7	1	<0.1	
NF02	0.7	0.5	2.3	1	0.6	0.8	0.5	0.9	1.1	0.4	2	0.4	0.9	0.6	0.8	0.6	0.7	
NF03	1.7	1.4	1.3	<0.1	1.6	<0.1	1.9	<0.1	<0.1	0.9	<0.1	<0.1	<0.1	1.4	<0.1	1.9	<0.1	
NF04	0.6	2.2	10.8	1	0.6	1.5	0.8	3.7	1.4	1.8	0.8	4	2.5	2.6	1	<0.1	1.7	
NF05	<0.1	0.1	0.4	<0.1	10.3	1.6	0.2	5.4	0.3	0.4	0.8	1.3	0.6	9.8	9.8	1.9	0.1	
NF06	0.9	1.5	1.7	<0.1	5.5	1.3	0.5	0.4	<0.1	3.8	5.2	0.9	19	6.5	2	1	1.2	
NF07	<0.1	<0.1	1.3	<0.1	1.6	1.7	0.1	1.4	0.1	2.6	<0.1	0.6	1.7	1.6	1.4	1.5	0.9	
NF08	1.7	3.3	5.4	1.1	3.7	6.6	7.6	2.2	2.7	4	7	8.4	1	12.9	4.7	22.2	13.4	
NF09	2.1	1.6	1.9	1.7	0.7	1.6	1.7	1.8	1.1	2	2.8	1.8	2.5	1.5	2.5	0.6	0.7	
NF10	0.7	0.6	2.5	1.2	4.5	2	2.1	7.5	6.3	2.1	4.4	2.5	0.6	1.2	2.9	1.9	1.5	
NF11	2.9	0.5	9.2	7.2	6.3	26.1	0.9	1.7	1.3	2.5	1.9	1.2	4.3	2.1	0.8	0.8	1.1	
NF12	2.2	7.3	0.7	<0.1	<0.1	0.7	5.7	7.6	4.5	3.6	8.3	2.1	0.2	<0.1	<0.1	<0.1	<0.1	
NF13	2.5	1.6	0.8	1.6	2.1	1.9	3.6	2.5	1.7	1.2	1.5	3.1	14.7	1.6	2.7	1.5	0.8	
NF14	0.8	1.1	<0.1	1.9	2.2	0.8	1.2	2.2	2.8	2.1	1.9	1.9	2.6	1.8	1.9	1.1	0.9	
NF15	<0.1	<0.1	<0.1	<0.1	<0.1	2	4.6	<0.1	<0.1	2.3	1.4	0.9	2.3	0.6	0.4	1.4	0.6	
NF16	2.3	0.5	4.3	3	1.6	2.1	1.3	1.2	2.6	2.3	1.8	2.6	3.2	0.9	1.7	2.8	3.9	
NF17	4.1	2.1	1.7	4.6	1.6	3.9	2.8	9.6	3.1	1.2	1.8	11.6	1.7	2.1	5.6	2.6	1.2	
NF18	1.3	4.3	3.1	2.8	1.1	4.6	2.1	2.6	3.1	0.6	2.1	1.9	2.4	2.6	1.3	2.6	2.6	
NF19	0.8	0.9	13.7	10.8	11.8	<0.1	3.3	0.5	1.8	10.7	1.8	0.9	5.5	3.4	1.9	1.1	1.4	
NF20	<0.1	2.4	1.5	1.1	1.3	1.7	3.1	1	2.6	1.4	0.9	1.6	2.2	2.7	3.3	3	2.1	
NF21	4.2	1.2	1.3	3.3	2.8	2.9	4.1	1.3	1.4	4.6	2.9	2.3	8.1	6.6	7.3	17.3	4.2	
NF22	0.9	2.4	2	2.4	2.9	1.8	1.2	1.5	3.3	3.6	3.2	0.3	2.5	1.6	1.8	1.1	3	
NF23	6.9	6.3	0.5	2.4	2.9	2.2	3.8	3.1	2.1	1.9	5.8	3.9	2.9	3.8	6.6	2.4	1.6	
NF24	1.1	0.8	1.3	0.6	1.8	1.6	1.6	1.8	2.2	1.3	1.9	1.9	1.9	4.6	2.2	1.4	2.5	
NF25	0.1	<0.1	0.6	1.3	2.3	0.8	0.1	0.8	1.3	1.6	3.1	1.7	1.3	0.8	2.8	0.1	0.1	
NF26	1.8	1.1	1.6	0.8	1.1	0.3	1.6	2.2	1	1	1.7	1.3	1.4	1.3	1.2	3.2	2.2	
NF27	4.2	0.6	2.1	0.2	0.2	0.4	1.9	1.7	0.7	0.4	0.5	0.6	0.2	0.2	0.1	0.4	0.7	
NF28	3.1	2.3	1.9	2.2	2.8	1.6	2	2.4	4.1	2.2	1.9	1.1	2.1	1.8	1.3	1.3	1.8	
MS29	<0.1	<0.1	<0.1	0.4	1.4	0.8	<0.1	0.9	2	1.3	1	2.5	0.6	0.8	<0.1	<0.1	0.6	
MS30	2.2	1.3	2.5	1	0.6	0.2	0.3	0.7	2.4	0.7	0.8	0.7	0.2	2.6	1	3.4	<0.1	
MS31	<0.1	<0.1	<0.1	<0.1	<0.1	1.3	<0.1	<0.1	0.5	0.5	<0.1	0.5	0.3	0.8	6.9	<0.1	<0.1	
MS32	1.2	0.8	2.4	0.6	1.4	0.6	2.5	1.9	1.3	1.3	2.7	<0.1	1.8	1.2	4	2.1	5.6	
MS33	<0.1	<0.1	<0.1	<0.1	7.6	<0.1	<0.1	3.5	0.4	<0.1	1.2	0.6	<0.1	<0.1	0.7	2.9	<0.1	
MS34	<0.1	<0.1	<0.1	<0.1	<0.1	<0.1	<0.1	<0.1	<0.1	<0.1	<0.1	<0.1	<0.1	<0.1	<0.1	<0.1	<0.1	
MS35	<0.1	4.1	<0.1	<0.1	<0.1	<0.1	<0.1	<0.1	<0.1	<0.1	<0.1	<0.1	<0.1	<0.1	<0.1	<0.1	<0.1	
MS36	<0.1	8.6	1.8	0.2	0.9	<0.1	<0.1	<0.1	<0.1	0.5	<0.1	<0.1	<0.1	0.7	<0.1	<0.1	<0.1	
MS37	11.4	0.5	0.7	<0.1	<0.1	<0.1	1.5	<0.1	<0.1	<0.1	2.1	<0.1	<0.1	<0.1	<0.1	<0.1	<0.1	
MS38	2.2	3.2	2.8	3.1	<0.1	0.8	<0.1	<0.1	1.2	0.5	<0.1	<0.1	<0.1	<0.1	<0.1	3.9	0.3	
MS39	<0.1	3.1	0.6	<0.1	2.1	<0.1	<0.1	1.1	1.4	<0.1	2.7	<0.1	<0.1	<0.1	<0.1	1	1	
MS40	<0.1	<0.1	<0.1	<0.1	1.9	<0.1	<0.1	<0.1	1.2	4.6	0.4	<0.1	1.8	<0.1	2.9	1	1.2	
MS41	0.9	2.8	5.1	3.9	1.4	2.9	4.2	1.3	4.2	4	1.3	2.3	2.2	1.1	2.5	0.8	3.4	
MS42	7	0.6	0.5	1.2	2.7	1.3	1.4	1.2	1.9	1.9	8.4	1.4	1.4	1.3	1.4	1.9	0.9	
MS43	2.6	<0.1	6.3	9.5	7.3	5.5	2.1	0.8	1.8	5.3	<0.1	0.1	0.7	0.7	0.8	1.6	4.8	
MS44	4.6	1	3.7	0.3	2	1.2	5.8	8.6	0.5	1.3	3.2	7.8	0.9	8	0.9	5.1	0.1	
MS45	6.4	2.9	3.3	1.8	4	0.7	3	1.8	2.4	1	1.6	0.7	1.8	0.7	16.1	11.5	4.2	

Table A2.1. (Cont.) Pebble count results in centimeters.

MS46	1.2	0.3	<0.1	4.7	<0.1	5.4	1.3	3	19	1.2	<0.1	2	20.5	0.9	<0.1	9.9	0.7
MS47	1.5	4.8	3.9	3.4	0.5	3.5	2	3.3	0.9	3.2	10.9	6.3	1.9	0.6	6.4	0.8	5.9
MS48	1.1	<0.1	<0.1	<0.1	<0.1	<0.1	<0.1	<0.1	<0.1	<0.1	<0.1	<0.1	<0.1	16.1	<0.1	<0.1	<0.1
MS49	7.2	6.5	<0.1	<0.1	6.9	3	1	4.8	1.1	<0.1	<0.1	3.1	<0.1	<0.1	4.1	4.3	<0.1
MS50	<0.1	<0.1	<0.1	<0.1	<0.1	<0.1	<0.1	<0.1	0.2	8	<0.1	<0.1	<0.1	10.5	<0.1	7.4	20.8
MS51	1.8	2.1	3.5	0.5	1.2	4.1	1.8	1.7	0.4	1	0.5	18.2	1.5	2.2	3.1	23.4	<0.1
MS52	<0.1	<0.1	<0.1	<0.1	0.7	<0.1	<0.1	1.6	<0.1	<0.1	0.5	<0.1	<0.1	1.6	<0.1	<0.1	<0.1
MS53	<0.1	<0.1	<0.1	<0.1	0.4	<0.1	<0.1	<0.1	<0.1	<0.1	<0.1	<0.1	<0.1	<0.1	<0.1	<0.1	18.9
MS54	<0.1	<0.1	19.1	>30	3.3	<0.1	12.3	<0.1	20.7	15.8	9.7	3.3	8.1	<0.1	5.7	<0.1	0.7
MS55	7.1	6.5	3	11.3	21.3	23.8	2	12.5	17.9	1.4	18.4	0.9	11.8	1.5	6.3	3.6	3
MS56	<0.1	6	1.8	2.2	<0.1	<0.1	<0.1	<0.1	4.8	2.1	<30	2.1	2	<0.1	<0.1	13	8.9
MS57	1.6	1.1	1.8	6	<0.1	1	2.7	2	1	1.9	<0.1	<0.1	<0.1	<0.1	1.4	2.1	2.4
MS58	<0.1	<0.1	<0.1	<0.1	2.1	<0.1	1.7	<0.1	<0.1	<0.1	<0.1	<0.1	<0.1	<0.1	<0.1	1.2	<0.1
MS59	<0.1	<0.1	<0.1	<0.1	<0.1	<0.1	<0.1	<0.1	<0.1	<0.1	<0.1	<0.1	<0.1	<0.1	<0.1	<0.1	<0.1
MS60	24.9	8.7	2.7	2.5	3.1	1	2.8	5.4	2.9	2.1	1.2	1.1	9.5	9.3	6.5	3.3	1.9
MS61	3	1.7	1.3	4.1	1.4	1.8	6.9	10.9	4.8	2.3	3.3	2.8	19.8	2.9	2.2	0.4	<0.1
MS62	<0.1	<0.1	<0.1	<0.1	<0.1	<0.1	<0.1	1.4	<0.1	<0.1	<0.1	<0.1	<0.1	<0.1	<0.1	<0.1	<0.1
MS63	<0.1	<0.1	18.2	13.5	1.8	<0.1	<0.1	<0.1	<0.1	<0.1	12.6	3	1.7	14.4	3	1.1	<0.1
MS64	1.3	2.4	<0.1	2.3	3.3	3.4	<0.1	<0.1	<0.1	2.5	1.4	<0.1	<0.1	3.2	3.1	4.4	1
MS65	<0.1	2.2	3.6	1.5	2.7	4	2	3.1	3.6	1.1	0.8	3.4	1.3	0.5	4.4	2.3	1.2
MS66	<0.1	2.5	1.9	<0.1	<0.1	4.1	3	>30	<0.1	<0.1	1.4	26.2	1.1	<0.1	<0.1	<0.1	2.7
MS67	2	1.5	3.4	<0.1	1.3	<0.1	1.6	<0.1	<0.1	<0.1	2.4	<0.1	1.5	1.5	<0.1	<0.1	<0.1
NF68	1.8	0.9	0.7	1.5	1.3	1.4	1.8	1.6	1.4	0.6	0.9	1.1	0.6	<0.1	0.9	1.4	1.5
NF69	1.1	2	1.2	1	2.1	<0.1	1	1.9	0.8	1	2.3	1.2	1	<0.1	2.4	1.5	2.5
NF70	1.6	1.8	1.6	2.6	0.8	<0.1	2.7	2.6	<0.1	<0.1	2.2	3.1	2.5	1.3	3.6	1.8	1.6
NF71	3.5	1.3	<0.1	<0.1	1.9	0.6	2.1	5.8	1	<0.1	0.2	3.6	<0.1	1.7	0.5	4.5	1.5
NF72	0.4	0.5	0.6	0.8	1.4	0.3	<0.1	0.4	0.9	0.3	0.3	1.6	1.2	0.2	<0.1	1.4	1
NF73	0.5	0.7	0.9	1.1	2	2.3	1.6	3	<0.1	2.6	1.2	3.3	1.6	2.6	3.1	2.5	1.4
NF74	2.6	4	0.9	1.7	1.5	2.9	3.1	2.6	4.6	1.4	2	4.2	1.2	2.1	1.2	1.9	1.4
NF75	<0.1	2.1	2.5	1.9	1.9	1.6	2.3	2.9	1.4	1.2	1.3	2.9	2.7	1.9	2.1	3.9	2.7
NF76	1.8	3.1	1.8	0.6	2.9	12	2.5	5.8	4	0.5	2.9	1.8	1.6	6.2	1.2	6	2.1
NF77	6.2	4.9	5.2	3.1	3	2.6	5	2.2	3.5	<0.1	5.3	1.6	2	1.6	0.5	3	2.6
NF78	2.1	2.6	0.9	0.9	1.5	4.6	3.5	1.4	1	16.2	2.3	1.3	0.9	0.4	0.9	0.8	1.5
NF79	3.5	1.8	0.2	2.7	2.7	0.9	14.1	2.1	2.1	1.9	1.8	6.9	1.7	23.6	0.8	1.6	1
NF80	1.9	1.1	1	1.9	3.4	1.6	2.3	1.1	2.3	1.9	2.8	1.1	2.2	1.9	1.9	13.3	1.5
NF81	1	1.3	4.8	0.9	3	1.6	1.2	2.6	1.3	4.5	3.4	<0.1	2	<0.1	1.1	3.1	1.6
NF82	1.6	4.3	7.8	1.5	<0.1	4.2	3	8.8	8	<0.1	1.5	4.2	13.5	2.6	6.8	3.1	7.4
NF83	2.8	4.1	7.2	1.9	11.8	2.5	2.4	0.1	3.7	17.3	2	8.9	7.2	6.9	>30	0.2	0.5
NF84	2.2	10.6	8.4	7.7	<0.1	8	8.8	3.1	<0.1	3.4	1.9	6.6	<0.1	4.2	2.7	5	7.3
NF85	<0.1	<0.1	<0.1	2.2	0.6	<0.1	2.2	0.9	<0.1	1.3	1	<0.1	2	1.1	<0.1	0.8	2.1
SF86	2.2	1.1	<0.1	<0.1	<0.1	3.2	2.1	0.8	<0.1	<0.1	1.8	4.7	2.9	0.7	<0.1	2.4	0.9
SF87	5.7	2.6	2	6.3	6.1	10.3	15.8	12.7	7.3	2.3	7.9	16.2	3.1	5.8	4.7	24.2	<0.1
SF88	0.6	0.9	1.5	4	<0.1	0.9	0.9	4.7	3	2.7	<0.1	1.9	0.8	1.5	17	3.4	>0.1
SF89	3	1.2	7	4.4	29.1	4.2	0.9	1.4	5.3	17.5	2.1	3.4	2.2	1.9	3.5	2.7	7.2
SF90	1.2	2.1	1.8	0.9	11.5	0.1	1.4	2.2	1.4	0.9	1	1.3	1.1	1.2	1	2.2	2.4

Table A2.1. (Cont.) Pebble count results in centimeters.

Site																		
MS46	<0.1	1.8	1.2	<0.1	<0.1	0.1	0.3	>30	0.8	7.2	2.8	5.9	1.8	<0.1	0.1	1.2	14.5	
MS47	6.2	1.5	6.8	8.1	2	5	7.2	15.9	3.8	5	4.2	8.8	1.1	2.8	1.5	7.4	7.4	
MS48	<0.1	<0.1	<0.1	<0.1	<0.1	<0.1	<0.1	<0.1	<0.1	<0.1	<0.1	<0.1	<0.1	<0.1	<0.1	1.9	2	
MS49	<0.1	<0.1	<0.1	<0.1	<0.1	<0.1	<0.1	<0.1	<0.1	0.4	6.4	4.2	<0.1	5.2	0.9	<0.1	1	
MS50	<0.1	<0.1	9.9	<0.1	<0.1	<0.1	<0.1	<0.1	<0.1	<0.1	1.4	19.4	<0.1	<0.1	<0.1	<0.1	<0.1	
MS51	3.9	11.4	1.3	3.1	3.1	0.8	4.4	<0.1	3.5	17.2	2.3	5.5	2.4	1.2	0.8	1.7	2.1	
MS52	<0.1	<0.1	<0.1	<0.1	1.9	<0.1	<0.1	<0.1	1.5	<0.1	2.4	<0.1	<0.1	<0.1	<0.1	<0.1	1.2	
MS53	<0.1	<0.1	<0.1	<0.1	<0.1	<0.1	<0.1	4.5	<0.1	<0.1	<0.1	<0.1	9.6	<0.1	<0.1	<0.1	<0.1	
MS54	<0.1	<0.1	<0.1	<0.1	12.4	11.8	2.6	1.8	3	1.2	<0.1	4.1	1.7	7.8	1.1	1.7	0.5	
MS55	3.3	2.7	3	3.1	1	2.6	3.1	3.3	1.5	2.5	11.7	>30	1.1	9.2	15.5	1.2	6.8	
MS56	<0.1	<0.1	1.8	<0.1	<0.1	<0.1	1.8	3.8	2.6	2.8	<0.1	3.3	0.4	<0.1	0.8	11	3	
MS57	4.1	<0.1	<0.1	<0.1	<0.1	27	1.3	2.7	2.7	0.9	<0.1	<0.1	<0.1	<0.1	<0.1	1.7	2.2	
MS58	<0.1	<0.1	1.8	<0.1	<0.1	<0.1	<0.1	<0.1	<0.1	<0.1	<0.1	<0.1	<0.1	<0.1	<0.1	<0.1	<0.1	
MS59	<0.1	<0.1	<0.1	<0.1	<0.1	<0.1	<0.1	<0.1	<0.1	<0.1	<0.1	<0.1	<0.1	<0.1	<0.1	<0.1	<0.1	
MS60	9.9	5.7	0.5	1.7	12.6	9.6	2.8	10.7	0.3	2.2	13.9	4.5	1.2	2.2	1.2	2.2	11.7	
MS61	3.8	4.1	3.4	1.4	0.5	2.6	0.8	1.1	1.1	0.9	1.9	5.2	3.4	1.2	1.7	8.8	1.4	
MS62	<0.1	<0.1	<0.1	1.1	2	<0.1	<0.1	<0.1	<0.1	<0.1	<0.1	1.6	<0.1	<0.1	<0.1	1.8	<0.1	
MS63	<0.1	1.3	19.3	2.6	3.6	<0.1	1.3	3.4	1.1	2.2	2.7	3.5	1	7.2	1.2	>30	0.7	
MS64	2.3	<0.1	1.7	<0.1	2.1	2.8	1.9	1.5	<0.1	1.5	0.8	<0.1	2.7	2.4	<0.1	2	<0.1	
MS65	3	23.1	1.1	6.8	0.9	1.2	<0.1	0.2	1	5.7	1	2.9	0.8	1.5	1.1	1.5	1	
MS66	<0.1	0.6	1.8	1.1	2	1.3	<0.1	0.4	4.2	1.2	1.7	<0.1	<0.1	<0.1	3.6	<0.1	<0.1	
MS67	<0.1	3.3	<0.1	0.3	1.7	<0.1	4.2	3	2	2.4	0.7	5.9	2.7	0.6	1.6	<0.1	2.1	
NF68	<0.1	2	2.3	0.6	0.7	2.7	0.9	0.7	<0.1	<0.1	2.6	0.9	0.9	1	3.9	1.1	<0.1	
NF69	1.4	<0.1	3.4	1.2	<0.1	1.8	1.5	2.6	0.6	2	2.1	2	1.4	3.9	4.5	2.3	1.3	
NF70	2.3	3.5	1.1	<0.1	3	<0.1	1.9	1.1	3.4	<0.1	0.8	1.8	<0.1	0.8	0.9	0.5	1.2	
NF71	<0.1	2	0.5	3.9	<0.1	0.1	1.7	3.4	1.4	2.4	<0.1	0.5	4.4	<0.1	0.5	0.2	0.4	
NF72	0.7	0.7	<0.1	1.9	0.7	0.4	3.9	0.5	0.9	0.1	0.5	1.5	1.5	0.8	2.6	1.1	2.3	
NF73	<0.1	<0.1	3.8	<0.1	0.4	1.1	1.8	3.2	1.6	6.4	5.2	3.2	1.8	4.8	4.1	1.5	0.9	
NF74	1.4	4	2	2.6	8.9	7.9	2.2	4.1	3.7	2.5	1.9	2.4	5	2	1.8	3.1	5.6	
NF75	3.3	1.8	1.6	2.6	6.9	1.7	3	4.4	2	4.6	2.4	1.2	3	1.8	2.7	1.5	1.3	
NF76	2.4	2.1	2.7	<0.1	4.9	4	2.5	1.8	8.9	5.3	3.9	1.3	1.6	3.5	3.5	3.5	2.5	
NF77	1.4	<0.1	0.4	5	3.5	3.8	1.6	1.9	1.3	1.3	0.6	4.4	5.1	<0.1	<0.1	2	1.9	
NF78	0.7	2.2	1.6	2.8	3.5	0.9	2.7	1.6	1.3	9	6.1	1.3	2.1	2.6	1	<0.1	4	
NF79	2.6	7.1	13.3	7	1.6	0.5	1.6	1.8	4.8	0.6	2.9	1.3	2.2	0.5	3.6	1.8	0.6	
NF80	2.3	3.3	2.5	1.6	1.6	1.4	0.7	2	2.6	0.7	0.1	1.8	2.1	3.1	2.2	16.5	2.9	
NF81	1.1	3.9	2.6	0.9	<0.1	<0.1	0.9	2.9	<0.1	1	2.4	5.7	1.7	0.9	<0.1	0.8	1.5	
NF82	6.9	8.5	5.3	1.5	12.3	1.8	2.2	0.6	2.7	2.3	2.1	2.2	5.1	>30	7.8	4.1	2.2	
NF83	2	2.5	12.7	27.4	4.4	7.1	2.2	3.2	1.6	1.3	7.8	2.5	6.5	0.5	16.1	5.1	0.9	
NF84	5.9	17.3	1.3	4.7	2.3	3.7	2.1	0.7	7.2	5.3	1.9	0.7	0.9	4.4	2.7	1.5	1.2	
NF85	1	1.2	<0.1	<0.1	<0.1	0.5	<0.1	1	<0.1	1.7	<0.1	1.5	1.3	<0.1	0.5	<0.1	<0.1	
SF86	1.6	2.2	<0.1	<0.1	0.6	1.7	2.2	<0.1	<0.1	<0.1	10.8	<0.1	<0.1	<0.1	<0.1	0.8	0.8	
SF87	3	7.9	5.3	<0.1	3.9	8.8	13.8	17.8	2	0.3	1.2	20.6	7.8	5.5	1.2	0.5	0.1	
SF88	1.8	1.4	0.9	3.9	3.3	1.9	0.8	<0.1	1.2	1.5	<0.1	0.3	1.9	2.9	4	1.8	<0.1	
SF89	>0.1	4.4	6.1	0.1	2.1	0.2	5.8	6.8	1.7	1	3	2.7	6.9	9.7	3.2	0.8	2.2	
SF90	1.9	0.8	1.3	2.7	0.8	0.6	2	1.9	2.6	1.4	0.1	0.2	1.4	<0.1	0.9	1.2	0.2	

Table A2.1. (Cont.) Pebble count results in centimeters.

Site																		
MS46	0.5	12.5	0.8	>30	0.6	8	10.6	2.6	<0.1	>30	1.3	4	<0.1	0.3	7.2	6.8	1.9	
MS47	2.3	3.5	2.1	3.7	5.5	5.2	3.3	5.7	2.5	1.6	1.7	1	5.6	1.2	2.2	8.2	0.6	
MS48	1.7	15.8	<0.1	<0.1	<0.1	<0.1	<0.1	<0.1	<0.1	<0.1	<0.1	<0.1	<0.1	<0.1	<0.1	<0.1	15.5	
MS49	<0.1	1.7	0.8	0.5	2.3	1	<0.1	9	<0.1	2.8	5	1	<0.1	5.7	<0.1	<0.1	6	
MS50	<0.1	<0.1	<0.1	15.5	<0.1	<0.1	<0.1	<0.1	<0.1	<0.1	<0.1	25.1	<0.1	<0.1	<0.1	<0.1	<0.1	
MS51	2.1	5.5	1.5	0.8	2.6	1.6	1.7	1.7	<0.1	1.3	1.8	1.8	1	1	<0.1	1.7	0.9	
MS52	<0.1	<0.1	1.5	<0.1	<0.1	<0.1	<0.1	2.9	<0.1	<0.1	<0.1	<0.1	<0.1	<0.1	<0.1	<0.1	<0.1	
MS53	<0.1	<0.1	6.6	<0.1	<0.1	<0.1	<0.1	<0.1	<0.1	0.5	<0.1	<0.1	<0.1	<0.1	<0.1	<0.1	<0.1	
MS54	2.2	<0.1	2.3	<0.1	2.2	2.1	1.2	3.3	1	0.9	1.3	2.4	2.1	1.7	2.6	10.5	10	
MS55	13.8	2.9	5.6	1	1	20.1	1.7	3.4	0.7	2.7	1.6	1.8	3.6	10.6	1.9	2.7	3.8	
MS56	<0.1	<0.1	2	<0.1	<0.1	<0.1	14.5	5.4	1.9	<0.1	1.3	2.3	5.4	<0.1	2	8.5	<0.1	
MS57	2.2	1.4	1.4	0.8	0.8	<0.1	1.8	<0.1	<0.1	<0.1	<0.1	<0.1	3.9	3.2	1.1	2.3	1.4	
MS58	<0.1	<0.1	<0.1	<0.1	<0.1	3	<0.1	1.5	<0.1	<0.1	<0.1	2.2	<0.1	<0.1	<0.1	<0.1	<0.1	
MS59	<0.1	<0.1	<0.1	<0.1	<0.1	<0.1	<0.1	<0.1	<0.1	<0.1	<0.1	<0.1	<0.1	<0.1	<0.1	<0.1	<0.1	
MS60	3.5	<0.1	11.4	1.8	1.6	4	10.9	8.7	2.5	1.1	2.3	24.7	6.7	1.6	10.5	3.8	1.5	
MS61	2.2	2.5	2.5	0.5	9.9	5.8	4	2.7	0.9	1	1.9	1.1	3.7	1.9	2.4	3.6	2.5	
MS62	<0.1	<0.1	<0.1	<0.1	<0.1	<0.1	<0.1	<0.1	<0.1	<0.1	<0.1	<0.1	2.6	<0.1	<0.1	0.4	0.4	
MS63	1	2.9	2.5	0.7	1.6	2.7	1.5	1.3	2	2.2	<0.1	<0.1	0.5	2.1	2.4	9.8	2.5	
MS64	<0.1	1.6	<0.1	0.9	1.7	0.9	1.9	<0.1	<0.1	<0.1	1.9	2.8	<0.1	<0.1	0.8	<0.1	0.4	
MS65	1	1.5	3	0.2	2.2	0.6	1.2	0.1	1.8	1.8	4	0.2	1.4	1.1	2.3	4.3	0.5	
MS66	<0.1	0.9	<0.1	1.3	2	<0.1	<0.1	<0.1	<0.1	1.5	<0.1	<0.1	<0.1	<0.1	<0.1	0.8	0.6	
MS67	<0.1	0.7	2.2	2.5	11.1	1.8	<0.1	4.1	12.6	1	2	2.3	<0.1	<0.1	0.7	3.9	14.5	
NF68	0.8	0.9	0.5	0.8	1.4	1.8	1	1.1	2.7	0.7	1.5	1.8	0.9	<0.1	0.9	1	<0.1	
NF69	1.7	<0.1	2.1	2.4	2.9	2.5	1.6	1.2	2.1	1.5	2	1.1	3.5	2.7	<0.1	<0.1	2.2	
NF70	3.9	1.6	3.3	<0.1	1.9	3.1	3.1	3.1	1	<0.1	5.6	<0.1	0.7	1.3	<0.1	2.5	3.6	
NF71	<0.1	2.1	0.7	<0.1	0.4	0.7	0.8	2.9	0.4	0.5	0.6	1.4	<0.1	0.5	<0.1	0.6	0.3	
NF72	2.8	2.2	0.2	0.8	2.4	0.2	0.3	2.5	0.5	0.6	4.7	0.6	0.3	0.2	2	0.4	2.9	
NF73	2.6	0.8	1.8	1.7	2.7	3.8	2.1	3.3	5.1	1.6	2.9	1.2	2.1	1.5	1.3	0.6	0.9	
NF74	1.5	1.7	0.5	0.6	2.2	2.9	1.2	2.1	2.5	1.2	3.2	<0.1	3.9	<0.1	2.1	13	1.6	
NF75	4.7	4.1	3.2	3.2	3.7	2.7	2.2	0.8	2	3.5	1.2	1.3	3.1	1.6	4	2.6	3.9	
NF76	11.3	2.5	1.5	2.3	0.9	6.9	3	2.1	2.7	2.5	3.5	2	2	29	5	3.6	1.9	
NF77	0.2	1.9	10.8	1.2	3.3	3	1.7	0.6	1.5	<0.1	2.6	2.5	1.9	0.6	1.7	10.1	2.2	
NF78	2.9	1.5	4.9	2	0.6	3.6	0.2	1.1	7	4	1.6	0.4	6.1	0.8	2.1	2.6	14.1	
NF79	17	2.5	7.8	0.9	8.5	3.4	1.1	1.1	1.5	1.1	2	0.6	4.9	1.4	3.8	6.1	13.6	
NF80	1.3	2.9	1	4.3	1.6	0.5	2.3	2.3	2.2	0.6	4.1	4.1	1.5	1	2.2	2.2	1.2	
NF81	0.6	0.8	3.4	1.5	1.3	2.3	1.2	1.2	1.9	0.4	2.1	0.7	3.5	0.3	0.5	0.7	2.8	
NF82	4.3	0.7	4.4	0.8	0.4	3.9	3.2	2	6.3	3	2	0.8	1.1	4.1	2.6	1.1	0.7	
NF83	2.1	0.9	7.7	2.2	2	4.2	2.8	6.3	1.1	11.3	1.6	2.8	2.1	0.9	1	4.1	6.2	
NF84	<0.1	1	9.9	<0.1	8.3	14.6	1.5	2.1	<0.1	5.4	1.4	<0.1	3.3	<0.1	1.1	3.5	11.4	
NF85	<0.1	1.5	<0.1	<0.1	<0.1	0.7	3.5	0.9	<0.1	2	1.9	2.4	0.3	0.9	<0.1	2.5	<0.1	
SF86	1.2	<0.1	0.4	1.5	<0.1	1.2	1.7	<0.1	2.6	<0.1	<0.1	<0.1	<0.1	0.9	<0.1	<0.1	<0.1	
SF87	8.7	1.1	2.7	1.3	17.8	2.6	2.2	6.2	4.1	0.6	0.4	1.7	2.6	2	1.8	0.7	11.5	
SF88	1.8	2	2.5	0.6	3.8	1.2	1.8	0.8	1.5	1.7	5.5	1.3	1	1.4	1.2	4.8	2.2	
SF89	5.7	3.7	0.8	3.3	9.2	7.4	2.5	6.5	9	3.2	2.7	0.6	6.6	1.2	3.1	1.1	10.6	
SF90	1.3	0.5	2.6	2.1	1.6	0.6	1.1	3.2	2.3	2.7	1.1	3.1	2.6	0.1	2.4	1.3	0.6	

Table A2.1. (Cont.) Pebble count results in centimeters.

Site																		
MS46	4.6	0.3	0.1	2.7	1.6	3.6	0.1	1.6	0.1	0.2	3.6	0.4	<0.1	2.8	3.1	0.4	2.2	
MS47	1.1	3.5	2.2	2.3	6	2.5	2.6	1.3	1.5	1.4	2.5	5.6	3.1	2.1	1.2	3	1.8	
MS48	<0.1	<0.1	<0.1	<0.1	<0.1	<0.1	<0.1	<0.1	<0.1	<0.1	<0.1	<0.1	<0.1	<0.1	<0.1	<0.1	<0.1	
MS49	0.4	1.5	1.8	<0.1	1.5	4.4	4.4	<0.1	1.6	<0.1	1.5	3	4.2	<0.1	3	3.2	<0.1	
MS50	<0.1	<0.1	<0.1	<0.1	<0.1	<0.1	<0.1	<0.1	<0.1	<0.1	<0.1	<0.1	<0.1	<0.1	<0.1	<0.1	<0.1	
MS51	2.1	0.6	0.4	1.7	3.2	1	<0.1	<0.1	10.2	11.6	1.7	1	4.1	2.2	0.7	1.5	1.5	
MS52	<0.1	<0.1	<0.1	1	<0.1	<0.1	1.2	<0.1	<0.1	<0.1	<0.1	1.7	<0.1	1.1	<0.1	<0.1	<0.1	
MS53	<0.1	<0.1	<0.1	<0.1	<0.1	<0.1	2.1	<0.1	<0.1	<0.1	<0.1	<0.1	<0.1	<0.1	<0.1	<0.1	<0.1	
MS54	<0.1	2	3.2	1.8	7.9	0.8	1.7	<0.1	2.8	2.4	2.8	7.9	0.6	2	2.6	<0.1	1.3	
MS55	3.2	1.3	0.6	<0.1	8.9	6.5	<0.1	1.4	<0.1	8.7	1.4	1.2	2	10.8	2.1	1.4	10.4	
MS56	3.3	4	2.2	<0.1	1.4	2.3	0.5	13.2	<0.1	1.5	2.6	11.8	1.7	1.4	1.3	<0.1	3.6	
MS57	0.3	0.6	1.1	<0.1	3.8	<0.1	2.4	0.5	<0.1	<0.1	<0.1	<0.1	<0.1	<0.1	0.4	4.2	<0.1	
MS58	<0.1	<0.1	<0.1	<0.1	<0.1	<0.1	<0.1	<0.1	<0.1	<0.1	<0.1	<0.1	<0.1	3.6	1.8	<0.1	<0.1	
MS59	<0.1	<0.1	<0.1	<0.1	<0.1	<0.1	<0.1	<0.1	<0.1	<0.1	<0.1	<0.1	<0.1	<0.1	<0.1	<0.1	<0.1	
MS60	2	2.2	1.1	3.8	10.1	1.5	1	3.1	1.6	7.5	3.5	1.6	2.2	3.2	1.4	2.3	2.3	
MS61	2	1.9	0.9	1.5	7.5	2.1	2.6	1.5	0.7	2	1.1	1.3	4.6	1.1	1.2	5.6	3.6	
MS62	<0.1	<0.1	1.8	<0.1	<0.1	<0.1	<0.1	<0.1	<0.1	1.1	<0.1	<0.1	<0.1	<0.1	<0.1	<0.1	<0.1	
MS63	1.6	4	1.1	0.8	1.2	2.6	3.2	9.9	1.4	0.3	2.4	1	1.1	1.2	2.8	10.6	2.6	
MS64	<0.1	1.9	3.5	<0.1	<0.1	<0.1	1.2	3.3	<0.1	<0.1	<0.1	<0.1	2.7	5	4	<0.1	<0.1	
MS65	1.5	1.9	1	0.3	0.8	1.9	1.1	0.8	1.5	0.5	1.4	2	1	2.2	4	<0.1	3	
MS66	<0.1	0.7	<0.1	2.5	1.6	<0.1	1	<0.1	2.4	<0.1	<0.1	3	<0.1	3.7	<0.1	<0.1	2.1	
MS67	2.4	0.9	1.2	1.2	3	<0.1	<0.1	<0.1	2.6	1.5	<0.1	13.4	0.8	<0.1	1.7	<0.1	3.2	
NF68	<0.1	1.5	1.1	1	<0.1	<0.1	1.2	1	1.9	<0.1	1.5	0.9	0.8	<0.1	<0.1	<0.1	1.2	
NF69	1	1.4	0.7	0.6	1.2	2.5	1.4	0.8	3	2	1	0.7	1.2	2.4	0.9	1.3	0.7	
NF70	1.6	1.2	1.5	<0.1	0.8	2	1.5	<0.1	<0.1	<0.1	3	1.6	1.8	<0.1	1.1	2.5	0.9	
NF71	0.5	2.2	1.9	1.2	1.5	<0.1	4.6	2.1	0.6	1.2	3.6	0.6	0.7	0.1	0.5	0.5	0.9	
NF72	1.7	1	0.6	1.5	3.8	0.7	0.5	0.7	0.2	1.3	1.1	1.6	1.9	0.5	1.8	4.6	0.7	
NF73	2.5	0.5	4.7	2.4	3.3	2.4	3.8	1.8	1.6	2.9	0.9	3.5	2.7	<0.1	2.4	1.2	3.7	
NF74	2.5	2.7	2.6	1	2.6	3.1	<0.1	1.3	2.1	3	9.8	2	5.5	2.4	3	1.6	1.6	
NF75	1.6	3.5	1.2	1.7	1	2.4	1.1	1.5	1	<0.1	2.2	2.3	1.5	0.6	4.5	3.6	2.7	
NF76	2.7	3.1	1	2.6	3.1	1.9	3.6	2.6	1	3	6	1.5	9.8	1.3	6.7	3.8	2.6	
NF77	4.2	3.6	2.6	0.6	2.1	9.6	4.3	2.2	2	9	6.5	2.9	3.9	2	3	0.5	1.5	
NF78	7.8	<0.1	3	1.8	1.4	1.7	3	1.5	1	2.3	1	2.6	1.6	2.6	2.5	2.6	3.7	
NF79	12.1	3.9	0.4	2.4	2.4	8.5	0.7	2.2	2	2.2	2.6	5.2	1.4	0.6	0.7	2.8	1.6	
NF80	21.3	1.5	1.3	1.4	1.2	2.4	0.6	0.4	1.4	0.6	0.3	6.9	1.3	0.6	4.5	1.1	5.2	
NF81	<0.1	<0.1	0.7	3.6	0.3	<0.1	0.6	0.6	0.6	2.7	1	2.5	1.9	1.2	0.7	<0.1	0.6	
NF82	7.8	10.5	3.1	4.1	4	7.1	2.3	3.9	0.4	2.2	1.8	11.5	1.4	6.2	1.8	4.8	3.9	
NF83	3.6	1.5	1.9	14.6	1.5	0.6	2.8	8.3	1.1	2.9	12.2	0.8	8.3	6.7	0.4	0.6	5.5	
NF84	9.5	0.9	9.7	4.2	11.1	<0.1	9.9	1.4	1	0.6	1.8	4.2	5.4	<0.1	<0.1	6.5	3	
NF85	<0.1	3.2	<0.1	<0.1	<0.1	0.4	0.4	<0.1	<0.1	<0.1	0.8	0.8	2.8	0.2	2.6	2.2	1.8	
SF86	<0.1	<0.1	<0.1	1	1.2	<0.1	<0.1	0.8	3.2	0.1	<0.1	<0.1	2.1	5.7	0.3	<0.1	1.4	
SF87	4.9	1.2	1.6	5.4	5.3	4.9	2.6	3.5	12.2	2.5	1.9	20	20.6	12	1.8	2.5	4.4	
SF88	2.1	2.3	3.4	5.5	2.3	1.4	1.8	2.2	1.1	1	0.8	4.6	1.6	3.7	3.2	0.6	0.1	
SF89	3.3	2.9	5.3	3.6	11.7	2.2	7.4	2.4	3.9	<0.1	6.9	4	0.8	6.3	4.1	2.3	2.1	
SF90	0.3	3.7	6	2.9	1	1	0.8	0.6	0.6	7.8	0.5	0.5	1.7	7.5	<0.1	1.3	1	

Table A2.1. (Cont.) Pebble count results in centimeters.

Site																		
MS46	3.4	0.4	2.4	<0.1	1.6	<0.1	<0.1	0.5	5.9	<0.1	24	<0.1	3	<0.1	<0.1	4.5	2.6	
MS47	1.2	4.4	1.8	3.9	2.8	15.5	2.6	2.7	22	13.9	1.9	9.5	2.1	2	3.4	2.6	2.8	
MS48	<0.1	8.9	<0.1	<0.1	<0.1	<0.1	<0.1	<0.1	<0.1	<0.1	<0.1	<0.1	<0.1	<0.1	<0.1	<0.1	<0.1	
MS49	0.7	4.7	3.5	2.2	1	1.6	0.9	3	1.1	1.2	3.1	3.3	2.8	1.3	1.9	2	<0.1	
MS50	<0.1	<0.1	<0.1	<0.1	<0.1	<0.1	<0.1	<0.1	<0.1	<0.1	<0.1	<0.1	<0.1	<0.1	<0.1	<0.1	<0.1	
MS51	<0.1	1.6	<0.1	1.9	1.8	0.4	1.1	1	0.4	1.4	1.3	0.8	1.3	0.6	0.3	17.8	2.4	
MS52	<0.1	<0.1	3.8	<0.1	<0.1	<0.1	<0.1	<0.1	<0.1	<0.1	<0.1	2.2	<0.1	<0.1	<0.1	<0.1	<0.1	
MS53	<0.1	<0.1	<0.1	2	<0.1	<0.1	3.2	<0.1	<0.1	<0.1	<0.1	<0.1	<0.1	3.1	2.6	<0.1	<0.1	
MS54	0.6	3	1.1	6.9	2.4	2.3	1.2	1.9	1.9	1.5	1.7	11.4	2.1	1.4	1	1.1	1.8	
MS55	7.6	7	2.1	1.9	2.3	3	3	2.2	4.1	6.7	6.5	5.5	<0.1	2.5	2	<0.1	3.6	
MS56	2.2	<0.1	2.5	1.2	0.9	2.1	3.8	16.2	<0.1	0.5	1.8	3.3	0.6	<0.1	3.2	<0.1	2.2	
MS57	<0.1	<0.1	3.2	<0.1	2.1	3.6	<0.1	0.5	<0.1	<0.1	<0.1	<0.1	<0.1	<0.1	<0.1	<0.1	2.6	
MS58	<0.1	1.3	1.5	<0.1	<0.1	<0.1	<0.1	<0.1	<0.1	1.3	<0.1	<0.1	1.9	<0.1	<0.1	<0.1	2.8	
MS59	<0.1	<0.1	<0.1	<0.1	<0.1	<0.1	<0.1	<0.1	<0.1	<0.1	<0.1	<0.1	<0.1	<0.1	<0.1	<0.1	<0.1	
MS60	0.5	0.7	<0.1	7	1.2	8.7	2.4	1.3	2.5	1.3	2.8	4.2	2.8	1.8	8	3.3	1.2	
MS61	2.3	2	2.4	1.1	2.2	0.7	1.2	0.8	3.6	3.1	2	7.3	4.5	1.4	2.1	1.2	1.5	
MS62	<0.1	0.8	<0.1	<0.1	<0.1	<0.1	<0.1	<0.1	<0.1	<0.1	<0.1	<0.1	<0.1	<0.1	<0.1	<0.1	<0.1	
MS63	0.7	1.2	0.4	2.7	2	2.7	1.7	<0.1	0.1	2.2	2.5	0.2	1.2	0.1	<0.1	1.6	0.9	
MS64	<0.1	<0.1	1.7	2.8	<0.1	2.4	2.5	<0.1	<0.1	<0.1	2.8	1.8	<0.1	<0.1	1.9	2.8	0.3	
MS65	2.8	0.7	4.6	3.5	2.1	2.5	7.2	2.6	1.6	3.5	<0.1	3.8	3	0.8	<0.1	0.8	1	
MS66	0.9	<0.1	1.5	1.1	0.9	1.3	<0.1	<0.1	0.5	<0.1	<0.1	1.5	1.7	1.1	1.4	<0.1	3.5	
MS67	1.5	2.5	<0.1	1.7	<0.1	1.2	13.9	0.2	1	0.8	0.1	0.8	1.2	1.9	2.4	1.3	1.3	
NF68	1	0.7	<0.1	0.5	1	2.3	<0.1	<0.1	0.6	0.6	<0.1	<0.1	0.6	0.6	0.8	1.5	<0.1	
NF69	2.1	1.8	1	6.1	1.1	1.9	0.8	1.5	1.2	1.4	2.7	1.2	2.5	1.6	1.4	3.3	0.8	
NF70	2.9	3.4	0.4	3.6	3.8	3.1	2.3	2.1	1.6	0.9	<0.1	0.6	1.3	0.8	0.8	1	2.1	
NF71	2.3	1	1.1	0.6	0.9	0.8	1.7	0.7	<0.1	1	0.6	2.4	<0.1	2.2	1.9	2	0.2	
NF72	0.3	0.6	1.5	2	0.3	1.2	0.7	1.1	1.1	0.8	0.9	1.2	1	0.1	1.2	3.1	0.6	
NF73	2.1	3.2	4.2	2.7	0.8	0.9	1	2.5	1.3	1.7	3.6	3.9	1.7	2.5	1.1	2.4	1.8	
NF74	<0.1	2.4	0.9	9.9	3.9	1	2.2	1.4	1.2	3	2.4	2.4	1.5	1.1	1.2	1.9	1.8	
NF75	3.6	2.1	1	2	4	1	0.9	2.5	0.8	2.7	2.2	3	3.4	3.2	2	5.5	1.7	
NF76	0.9	14.6	0.8	2.5	2.5	2.6	1.7	6.7	1.5	4.6	1.4	2.3	4.5	0.3	0.8	2.3	3.1	
NF77	2.2	2.1	1.2	2.7	1.3	2.3	3.4	3.2	1.3	3.4	1.1	1.3	<0.1	2	2.7	7.4	1.5	
NF78	2.7	1.3	1.3	1.9	3.5	1.5	7.6	2.5	1.9	1.3	1.5	4.3	1	2.9	<0.1	<0.1	2	
NF79	1.1	4.1	6.2	2.3	0.7	0.5	0.5	0.5	1.7	3.3	2.8	2.3	1.5	2.9	1.6	0.6	6.6	
NF80	1.2	3	0.7	5.5	0.7	4.3	0.4	1.2	1.9	3.1	1.4	3.2	4.8	0.6	1	1.7	2.3	
NF81	2.5	2.3	0.5	1	0.9	1.5	1.9	0.9	1.9	0.2	0.8	2.7	3.5	1.1	2.2	0.5	0.6	
NF82	3.7	3.3	3.3	1.3	0.9	0.8	5.6	4.3	2	3.5	1	0.8	0.8	1	1.3	3.7	1	
NF83	0.8	2.6	0.6	1.2	3	8.1	0.6	9.4	<0.1	3.7	6.1	2.4	6.3	4.3	0.7	0.5	13.2	
NF84	1.3	8.4	4.7	5.7	3	0.9	0.6	1.7	13	1.3	2.5	<0.1	2.1	0.9	1.6	4.4	0.6	
NF85	<0.1	<0.1	0.3	0.9	<0.1	0.6	1.7	2	<0.1	<0.1	<0.1	<0.1	<0.1	<0.1	1.1	<0.1	2.7	
SF86	0.3	<0.1	<0.1	<0.1	2	3	0.3	<0.1	1.9	0.7	<0.1	<0.1	<0.1	1	3	<0.1	<0.1	
SF87	3.5	1.7	1.3	4.2	3	10.4	3.6	24.3	12.5	1.5	7	3	6.7	1	22.5	1	<0.1	
SF88	1.9	<0.1	0.4	2.2	2.6	3.1	<0.1	1.6	2.3	1	0.6	0.8	1.3	1.5	0.1	0.9	<0.1	
SF89	6.2	2.6	6.7	4.7	4	0.4	2.4	7.3	0.9	1.2	3.1	1.8	2.5	2	3.4	4	1.6	
SF90	0.3	0.5	1.2	1.5	1	0.6	1	0.6	<0.1	1.1	0.5	0.1	3.1	0.4	3	1.2	1.4	

Table A2.1. (Cont.) Pebble count results in centimeters.

Site															
MS46	1.9	0.1	1.9	4.3	2.1	6.2	1.8	0.1	0.1	<0.1	1	0.3	1.8	0.7	1.2
MS47	0.8	1.1	1.5	3.7	1.7	3.5	1.8	1.3	1.1	0.6	1.9	4.8	4.6	0.9	1.5
MS48	<0.1	<0.1	<0.1	<0.1	<0.1	<0.1	<0.1	<0.1	0.5	6.8	<0.1	<0.1	<0.1	<0.1	<0.1
MS49	<0.1	<0.1	3.3	0.9	1	<0.1	1.5	1.8	1	<0.1	1.9	2.2	2	1.1	1.6
MS50	<0.1	<0.1	<0.1	<0.1	<0.1	<0.1	<0.1	<0.1	<0.1	<0.1	<0.1	<0.1	<0.1	<0.1	<0.1
MS51	1.2	1.8	2.9	1.4	2.6	1.8	1.2	<0.1	1.1	3.2	3.9	1.1	1	2.3	1.1
MS52	<0.1	<0.1	<0.1	<0.1	<0.1	<0.1	<0.1	<0.1	<0.1	<0.1	<0.1	<0.1	0.9	<0.1	0.8
MS53	<0.1	<0.1	<0.1	<0.1	<0.1	<0.1	<0.1	<0.1	<0.1	<0.1	<0.1	7.8	<0.1	<0.1	<0.1
MS54	1.8	10.2	15.2	9.4	14.3	>30	27.5	1.9	0.8	3.2	0.6	1.2	2	0.6	2.2
MS55	0.8	1.5	3.1	2	0.9	1.5	2.2	3.8	2.8	2.3	0.8	<0.1	1.9	14.7	1.6
MS56	2.8	2.1	<0.1	2.6	2.5	3.2	<0.1	<0.1	<0.1	<0.1	0.6	4.6	1.8	<0.1	1.5
MS57	<0.1	<0.1	<0.1	1.5	3	<0.1	<0.1	2.3	1.3	0.7	<0.1	<0.1	<0.1	2.5	<0.1
MS58	1.1	<0.1	<0.1	4.1	<0.1	<0.1	0.8	<0.1	<0.1	<0.1	<0.1	1.2	<0.1	<0.1	<0.1
MS59	<0.1	<0.1	<0.1	<0.1	<0.1	<0.1	<0.1	<0.1	<0.1	<0.1	4.2	<0.1	<0.1	<0.1	<0.1
MS60	3.1	2.3	<0.1	5.8	0.8	7.4	1.5	8.9	1.8	0.6	1.7	1.2	1.2	3.5	1.4
MS61	0.5	8.6	3.6	1.5	3.4	7.6	5	0.8	7	1.3	2.4	3	2.1	2.7	1.7
MS62	<0.1	<0.1	<0.1	<0.1	<0.1	<0.1	<0.1	<0.1	<0.1	0.7	<0.1	<0.1	<0.1	<0.1	<0.1
MS63	1.7	2.6	0.8	2	0.7	3	1.1	2.8	1.6	2.4	<0.1	3.1	2.6	0.4	1.1
MS64	<0.1	<0.1	1.4	2.4	0.6	3.7	5.1	2.5	3	<0.1	<0.1	1	0.5	1.4	<0.1
MS65	0.8	1.9	1	0.6	2.5	0.9	1.6	1.5	2.2	1	2.5	1	0.4	1.5	1.2
MS66	<0.1	<0.1	0.7	1	<0.1	<0.1	<0.1	<0.1	<0.1	<0.1	1.1	1.5	<0.1	1.8	<0.1
MS67	0.8	<0.1	1.2	1.2	1.7	<0.1	<0.1	2.8	<0.1	1.8	2.3	0.9	2.4	<0.1	<0.1
NF68	<0.1	1.5	1.7	1.7	<0.1	0.5	1.3	0.5	0.6	<0.1	<0.1	0.3	1	1	<0.1
NF69	1.1	2.2	1.3	0.7	0.9	1.5	2.6	2.3	1.2	0.6	0.8	1	0.8	4.9	0.6
NF70	2.4	2.6	2.9	2.6	<0.1	<0.1	2.3	1.2	1.9	1.3	2.4	1.4	2.5	3.2	1.4
NF71	0.8	0.7	1.2	0.7	2.1	2.9	1.1	0.8	<0.1	3.5	3.7	2.4	3.3	1.2	<0.1
NF72	2.3	1	0.7	0.5	0.8	0.6	0.7	0.5	0.8	2	1	0.1	1.5	0.4	0.4
NF73	2.2	4.7	0.6	2.6	0.5	0.9	0.8	8.1	<0.1	<0.1	2.8	<0.8	2.1	1.1	1.8
NF74	1.6	1.5	2.3	2.3	2.5	2.1	2.6	2.3	2	2	2.6	1	1.1	1.2	0.9
NF75	3.5	2.5	1.8	<0.1	4.5	<0.1	1	0.9	0.9	0.3	2.4	0.6	0.9	1.8	1.4
NF76	4	2.2	2.6	2.1	2.9	0.7	2.9	1.5	1	1.2	3.4	1.4	2.5	3.3	2.6
NF77	1.9	2.5	1.1	1.9	4.1	2.2	3	1.5	12.7	2.2	2.3	3.3	1.3	1.2	1.5
NF78	1	5.3	2	4.1	2.8	2.6	2.5	2.5	1.5	8.5	2.4	<0.1	5.6	1.7	1.7
NF79	1.5	2.7	14.6	3.9	1.7	0.4	7.6	1.7	2.9	1.1	1.6	2.6	3.7	5.3	4.3
NF80	4	3.2	<0.1	1	2.1	>30	2	16.1	5.4	20.5	0.9	0.5	2.7	1	2
NF81	1.7	1.5	1	1.3	0.6	1.7	0.7	0.6	0.6	0.7	1.5	0.9	3	0.2	0.8
NF82	10.3	1.7	10.7	1.8	2.7	1	11.6	1.1	0.8	1.8	2.7	2	7	1	2.5
NF83	2.3	4.3	1.5	5.5	0.4	1.8	1.8	0.9	1.1	1.2	8.1	7.9	2.7	0.3	1.1
NF84	6.5	3.4	3.5	1.1	7	2	0.5	0.7	0.7	19	1.4	1.4	2.3	3.5	4
NF85	<0.1	<0.1	<0.1	0.9	1.3	1.6	2.3	0.5	1.7	<0.1	<0.1	1	2.9	1.3	0.6
SF86	<0.1	0.4	2.2	<0.1	<0.1	1.8	<0.1	<0.1	2	1.3	1.3	<0.1	<0.1	1.6	1
SF87	1.4	0.9	0.8	2.8	0.9	0.9	0.9	5	4.5	2.6	6.6	6.5	7.9	8.1	1.8
SF88	0.9	0.6	2.7	0.5	0.4	4.2	1.2	3.4	<0.1	0.6	0.2	1.2	2.9	2.3	1
SF89	9.4	9.1	1.3	3.6	2.4	3.9	2.2	1.9	0.5	0.9	2.7	5	4.1	1	1.6
SF90	2	0.9	1.1	0.5	1.9	1.3	0.5	0.6	1.9	2.4	2.5	0.9	1.2	<0.1	0.7

Table A2.1. (Cont.) Pebble count results in centimeters.

Site																		
SF91	1.4	1.3	0.4	0.4	0.5	<0.1	2.8	2.6	2.3	1.8	<0.1	1.2	0.7	1.6	1	0.7	<0.1	
SF92	7.5	22.2	0.4	13.4	9.7	6.4	5.2	5.2	5.8	3.4	<0.1	4.8	9.1	4.3	8.2	3.4	1.8	
SF93	0.6	0.8	1.2	1.3	1.7	0.2	6.9	0.5	0.9	12.7	0.1	4.3	1.4	24.2	0.8	0.9	0.8	
SF94	1.9	2.4	1.4	1.6	2.7	1.5	0.9	1.8	1.3	0.7	1.4	0.4	0.8	0.9	0.9	1.1	1.5	
SF95	3	1.5	1.1	4	0.2	1.5	2	2	1.5	25.3	1.6	2.8	0.8	1.3	0.9	1.1	1.3	
SF96	22.1	1	<0.1	0.2	4.5	2.3	1.1	1.3	2.1	2.6	1.2	1.6	0.7	<0.1	1.7	1.6	1.2	
SF97	<0.1	1.2	3.2	15.5	<0.1	11.4	9.5	6	<0.1	13.7	0.6	2.5	6.9	5	5.6	5.3	12.7	
SF98	<0.1	<0.1	<0.1	<0.1	<0.1	<0.1	15	<0.1	<0.1	<0.1	<0.1	<0.1	<0.1	<0.1	<0.1	<0.1	<0.1	
SF99	0.3	0.7	1.1	0.4	0.9	0.3	0.3	0.7	0.3	0.9	0.4	3.3	0.8	0.4	0.8	1	<0.1	
SF100	<0.1	<0.1	<0.1	<0.1	<0.1	<0.1	<0.1	<0.1	<0.1	<0.1	<0.1	<0.1	<0.1	<0.1	<0.1	<0.1	<0.1	
SF101	<0.1	<0.1	<0.1	<0.1	<0.1	<0.1	<0.1	<0.1	<0.1	0.4	<0.1	<0.1	<0.1	<0.1	<0.1	<0.1	<0.1	
SF102	2.2	13.8	<0.1	<0.1	<0.1	<0.1	<0.1	<0.1	<0.1	<0.1	13.6	<0.1	<0.1	<0.1	<0.1	<0.1	<0.1	
SF103	<0.1	<0.1	<0.1	<0.1	<0.1	<0.1	<0.1	<0.1	<0.1	<0.1	<0.1	<0.1	1.2	<0.1	<0.1	<0.1	<0.1	
SF104	<0.1	<0.1	<0.1	<0.1	<0.1	<0.1	<0.1	<0.1	<0.1	<0.1	<0.1	<0.1	<0.1	<0.1	<0.1	<0.1	<0.1	
SF105	<0.1	2.7	<0.1	4.2	4.4	<0.1	1.7	<0.1	18.3	0.7	<0.1	<0.1	<0.1	<0.1	<0.1	<0.1	<0.1	
MS106	0.3	1	1.5	1.2	2.6	2.2	1.2	0.8	1.4	1.5	1	2.5	2.1	1.5	3.2	2.4	4.5	
MS107	<0.1	13.4	<0.1	0.7	2	3.7	6	0.9	6.7	2.2	7.9	4.7	2.5	4.7	<0.1	6.6	2.9	
MS108	2.4	1	3.4	1.4	4	10.5	2.2	3.1	5.7	13.5	11.5	3	6.9	6	4.1	10.5	1.9	
MS109	2.7	1.3	7.2	1.1	4	<0.1	4.1	5.6	<0.1	1.2	3	11.5	3.7	3.3	0.5	<0.1	<0.1	
NF110	3.3	4.9	1.8	1.2	3.3	3.4	2.8	1	1	5.9	10	5.1	3.3	1.2	1.5	2	0.5	
NF111	16	1.6	1.6	1.2	10.6	2	1.8	5.6	1.3	2.6	1.5	4	2.8	2.7	1.4	2.9	4.6	
NF112	6.6	5.3	2.6	4	3.8	1.6	2.4	2.6	8.3	4.6	4.6	1.8	1.8	4.1	1.7	2.8	2.6	
NF113	14.4	19	6.8	1.4	5	3.2	1.9	1.6	2.6	2.2	3.4	6.1	17.2	3.4	10.3	4.4	2.5	
NF114	2	2	2.4	3.1	2.2	1.1	0.7	1.5	2.8	4.7	4.5	8.3	1.2	1.8	0.8	1.2	1.1	
SF115	19	1.2	3.2	5.3	4.2	1.4	0.5	1.9	<0.1	<0.1	<0.1	1.4	<0.1	0.3	0.9	0.5	2.9	
SF116	1.9	2.5	1.5	2.6	2.5	0.8	0.6	2.8	3.9	1.2	1.8	1	1.5	1.3	1.9	2.1	1.8	
SF117	8.2	1.1	5.7	0.5	2.4	3.3	1.2	1.3	0.4	<0.1	0.9	0.6	0.9	0.5	<0.1	7.7	0.8	
SF118	4.4	2.5	2.6	3.7	2	2.8	<0.1	<0.1	3.9	2.3	29.7	0.4	<0.1	1.9	4.4	0.5	5.5	
MS119	<0.1	<0.1	<0.1	<0.1	<0.1	<0.1	<0.1	<0.1	<0.1	<0.1	18.2	1.2	<0.1	<0.1	<0.1	<0.1	0.9	
MS120	3.2	3.7	<0.1	14.9	1	3.8	2.9	<0.1	0.7	1.8	3.8	<0.1	2.7	3.3	2.5	0.6	1.2	
MS121	<0.1	2.4	<0.1	<0.1	4	9.2	1.7	<0.1	1.5	<0.1	5.4	2.9	1.9	<0.1	1.2	<0.1	3.3	
MS122	<0.1	<0.1	<0.1	<0.1	<0.1	<0.1	24.1	5.1	2.9	3.3	3.2	<0.1	<0.1	<0.1	<0.1	19.5	8.4	
MS123	2.5	1.1	2.8	0.9	1.6	2.3	1.2	2	<0.1	1.3	2.3	1.3	1.6	2.2	0.6	1	1.8	
MS124	0.4	2.9	1.4	2.3	3.2	5	13.5	3.2	1	1.4	17.1	0.5	3.7	3.2	9.7	2	3.9	

Table A2.1. (Cont.) Pebble count results in centimeters.																	
Site																	
SF91	1.5	1.1	1.6	<0.1	0.7	2.2	1.4	1	0.8	2.2	1.6	1.1	0.6	0.8	1.2	0.6	1.9
SF92	1.2	2.8	1.3	11.1	>30	6.5	1.9	3.8	9.3	4.2	2.1	6.8	<0.1	4.6	6.2	0.4	6.3
SF93	1.6	>0.1	6.4	1.2	1.9	11.8	<0.1	5.6	2.8	1.9	5.4	1.9	0.3	0.5	9.8	<0.1	0.6
SF94	0.6	1	2.2	1.3	2.3	0.5	0.6	1	0.9	1	1.2	0.9	0.4	1.3	2.3	0.6	<0.1
SF95	1.7	0.4	5.8	0.5	1.6	2.6	5.6	0.4	2.9	0.8	10.7	3.1	0.7	1.1	14.2	3.5	1.1
SF96	2.1	0.9	5	1.8	1.5	1.6	0.6	2.3	3.6	<0.1	<0.1	2.9	2.7	5.1	2.2	4.4	2
SF97	1.8	4.3	1.5	1.9	14.3	<0.1	1.5	2.2	<0.1	<0.1	0.2	1.7	3	0.5	0.6	2.2	0.6
SF98	<0.1	<0.1	<0.1	<0.1	<0.1	<0.1	<0.1	<0.1	<0.1	<0.1	<0.1	<0.1	<0.1	<0.1	<0.1	<0.1	<0.1
SF99	0.2	2.6	1.8	<0.1	<0.1	1.3	1.1	2.1	1.2	1	<0.1	<0.1	0.6	<0.1	2.4	0.8	0.4
SF100	<0.1	<0.1	<0.1	<0.1	<0.1	<0.1	<0.1	<0.1	<0.1	<0.1	<0.1	<0.1	<0.1	0.3	<0.1	<0.1	<0.1
SF101	<0.1	<0.1	<0.1	<0.1	<0.1	<0.1	<0.1	<0.1	<0.1	<0.1	<0.1	<0.1	<0.1	<0.1	<0.1	<0.1	<0.1
SF102	<0.1	<0.1	<0.1	<0.1	<0.1	<0.1	<0.1	<0.1	<0.1	<0.1	<0.1	<0.1	<0.1	<0.1	<0.1	<0.1	1
SF103	<0.1	<0.1	<0.1	<0.1	<0.1	<0.1	<0.1	<0.1	<0.1	<0.1	1.2	2.5	12	10.6	<0.1	<0.1	<0.1
SF104	<0.1	<0.1	<0.1	<0.1	<0.1	<0.1	<0.1	<0.1	<0.1	<0.1	<0.1	<0.1	<0.1	<0.1	<0.1	<0.1	<0.1
SF105	<0.1	<0.1	<0.1	<0.1	<0.1	<0.1	<0.1	<0.1	<0.1	6	<0.1	<0.1	<0.1	1.5	<0.1	<0.1	<0.1
MS106	4.1	3.4	4	2.5	5.4	2	2.3	1.5	4.5	4	3.1	1.5	1	1.6	2.1	2	2
MS107	6.1	8.9	6.6	0.9	5.8	2.2	6.6	<0.1	<0.1	5.1	11	3.7	6.7	4.7	3.1	3.2	<0.1
MS108	2.8	3.5	16.5	5.8	3.2	4.1	7.9	8.8	4.4	4.2	9.8	1.6	2.2	2.9	10.7	9.5	1.7
MS109	0.6	2.1	4.7	1.6	0.7	1.4	7.5	<0.1	8.1	2.8	<0.1	2.8	5	6	1.2	0.9	<0.1
NF110	9.2	2.4	3.3	4.3	0.9	4.2	7.9	3.8	1.9	3.1	2.2	0.9	6.2	5.8	2.7	6	1.4
NF111	1.7	0.5	2.8	2.5	3.2	1.5	9.8	8.4	1.6	3.4	2.1	21.9	3.1	1.6	2.9	1.8	1.1
NF112	2.2	1.1	1.2	1.1	3.2	2.5	1.7	1.6	1.2	2.7	2.6	1.1	1.2	1	1.1	1.2	1.4
NF113	3.2	2.2	2.7	1.6	2.4	4.1	2.6	2.6	3.1	4	0.8	1.2	1.1	1.4	4.2	2.1	1.2
NF114	0.7	0.9	0.6	0.7	0.4	0.6	2.2	1.3	3.8	2.9	1.1	0.8	0.8	0.7	13	1.9	1.9
SF115	2.7	2.1	2.8	11.5	1.4	2.2	4.1	8.3	5.1	0.9	2.1	2.2	1.1	1.7	1.1	8.8	22.3
SF116	0.5	2	1.7	3.2	1.5	2.3	0.8	1.4	4.8	2.9	0.9	1.4	0.6	3.2	2.6	0.9	2.2
SF117	0.3	7.7	0.8	1.4	4.8	0.9	<0.1	0.4	<0.1	2.5	<0.1	3.8	1.2	2.7	<0.1	1.9	0.6
SF118	<0.1	<0.1	2.3	1.2	6.9	25.4	0.2	0.3	1.8	6.3	0.8	0.4	<0.1	1.2	1.2	5.2	2.4
MS119	1.2	<0.1	<0.1	<0.1	<0.1	<0.1	<0.1	1	<0.1	8.8	2.2	<0.1	1.4	<0.1	4.8	<0.1	3.2
MS120	5.7	2.6	1.2	2.6	3.1	1.5	<0.1	1.6	0.4	1.2	1.7	4.2	1.8	<0.1	2.1	3.5	2.7
MS121	<0.1	<0.1	4.3	<0.1	1.8	<0.1	<0.1	<0.1	3.4	<0.1	>30	<0.1	<0.1	<0.1	0.8	<0.1	2.2
MS122	26	<0.1	>30	24.7	1.1	1.1	4.7	<0.1	<0.1	<0.1	<0.1	1.4	3.3	2.6	1.8	<0.1	<0.1
MS123	1.1	3.5	4.6	0.5	0.9	<0.1	2.2	<0.1	1.8	2.1	1.2	2.6	1.7	1	2.2	<0.1	0.5
MS124	4.3	0.1	2.3	1.9	1	4	1.6	10.4	1.1	0.2	2.1	1.8	2.5	2.8	5.5	0.6	0.9

Table A2.1. (Cont.) Pebble count results in centimeters.

Site																		
SF91	2.3	1.2	0.4	1.4	1	0.9	1.6	0.4	1.3	1.2	1.6	0.3	1.5	18.2	1.2	1.3	0.6	
SF92	9.8	0.7	1.2	1.9	3.8	5.6	8.2	<0.1	7.7	1.4	5.5	2.2	4.9	2.4	1.4	4	4.1	
SF93	2.4	1.2	1	1.7	4.1	0.8	0.6	0.5	6.8	<0.1	1.2	0.3	1.6	0.9	<0.1	1.5	26.8	
SF94	<0.1	0.9	0.6	0.9	2	1.5	1.1	1	4.7	1.9	1.3	1.3	1	0.8	3.3	2.2	<0.1	
SF95	10	1	1.1	1.4	1.5	1.4	1.6	1	2.2	0.8	0.3	1.5	1.2	0.8	0.7	1.2	3.8	
SF96	2.5	1.5	5.7	5.6	0.9	14.3	2.3	1.9	4.1	0.9	1.2	1.2	<0.1	2.3	2.9	2.2	1.5	
SF97	2.6	4.4	4.6	1.2	0.7	2.3	2.3	1.1	1.9	1	10	1.3	1.6	<0.1	3	1.2	10.6	
SF98	<0.1	<0.1	<0.1	<0.1	<0.1	<0.1	<0.1	<0.1	<0.1	<0.1	<0.1	<0.1	<0.1	<0.1	<0.1	<0.1	<0.1	
SF99	0.6	1.9	1.3	<0.1	<0.1	<0.1	0.2	2.9	1.2	0.4	1.5	0.9	0.6	0.4	2.6	0.5	1	
SF100	0.5	<0.1	<0.1	<0.1	<0.1	<0.1	<0.1	1.3	<0.1	0.7	<0.1	<0.1	<0.1	<0.1	<0.1	<0.1	<0.1	
SF101	<0.1	<0.1	<0.1	<0.1	<0.1	<0.1	<0.1	<0.1	<0.1	<0.1	<0.1	<0.1	<0.1	<0.1	<0.1	<0.1	<0.1	
SF102	<0.1	3.9	<0.1	<0.1	<0.1	<0.1	<0.1	11.3	<0.1	<0.1	<0.1	3.7	<0.1	<0.1	<0.1	<0.1	<0.1	
SF103	<0.1	<0.1	<0.1	<0.1	<0.1	<0.1	<0.1	0.6	<0.1	<0.1	<0.1	<0.1	<0.1	<0.1	0.8	<0.1	<0.1	
SF104	<0.1	<0.1	<0.1	<0.1	<0.1	<0.1	<0.1	<0.1	<0.1	<0.1	<0.1	<0.1	<0.1	<0.1	<0.1	<0.1	<0.1	
SF105	<0.1	<0.1	<0.1	<0.1	<0.1	<0.1	<0.1	<0.1	<0.1	3.9	5.7	<0.1	4	<0.1	<0.1	<0.1	<0.1	
MS106	3	1.5	3	2.5	2	1.9	1.6	3	1.9	3	0.8	1.1	4.2	1.9	4.6	2.2	1.8	
MS107	<0.1	<0.1	5.7	1.7	3.5	7.8	<0.1	6.9	<0.1	5.6	<0.1	<0.1	3.7	3.8	1.6	8.9	8.5	
MS108	5.4	<0.1	3.2	3.7	1.5	2.5	3.3	2.9	5.9	4.3	9	4.4	3.5	6.9	4.9	5.3	4.4	
MS109	1	1.8	4.9	6	8.2	5	3.1	1.2	1.3	22.2	0.9	9.2	6	1.9	0.7	2.6	1.6	
NF110	4.4	2.5	0.8	0.4	1.6	3	1.2	0.6	1	2	2.2	0.6	1.9	1.7	2	0.7	3.3	
NF111	7	7.6	10.6	5.6	2.8	4.5	1.1	3.2	0.9	1.6	0.4	1.9	1.5	1.3	10.4	0.5	3.6	
NF112	0.7	0.8	0.7	0.4	0.6	1.1	0.4	0.6	0.4	0.4	0.3	0.3	0.1	1.2	3.9	3.4	2.3	
NF113	0.6	0.4	0.2	1.1	0.6	0.2	0.4	0.5	0.7	0.2	0.3	0.7	4.6	1.1	3.1	1.2	2.1	
NF114	1.6	1.4	1.8	4	2.8	2.5	0.4	0.6	2.7	1.3	2	2.4	1	1.2	1.1	2.2	1.8	
SF115	1.3	0.2	2.6	0.8	<0.1	<0.1	0.9	1.3	2.9	1.2	0.3	15.6	<0.1	2.1	2.9	3.6	0.8	
SF116	1.3	0.8	3.2	2.1	1.2	1.7	0.8	1.3	2.3	1.3	1.4	1.4	2.7	2.8	2.1	2.2	2.5	
SF117	<0.1	2	<0.1	2.8	<0.1	1.2	<0.1	0.9	7.7	0.8	<0.1	4.2	2.3	1	3.3	<0.1	1	
SF118	2.7	<0.1	1.9	5.5	5.2	2.6	1.6	<0.1	1.2	3.7	<0.1	2.1	1.7	1.7	0.3	<0.1	12.7	
MS119	1.6	<0.1	<0.1	<0.1	<0.1	1.1	<0.1	1.7	1.1	14.4	<0.1	1	<0.1	<0.1	<0.1	<0.1	<0.1	
MS120	3.4	<0.1	2.5	<0.1	2.2	9.2	14.4	<0.1	<0.1	1.8	1.9	1.2	<0.1	3	2.2	0.8	1.9	
MS121	<0.1	0.8	<0.1	0.8	<0.1	2.5	3.3	0.1	3.7	<0.1	2.7	2.1	<0.1	0.4	2.7	3	<0.1	
MS122	<0.1	<0.1	2.2	<0.1	<0.1	0.8	0.9	2.1	3.3	1	<0.1	6.8	9.6	<0.1	<0.1	<0.1	17.2	
MS123	<0.1	4	0.9	1.3	0.9	2.1	0.9	3.1	0.8	2.6	4.7	1.8	3.6	0.8	0.5	2.1	2	
MS124	2.1	2.1	3.3	1.7	2.1	0.6	0.6	2.6	3.1	3.3	1.8	2.1	0.5	<0.1	2.3	1.5	2.5	

Table A2.1. (Cont.) Pebble count results in centimeters.

Site																		
SF91	1.2	0.2	0.5	2	>30	0.9	<0.1	1.5	5.3	0.1	1.7	0.6	<0.1	2.3	1.7	1.5	1.5	
SF92	2.1	1.5	0.6	2.4	4	0.4	2.9	5.2	0.8	3.8	11.4	1.6	0.6	1	5.4	7.8	1	
SF93	<0.1	12.3	<0.1	2.4	0.3	1.3	0.6	1.2	2.1	3	7.2	2.4	3.7	0.9	3.1	0.8	7.7	
SF94	1.4	1	1.2	0.4	0.8	0.9	1.9	1.1	1.4	1.3	1.2	0.4	1.7	1.3	1.4	0.8	1	
SF95	0.7	1.2	1.1	2	2.7	1.2	2.2	1.7	2	2.3	1.6	4.2	1.9	1.3	2.1	2.2	1.3	
SF96	2.7	3.4	2.4	0.9	9.8	1.9	1.5	14.8	6.5	2.9	4.2	1.3	1.2	2	0.6	1.8	0.8	
SF97	15.3	26.6	18.4	2.3	7.8	0.9	2.6	<0.1	2.2	2.3	4.1	1.9	2	2.4	2.1	2.4	2.1	
SF98	<0.1	<0.1	<0.1	<0.1	<0.1	<0.1	<0.1	<0.1	<0.1	<0.1	<0.1	<0.1	<0.1	<0.1	<0.1	<0.1	<0.1	
SF99	0.4	0.6	0.3	0.6	0.5	0.3	0.3	3.2	<0.1	<0.1	0.4	<0.1	<0.1	0.6	<0.1	0.3	0.3	
SF100	<0.1	<0.1	<0.1	<0.1	<0.1	<0.1	<0.1	<0.1	<0.1	<0.1	<0.1	<0.1	<0.1	0.4	<0.1	<0.1	<0.1	
SF101	<0.1	<0.1	<0.1	<0.1	<0.1	<0.1	<0.1	<0.1	<0.1	<0.1	<0.1	<0.1	<0.1	<0.1	<0.1	0.5	<0.1	
SF102	8.5	<0.1	<0.1	0.1	<0.1	<0.1	<0.1	2.2	<0.1	<0.1	<0.1	<0.1	8.9	0.3	<0.1	<0.1	<0.1	
SF103	<0.1	0.5	<0.1	<0.1	<0.1	<0.1	<0.1	<0.1	<0.1	<0.1	<0.1	<0.1	1.3	<0.1	<0.1	<0.1	6.9	
SF104	<0.1	<0.1	<0.1	<0.1	<0.1	<0.1	<0.1	<0.1	<0.1	<0.1	<0.1	<0.1	<0.1	<0.1	<0.1	<0.1	<0.1	
SF105	<0.1	1.5	0.6	3.6	<0.1	<0.1	<0.1	<0.1	<0.1	<0.1	<0.1	1.4	<0.1	<0.1	<0.1	<0.1	<0.1	
MS106	3.6	1.6	2.1	3.6	1.6	2.4	1.5	1.8	1	1.5	1.4	1.9	0.7	2.6	1.5	2.5	3.8	
MS107	20.7	2.4	5.8	0.8	9.7	2.3	5.5	11.7	2.3	0.7	0.3	5.3	<0.1	<0.1	<0.1	1.8	1.3	
MS108	0.4	1	9.8	6.7	2.2	3.5	3.9	1.1	2.7	5.6	7.4	3.9	5.9	4.5	1.1	7.7	14	
MS109	0.4	0.6	2.5	7.3	4.1	3.7	1.9	6.9	1	3	1.1	1.3	1.9	1.8	1.3	2.6	2.1	
NF110	2.2	5.8	2.9	2.9	2.9	2.7	2.6	3.8	1.4	1.3	3.8	1.8	3	3.3	1.9	1.1	3.1	
NF111	3.5	16.9	2.8	1.5	0.8	1.2	3.1	1.7	3	2.9	3.9	1.1	0.5	0.6	4.1	9.9	0.8	
NF112	2.4	3	5.1	3.3	2.4	2.6	3.4	2.7	2.4	1.7	2.1	1.8	3.1	2.9	1.3	3.6	2.7	
NF113	0.8	0.3	0.1	0.1	0.2	0.2	19.8	2.3	3	2.1	2.4	0.9	0.4	0.3	0.3	0.6	0.7	
NF114	2.1	1.6	2.9	2	1.7	3.8	1.7	3	1.2	1.8	1.6	1	1.4	2	1.8	2.2	1.9	
SF115	1.7	<0.1	2.4	1	16.1	0.6	16.4	2.9	<0.1	<0.1	1.1	25.5	0.7	2	9	11	<0.1	
SF116	1.6	1.2	2.9	1.8	1	2.2	2.8	6.2	3.1	2.6	4.2	1.4	2.7	3	0.4	1.4	3.2	
SF117	0.4	<0.1	1.2	2.6	6.4	<0.1	1	1.1	0.9	21.3	2.5	<0.1	0.8	0.9	1.8	2.5	2.1	
SF118	3.1	10.8	2.1	8.5	1	2.6	<0.1	1.6	7.8	14	3.1	2.9	2	3	2.4	6.4	5.5	
MS119	<0.1	<0.1	<0.1	1.8	<0.1	<0.1	0.8	0.9	<0.1	<0.1	<0.1	0.6	1.5	18.8	<0.1	1.1	0.8	
MS120	1.8	>30	1.8	4.4	0.3	0.5	2.2	0.9	2.9	3.9	11.3	1.1	1.4	2.6	<0.1	<0.1	3.4	
MS121	1.6	3	<0.1	1.6	1.2	3.3	<0.1	<0.1	1.8	1.3	1.2	<0.1	<0.1	0.7	<0.1	<0.1	1.5	
MS122	1.9	2.3	<0.1	10.7	4.7	1.4	2.5	1.4	<0.1	<0.1	1.1	<0.1	<0.1	26.3	2.8	<0.1	<0.1	
MS123	1.9	0.8	2.3	0.3	<0.1	1.7	2.2	2	2.6	2.1	1.7	<0.1	<0.1	0.9	1.5	1.8	1.3	
MS124	0.7	3.1	2.3	1.2	5.4	<0.1	2.1	2.1	3.3	21.7	<0.1	1.3	0.7	<0.1	2.4	2.1	2.9	

Table A2.1. (Cont.) Pebble count results in centimeters.

Site																		
SF91	1.2	10.6	1.1	<0.1	0.8	1.9	2.1	0.8	0.3	0.2	0.2	0.7	1.9	1	1.6	1.1	7.8	
SF92	0.7	1.5	1.6	2.5	2.7	7.6	1.9	3.9	4.6	4.9	4.6	3.4	1.8	0.5	1.6	0.6	0.4	
SF93	<0.1	7	7.4	1.9	3.5	<0.1	<0.1	<0.1	2.9	3.4	1.2	3.9	7	8.4	0.3	6.9	3.6	
SF94	0.9	0.9	1.1	1.4	1.4	1.9	0.1	1.2	3.2	0.7	1.9	1.6	2	<0.1	2.5	2.1	1.5	
SF95	1.5	1.2	1.9	0.8	0.7	1.6	1.1	1.7	2.3	1.3	0.8	0.6	1.3	0.4	1	1.1	1.7	
SF96	7.2	8.9	1.3	2	7.7	5.9	3.8	1	0.6	2.6	1.6	0.9	10.5	1.5	1.5	6.7	3.5	
SF97	1.3	3	2.4	1.3	3.9	2.1	2.1	<0.1	1.9	2	1	3.3	0.1	1	1.5	3.6	6.4	
SF98	<0.1	<0.1	<0.1	<0.1	<0.1	<0.1	<0.1	<0.1	<0.1	<0.1	<0.1	<0.1	<0.1	<0.1	<0.1	<0.1	<0.1	
SF99	0.9	<0.1	2	0.9	0.3	0.5	0.2	2.6	20	1.7	0.3	<0.1	1.7	1.3	0.9	0.3	1.6	
SF100	<0.1	<0.1	<0.1	<0.1	<0.1	<0.1	<0.1	<0.1	0.3	<0.1	<0.1	<0.1	<0.1	<0.1	<0.1	<0.1	<0.1	
SF101	<0.1	<0.1	<0.1	<0.1	<0.1	<0.1	<0.1	<0.1	1.2	<0.1	<0.1	<0.1	<0.1	<0.1	<0.1	<0.1	<0.1	
SF102	0.8	<0.1	<0.1	<0.1	<0.1	1.6	<0.1	1.6	<0.1	<0.1	2.7	<0.1	<0.1	<0.1	2	<0.1	2	
SF103	<0.1	<0.1	<0.1	<0.1	1.7	<0.1	<0.1	<0.1	<0.1	<0.1	<0.1	<0.1	<0.1	<0.1	<0.1	<0.1	<0.1	
SF104	<0.1	<0.1	<0.1	<0.1	<0.1	<0.1	<0.1	<0.1	<0.1	<0.1	<0.1	<0.1	<0.1	<0.1	<0.1	<0.1	<0.1	
SF105	5.7	1.9	3.1	2.2	<0.1	<0.1	1.1	<0.1	<0.1	<0.1	<0.1	1.9	<0.1	<0.1	1.8	<0.1	<0.1	
MS106	3	1	1.7	5	1.5	2.4	1.6	2.8	1.7	4.1	1.4	3.2	4.3	2.5	2	2.1	1.5	
MS107	<0.1	2.8	8	8.9	<0.1	6.7	0.6	6.9	0.9	1.6	1.7	2.1	1.9	1.3	8.5	7.6	2.3	
MS108	6.1	17.9	5.6	2.3	7.5	1.3	6	10.2	1.9	10.4	2.3	1.8	2	1.6	7.2	2.1	2.9	
MS109	1.5	<0.1	6.3	3.6	5.4	2.3	9	2.2	3.2	0.6	6.9	0.4	0.4	4.4	1.6	5.7	<0.1	
NF110	3.5	1.3	1.3	0.2	0.9	3	1.2	1.6	14.2	0.4	0.5	0.3	2.1	0.7	1.3	0.8	1	
NF111	1.9	3.6	3.2	1.9	1.6	2.5	3	1.2	2.7	2.2	4.3	10.2	1	3.2	2.3	1.1	1.6	
NF112	2.3	1.7	1.4	2.1	3.3	2.2	1.6	2.8	2.1	1.8	1.4	2.3	1.4	1.3	2.1	2.1	2.2	
NF113	0.9	4	3.5	3.2	3	3.6	2.1	2.3	1.2	1.1	0.8	0.4	1.1	0.6	0.4	0.9	0.4	
NF114	3.2	3.9	1.8	1.9	2.2	2.3	1.5	1.8	1.8	2.6	2.2	1.9	7.3	5.3	3.2	2.6	2	
SF115	<0.1	2.5	<0.1	1.7	2.9	2.5	2.1	0.8	1	10.9	1.9	9.9	2.8	<0.1	1.9	1.7	1.9	
SF116	4.9	2.6	5.3	2.1	2.1	3.9	3.7	1.8	1.4	5.6	2.4	3.8	3.8	0.9	0.4	0.4	2.6	
SF117	0.6	<0.1	5.8	<0.1	10.6	1.1	0.9	2.3	<0.1	<0.1	0.6	<0.1	1.6	2.8	<0.1	<0.1	<0.1	
SF118	1.3	3.4	2.8	1.9	2.4	3.4	5.2	1.1	13.1	2.3	2.8	2.3	3.9	3	2.4	6.9	1.1	
MS119	1.7	1.2	0.6	2.8	<0.1	2.7	<0.1	<0.1	1.3	4.7	<0.1	0.9	<0.1	1.3	0.9	5.1	<0.1	
MS120	3.7	1.1	1.3	1.4	1.1	2.7	5.5	1.6	0.7	3.1	2.1	0.5	<0.1	1.2	<0.1	3.5	<0.1	
MS121	1.6	<0.1	3.4	<0.1	<0.1	<0.1	<0.1	3.2	15.5	<0.1	1.3	<0.1	2.9	0.9	2.4	<0.1	<0.1	
MS122	<0.1	3.8	1.8	8	4.4	<0.1	<0.1	<0.1	0.1	<0.1	<0.1	<0.1	5.3	<0.1	<0.1	<0.1	0.6	
MS123	2.9	<0.1	2.2	1.3	2.9	0.5	1.3	2.3	1.1	1.3	0.1	0.8	0.8	2.4	4.8	2.7	1.1	
MS124	1.5	0.6	2	1.6	2.2	1.7	0.6	0.7	2.2	1	8.4	<0.1	2.7	1.6	0.1	4.1	1.6	

Table A2.1. (Cont.) Pebble count results in centimeters.

Site																
SF91	1.4	0.5	0.9	0.2	8.7	0.1	0.3	0.2	<0.1	1.1	0.9	1	0.6	7.4	1.2	
SF92	1.9	0.3	1.5	<0.1	12.7	1.3	1.9	0.7	0.8	<0.1	1.3	0.3	<0.1	<0.1	0.8	
SF93	1.3	<0.1	1.2	<0.1	2	0.8	0.8	<0.1	1.1	2.9	0.8	1.1	1.3	8.3	2	
SF94	1.5	0.3	1.1	0.8	1.6	1.1	0.6	1	1.1	2.2	0.6	1	1.3	0.7	2.2	
SF95	0.7	2.2	0.9	0.8	1.2	0.8	1	6.6	1.9	1.5	1.4	0.9	2.5	0.9	0.9	
SF96	1.8	1.7	<0.1	5.7	7.6	<0.1	1	3.6	0.9	3.9	3.1	0.5	0.8	3.6	1.7	
SF97	0.1	0.8	2.4	2.3	1.4	2.1	0.7	1.2	0.9	3.2	1.8	2.1	0.7	0.7	1.6	
SF98	<0.1	<0.1	<0.1	<0.1	<0.1	<0.1	<0.1	<0.1	<0.1	<0.1	<0.1	<0.1	<0.1	<0.1	<0.1	
SF99	0.4	<0.1	0.7	0.3	<0.1	<0.1	0.6	0.1	0.8	0.2	<0.1	2.2	<0.1	2	<0.1	
SF100	<0.1	<0.1	<0.1	<0.1	<0.1	<0.1	<0.1	<0.1	0.4	<0.1	<0.1	<0.1	<0.1	0.2	<0.1	
SF101	<0.1	<0.1	<0.1	<0.1	<0.1	<0.1	<0.1	<0.1	<0.1	<0.1	<0.1	<0.1	<0.1	<0.1	<0.1	
SF102	7.5	<0.1	3.3	<0.1	<0.1	<0.1	0.5	0.4	2.3	<0.1	<0.1	<0.1	1.2	<0.1	1.5	
SF103	<0.1	1.4	0.5	1.8	<0.1	1.1	<0.1	<0.1	<0.1	<0.1	2.9	<0.1	<0.1	<0.1	<0.1	
SF104	<0.1	<0.1	<0.1	<0.1	<0.1	<0.1	<0.1	<0.1	<0.1	<0.1	<0.1	<0.1	<0.1	<0.1	<0.1	
SF105	<0.1	<0.1	3.4	<0.1	1.8	<0.1	<0.1	<0.1	<0.1	<0.1	1.9	<0.1	<0.1	<0.1	<0.1	
MS106	1.2	2.3	2.1	2.2	1.1	2.5	3	2.8	2.5	2.3	1.5	2	3.9	1.5	2	
MS107	3.1	4.9	3.3	<0.1	4.7	16.5	1.3	2	6.8	2.2	7.6	5.8	<0.1	0.9	9.1	
MS108	1.5	1	2.6	5.1	1.5	15.3	3.5	7.6	4.5	12.4	11	1.1	14.2	3.2	1.9	
MS109	1	4.4	5.6	<0.1	4	6.2	4.8	4.8	4.7	0.6	2.7	1.2	0.6	2.5	21.9	
NF110	1.2	0.5	2	1.9	>30	1.8	2	1.1	1.9	0.3	1.4	10.6	1.1	0.8	0.6	
NF111	8.2	3.4	1.8	1.1	0.9	7.6	16.5	0.5	1.7	1.1	2.7	0.9	2.4	1.8	1.6	
NF112	1.7	1.8	3.1	4.1	1.4	1.9	1.9	1.4	1.6	1.1	1.1	1.8	1.3	0.9	2.4	
NF113	0.3	0.2	0.2	0.1	14.7	3.6	4.7	4.4	2.8	1.7	3	2.1	2.2	1.4	0.6	
NF114	3	2.2	1.8	2.2	2.5	1.7	1.8	1.6	2.2	1.4	1.3	1.6	3	5.8	1.8	
SF115	21	0.9	1.1	0.8	1.8	<0.1	1.7	12.3	1	1.6	2.4	1.4	1.2	1.8	2	
SF116	1.1	2.9	0.6	1.9	2.4	2	1.4	0.4	0.3	1.4	1.1	<0.1	3	2.7	2.7	
SF117	8.4	0.5	0.7	0.5	2.5	0.9	1.2	<0.1	1.6	1.2	<0.1	<0.1	0.9	<0.1	<0.1	
SF118	1	2.9	2.1	2.3	1.1	1.5	0.9	3.8	1.6	2.2	<0.1	5.1	1.8	1.8	<0.1	
MS119	<0.1	<0.1	2.9	<0.1	1.5	1.3	1.5	<0.1	<0.1	<0.1	<0.1	0.5	<0.1	<0.1	1.7	
MS120	0.8	1.9	1.5	3.5	2.4	<0.1	0.7	2	3.5	0.1	3.6	3.2	1.4	2	2	
MS121	0.3	<0.1	<0.1	<0.1	<0.1	1.7	<0.1	<0.1	2	1.5	2	1	<0.1	<0.1	1.8	
MS122	<0.1	0.8	<0.1	2.8	<0.1	3.5	0.1	0.5	2.1	8.6	<0.1	<0.1	<0.1	1.3	<0.1	
MS123	0.7	3.2	1.3	2.5	1.6	0.3	1.1	<0.1	2.5	1.7	0.7	0.3	2.6	1.7	1.1	
MS124	2	0.8	0.9	0.9	>30	2.8	1.1	1.3	0.6	1.3	2.1	0.9	1.4	1.1	0.8	

Table A2.2. Canopy cover measured with a densiometer.

Site	North	East	South	West	Average
NF01	14	39	1	4	15
NF02	7	17	0	0	6
NF03	6	17	3	0	7
NF04	84	92	96	93	95
NF05	55	69	91	21	61
NF06	50	17	71	92	60
NF08	0	0	14	18	8
NF09	4	5	48	30	23
NF10	10	28	89	75	53
NF11	14	15	75	89	50
NF12	13	90	96	96	77
NF13	0	0	29	39	18
NF14	52	91	96	55	76
NF15	41	78	3	2	32
NF16	82	84	11	40	56
NF17	5	1	0	0	2
NF18	7	10	18	4	10
NF19	79	30	86	73	70
NF20	54	34	77	69	61
NF21	74	54	92	80	78
NF22	85	81	79	86	86
NF23	81	81	82	71	82
NF24	9	0	0	26	9
NF25	86	95	95	45	83
NF26	3	12	0	0	4
NF27	9	0	0	0	2
NF28	30	0	1	48	21
MS29	83	82	62	30	67
MS30	0	1	0	0	0
MS31	20	72	94	29	56
MS32	14	78	95	61	64
MS33	41	82	77	8	54
MS34	72	33	84	93	73
MS35	85	95	92	77	91
MS36	80	95	94	74	89
MS37	10	31	80	52	45
MS38	54	85	92	69	78
MS39	11	20	87	72	49
MS40	96	91	94	79	94
MS41	50	70	95	72	75
MS42	84	88	93	94	93
MS43	96	91	96	92	98
MS44	88	87	91	95	94
MS45	94	93	96	95	98
MS46	81	93	81	85	88

Table A2.2. (Cont.) Canopy cover measured with a densiometer.

Site	North	East	South	West	Average
MS47	81	81	62	38	68
MS48	37	90	96	82	79
MS49	73	85	96	96	91
MS50	79	82	90	91	89
MS51	93	96	96	96	99
MS52	96	86	65	94	89
MS53	56	20	12	4	24
MS54	86	82	72	86	85
MS55	94	92	93	91	96
MS56	91	90	93	95	96
MS57	96	95	95	96	99
MS58	94	84	95	93	95
MS59	80	81	69	69	78
MS60	90	92	96	96	97
MS61	84	91	78	94	90
MS62	94	91	92	92	96
MS63	89	96	83	96	95
MS64	90	88	96	96	96
MS65	96	93	93	96	98
MS66	86	91	86	89	92
MS67	95	87	96	94	97
NF68	0	0	5	1	2
NF69	4	33	12	2	13
NF70	9	18	92	87	54
NF71	64	33	96	96	75
NF72	22	0	10	5	10
NF73	0	0	14	19	9
NF74	94	90	80	91	92
NF75	57	76	0	0	35
NF76	96	19	28	46	49
NF77	88	2	22	14	33
NF78	19	42	66	85	55
NF79	57	93	82	74	80
NF80	72	91	87	70	83
NF81	73	85	64	68	75
NF82	92	91	93	94	96
NF83	74	94	76	75	83
NF84	93	55	83	91	84
NF85	94	96	96	96	99
SF86	70	39	28	63	52
SF87	84	96	96	92	96
SF88	87	95	80	72	87
SF89	82	93	96	78	91
SF90	6	8	6	28	12

Table A2.2. (Cont.) Canopy cover measured with a densiometer.					
Site	North	East	South	West	Average
SF91	0	0	0	0	0
SF92	81	75	38	48	63
SF93	88	96	91	85	94
SF94	96	71	82	94	89
SF95	92	81	78	79	86
SF96	96	90	96	94	98
SF97	87	72	66	93	83
SF98	44	14	96	94	64
SF99	95	96	96	96	100
SF100	3	0	2	21	7
SF101	7	2	68	81	41
SF102	73	14	24	78	49
SF103	53	14	5	34	28
SF104	22	3	0	15	10
SF105	96	96	96	74	94
MS106	94	93	90	94	96
MS107	93	90	95	92	96
MS108	90	93	94	92	96
MS109	86	94	94	94	96
NF110	94	88	95	92	96
NF111	52	80	85	85	79
NF112	88	14	22	60	48
NF113	0	9	54	4	17
NF114	4	4	0	2	3
SF115	84	92	96	95	95
SF116	79	95	92	96	94
SF117	68	84	52	27	60
SF118	64	80	81	93	83
MS119	96	96	95	77	95
MS120	29	24	75	91	57
MS121	46	94	92	84	82
MS122	41	10	3	46	26
MS123	93	51	95	96	87
MS124	89	88	95	89	94

Figure A2.3. 2021 site characterization used in random forest analysis.

Site	SSFP*	Drainage Area (m ²)	Carbonates (%)	Colluvium (%)	Metased (%)	Slope (degrees)	Aspect (degree)	Elevation (ft)
NF03	1	187165.3	0.00	0.13	99.87	13.0	230.5	1939
NF04	0	544951.9	0.00	0.13	91.45	16.1	220.3	1870
NF05	0	544951.9	0.00	0.13	91.45	25.9	209.6	1872
NF06	0	504580.9	0.00	0.13	91.45	22.2	121.6	1878
NF07	1	102805.8	0.00	0.13	91.45	23.8	105.3	1957
NF08	0	955390.8	0.00	1.84	93.59	7.8	72.5	1944
NF09	0	941433.8	0.00	1.84	93.59	12.6	71.4	1945
NF10	0	927467	0.00	1.84	93.59	17.1	63.9	1946
NF11	0	913508.2	0.00	1.84	93.59	17.7	51.8	1948
NF12	0	899549	0.00	1.84	93.59	19.9	45.9	1949
NF13	0	2892662	0.00	0.00	54.76	5.7	93.3	1950
NF14	0	2877395	0.00	0.00	54.76	6.6	76.5	1951
NF15	0	2862130	0.00	0.00	54.76	14.6	64.7	1952
NF16	0	2846863	0.00	0.00	54.76	5.2	131.6	1952
NF17	0	2831598	0.00	0.00	54.76	8.3	178.7	1954
NF18	0	2770539	0.00	0.00	54.76	8.8	75.5	1959
NF19	0	2709481	0.00	0.00	54.76	14.4	58.4	1961
NF20	0	2694221	0.00	0.00	54.76	13.3	179.2	1962
NF21	0	2678957	0.00	0.00	54.76	24.3	213.9	1963
NF22	0	2663688	0.00	0.00	54.76	8.3	125.1	1965
NF23	0	2648425	0.00	0.00	54.76	9.0	62.0	1966
NF24	0	2358757	0.00	0.00	54.76	14.3	211.3	1981
NF25	0	2343495	0.00	0.00	54.76	13.1	210.9	1982
NF26	0	2328234	0.00	0.00	54.76	5.8	199.6	1983
NF27	0	2312965	0.00	0.00	54.76	14.8	211.6	1984
NF28	0	2297701	0.00	0.00	54.76	17.2	241.1	1984
MS29	0	881188.1	0.00	23.05	76.93	30.3	143.0	1684
MS30	0	635854.3	0.00	23.05	76.93	22.8	215.9	1754
MS31	1	583507.2	0.00	23.05	76.93	26.8	45.2	1770
MS32	1	576964.3	0.00	23.05	76.93	32.5	59.7	1770
MS119	1	570419.7	0.00	23.05	76.93	24.6	75.2	1772
MS33	0	563876.9	0.00	23.05	76.93	26.0	34.7	1774
MS34	0	557331.3	0.00	23.05	76.93	24.9	77.0	1776
MS35	0	550789.4	0.00	23.05	76.93	23.8	93.1	1780
MS36	0	541541.8	0.00	23.05	76.93	18.6	73.1	1784
MS37	0	534998	0.00	23.05	76.93	15.3	78.2	1785
MS38	0	528455.3	0.00	23.05	76.93	9.0	63.8	1787
MS39	0	483200.8	0.00	23.05	76.93	11.1	42.8	1801
MS40	1	7573343	0.00	2.56	15.24	18.0	194.9	1775
MS41	1	7565228	0.00	2.51	15.23	17.0	209.6	1776
MS42	1	7557114	0.00	2.47	15.22	13.4	180.9	1777
MS43	1	7549002	0.00	2.42	15.21	6.2	174.1	1779
MS44	1	7540887	0.00	2.38	15.20	13.6	178.8	1780

Figure A2.3. (Cont.) 2021 site characterization used in random forest analysis.

Site	Upstream Distance (m)	Loam (%)	Silt Loam (%)	PCM (cm)	PCIQR (cm)	Canopy Cover (%)	Trees (%)	Faults Upstream
NF03	5788	36.01	64.01	0.2	1.4	6.76	2.47	0
NF04	4434	88.21	15.83	1.6	2.325	94.9	4.35	0
NF05	4459	91.60	15.83	1.3	2.675	61.36	4.35	0
NF06	4484	88.21	15.83	2.9	3.8	59.8	4.35	0
NF07	4982	88.21	15.83	0.9	1.625	NA	4.35	0
NF08	5911	14.38	42.53	3.5	5.575	8.32	14.76	0
NF09	5923	14.38	42.53	1.25	0.9	22.62	14.76	0
NF10	5936	14.38	42.53	1.75	2.4	52.52	14.76	0
NF11	5948	14.38	42.53	2.25	2.9	50.18	14.76	0
NF12	5961	14.38	42.53	2.6	3.875	76.7	14.76	0
NF13	6087	38.12	14.72	2.5	2.225	17.68	6.52	3
NF14	6100	38.12	14.72	2.1	2.5	76.44	6.52	3
NF15	6112	38.12	14.72	1.4	2.2	32.24	6.52	3
NF16	6125	38.12	14.72	2.15	2.225	56.42	6.52	3
NF17	6137	38.12	14.72	2.3	1.5	1.56	6.52	3
NF18	6187	38.12	14.72	2.5	2.025	10.14	6.52	3
NF19	6237	38.12	14.72	2.1	2.125	69.68	6.52	3
NF20	6250	38.12	14.72	2	1.825	60.84	6.52	3
NF21	6262	38.12	14.72	2.7	2.525	78	6.52	3
NF22	6275	38.12	14.72	2.05	1.7	86.06	6.52	3
NF23	6287	38.12	14.72	2.55	2.6	81.9	6.52	3
NF24	6524	38.12	14.72	1.8	1.025	9.1	6.52	2
NF25	6537	38.12	14.72	1.75	2.025	83.46	6.52	2
NF26	6549	38.12	14.72	1.8	1.2	3.9	6.52	2
NF27	6562	38.12	14.72	1.85	2.15	2.34	6.52	2
NF28	6574	38.12	14.72	2.05	1.325	20.54	6.52	2
MS29	2150	0.26	53.52	0	0.1	66.82	3.64	1
MS30	2619	0.26	53.52	1.3	1.625	0.26	3.64	0
MS31	2718	0.26	53.52	0.1	0.925	55.9	3.64	0
MS32	2731	0.26	53.52	1.2	1.425	64.48	3.64	0
MS119	2743	0.26	53.52	0.4	2.375	54.08	3.64	0
MS33	2756	0.26	53.52	0	0	73.32	3.64	0
MS34	2768	0.26	53.52	0	0	90.74	3.64	0
MS35	2781	0.26	53.52	0	1.125	89.18	3.64	0
MS36	2799	0.26	53.52	0	0.925	44.98	3.64	0
MS37	2811	0.26	53.52	0.6	1.7	78	3.64	0
MS38	2824	0.26	53.52	0	1.1	49.4	3.64	0
MS39	2910	0.26	53.52	0	0.925	93.6	3.64	0
MS40	2675	0.06	7.08	2.6	2.225	74.62	9.03	0
MS41	2687	0.06	7.02	2.1	2.45	93.34	9.03	0
MS42	2700	0.05	6.97	2.1	4	96.72	9.02	0
MS43	2712	0.05	6.91	2.65	4.45	93.86	9.02	0
MS44	2725	0.05	6.86	2.4	5.325	98.28	9.02	0

Figure A2.3. (Cont.) 2021 site characterization used in random forest analysis.

Site	Geomorphic Depth (cm)	Geomorphic Width (cm)
NF03	15	29
NF04	18	198
NF05	13	83
NF06	20	152
NF07	5	19
NF08	16	71
NF09	12	130
NF10	13	95
NF11	16	127
NF12	18	97
NF13	19	57
NF14	6	70
NF15	8	35
NF16	18	86
NF17	13	102
NF18	13	47
NF19	11	59
NF20	12	36
NF21	16	57
NF22	15	95
NF23	14	81
NF24	10	102
NF25	13	75
NF26	10	72
NF27	12	79
NF28	9	83
MS29	18	51
MS30	15	62
MS31	15	87
MS32	15	77
MS119	18	84
MS33	16	104
MS34	18	102
MS35	17	66
MS36	14	38
MS37	13	31
MS38	10	65
MS39	20	74
MS40	12	74
MS41	17	118
MS42	19	96
MS43	16	119
MS44	25	169

Figure A2.3. (Cont.) 2021 site characterization used in random forest analysis.

Site	SSFP*	Drainage Area (m2)	Carbonates (%)	Colluvium (%)	Metased (%)	Slope (degrees)	Aspect (degree)	Elevation (ft)
MS45	1	7453472	0.00	1.90	15.10	12.7	163.0	1796
MS46	1	7445356	0.00	1.86	15.09	9.9	175.4	1798
MS47	1	7437242	0.00	1.81	15.09	27.5	219.0	1799
MS48	0	7429127	0.00	1.77	15.08	14.2	105.3	1803
MS49	0	7421010	0.00	1.72	15.07	9.6	136.7	1804
MS50	0	7154546	0.00	0.17	14.75	17.7	106.2	1855
MS51	0	1071455	0.00	0.00	56.73	13.9	76.3	1868
MS52	0	810091.1	0.00	0.00	56.73	22.0	190.0	1891
MS53	1	715381.9	0.00	0.00	56.73	30.7	37.4	1902
MS54	0	693724.7	0.00	0.00	56.73	41.0	69.1	1904
MS55	0	672060.2	0.00	0.00	56.73	26.6	99.1	1908
MS56	0	650400.4	0.00	0.00	56.73	13.8	132.0	1911
MS57	0	628749.8	0.00	0.00	56.73	15.6	117.5	1914
MS58	0	5950716	0.00	0.00	6.79	12.3	149.6	1861
MS59	0	5853129	0.00	0.00	6.79	11.7	137.9	1863
MS60	0	5756307	0.00	0.00	6.79	10.5	184.2	1866
MS61	0	5419087	0.00	0.00	6.79	8.2	128.9	1871
MS62	0	3564375	0.00	0.00	6.79	7.1	207.6	1898
MS63	0	3466792	0.00	0.00	6.79	9.3	203.1	1899
MS64	0	3369180	0.00	0.00	6.79	9.7	238.4	1900
MS65	0	3271588	0.00	0.00	6.79	23.8	240.9	1902
MS66	0	3174008	0.00	0.00	6.79	25.2	114.7	1903
MS67	1	1285703	0.00	1.84	93.59	4.1	36.9	1921
NF68	1	1271740	0.00	1.84	93.59	6.5	25.8	1922
NF69	1	1257784	0.00	1.84	93.59	7.2	49.2	1923
NF70	1	1243817	0.00	1.84	93.59	15.5	27.1	1925
NF71	1	1229853	0.00	1.84	93.59	9.5	353.8	1926
NF72	1	1174010	0.00	1.84	93.59	13.4	342.2	1930
NF73	0	1118162	0.00	1.84	93.59	5.9	90.0	1934
NF74	0	1104206	0.00	1.84	93.59	8.0	42.1	1935
NF75	0	1092484	0.00	1.84	93.59	9.1	13.0	1936
NF76	0	1078530	0.00	1.84	93.59	5.5	68.0	1936
NF77	0	1064575	0.00	1.84	93.59	7.2	19.9	1936
NF78	0	843705.1	0.00	1.84	93.59	24.8	41.5	1950
NF79	0	787859	0.00	1.84	93.59	7.4	210.7	1953
NF80	0	773902.7	0.00	1.84	93.59	12.5	232.7	1954
NF81	0	759936.9	0.00	1.84	93.59	21.7	235.1	1955
NF82	0	745978.8	0.00	1.84	93.59	16.5	95.8	1955
NF83	0	732019.2	0.00	1.84	93.59	6.4	107.2	1957
NF84	0	162401.8	0.00	1.84	93.59	18.5	266.4	1990
NF85	0	5002283	3.60	5.81	22.03	18.3	169.0	1890
SF86	0	4999011	3.59	5.76	22.04	30.1	120.0	1890
SF87	1	4995739	3.59	5.70	22.05	19.2	167.4	1891

Figure A2.3. (Cont.) 2021 site characterization used in random forest analysis.

Site	Upstream Distance (m)	Loam (%)	Silt Loam (%)	PCM (cm)	PCIQR (cm)	Canopy Cover (%)	Trees (%)	Faults Upstream
MS45	2859	0.04	6.26	1.25	3.35	88.4	9.00	0
MS46	2872	0.04	6.20	2.65	3.275	68.12	9.00	0
MS47	2884	0.04	6.14	0	0	79.3	8.99	0
MS48	2897	0.04	6.09	1.1	3	91	8.99	0
MS49	2909	0.04	6.03	0	0	88.92	8.99	0
MS50	3320	0.00	4.09	1.6	1.4	99.06	8.92	0
MS51	3398	0.00	17.09	0	0	88.66	18.88	0
MS52	3549	0.00	17.09	0	0	23.92	18.88	0
MS53	3604	0.00	17.09	1.95	2.325	84.76	18.88	0
MS54	3616	0.00	17.09	2.75	5	96.2	18.88	0
MS55	3629	0.00	17.09	1.75	2.8	95.94	18.88	0
MS56	3641	0.00	17.09	0.15	1.825	99.32	18.88	0
MS57	3654	0.00	17.09	0	0	95.16	18.88	0
MS58	3370	0.00	1.38	0	0	77.74	7.03	0
MS59	3382	0.00	1.38	2.45	4.25	97.24	7.03	0
MS60	3394	0.00	1.38	2.15	2.3	90.22	7.03	0
MS61	3438	0.00	1.38	0	0	95.94	7.03	0
MS62	3675	0.00	1.38	1.6	2	94.64	7.03	0
MS63	3688	0.00	1.38	0.9	2.4	96.2	7.03	0
MS64	3700	0.00	1.38	1.5	1.625	98.28	7.03	0
MS65	3713	0.00	1.38	0	1.5	91.52	7.03	0
MS66	3725	0.00	1.38	1.2	2.3	96.72	7.03	0
MS67	5615	14.38	42.53	0.9	1.175	1.56	14.76	0
NF68	5627	14.38	42.53	1.4	1.125	13.26	14.76	0
NF69	5640	14.38	42.53	1.6	1.725	53.56	14.76	0
NF70	5652	14.38	42.53	0.8	1.6	75.14	14.76	0
NF71	5665	14.38	42.53	0.8	1	9.62	14.76	0
NF72	5715	14.38	42.53	1.8	1.825	8.58	14.76	0
NF73	5765	14.38	42.53	2.1	1.35	92.3	14.76	0
NF74	5777	14.38	42.53	2.1	1.7	34.58	14.76	0
NF75	5788	14.38	42.53	2.55	1.75	49.14	14.76	0
NF76	5800	14.38	42.53	2.2	1.95	32.76	14.76	0
NF77	5813	14.38	42.53	2	1.6	55.12	14.76	0
NF78	6011	14.38	42.53	2.15	2.575	79.56	14.76	0
NF79	6061	14.38	42.53	1.9	1.8	83.2	14.76	0
NF80	6073	14.38	42.53	1.1	1.425	75.4	14.76	0
NF81	6086	14.38	42.53	2.7	3.025	96.2	14.76	0
NF82	6098	14.38	42.53	2.55	5.175	82.94	14.76	0
NF83	6111	14.38	42.53	2.4	4.475	83.72	14.76	0
NF84	6620	14.38	42.53	0.45	1.3	99.32	14.76	0
NF85	4845	22.42	22.34	0.2	1.525	52	36.01	1
SF86	4857	22.43	22.29	3.5	5.75	95.68	36.00	1
SF87	4870	22.44	22.24	1.5	1.55	86.84	36.00	1

Figure A2.3. (Cont.) 2021 site characterization used in random forest analysis.

Site	Geomorphic Depth (cm)	Geomorphic Width (cm)
MS45	30	165
MS46	14	67
MS47	13	110
MS48	12	30
MS49	10	25
MS50	16	74
MS51	9	53
MS52	8	73
MS53	18	33
MS54	16	27
MS55	12	62
MS56	12	43
MS57	17	104
MS58	15	100
MS59	23	115
MS60	16	100
MS61	1	13
MS62	20	99
MS63	12	53
MS64	16	43
MS65	16	52
MS66	14	45
MS67	16	75
NF68	13	100
NF69	11	37
NF70	20	137
NF71	19	80
NF72	18	88
NF73	20	100
NF74	16	50
NF75	19	40
NF76	93	19
NF77	17	100
NF78	21	143
NF79	15	150
NF80	9	84
NF81	13	85
NF82	25	116
NF83	33	111
NF84	21	159
NF85	13	75
SF86	18	81
SF87	19	67

Figure A2.3. (Cont.) 2021 site characterization used in random forest analysis.

Site	SSFP*	Drainage Area (m ²)	Carbonates (%)	Colluvium (%)	Metased (%)	Slope (degrees)	Aspect (degree)	Elevation (ft)
SF88	1	4992467	3.58	5.65	22.07	19.5	156.6	1890
SF89	1	4989197	3.57	5.60	22.08	14.2	126.7	1891
SF90	0	1305806	0.00	21.19	69.27	7.8	56.3	1894
SF91	0	1284906	0.00	20.61	69.69	17.7	354.5	1900
SF92	0	1279544	0.00	20.46	69.80	18.4	126.8	1902
SF93	0	1274184	0.00	20.31	69.91	6.1	92.9	1905
SF94	0	1268821	0.00	20.15	70.02	5.1	111.5	1906
SF95	0	1263460	0.00	20.00	70.14	7.2	168.0	1907
SF96	0	1220026	0.00	18.68	71.10	3.4	130.9	1918
SF97	1	181489.4	0.00	59.45	22.93	10.0	75.3	1939
SF98	0	742490.1	0.00	4.97	86.33	8.0	141.0	1943
SF99	0	2960454	4.75	0.14	6.39	8.7	90.5	1905
SF100	1	2888692	4.75	0.14	6.39	8.1	86.9	1906
SF101	1	2816955	4.75	0.14	6.39	8.8	111.9	1907
SF102	1	2745199	4.75	0.14	6.39	14.4	69.4	1908
SF103	1	2673453	4.75	0.14	6.39	13.6	101.3	1910
SF104	1	429028.8	42.24	0.13	0.00	34.4	314.8	1871
SF105	0	31927925	8.27	3.74	31.82	3.8	140.7	1654
MS106	0	31963465	8.28	3.74	31.78	7.2	43.0	1653
MS107	0	41739986	6.41	4.15	27.49	14.9	348.0	1645
MS109	1	185854.3	0.00	0.10	99.90	36.9	184.4	1752
NF110	1	4175317	0.00	0.00	23.24	17.6	115.4	1940
NF111	0	2224249	0.00	0.00	54.76	29.4	198.9	1987
NF112	0	2193718	0.00	0.00	54.76	24.9	14.4	1991
NF113	0	2375761	0.00	0.00	54.76	12.1	212.6	1981
NF114	0	1214666	0.00	18.51	71.22	7.9	136.3	1919
SF115	0	1209306	0.00	18.34	71.34	8.2	98.4	1919
SF116	0	1203943	0.00	18.17	71.47	4.7	65.8	1921
SF117	0	1198580	0.00	17.99	71.60	13.4	61.7	1922
SF118	0	8267118	0.00	5.97	15.93	7.3	135.9	1650
MS120	0	2406388	0.00	0.00	6.79	18.6	111.9	1917
MS121	0	2503968	0.00	0.00	6.79	11.2	150.9	1914
MS122	0	2601574	0.00	0.00	6.79	9.1	188.7	1911
MS123	0	2699152	0.00	0.00	6.79	22.4	85.5	1910
MS124	0	2796745	0.00	0.00	6.79	16.4	123.2	1910

Figure A2.3. (Cont.) 2021 site characterization used in random forest analysis.

Site	Upstream Distance (m)	Loam (%)	Silt Loam (%)	PCM (cm)	PCIQR (cm)	Canopy Cover (%)	Trees (%)	Faults Upstream
SF88	4882	22.45	22.19	3.1	3.525	90.74	36.00	1
SF89	4895	22.47	22.14	1.2	1.4	12.48	36.00	1
SF90	4942	40.23	54.48	1.1	1.025	0	10.05	1
SF91	4991	37.97	54.07	2.45	4.1	62.92	9.89	1
SF92	5003	37.38	53.96	1.3	2.825	93.6	9.85	1
SF93	5016	36.78	53.85	1.1	0.65	89.18	9.80	1
SF94	5028	36.18	53.74	1.4	1.05	85.8	9.76	1
SF95	5041	35.57	53.63	1.9	2.425	97.76	9.72	1
SF96	5142	30.45	52.68	2.1	2.225	82.68	9.35	1
SF97	5342	5.80	73.42	0	0	64.48	25.33	0
SF98	5342	29.24	45.28	0.5	0.825	99.58	4.21	1
SF99	5058	15.94	11.09	0	0	6.76	44.66	0
SF100	5070	15.88	11.09	0	0	41.08	44.66	0
SF101	5083	15.81	11.09	0	0.025	49.14	44.66	0
SF102	5095	15.75	11.09	0	0	27.56	44.66	0
SF103	5108	15.67	11.09	0	0	10.4	44.66	0
SF104	4694	5.44	39.89	0	0.15	94.12	44.82	0
SF105	1651	25.46	20.79	2.05	1.35	96.46	20.31	17
MS106	1642	25.46	20.77	3	5.7	96.2	20.29	17
MS107	1519	19.61	18.28	2.4	3.8	95.68	17.46	18
MS109	3251	52.75	47.26	1.95	2.2	95.94	6.39	0
NF110	5932	6.18	3.77	2.35	2.025	78.52	7.00	0
NF111	6634	38.12	14.72	1.85	1.5	47.84	6.52	2
NF112	6659	38.12	14.72	1.65	2.525	17.42	6.52	2
NF113	6510	38.12	14.72	1.85	1.2	2.6	6.52	2
NF114	5154	29.79	52.56	1.7	2.1	95.42	9.30	1
SF115	5167	29.12	52.44	1.95	1.4	94.12	9.25	1
SF116	5179	28.45	52.32	0.9	2.3	60.06	9.20	1
SF117	5192	27.78	52.19	2.3	2.6	82.68	9.16	1
SF118	1606	0.13	11.37	0	1.2	94.64	9.19	1
MS120	3823	0.00	1.38	1.8	2.325	56.94	7.03	0
MS121	3811	0.00	1.38	0.35	2	82.16	7.03	0
MS122	3798	0.00	1.38	0.1	2.825	26	7.03	0
MS123	3786	0.00	1.38	1.4	1.4	87.1	7.03	0
MS124	3773	0.00	1.38	1.95	1.925	93.86	7.03	0

Figure A2.3. (Cont.) 2021 site characterization used in random forest analysis.

Site	Geomorphic Depth (cm)	Geomorphic Width (cm)
SF88	16	64
SF89	17	73
SF90	13	113
SF91	17	40
SF92	19	90
SF93	18	92
SF94	20	188
SF95	25	148
SF96	28	42
SF97	15	167
SF98	20	60
SF99	20	58
SF100	9	45
SF101	4	35
SF102	7	37
SF103	12	47
SF104	29	130
SF105	41	303
MS106	19	188
MS107	23	124
MS109	22	33
NF110	24	153
NF111	10	61
NF112	14	56
NF113	17	178
NF114	22	193
SF115	29	105
SF116	11	111
SF117	7	80
SF118	0	0
MS120	15	103
MS121	15	62
MS122	20	106
MS123	11	39
MS124	15	54

Table A2.4. Calibration curves selected thresholds for every STIC used in Gibson Jack.

Serial Number	2020 ID	2021 ID	AdjR2	Intercept	Intercept SE	Intercept + SE	Intercept - SE	2020 Threshold	2021 Threshold
20284742	2H0_40	MS40	0.951	9940	6647	16586	3293	9940	9940
20848644	2H12_65	MS65	0.983	2153	4891	7044	-2738	1000	2153
20600954	A-_34	MS34	0.995	4560	2860	7420	1700	4560	1700
20600940	A0_32	MS32	0.924	6076	11368	17444	-5292	6076	6076
20641933	A100_33	MS33	NA	NA	NA	NA	NA	5000	0
20600961	A12_31	MS31	0.990	5335	3372	8707	1964	5335	1300
20641928	A25_30	MS30	0.953	8081	10927	19008	-2847	8081	8081
20895998	A37	MS61	0.997	2627	2072	4699	555	2627	2627
20848639	AB0_76	NF76	0.975	8090	5520	13610	2570	6000	1300
20848635	AB12_80	NF80	0.995	1041	2037	3077	-996	4500	2000
20848629	AB25_79	NF79	0.991	179	5395	5574	-5216	12321	2794
20848637	AB37_77	NF77	0.944	12321	9526	21847	2794	4093	4093
20892201	AB50_78	NF78	NA	NA	NA	NA	NA	8090	2570
20896004	B0_58	MS58	0.963	3185	10579	13764	-7394	3185	3185
20600942	B100_36	MS36	0.957	8409	5973	14381	2436	8409	8409
20896003	B12_59	MS59	0.996	4273	2846	7119	1427	4273	4273
20641931	B25_35	MS35	0.992	2009	4104	6113	-2096	2009	2009
20284729	B37_38	MS38	0.994	3948	2488	6436	1459	3948	3948
20641934	B50_39	MS39	0.957	3287	3984	7271	-697	3287	3287
20895979	Below0_89	SF89	NA	NA	NA	NA	NA	6426	5212
20895989	Below100_84	NF84	0.995	2487	2287	4774	200	15000	8435
20895984	Below12_88	SF88	0.995	1041	2037	3077	-996	5492	12590
20895980	Below25_87	SF87	0.983	5212	5416	10628	-204	4364	2818
20895981	Below37_86	SF86	0.876	12590	9613	22203	2978	0	2695
20895986	Below50_85	NF85	0.927	7365	7128	14493	237	4764	9550
20284734	C0_21	MS108	NA	NA	NA	NA	NA	Unused	Unused
20302367	C100_17	NF13	0.994	4975	3103	8078	1871	12253	800
20896014	C12_47	MS47	0.969	5894	4112	10006	1782	5894	2100
20600946	C25_12	NF17	0.805	16497	17194	33692	-697	6116	2500
20896010	C37_48	MS48	0.990	4748	3169	7917	1580	4748	0
20641925	C50_13	NF12	0.834	12253	14634	26887	-2381	442	442
20641929	D0_5	NF05	0.979	6517	4914	11431	1602	6517	6517
20600952	D100_28	NF28	0.998	2353	1853	4206	499	4008	4008
20284730	D12_4	NF04	0.988	5093	3580	8673	1512	5093	5093
20896011	D25_50	MS50	0.993	4445	3659	8104	786	4445	4445
20896018	D37_49	MS49	0.958	3737	5883	9620	-2146	3737	3737
20600951	D50_22	NF22	0.998	-2163	1621	-542	-3784	4255	4255
20600956	E0_27	NF27	0.955	4008	6801	10809	-2794	10975	4069
20284741	E100_23	SF105	0.992	1476	2564	4040	-1088	376	376
20641935	E1000_16	NF03	0.902	13958	16840	30798	-2883	13958	13958
20896012	E12_50	MS51	0.970	7535	5317	12851	2218	7535	7535
20641924	E25_9	NF09	0.999	-1228	767	-461	-1995	500	80
20896015	E37_49	MS52	0.995	2356	2639	4995	-283	2356	2356
20600960	E50_14	NF14	0.983	6329	5337	11665	992	4975	4975

Table A2.4. (Cont.) Calibration curves selected thresholds for every STIC used in Gibson Jack.

Serial Number	2020 ID	2021 ID	AdjR2	Intercept	Intercept SE	Intercept + SE	Intercept - SE	2020 Threshold	2021 Threshold
20600943	F0_26	NF26	0.964	10975	6907	17882	4069	7501	2500
20600945	F100_20	NF20	0.946	14251	11735	25985	2516	3032	3032
20895992	F12_99	SF99	NA	NA	NA	NA	NA	14623	14623
20600957	F25_24	NF24	0.978	9247	6652	15899	2596	4126	4126
20895997	F37_100	SF100	0.940	14633	9144	23777	5489	2487	2487
20600962	F50_3	NF16	0.855	6116	8527	14643	-2411	6319	4000
20641927	G0_7	NF07	0.891	-9472	12285	2813	-21757	2813	3500
20600958	G100_10	NF10	0.976	2748	5531	8280	-2783	2748	2748
20848642	G12_60	NF18	0.829	12935	11589	24523	1346	16497	3500
20454811	G25_8	NF08	0.930	4282	6741	11024	-2459	4282	80
20848645	G37_61	MS62	0.977	7219	4829	12048	2390	7219	7219
20641932	G50_11	NF11	0.975	5312	4682	9994	630	5312	586
20600953	Gib0_29	MS29	0.946	6635	6063	12698	571	6635	6635
20892202	Gib100_74	NF74	0.973	6426	4533	10959	1893	7943	4450
20848631	Gib12_75	NF75	0.997	4093	2652	6745	1440	5492	4450
20848636	Gib25_71	NF71	0.996	4364	3180	7543	1184	40000	4800
20848638	Gib37_72	NA	NA	NA	NA	NA	NA	1000	
20848641	Gib50_73	NF73	0.973	6426	4533	10959	1893	4364	4364
20600948	H0_25	NF25	0.928	7501	7539	15039	-38	9247	2500
20600950	H100_19	NF19	0.994	3032	2091	5123	941	12935	1346
20896002	H12_63	MS63	0.954	8138	5432	13569	2706	8138	8138
20896001	H37_64	MS64	0.978	5917	4325	10243	1592	5917	5917
20284731	H50_6	NF06	0.820	11703	13825	25528	-2123	11703	11703
20895985	Jack0_90	SF90	0.995	1111	2007	3118	-897	1041	1041
20895994	Jack100_94	SF94	0.984	2042	4077	6119	-2034	2465	2465
20895990	Jack12_91	SF91	0.987	-569	5217	4648	-5785	0	5300
20895982	Jack25_92	SF92	0.973	2465	6192	8658	-3727	1111	3000
20895983	Jack37_93	SF93	0.958	8815	6945	15761	1870	0	4648
20895988	Jack50_95	NA	NA	NA	NA	NA	NA	1000	
20869017	LE0_53	MS53	NA	NA	NA	NA	NA	15000	1100
20896008	LE12_54	MS54	0.979	3529	7926	11455	-4397	3529	3529
20896000	LE25_57	MS57	0.986	5043	3667	8710	1377	5043	5043
20896019	LE37_55	MS55	0.973	6139	5128	11267	1011	6139	6139
20896006	LE50_56	MS56	0.987	5294	3320	8613	1974	5294	5294
20848634	Lower0_81	NF81	0.921	5198	8114	13311	-2916	179	179
20895978	Lower100_98	SF98	NA	NA	NA	NA	NA	2487	6541
20895993	Lower12_82	NF82	0.782	8435	13333	21768	-4899	4008	1041
20895987	Lower25_83	NF83	0.933	9550	12179	21729	-2629	5198	500
20895996	Lower37_96	SF96	0.970	6541	4119	10661	2422	2042	2042
20895995	Lower50_97	SF97	0.860	14623	9144	23768	5479	14215	4900
20848646	lowH0_66	MS66	0.996	2523	1745	4269	778	2523	2523
20848643	lowH12_67	MS67	0.940	9283	6630	15912	2653	9283	9283
20848633	lowH25_68	NF68	0.855	7524	11917	19441	-4393	2353	2353
20848632	lowH37_69	NF69	0.986	4764	3621	8385	1143	7524	5100

Table A2.4. (Cont.) Calibration curves selected thresholds for every STIC used in Gibson Jack.

Serial Number	2020 ID	2021 ID	AdjR2	Intercept	Intercept SE	Intercept + SE	Intercept - SE	2020 Threshold	2021 Threshold
20848630	lowH50_70	NF70	0.982	7943	6955	14898	987	4764	4650
20600944	MBO_42	MS42	0.992	618	2789	3407	-2171	618	618
20896016	MB12_43	NA	NA	NA	NA	NA	NA	18000	
20896007	MB25_44	MS44	0.975	5309	4374	9683	936	5309	5309
20896009	MB37_45	MS45	NA	NA	NA	NA	NA	15500	1400
20895999	MB50_46	MS46	0.857	13477	13192	26669	284	13477	13477
20600949	NA	MS106	0.946	15486	13619	29106	1867	Unused	15486
21059637	NA	MS107	0.907	8789	8549	17338	240	Unused	8789
21064707	NA	MS109	0.940	4738	7916	12654	-3178	Unused	4738
Unknown	NA	MS119	NA	NA	NA	NA	NA	Unused	4000
21059638	NA	MS120	0.995	4047	2527	6573	1520	Unused	4047
21064703	NA	MS121	0.946	7329	6431	13760	898	Unused	4500
21059639	NA	MS122	0.977	2458	3700	6158	-1241	Unused	2458
21059631	NA	MS123	0.991	1498	2484	3982	-986	Unused	1498
21059622	NA	MS124	0.871	6453	9912	16365	-3459	Unused	1500
20600947	NA	MS37	0.960	7436	5497	12933	1939	Unused	7436
21059623	NA	MS41	0.968	8364	6038	14402	2326	Unused	8364
2089016	NA	MS43	0.930	8330	8294	16624	35	Unused	8330
20896013	NA	MS60	0.996	3037	2115	5152	922	Unused	3037
20600963	NA	NF02	NA	NA	NA	NA	NA	Unused	
Unknown	NA	NF110	0.998	586	1333	1918	-747	Unused	4000
2105921	NA	NF111	0.970	3072	5253	8325	-2181	Unused	3072
21059630	NA	NF112	0.944	16061	12229	28290	3832	Unused	28290
21064700	NA	NF113	0.852	15451	15404	30855	47	Unused	15451
21059626	NA	NF114	0.996	442	1948	2390	-1506	Unused	5312
20600959	NA	NF15	0.962	6319	5399	11718	920	Unused	2600
10870155	NA	NF21	0.989	4255	3452	7707	804	Unused	4000
20641926	NA	NF23	0.942	4126	6110	10237	-1984	Unused	4000
Unknown	NA	NF72	0.981	5492	3450	8943	2042	Unused	4450
21064706	NA	SF101	NA	NA	NA	NA	NA	Unused	7365
21064705	NA	SF102	0.959	12227	7654	19881	4574	Unused	14633
Unknown	NA	SF103	0.998	376	1440	1816	-1063	Unused	2000
21059636	NA	SF115	0.886	11609	9896	21505	1713	Unused	3812
21059625	NA	SF116	0.994	1198	2445	3643	-1247	Unused	1476
21064702	NA	SF117	0.922	10292	7597	17889	2695	Unused	3000
21064701	NA	SF118	0.995	-311	3128	2818	-3439	Unused	1198
20895986	NA	SF95	0.820	14215	13422	27637	793	Unused	1870
21064708	NA	SF104	0.993	3812	2380	6192	1432	Unused	12227

Table A2.5. Spatial models created from 2020 data.

Explanatory Variable	Shape	VIF	AUC	False Positive	False Negative	Partial Sill	Range	Nugget	Sig of 1 st Variable	Sig of 2 nd Variable
Drainage Area + Faults	Mariah	10.6	99.81	0	0	0.21	7324	2.32E-09	0.001	0.464
Loam + Silt Loam	Exponential	8.99	99.81	0	0	0.47	4826	2.06E-09	0.012	0.032
Metaseds	NULL	NA	99.76	40	0	1.02	NA	NA	0.978	NA
Colluvium + Loam	Exponential	8.99	99.76	0	0	0.37	4826	2.16E-08	0.000	0.448
Silt Loam	Mariah	NA	99.71	0	0	0.23	7324	2.07E-09	0.053	NA
Silt Loam	Spherical	NA	99.71	0	0	0.35	2343	2.06E-09	0.032	NA
Colluvium	LinearSill	NA	99.66	0	0	0.49	7324	2.06E-09	0.482	NA
Faults + Elevation	Mariah	2.16	99.66	0	0	0.17	7324	2.06E-09	0.002	0.000
Metaseds	Mariah	NA	99.61	0	0	0.23	7324	2.11E-09	0.547	NA
Colluvium	Exponential	NA	99.61	0	0	0.25	7324	2.06E-09	0.152	NA
Colluvium	Spherical	NA	99.61	0	0	0.34	7324	2.06E-09	0.295	NA
Colluvium	Mariah	NA	99.61	0	0	0.24	7324	2.18E-09	0.058	NA
Loam	Mariah	NA	99.61	0	0	0.23	7324	2.08E-09	0.134	NA
Slope	Exponential	NA	99.61	0	0	0.27	7324	2.06E-09	0.986	NA
Silt Loam	Exponential	NA	99.61	0	0	0.45	4826	2.06E-09	0.067	NA
Elevation + Loam	Spherical	8.99	99.61	0	0	1.41	1285	3.41E-09	0.091	0.130
1 Mariah	Mariah	NA	99.56	0	0	0.23	7324	2.38E-09	NA	NA
Carbonates	Mariah	NA	99.56	0	0	0.22	7324	2.08E-09	0.008	NA
Trees	Exponential	NA	99.56	0	0	0.26	7324	2.06E-09	0.920	NA
Trees	Mariah	NA	99.56	0	0	0.23	7324	2.12E-09	0.744	NA
Drainage Area	Mariah	NA	99.56	0	0	0.21	7324	2.06E-09	0.000	NA
Colluvium	Exponential	NA	99.56	0	0	0.47	4826	2.06E-09	0.006	NA
Slope	LinearSill	NA	99.52	0	0	0.55	7324	2.06E-09	0.967	NA
Slope	Mariah	NA	99.52	0	0	0.23	7324	2.06E-09	0.801	NA
Aspect	Mariah	NA	99.52	0	0	0.27	7324	2.27E-09	0.814	NA
Slope	Exponential	NA	99.52	0	0	0.44	4826	2.06E-09	0.946	NA
Slope	Spherical	NA	99.47	0	0	0.36	7324	2.06E-09	0.955	NA
Aspect	Exponential	NA	99.47	0	0	0.27	7324	2.06E-09	0.808	NA
Loam	Exponential	NA	99.47	0	0	0.39	4826	2.06E-09	0.021	NA
1 LinearSill	LinearSill	NA	99.42	0	0	0.44	7324	2.06E-09	NA	NA
Metaseds	LinearSill	NA	99.42	0	0	0.55	7324	2.06E-09	0.274	NA
Metaseds	Spherical	NA	99.42	0	0	0.38	7324	2.06E-09	0.302	NA
Loam	LinearSill	NA	99.42	0	0	0.56	7324	2.06E-09	0.186	NA
Loam	Spherical	NA	99.42	0	0	0.39	7324	2.06E-09	0.156	NA

Notes: Colors correspond with model type: Orange for Cartesian, blue for tail up, and grey for non-spatial. NA indicates not applicable.

Table A2.5. (Cont.) Spatial models created from 2020 data.

Explanatory Variable	Shape	VIF	AUC	False Positive	False Negative	Partial Sill	Range	Nugget	Sig of 1 st Variable	Sig of 2 nd Variable
Carbonates + Faults	Mariah	1.14	99.42	0	0	0.19	7324	2.20E-09	0.373	0.001
Faults + upDist	Mariah	1.63	99.42	0	0	0.14	7324	2.16E-09	0.000	0.000
1	Exponential	NA	99.37	0	0	0.26	7324	2.07E-09	NA	NA
Loam	Exponential	NA	99.37	0	0	0.27	7324	2.06E-09	0.135	NA
Metaseds	Exponential	NA	99.37	0	0	0.40	4826	2.06E-09	0.072	NA
Aspect	LinearSill	NA	99.32	0	0	0.50	7324	2.06E-09	0.825	NA
Colluvium + Silt Loam	Exponential	8.99	99.32	0	0	0.51	4826	1.42E-08	0.028	0.111
Metaseds	Exponential	NA	99.27	0	0	0.27	7324	2.06E-09	0.367	NA
Aspect	Spherical	NA	99.27	0	0	0.36	7324	2.06E-09	0.797	NA
Elevation + Colluvium	Exponential	8.99	99.27	0	0	0.47	4826	2.16E-09	0.001	0.006
Metaseds	Epanech	NA	99.23	0	0	0.49	7324	2.06E-09	0.294	NA
Loam	Epanech	NA	99.23	0	0	0.50	7324	2.06E-09	0.185	NA
Aspect	Exponential	NA	99.23	0	0	0.42	4826	2.06E-09	0.740	NA
Carbonates	Exponential	NA	99.18	0	0	0.26	7324	2.06E-09	0.002	NA
Silt Loam	Exponential	NA	99.13	0	0	0.26	7324	2.06E-09	0.279	NA
Silt Loam	Spherical	NA	99.13	0	0	0.34	7324	2.06E-09	0.684	NA
Loam	Spherical	NA	99.13	0	0	0.68	4826	2.06E-09	0.021	NA
1	Exponential	NA	99.08	0	0	0.41	4826	2.06E-09	NA	NA
Metaseds	Spherical	NA	99.03	0	0	0.73	4826	2.06E-09	0.074	NA
Colluvium	Epanech	NA	98.94	0	0	0.44	7324	2.06E-09	0.403	NA
Silt Loam	LinearSill	NA	98.94	0	0	0.50	7324	2.06E-09	0.864	NA
Elevation	Mariah	NA	98.89	0	0	0.17	7324	2.07E-09	0.000	NA
Carbonates	Exponential	NA	98.89	0	0	0.44	4826	2.06E-09	0.706	NA
Trees	Spherical	NA	98.89	0	0	0.35	2332	2.06E-09	0.069	NA
Silt Loam	Epanech	NA	98.84	0	0	0.47	7324	2.06E-09	0.971	NA
Carbonates + Elevation	Mariah	1.34	98.84	0	0	0.17	7324	2.19E-09	0.946	0.000
Elevation + upDist	Mariah	8.99	98.79	0	0	0.20	7324	2.17E-09	0.001	0.563
upDist	Mariah	NA	98.74	0	0	0.20	7324	2.14E-09	0.000	NA
Slope	Spherical	NA	98.69	0	0	0.90	4826	2.06E-09	0.925	NA
Elevation	Exponential	NA	98.60	0	0	0.23	7324	2.06E-09	0.000	NA
Elevation	LinearSill	NA	98.60	0	0	0.41	7324	2.06E-09	0.000	NA
Elevation	Spherical	NA	98.60	0	0	0.32	7324	2.06E-09	0.000	NA
Elevation	Epanech	NA	98.60	0	0	0.41	7324	2.06E-09	0.000	NA
Carbonates + Elevation	Exponential	1.34	98.60	0	0	0.22	7324	2.06E-09	0.652	0.000

Notes: Colors correspond with model type: Orange for Cartesian, blue for tail up, and grey for non-spatial. NA indicates not applicable.

Table A2.5. (Cont.) Spatial models created from 2020 data.

Explanatory Variable	Shape	VIF	AUC	False Positive	False Negative	Partial Sill	Range	Nugget	Sig of 1 st Variable	Sig of 2 nd Variable
Carbonates + Elevation	LinearSill	1.34	98.60	0	0	0.40	7324	2.06E-09	0.011	0.000
Carbonates + Elevation	Spherical	1.34	98.60	0	0	0.31	7324	2.06E-09	0.990	0.000
Carbonates + Elevation	Epanech	1.34	98.60	0	0	0.40	7324	2.06E-09	0.745	0.000
Elevation + upDist	LinearSill	8.99	98.60	0	0	0.38	7324	2.06E-09	0.009	0.193
Elevation + upDist	Spherical	8.99	98.60	0	0	0.30	7324	2.06E-09	0.011	0.259
Upstream Distance	Exponential	NA	98.60	0	0	0.78	4826	3.43E-08	0.246	NA
Aspect	Spherical	NA	98.60	0	0	0.91	4826	2.06E-09	0.792	NA
Elevation + upDist	Exponential	8.99	98.55	0	0	0.25	7324	2.06E-09	0.008	0.471
Elevation	Exponential	NA	98.55	0	0	0.69	4826	2.07E-09	0.031	NA
Carbonates + upDist	Mariah	1.2	98.50	0	0	0.18	7324	2.07E-09	0.119	0.000
Elevation	Spherical	NA	98.50	0	0	0.36	2295	5.55E-09	0.002	NA
Elevation + upDist	Epanech	8.99	98.45	0	0	0.37	7324	2.06E-09	0.021	0.193
Trees	Exponential	NA	98.45	0	0	0.41	4826	2.06E-09	0.227	NA
Trees	LinearSill	NA	98.40	0	0	0.44	7324	2.06E-09	0.633	NA
Trees	Epanech	NA	98.40	0	0	0.41	7324	2.06E-09	0.681	NA
upDist	LinearSill	NA	98.40	0	0	0.50	7324	2.06E-09	0.001	NA
upDist	Spherical	NA	98.40	0	0	0.37	7324	2.06E-09	0.000	NA
upDist	Epanech	NA	98.40	0	0	0.47	7324	2.30E-09	0.002	NA
Upstream Distance	Spherical	NA	98.40	0	0	0.61	2323	2.10E-09	0.067	NA
Trees	Spherical	NA	98.31	0	0	0.36	7324	2.07E-09	0.935	NA
upDist	Exponential	NA	98.31	0	0	0.25	7324	2.06E-09	0.000	NA
Faults	Mariah	NA	98.31	0	0	0.19	7324	2.40E-09	0.000	NA
Aspect	Epanech	NA	98.31	0	0	0.44	7324	2.06E-09	0.790	NA
Faults + Colluvium	Spherical	8.99	98.31	0	0	0.35	2305	2.07E-09	0.002	0.074
Faults + Silt Loam	Spherical	8.99	98.31	0	1	0.35	2281	2.08E-09	0.001	0.339
Slope	Epanech	NA	98.21	0	0	0.45	7324	2.06E-09	0.935	NA
1	Spherical	NA	98.21	0	0	0.90	4826	1.17E-08	NA	NA
1	Spherical	NA	98.16	0	0	0.36	7324	2.07E-09	NA	NA
1	Epanech	NA	98.16	0	0	0.41	7324	2.06E-09	NA	NA

Notes: Colors correspond with model type: Orange for Cartesian, blue for tail up, and grey for non-spatial. NA indicates not applicable.

Table A2.5. (Cont.) Spatial models created from 2020 data.

Explanatory Variable	Shape	VIF	AUC	False Positive	False Negative	Partial Sill	Range	Nugget	Sig of 1 st Variable	Sig of 2 nd Variable
Carbonates	Spherical	NA	98.16	0	0	0.91	4826	2.06E-09	0.929	NA
Carbonates + upDist	Exponential	1.2	98.11	0	0	0.25	7324	2.06E-09	0.134	0.000
Carbonates + upDist	LinearSill	1.2	98.11	0	0	0.38	7324	2.06E-09	0.377	0.000
Carbonates + upDist	Spherical	1.2	98.11	0	0	0.39	7324	2.06E-09	0.792	0.000
Carbonates + upDist	Epanech	1.2	98.11	0	0	0.39	7324	3.93E-08	0.390	0.000
Faults + Elevation	Spherical	8.99	97.73	0	1	0.18	1204	2.07E-09	0.002	0.000
Faults + Elevation	Exponential	8.99	97.68	0	1	0.47	4826	2.06E-09	0.003	0.004
Faults	Spherical	NA	96.42	0	1	0.34	2258	2.07E-09	0.001	NA
Faults	Exponential	NA	96.42	0	1	0.44	4826	2.08E-09	0.001	NA
Faults + Colluvium	Exponential	8.99	96.42	0	1	0.40	4826	2.10E-09	0.002	0.077
Faults + Loam	Spherical	8.99	96.42	0	1	1.38	4826	2.14E-09	0.029	0.097
Faults + Loam	Exponential	8.99	96.42	0	1	0.61	4826	2.11E-09	0.007	0.059
Faults + Silt Loam	Exponential	8.99	96.42	0	1	0.41	4826	2.08E-09	0.002	0.363
Faults + upDist	NULL	1.63	93.95	6	8	0.63	NA	NA	0.000	0.000
Faults + Elevation	NULL	2.16	90.42	6	8	0.70	NA	NA	0.001	0.000
Drainage Area + upDist	NULL	1.96	88.97	1	8	0.72	NA	NA	0.000	0.006
Drainage Area + upDist	Mariah	1.96	87.76	0	6	0.17	7324	2.62E-09	0.000	0.001
Carbonates + Elevation	NULL	1.34	87.57	6	13	0.73	NA	NA	0.786	0.000
Elevation	NULL	NA	87.32	6	11	0.73	NA	NA	0.000	NA
Drainage Area + Faults	NULL	10.6	86.02	0	8	0.82	NA	NA	0.000	0.648
Drainage Area	NULL	NA	85.97	0	8	0.81	NA	NA	0.000	NA
Elevation + upDist	NULL	8.99	84.86	6	8	0.77	NA	NA	0.000	0.058

Notes: Colors correspond with model type: Orange for Cartesian, blue for tail up, and grey for non-spatial. NA indicates not applicable.

Table A2.5. (Cont.) Spatial models created from 2020 data.

Explanatory Variable	Shape	VIF	AUC	False Positive	False Negative	Partial Sill	Range	Nugget	Sig of 1 st Variable	Sig of 2 nd Variable
Trees	NULL	NA	81.37	40	0	1.02	NA	NA	0.802	NA
upDist	NULL	NA	81.13	11	11	0.90	NA	NA	0.000	NA
Carbonates + upDist	NULL	1.2	80.26	16	16	0.81	NA	NA	0.079	0.000
Carbonates + Faults	NULL	1.14	75.47	6	13	0.75	NA	NA	0.127	0.000
Faults	NULL	NA	74.14	6	13	0.75	NA	NA	0.000	NA
Colluvium	NULL	NA	64.30	28	0	0.98	NA	NA	0.020	NA
Aspect	NULL	NA	63.28	24	15	1.02	NA	NA	0.018	NA
Loam	NULL	NA	56.10	40	0	1.02	NA	NA	0.330	NA
Carbonates	NULL	NA	55.68	6	29	0.95	NA	NA	0.002	NA
Slope	NULL	NA	54.91	31	11	1.02	NA	NA	0.087	NA
Silt Loam	NULL	NA	53.87	23	0	1.03	NA	NA	0.013	NA

Notes: Colors correspond with model type: Orange for Cartesian, blue for tail up, and grey for non-spatial. NA indicates not applicable.

Table A2.6. Spatial models created from 2021 data.

Explanatory Variable	Shape	AUC	False Positive	False Negative	Partial Sill	Range	Nugget	Significance of Variable
Trees	Cauchy	95.98566	5	8	0.886725	95.98	0.09546	0.06751
Trees	Exponential	95.87814	6	9	1.057908	237.39	0.001637	0.04858
Trees	Gaussian	95.77061	6	8	0.871419	80.143	0.107296	0.10946
Drainage Area	Mariah	95.69892	5	9	1.047147	3524.5	4.38E-08	0.49878
Trees	Spherical	95.62724	7	9	1.128821	167.51	0.025879	0.07463
Trees	Exponential	95.5914	6	9	1.03481	237.13	3.40E-05	0.13681
Faults	LinearSill	95.5914	6	8	0.887486	60.195	0.010841	0.06996
Trees	Mariah	95.55556	4	9	1.065196	3337.7	8.22E-08	0.1967
Faults	Epanech	95.51971	6	8	0.875794	80.843	0.043167	0.0785
Trees	Epanech	95.44803	6	9	1.016294	107.25	0.034651	0.15867
Trees	LinearSill	95.44803	6	9	1.29808	124.97	0.016584	0.20775
Trees	Spherical	95.44803	6	9	1.039794	133.29	0.011527	0.14703
Faults	Spherical	95.44803	6	8	0.901929	89.628	0.005666	0.07701
Drainage Area	Exponential	95.37634	7	8	1.023234	243.21	0.002473	0.50318
1	Mariah	95.19713	5	9	1.024377	3471.1	3.45E-08	NA
1	Cauchy	95.16129	7	8	0.882326	94.045	0.090217	NA
Drainage Area	Spherical	95.16129	6	8	1.033634	130.51	0.01164	0.50131
Carbonates	Cauchy	95.12545	7	7	0.887372	94.217	0.091331	0.29362
Upstream Distance	Cauchy	95.05376	7	8	0.904995	95.753	0.091245	0.9481
Carbonates	Exponential	95.05376	8	7	1.005393	231.41	9.79E-08	0.30223
Carbonates	Exponential	95.05376	7	8	1.01909	233.89	1.42E-06	0.32379
Drainage Area	Epanech	94.98208	6	8	1.001617	99.759	0.032334	0.49615
1	Exponential	94.98208	7	8	1.004652	233.68	1.73E-06	NA
Slope	Mariah	94.98208	3	11	1.008983	3378.9	1.05E-07	0.56951
Elevation	Mariah	94.98208	6	8	1.06307	3609.7	4.26E-08	0.71716
Elevation	Exponential	94.94624	7	8	1.03551	244.6	0.001546	0.8558
Upstream Distance	Gaussian	94.94624	6	8	0.894659	79.807	0.10699	0.97285
Elevation	Cauchy	94.91039	7	8	0.903645	95.723	0.09036	0.88257
1	Gaussian	94.91039	6	8	0.875309	78.83	0.106815	NA
Carbonates	Gaussian	94.87455	6	8	0.877512	78.615	0.107709	0.2773
Elevation	Gaussian	94.87455	6	8	0.892578	79.765	0.106356	0.79426
Metaseds	Mariah	94.87455	6	9	1.06869	3749.1	4.72E-08	0.56552
Drainage Area	LinearSill	94.80287	7	8	1.192036	112.47	0.021147	0.53541
1	Exponential	94.76703	8	8	0.987678	227.31	6.70E-08	NA

Notes: Colors correspond with model type: Orange for Cartesian, blue for tail up, and grey for non-spatial. NA indicates not applicable.

Table A2.6. (Cont.) Spatial models created from 2021 data.

Explanatory Variable	Shape	AUC	False Positive	False Negative	Partial Sill	Range	Nugget	Significance of Variable
Elevation	Exponential	94.76703	8	8	1.02054	237.48	1.27E-07	0.94628
Carbonates	Spherical	94.69534	8	7	1.07185	142.81	0.013692	0.29904
Metaseds	Gaussian	94.62366	6	8	0.8895	80.502	0.104877	0.58829
Metaseds	Cauchy	94.58781	6	8	0.907938	98.514	0.088391	0.36031
Slope	Exponential	94.58781	7	10	0.994528	235.01	0.00192	0.67043
Loam	Mariah	94.58781	6	9	1.060333	3603.5	1.59E-07	0.90664
1	Spherical	94.58781	8	8	1.069624	145.71	0.014275	NA
Metaseds	Exponential	94.55197	7	7	1.036534	249.95	2.94E-05	0.57136
Upstream Distance	Mariah	94.55197	6	8	1.076927	3511.4	1.46E-07	0.52523
Silt Loam	Gaussian	94.48029	6	8	0.901823	79.072	0.111645	0.50777
Silt Loam	Cauchy	94.44444	7	8	0.903783	94.677	0.092908	0.65739
Slope	Cauchy	94.44444	7	9	0.876336	94.37	0.091261	0.76114
Metaseds	Exponential	94.44444	8	8	1.079109	269.07	1.35E-07	0.20693
Slope	Gaussian	94.44444	6	8	0.870971	79.373	0.107616	0.7885
Elevation	Spherical	94.4086	9	8	1.123569	159.41	0.016867	0.89006
Carbonates	Mariah	94.33692	5	9	1.048369	3473.8	6.19E-08	0.37344
Silt Loam	Mariah	94.33692	6	9	1.076231	3453.2	9.67E-08	0.44688
1	Spherical	94.33692	6	8	1.025635	129.91	0.01144	NA
Metaseds	Spherical	94.30108	8	7	1.128911	164.26	0.015111	0.30647
Carbonates	Spherical	94.30108	6	8	1.037653	130.68	0.012075	0.30596
Elevation	Spherical	94.26523	6	8	1.046764	131.87	0.01072	0.96609
Elevation	Epanech	94.22939	6	8	1.014707	100.94	0.031248	0.91611
1	Epanech	94.19355	6	8	0.990783	98.383	0.031272	NA
Metaseds	Epanech	94.19355	6	8	1.02252	105.58	0.031981	0.67626
Slope	Exponential	94.19355	8	10	0.979752	225.35	4.76E-08	0.6433
Upstream Distance	Exponential	94.19355	7	8	1.042142	243.19	0.003108	0.66851
Aspect	Gaussian	94.19355	5	8	0.87851	74.871	0.109097	0.12436
Metaseds	Spherical	94.19355	7	7	1.121863	167.1	0.023319	0.54704
Upstream Distance	Exponential	94.15771	8	8	1.026026	236.94	1.13E-07	0.87845
Slope	Spherical	94.15771	6	9	1.015562	130.8	0.013232	0.72199
Carbonates	Epanech	94.12186	6	8	1.001981	99.508	0.03252	0.29494
Upstream Distance	Epanech	94.05018	6	8	1.01731	100.97	0.032755	0.86894
1	LinearSill	94.05018	6	8	1.276426	124.97	0.020221	NA
Silt Loam	Epanech	94.01434	6	8	1.022452	96.792	0.034084	0.4412
Aspect	Mariah	94.01434	4	7	1.029298	3376.4	6.04E-08	0.21703
Aspect	Epanech	93.97849	5	8	0.981708	88.112	0.027482	0.15233
Silt Loam	Exponential	93.97849	7	8	1.043543	241.07	0.003939	0.5226

Notes: Colors correspond with model type: Orange for Cartesian, blue for tail up, and grey for non-spatial. NA indicates not applicable.

Table A2.6. (Cont.) Spatial models created from 2021 data.

Explanatory Variable	Shape	AUC	False Positive	False Negative	Partial Sill	Range	Nugget	Significance of Variable
Upstream Distance	Spherical	93.97849	6	8	1.050065	131.51	0.012059	0.81802
Loam	Spherical	93.94265	6	8	1.048759	131.61	0.011238	0.93051
Silt Loam	Spherical	93.94265	6	8	1.060182	128.83	0.013262	0.49248
Loam	Exponential	93.90681	7	8	1.036474	239.9	0.000659	0.84458
Upstream Distance	Spherical	93.90681	9	8	1.127016	159.16	0.017833	0.9041
Loam	Epanech	93.83513	6	8	1.016797	101.21	0.031867	0.97964
Silt Loam	Exponential	93.83513	9	8	1.013082	230.98	5.56E-08	0.76273
Carbonates	LinearSill	93.83513	6	7	1.299275	124.97	0.020329	0.3635
Metaseds	LinearSill	93.83513	6	7	1.30333	124.97	0.014079	0.5953
Silt Loam	LinearSill	93.83513	6	8	1.32303	124.97	0.022828	0.58122
Loam	Gaussian	93.79928	6	8	0.893626	79.879	0.10623	0.89688
Slope	LinearSill	93.79928	6	9	1.257396	124.97	0.022426	0.77137
Loam	Cauchy	93.76344	7	8	0.901698	96.079	0.089527	0.85344
Slope	Spherical	93.76344	8	9	1.057658	144.64	0.015319	0.75803
Aspect	Cauchy	93.7276	5	8	0.894282	90.798	0.091751	0.15233
Loam	Spherical	93.7276	9	8	1.121469	159.51	0.016398	0.90008
Silt Loam	Spherical	93.7276	8	8	1.099975	147.25	0.015959	0.62861
Slope	Epanech	93.69176	6	9	0.984507	99.406	0.032811	0.75599
Aspect	Exponential	93.62007	6	7	1.002366	221.09	4.11E-07	0.20551
Elevation	LinearSill	93.54839	6	8	1.306134	124.97	0.017841	0.98958
Aspect	Spherical	93.44086	5	8	1.031158	121.36	0.00908	0.16783
Loam	LinearSill	93.40502	6	8	1.312202	124.97	0.019829	0.8523
Aspect	Exponential	93.33333	6	7	0.986971	215.99	1.15E-07	0.21423
Upstream Distance	LinearSill	93.18996	6	7	1.707129	260.73	0.079759	0.53848
Aspect	LinearSill	93.18996	5	8	1.21509	112.47	0.023431	0.16883
Aspect	Spherical	93.18996	7	8	1.050726	127.45	0.008819	0.14969
Loam	Exponential	92.22222	8	8	1.021235	242.9	9.31E-08	0.78067
Colluvium	Gaussian	91.97133	6	8	0.897101	79.922	0.107516	0.74491
Colluvium	Exponential	91.64875	7	8	1.032987	243.61	0.001243	0.79956
Colluvium	Mariah	91.57706	5	9	1.057438	3603.8	1.01E-07	0.70024
Colluvium	Exponential	91.46953	9	8	1.021853	237.59	5.78E-08	0.62864
Colluvium	Epanech	91.32616	6	8	1.018135	100.49	0.031464	0.73551
Colluvium	Spherical	91.11111	9	8	1.127723	160.54	0.018018	0.59211
Colluvium	Spherical	91.07527	6	8	1.049688	131.59	0.010863	0.7645
Colluvium	LinearSill	91.03943	6	8	1.307903	124.97	0.01828	0.80698
Carbonates	NULL	75.41219	3	30	1.001973	NA	NA	0.09383
Aspect	NULL	60.57348	0	31	1.018484	NA	NA	0.48428
Faults	NULL	59.49821	0	31	0.877266	NA	NA	0.00648

Notes: Colors correspond with model type: Orange for Cartesian, blue for tail up, and grey for non-spatial. NA indicates not applicable.

Table A2.6. (Cont.) Spatial models created from 2021 data.

Explanatory Variable	Shape	AUC	False Positive	False Negative	Partial Sill	Range	Nugget	Significance of Variable
Elevation	NULL	59.24731	5	31	0.997173	NA	NA	0.04633
Trees	NULL	58.49462	3	23	1.034143	NA	NA	0.00168
Loam	NULL	51.29032	0	31	1.036244	NA	NA	0.13982
Slope	NULL	48.78136	1	31	1.017394	NA	NA	0.12345
Metaseds	NULL	48.56631	0	31	1.031332	NA	NA	0.10119
Upstream Distance	NULL	46.02151	0	31	1.009209	NA	NA	0.15385

Notes: Colors correspond with model type: Orange for Cartesian, blue for tail up, and grey for non-spatial. NA indicates not applicable.

Table A2.7. Spatial models created from 2020 and 2021 data.

Explanatory Variable	Shape	VIF	AUC	False Positive	False Negative	Partial Sill	Range	Nugget	Sig of 1 st Variable	Sig of 2 nd Variable
Metaseds	Exponential	NA	98.01	8	6	1.10	469	6.86E-09	0.139	NA
Metaseds	Spherical	NA	97.97	7	7	1.35	302	1.57E-07	0.190	NA
Loam	Exponential	NA	97.92	8	5	1.11	473	2.29E-08	0.201	NA
Loam	Spherical	NA	97.83	7	7	1.34	302	1.26E-07	0.276	NA
Trees	Exponential	NA	97.82	8	6	1.10	455	1.82E-08	0.123	NA
Trees	Spherical	NA	97.72	8	7	1.37	302	6.64E-08	0.150	NA
Metaseds	Cauchy	NA	97.69	6	8	0.84	117	5.26E-02	0.280	NA
Aspect	Exponential	NA	97.68	6	5	1.03	434	1.71E-08	0.255	NA
Aspect	Cauchy	NA	97.61	6	6	0.83	115	5.28E-02	0.167	NA
Loam	Cauchy	NA	97.60	7	8	0.85	118	5.25E-02	0.426	NA
Aspect	Spherical	NA	97.58	5	5	1.34	301	4.82E-08	0.260	NA
Trees	Cauchy	NA	97.55	8	8	0.84	117	5.34E-02	0.228	NA
Metaseds	Mariah	NA	97.54	7	9	1.12	6460	6.21E-09	0.759	NA
Aspect	Mariah	NA	97.53	6	6	1.09	6103	5.63E-09	0.280	NA
Faults	Cauchy	NA	97.53	8	7	0.83	110	5.32E-02	0.098	NA
Loam	Mariah	NA	97.47	7	9	1.13	6483	9.12E-09	0.814	NA
Trees	Mariah	NA	97.47	7	8	1.13	6479	1.86E-08	0.600	NA
Metaseds	Exponential	NA	97.45	8	7	1.04	442	2.55E-09	0.552	NA
Aspect	Exponential	NA	97.45	5	7	1.01	422	3.17E-08	0.247	NA
1	Spherical	NA	97.43	11	4	13.27	3089	1.82E-02	NA	NA
Faults	Mariah	NA	97.39	9	8	1.11	6203	1.37E-08	0.363	NA
Upstream Distance + Carbonates	Exponential	1.13	97.39	8	6	1.05	434	1.08E-08	0.198	NA
Carbonates	Cauchy	NA	97.36	9	6	0.81	111	5.38E-02	0.054	NA
1	Cauchy	NA	97.33	8	6	0.84	116	5.25E-02	NA	NA
Metaseds	LinearSill	NA	97.32	8	6	1.18	162	5.08E-09	0.390	NA
Loam	Exponential	NA	97.32	8	7	1.05	445	1.53E-08	0.700	NA
Faults	Exponential	NA	97.31	8	7	1.04	413	1.60E-08	0.149	NA
Elevation + Carbonates	Exponential	1.13	97.31	8	4	1.08	421	1.15E-08	0.071	NA
Faults	Exponential	NA	97.29	9	4	1.01	418	1.26E-08	0.378	NA
Loam	LinearSill	NA	97.28	8	6	1.18	162	9.87E-09	0.574	NA
Carbonates	Mariah	NA	97.25	8	7	1.12	6066	1.25E-08	0.250	NA
Faults	Spherical	NA	97.25	9	5	1.35	299	6.18E-08	0.410	NA
Aspect	Spherical	NA	97.24	7	6	0.96	192	3.92E-08	0.256	NA
Carbonates	Exponential	NA	97.23	8	6	1.01	401	1.68E-08	0.121	NA
Upstream Distance	Exponential	NA	97.23	8	6	1.06	436	6.64E-09	0.148	NA
Elevation	Exponential	NA	97.23	9	6	1.05	410	1.24E-08	0.044	NA
Silt Loam	Exponential	NA	97.22	8	6	1.08	436	2.20E-08	0.273	NA

Notes: Colors correspond with model type: Orange for Cartesian, blue for tail up, and grey for non-spatial. NA indicates not applicable.

Table A2.7. (Cont.) Spatial models created from 2020 and 2021 data.

Explanatory Variable	Shape	VIF	AUC	False Positive	False Negative	Partial Sill	Range	Nugget	Sig of 1 st Variable	Sig of 2 nd Variable
1	Mariah	NA	97.21	7	9	1.10	6231	1.10E-08	NA	NA
Elevation + Faults	Exponential	1.13	97.21	9	6	1.07	414	6.99E-09	0.069	NA
Carbonates	Spherical	NA	97.19	10	6	0.99	191	2.30E-08	0.059	NA
Elevation + Carbonates	Mariah	1.13	97.19	8	6	1.21	6393	1.29E-08	0.091	0.418
Trees	Exponential	NA	97.17	8	8	1.04	440	1.45E-08	0.494	NA
Slope	Cauchy	NA	97.16	8	7	0.84	115	5.27E-02	0.579	NA
Drainage Area	Mariah	NA	97.15	4	12	1.76	7354	2.63E-08	0.562	NA
Aspect	LinearSill	NA	97.12	6	6	1.18	162	5.10E-09	0.340	NA
Trees	LinearSill	NA	97.11	9	6	1.18	162	3.49E-09	0.372	NA
Slope	Mariah	NA	97.10	8	10	1.10	6199	7.16E-09	0.906	NA
Upstream Distance + Carbonates	Cauchy	1.13	97.10	10	6	0.83	111	5.25E-02	0.088	NA
Metaseds	Spherical	NA	97.08	7	7	1.35	301	7.17E-08	0.582	NA
Upstream Distance	Spherical	NA	97.08	9	6	1.36	300	1.25E-08	0.205	NA
Upstream Distance + Faults	Cauchy	1.13	97.08	10	7	0.85	111	5.30E-02	0.120	NA
Slope	LinearSill	NA	97.05	7	7	1.20	162	3.54E-08	0.564	NA
Upstream Distance	Cauchy	NA	97.04	10	7	0.84	113	5.32E-02	0.043	NA
1	Exponential	NA	97.03	8	7	1.02	431	1.30E-08	NA	NA
Trees	Spherical	NA	97.01	8	7	1.34	302	2.74E-07	0.525	NA
Elevation + Carbonates	Cauchy	1.13	97.01	10	5	0.86	108	5.51E-02	0.018	NA
Loam	Spherical	NA	97.00	7	7	1.35	303	9.42E-08	0.747	NA
Faults	Spherical	NA	96.99	8	6	1.39	289	4.45E-07	0.169	NA
Carbonates	Spherical	NA	96.98	8	6	1.36	297	7.95E-08	0.134	NA
Carbonates	Exponential	NA	96.98	8	5	1.00	409	6.61E-09	0.119	NA
Elevation	Cauchy	NA	96.98	10	6	0.85	109	5.56E-02	0.006	NA
Elevation	Mariah	NA	96.97	8	6	1.16	6145	3.96E-08	0.056	NA
Aspect	Gaussian	NA	96.97	5	6	0.86	93	6.32E-02	0.138	NA
Silt Loam	Cauchy	NA	96.96	7	8	0.84	113	5.45E-02	0.315	NA
Slope	Exponential	NA	96.96	10	7	1.04	439	1.53E-08	0.747	NA
Metaseds	Gaussian	NA	96.95	8	6	0.88	94	6.20E-02	0.380	NA
Silt Loam	Mariah	NA	96.95	8	9	1.12	6377	1.31E-08	0.869	NA
Elevation	Spherical	NA	96.95	9	5	1.42	298	1.63E-07	0.072	NA

Notes: Colors correspond with model type: Orange for Cartesian, blue for tail up, and grey for non-spatial. NA indicates not applicable.

Table A2.7. (Cont.) Spatial models created from 2020 and 2021 data.

Explanatory Variable	Shape	VIF	AUC	False Positive	False Negative	Partial Sill	Range	Nugget	Sig of 1 st Variable	Sig of 2 nd Variable
1	Exponential	NA	96.94	9	5	1.04	441	1.14E-08	NA	NA
Slope	Exponential	NA	96.93	8	8	1.03	429	1.58E-08	0.794	NA
Elevation + Carbonates	Exponential	1.13	96.93	9	6	1.03	395	8.97E-09	0.081	0.298
1	LinearSill	NA	96.92	7	6	1.72	287	8.73E-03	NA	NA
Elevation + Faults	Cauchy	1.13	96.92	10	6	0.86	109	5.56E-02	0.023	NA
Trees	Gaussian	NA	96.90	9	6	0.87	95	6.25E-02	0.292	NA
Elevation + Faults	Spherical	1.13	96.89	9	5	1.42	298	1.28E-07	0.102	NA
Upstream Distance	Mariah	NA	96.88	7	6	1.14	6295	1.33E-08	0.156	NA
Slope	Spherical	NA	96.88	9	6	1.34	301	3.07E-08	0.720	NA
Carbonates	LinearSill	NA	96.86	9	7	0.95	112	1.06E-08	0.035	NA
Loam	Gaussian	NA	96.85	8	6	0.88	94	6.20E-02	0.646	NA
Silt Loam	Exponential	NA	96.78	8	8	1.04	428	1.72E-08	0.522	NA
Drainage Area	Exponential	NA	96.76	8	7	1.06	418	1.29E-08	0.114	NA
Faults	LinearSill	NA	96.73	6	6	2.36	422	1.60E-02	0.336	NA
1	Spherical	NA	96.71	8	6	1.34	298	2.95E-07	NA	NA
Elevation	Exponential	NA	96.65	9	5	1.02	390	2.17E-08	0.032	NA
Aspect	Epanech	NA	96.65	8	7	1.06	143	2.82E-08	0.244	NA
Drainage Area	Cauchy	NA	96.64	9	7	0.83	108	5.31E-02	0.047	NA
Upstream Distance	Exponential	NA	96.62	10	6	1.03	420	1.60E-08	0.155	NA
Carbonates	Gaussian	NA	96.59	10	5	0.85	89	6.50E-02	0.022	NA
Loam	Epanech	NA	96.56	9	7	1.21	171	2.24E-07	0.702	NA
1	Gaussian	NA	96.56	8	6	0.87	93	6.23E-02	NA	NA
1	Epanech	NA	96.55	9	7	1.21	170	7.72E-07	NA	NA
Metaseds	Epanech	NA	96.54	9	7	1.21	171	9.32E-08	0.477	NA
Faults + Drainage Area	Cauchy	1.13	96.54	7	8	0.84	110	5.39E-02	0.202	NA
Trees	Epanech	NA	96.51	10	7	1.21	172	2.02E-07	0.481	NA
Slope	Gaussian	NA	96.49	8	7	0.87	93	6.29E-02	0.587	NA
Faults	Gaussian	NA	96.48	9	6	0.87	88	6.48E-02	0.029	NA
Upstream Distance + Carbonates	Gaussian	1.13	96.47	10	6	0.86	89	6.35E-02	0.049	NA
Silt Loam	Gaussian	NA	96.42	8	6	0.87	91	6.57E-02	0.299	NA

Notes: Colors correspond with model type: Orange for Cartesian, blue for tail up, and grey for non-spatial. NA indicates not applicable.

Table A2.7. (Cont.) Spatial models created from 2020 and 2021 data.

Explanatory Variable	Shape	VIF	AUC	False Positive	False Negative	Partial Sill	Range	Nugget	Sig of 1 st Variable	Sig of 2 nd Variable
Elevation + Upstream Distance	Exponential	1.13	96.40	9	7	1.16	317	1.34E-08	0.046	NA
Drainage Area	LinearSill	NA	96.38	6	6	2.37	422	1.51E-02	0.315	NA
Slope	Spherical	NA	96.35	8	8	1.34	296	1.56E-07	0.761	NA
Faults	Epanech	NA	96.32	8	6	1.72	305	2.43E-02	0.215	NA
Elevation + Upstream Distance	Cauchy	1.13	96.28	11	5	0.99	100	7.55E-02	0.017	NA
Carbonates	Epanech	NA	96.26	9	6	1.66	297	2.35E-02	0.201	NA
Elevation + Upstream Distance	Spherical	1.13	96.25	12	5	1.27	166	9.87E-08	0.025	NA
Drainage Area	Spherical	NA	96.24	8	6	1.41	293	6.48E-08	0.143	NA
Colluvium	Exponential	NA	96.23	10	5	1.05	329	2.02E-08	0.242	NA
Elevation + Carbonates	Gaussian	1.13	96.23	10	5	0.88	86	6.72E-02	0.006	NA
Upstream Distance	Gaussian	NA	96.20	11	8	0.87	91	6.41E-02	0.016	NA
Elevation + Carbonates	Spherical	1.13	96.11	12	5	1.03	191	2.23E-08	0.046	0.248
Elevation	Gaussian	NA	96.11	10	6	0.87	88	6.79E-02	0.001	NA
Slope	Epanech	NA	96.08	9	8	1.23	171	2.02E-05	0.590	NA
Silt Loam	Epanech	NA	96.07	9	7	1.11	145	2.97E-08	0.375	NA
Upstream Distance	Spherical	NA	96.06	8	7	1.35	292	3.13E-07	0.205	NA
Colluvium	Cauchy	NA	95.97	6	7	0.88	79	6.20E-02	0.147	NA
Silt Loam	Spherical	NA	95.93	12	3	11.94	2395	4.49E-02	0.433	NA
Silt Loam	LinearSill	NA	95.92	8	7	1.24	160	6.01E-09	0.335	NA
Elevation	Spherical	NA	95.89	11	5	1.02	190	1.23E-08	0.013	NA
Elevation + Carbonates	LinearSill	1.13	95.87	10	5	1.98	273	9.83E-07	0.227	0.430
Upstream Distance + Faults	Gaussian	1.13	95.86	10	7	0.88	89	6.41E-02	0.093	NA
Upstream Distance	LinearSill	NA	95.85	10	6	1.23	162	4.42E-08	0.130	NA
Silt Loam	Spherical	NA	95.84	7	7	1.36	290	2.57E-07	0.510	NA
Colluvium	Epanech	NA	95.77	8	7	1.17	87	2.53E-06	0.179	NA

Notes: Colors correspond with model type: Orange for Cartesian, blue for tail up, and grey for non-spatial. NA indicates not applicable.

Table A2.7. (Cont.) Spatial models created from 2020 and 2021 data.

Explanatory Variable	Shape	VIF	AUC	False Positive	False Negative	Partial Sill	Range	Nugget	Sig of 1 st Variable	Sig of 2 nd Variable
Upstream Distance	Epanech	NA	95.74	11	7	1.06	140	2.93E-08	0.057	NA
Elevation + Faults	Gaussian	1.13	95.74	10	6	0.89	87	6.77E-02	0.012	NA
Faults + Drainage Area	Gaussian	1.13	95.68	9	7	0.90	88	6.54E-02	0.311	NA
Colluvium	Spherical	NA	95.64	8	7	1.18	123	4.68E-07	0.168	NA
Elevation	LinearSill	NA	95.60	9	6	1.91	273	2.07E-03	0.129	NA
Colluvium	Mariah	NA	95.59	9	7	1.12	3536	1.72E-08	0.326	NA
Colluvium	Exponential	NA	95.57	7	9	1.10	218	3.31E-08	0.184	NA
Elevation + Carbonates	Epanech	1.13	95.53	9	5	1.75	298	2.45E-02	0.188	0.400
Colluvium	LinearSill	NA	95.52	7	9	1.28	110	2.49E-01	0.313	NA
Elevation	Epanech	NA	95.52	11	6	1.07	133	2.20E-08	0.007	NA
Drainage Area	Epanech	NA	95.40	8	6	1.76	305	2.28E-02	0.194	NA
Slope	NULL	NA	84.15	0	83	1.01	NA	NA	0.857	NA
Elevation + Carbonates	NULL	1.13	78.62	15	36	1.10	NA	NA	0.000	0.037
Elevation	NULL	NA	77.80	19	38	1.02	NA	NA	0.000	NA
Drainage Area	NULL	NA	72.83	13	31	0.97	NA	NA	0.000	NA
Upstream Distance	NULL	NA	72.15	27	42	0.97	NA	NA	0.000	NA
Colluvium	NULL	NA	65.61	0	83	1.01	NA	NA	0.042	NA
Carbonates	NULL	NA	63.68	12	52	0.99	NA	NA	0.000	NA
Aspect	NULL	NA	57.75	13	71	1.01	NA	NA	0.007	NA
Trees	NULL	NA	57.60	9	64	1.01	NA	NA	0.003	NA
Metaseds	NULL	NA	52.61	0	83	1.01	NA	NA	0.031	NA
Silt Loam	NULL	NA	51.27	0	83	1.00	NA	NA	0.031	NA
Loam	NULL	NA	51.25	0	83	1.01	NA	NA	0.187	NA
Faults	NULL	NA	46.52	3	60	1.05	NA	NA	0.000	NA

Notes: Colors correspond with model type: Orange for Cartesian, blue for tail up, and grey for non-spatial. NA indicates not applicable.

Table A2.8. Summary of kriging models.

Data	Model Type	Count	AUC (as a percent)	Partial Sill*		Nugget*		Range (m)*			
				Mean	S Dev	Mean	S Dev	Mean	S Dev	Max	Min
2020	Cartesian	36	98.50	0.56	0.28	4.25E-09	6.56E-09	4137	1231	4826	1204
2020	Tail-up	74	98.83	0	0.00	2.60E-09	4.32E-09	7324	0	7324	7324
2020	Non-spatial	20	77.27	NA	NA	NA	NA	NA	NA	NA	NA
2021*	Cartesian	43	94.26	7.12	1.20	5.29E-02	4.71E-02	142	63	269	75
2021*	Tail Up	63	94.19	5.97	0.76	1.44E-02	1.51E-02	787	1332	3749	60
2021*	Non-spatial	9	56.43	NA	NA	NA	NA	NA	NA	NA	NA
MY	Cartesian	64	96.96	8.64	1.51	3.35E-02	2.97E-02	296	469	3089	79
MY	Tail Up	70	96.65	8.13	1.37	5.52E-03	3.02E-02	1447	2405	7354	87
MY	Non-spatial	13	63.99	NA	NA	NA	NA	NA	NA	NA	NA

*Empirical toregram revealed a pure nugget.

Appendix 3: How to Create a .ssn object using STARS

A3.1. Introduction

The Stream Statistical Network (SSN) package in R facilitates the production of torgegrams for a variety of studies. However, the SSN package requires the use of a .ssn (“dot s-s-n”) object that can’t be created in R; therefore, to use the SSN package, we create the .ssn object in ArcMap using The Spatial Tools for the Analysis of River Systems (STARS) toolbox. In creating this standard operating procedure, I hope to introduce new users (you) to the STARS toolbox by giving step-by-step instructions on the use of STARS (i.e., this SOP will leave you “starstruck”!). The instructions here come from my personal experience using STARS in the geology teaching computer lab at Idaho State University, though it is my hope that these tools can easily be applied to other computers in other labs.

A.3.2. Part 1: Software Requirements and Installation

Currently, STARS requires the following software before you begin working. If you don’t have administrative privileges on the computer that you’re using for this analysis, talk to your Internal Technical (IT) staff about ensuring that the following software configurations are available to you.

- A. ArcGIS version \geq 10.6 (not ArcGIS Online or ArcGIS Pro)
- B. Active “Advanced” license and “Spatial Analyst extension”
- C. Python version 2.7.14

- D. STARS version 2.0.7 geoprocessing toolbox for ArcGIS
- E. PythonWin build 221, 32 bit: must be downloaded and installed separately from Python.

As of 3 Feb 2022, all the computers in the ISU teaching computer lab already have A, B and C installed. To install D and E, follow the steps below. First, download the current release of STARS at https://www.fs.fed.us/rm/boise/AWAE/projects/SSN_STARS/software_data.html#SSN by clicking on the blue “STARS Current Release” button under the STARS header. After downloading and unzipping this file, assuming that Python is already installed, you can add it as a toolbox to the ArcToolbox menu via the following steps:

1. Right-click on the ArcToolbox folder at the top of the menu and select add toolbox.
2. In the pop-up menu, select the “connect to folder” icon that looks like a folder with a + sign.
3. To connect the STARS folder, navigate to the folder where STARS is located (e.g., “C:\software\stars_v2.0.7_2019\stars_v2.07”), click on the folder, then press OK.
4. To add the toolbox to Arc, repeat step 1, navigate to the connected folder where STARS is located, and select the STARS toolbox by clicking on the icon that looks like a red toolbox.
5. **Check your work:** If you have added the toolbox correctly, the STARS toolbox will now appear in the ArcToolbox menu. When you open the toolbox you will see three subtoolboxes: ‘Pre-processing’, ‘Calculate’, and ‘Export’.

Finally, you can download PythonWin at <http://sourceforge.net/projects/pywin32/files/pywin32/> from Build 221. Note that both Python and PythonWin need to be version 2.7 for 32 bit. Version 3 won't work and neither will 64 bit. You will need administrator access to install PythonWin, so if you don't have access, talk to your IT staff or the computer lab manager for help. As of 29 Jul 2022, ISU computer C8STATION17, C8STATION18, and the presenting computer at the front of the classroom are the only computers at ISU that have all of the required software downloaded.

A3.3. Part 2: Getting Started in ArcMap

To use STARS, you will need the following data for your site, examples of which are included in the zip file attached to this thesis.

1. DEM (GJDEM in the example)
2. Stream shapefile (StreamGJ_NeedsFixing and/or StreamGJ_Fixed in the example)
3. Observations shapefile (STICs in the example)
4. Attribute rasters or shapefiles that might be covariates that would explain variation in your data that shouldn't be explained by spatial autocorrelation (Colluv in the example, representing the surficial geology covered by colluvium, digitized from mapping by Rodgers and Othberg, 1999)

Start by moving the required data from the Catalog to the Table of Contents, ensuring that it is all in the same projection. If it is not, use the **'Project'** and **'Project Raster'** tools in the 'Projections and Transformations' subtoolbox in the Data Management

Tools toolbox. Next, create a file geodatabase that will become your default. To do this, right click under a folder in the catalog, hover the mouse over “New”, then select “Folder”. “File Geodatabase”. Then set the geoprocessing extent to appropriate values by going to the menu at the top, hovering over ‘Geoprocessing’, and clicking on ‘Environments’. When the Environment Settings pop-ups appear, do the following in any order:

1. If you have not already, set your desired default geodatabase by going to ‘Workspace’, and under ‘Current Workspace’, inputting the path to the geodatabase you created before.
2. Under ‘Processing Extent’, use the dropdown menu to make ‘Extent’ “Same as DEM”.
3. Under ‘M Values’, set ‘Output has M Values’ to “Disabled”.
4. Under ‘Z Values’, set ‘Output has Z Values’ to “Disabled”.

Once you’ve completed all four steps, click OK.

This is a good time to check that the Spatial Analyst extension is enabled. To do so, go to the menu at the top, hover over ‘Customize’ and click on ‘Extensions’. If there is not a checkmark next to ‘Spatial Analyst’, then click on the empty box next to it to toggle it to “enabled”.

Finally, create a folder in your home directory called “temp”. To do this in the catalog, right click under a folder, hover the mouse over “New”, then select “Folder”. We will use this folder in several of the STARS scripts for intermediate processing steps, so setting it up now is wise. Note that as we move forward, you will find that you can drag

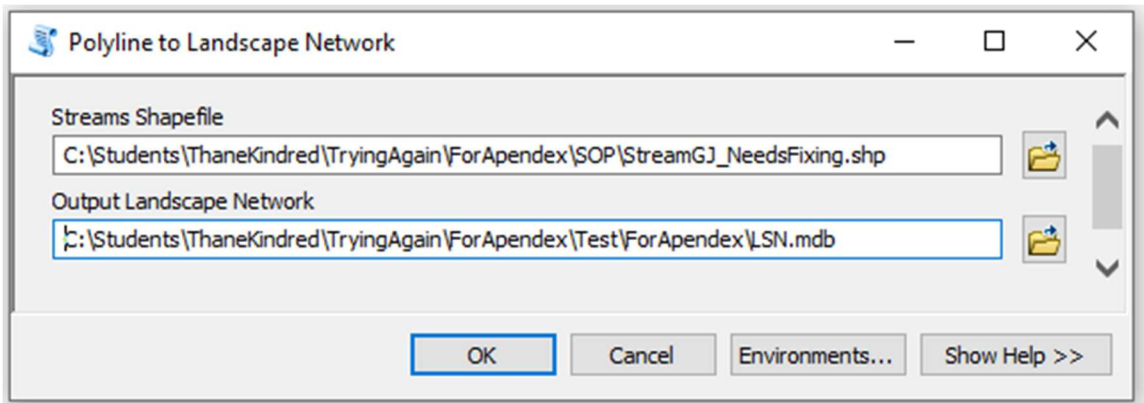
and drop some feature classes into a parameter field for some scripts in STARS, but not for all. If the drag and drop method doesn't work, don't panic. The icon next to the field with an arrow on it will allow you to navigate to the feature class so that you can still run the script.

A3.4. Part 3: Build a Landscape Network

Once you have the required software installed and configured properly, you need to create a LandScape Network (LSN). The LSN is a personal geodatabase that serves mostly as an organizational tool. You will store all the completed feature classes here before they go into your .ssn object so that they don't get mixed up in all the other feature classes you make. To create the LSN, follow these steps:

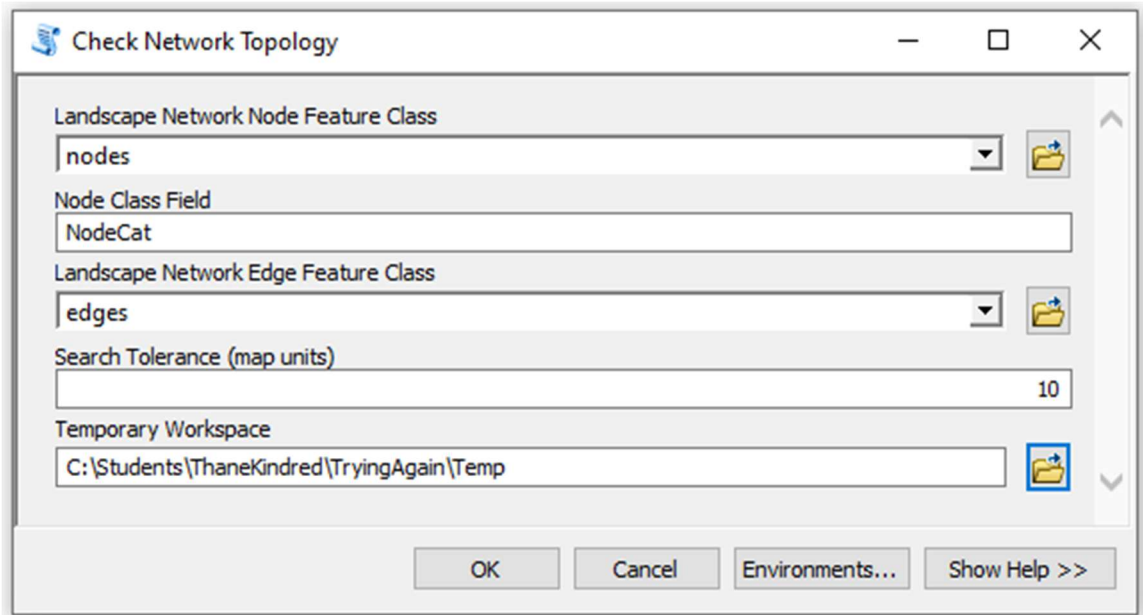
1. Ensure that your streams shapefile is in the correct format.
 - a. Each reach should be its own feature that starts at a source or confluence and ends at a confluence or outlet.
 - b. All features should point downstream. You can check this by changing the symbology of the feature class to "Arrow at End" and then visually examining each feature.
 - c. Each confluence should have three features meeting at a single point.
 - d. The sample data provided has six problems with it. If you're familiar with Arc, see if you can find and fix them now, but if you can't find all six problems, you can move on to the next step. The problems will become more obvious in step 3, so we can fix them at that point.
2. Select the '**Polyline to Landscape Network**' script from the 'Pre-processing' subtoolbox in the STARS toolbox and enter the parameters below. Make sure

that you include the “.shp” under ‘Streams Shapefile’ and the “.mdb” in ‘Output Landscape Network’.



Note that the Output Landscape Network does not need to exist before you run the script. This tool will create the following components with the LSN's newly generated geodatabase:

- a. Nodes (point feature class): a point at each source, outlet, and confluence in your stream network.
 - b. Edges (polyline feature class): a line connecting each of the nodes in your network.
 - c. A series of tables that allow quick analysis of topological relationships between edges, sites, and nodes.
 - i. Relationships (table)
 - ii. Noderelationships (table)
 - iii. Nodexy (table)
3. Add the nodes and edges feature classes (a and b created above in part 2) to your display and then run the ‘**Check Network Topology**’ script in the ‘Pre-processing’ subtoolbox in the STARS toolbox.



Note that for this tool to run, the folder under “Temporary Workspace” needs to be empty. If the tool fails in less than 0.10 seconds, you probably don’t have PythonWin installed correctly. This tool creates a new field in the nodes attribute table called NodeCat that will identify each node as one of the following node types:

- a. Source: this is the top of a tributary. These are good. You should have lots of them in any complex network.
- b. Outlet: this is the bottom of your network. You should only have one of these per stream system in your network. In the example data, you should only have one outlet.
- c. Converging stream: this is where two tributaries meet, but they do not flow into a downstream edge. These will cause problems later on and we’ll learn how to deal with them.

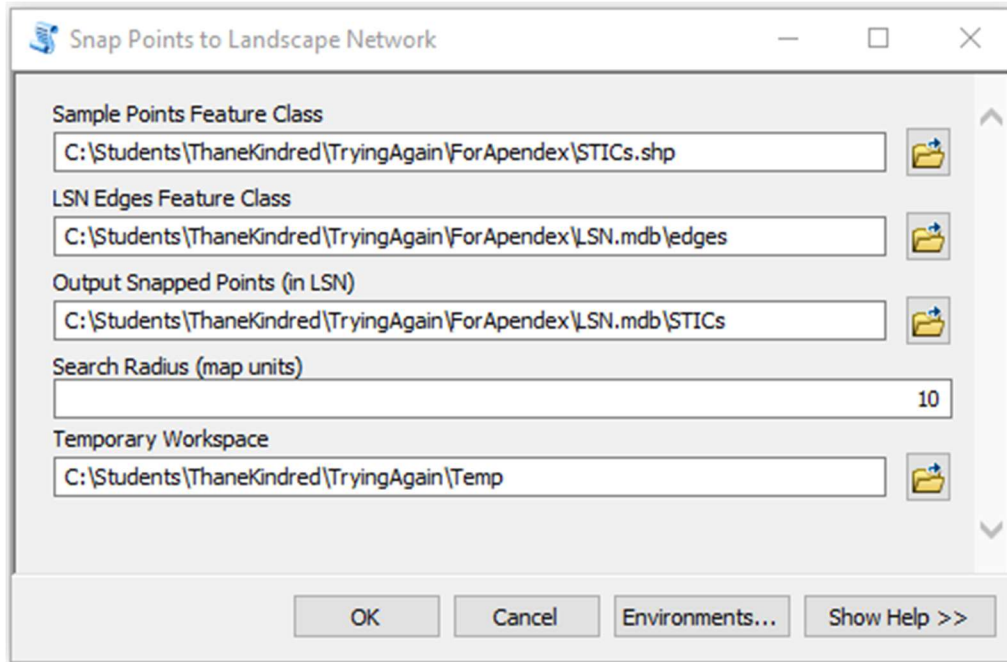
- d. Pseudo: this is where an upstream and downstream edge meet, but it is not classified as a confluence. These will cause problems later on and we'll learn how to deal with them.
 - e. Confluence nodes: this is where two tributaries meet and flow into a downstream edge. These are good! You should have lots of them in any complex network!
 - f. Downstream divergence: this is where one upstream edge flows into two downstream edges. These will cause problems later on and we'll learn how to deal with them.
4. **Check your work:** If you have done everything correctly, the nodes at the top of the tributary will be identified as sources, the nodes at confluences will be identified as confluences, and the node at the bottom of the tributary will be identified as an outlet in the NodeCat field. If you have any other type of node or any of the nodes are identified incorrectly, delete the LSN and start at the beginning of this part. You'll need to correct the original stream feature class to ensure that none of the problematic nodes described above are present in your stream network. This usually involves editing the features to add or remove nodes.
- a. Note that to edit the original stream feature class in ArcMap, you will need to right click on the feature class in the table of contents, hover over "Edit Features" and click "Start Editing". Once you begin editing, you have four tools that will help you fix the streams feature class:

- b. To flip reaches that are facing the wrong direction go to the original stream layer, highlight the reach that's problematic, then right-click on reach and click edit vertices. Then highlight "modify sketch vertices", right-click on the segment and click flip. Then save your edits.
- c. If a reach erroneously doesn't connect to others, click on the erroneously unconnected reach and select "edit vertices" from the edit toolbar. Then pull the reaches end to match the top of the downstream segment. It is often wise to remove all other points from the map when doing this so that vertices snap to the end of the feature, rather than to other points. These should be all connected now, so save your edits.
- d. You can combine polyline features together by selecting the features you want to combine, hovering over the 'Editor' dropdown on the Editor Toolbar and selecting 'Merge'.
- e. Conversely, you can split a polyline feature by selecting the 'Split Tool' from the Editor Toolbar and clicking where you want to make the split.
- f. Sometimes recreating lsn.mdb is quite finicky, requiring deleting the lsn.mdb from before the network was fixed and/or restarting Arc altogether with a new map.

A3.5. Part 4: Incorporating points in the LSN

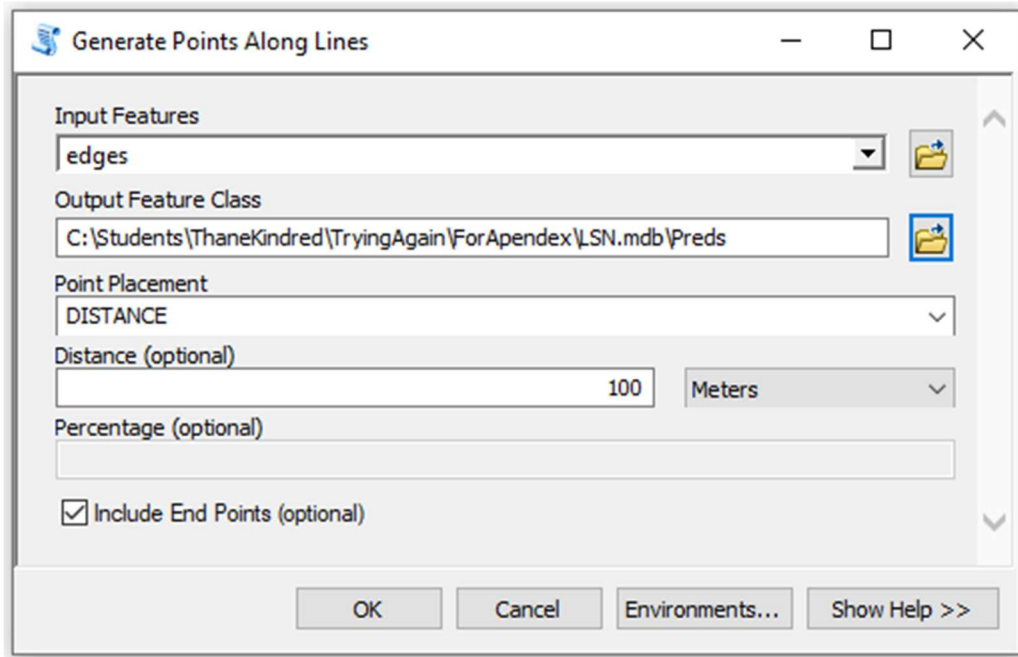
Next, you need to add at least two point-feature classes to the .ssn: the observation sites and the prediction points. Every point in these feature classes must fall EXACTLY on the edges line you created in Part 2. To ensure that the points fall on the edges line, we can use the '**Snap Points to Landscape Network**' script in the 'Pre-

processing' subtoolbox in the STARS toolbox using the parameters shown below.



Note that the input “Sample Points Feature Class” needs to be a shapefile (i.e., not in a gdb). You should specify the output in your LSN personal geodatabase: in this example “C:\Students\ThaneKindred\TryingAgain\forApendex\LSN.mdb”.

When creating prediction points you have several options, but I found one of those options was the most reliable. Theoretically, you could create them using the **‘Create Prediction Points’** script in the ‘Pre-processing’ subtoolbox in the STARS toolbox, however that script never worked when I tried to run it. Alternatively, you could use the **‘Feature to Points’** tool in the ‘Features’ subtoolbox in the Data Analysis Tools toolbox to create a point for every reach. Then you could snap those points to the LSN edges using the **‘Snap Points to Landscape Network’** described above. Instead, I chose to use the **‘Generate Points Along Lines’** script in the ‘Sampling’ subtoolbox in the Data Management Tools toolbox.

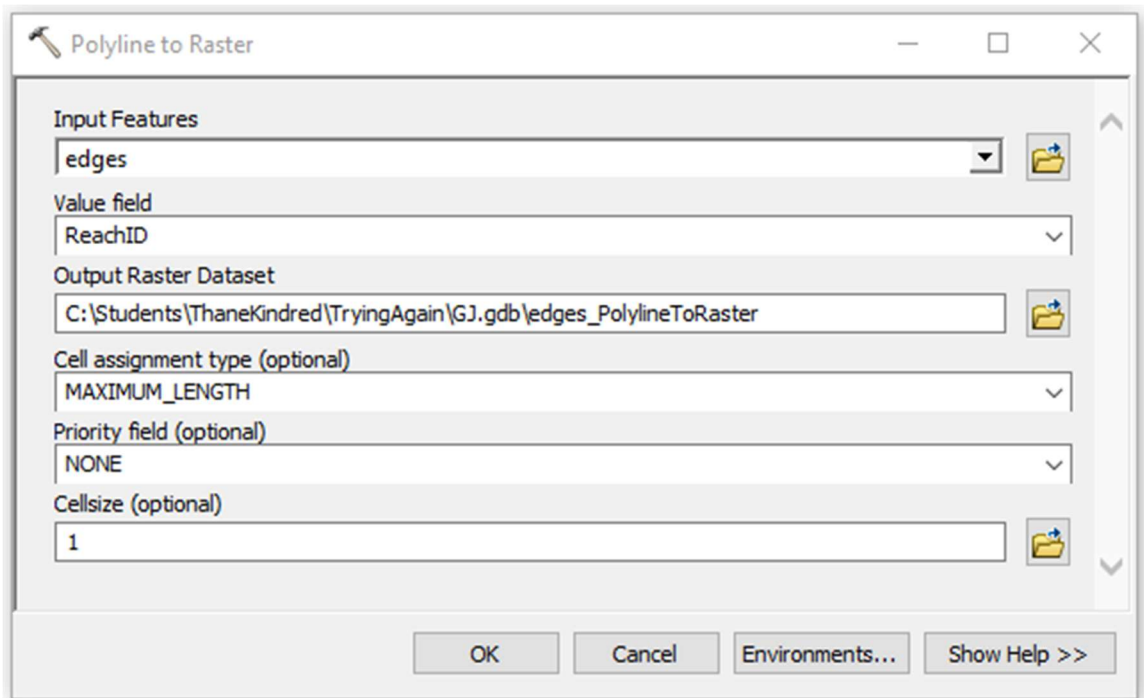


Quick note that if you want predictions more closely spaced (e.g., for this thesis, we used 12.5m), then you'll want to change the numeric distance entry accordingly. Smaller numbers will increase run time for the rest of this tutorial and in R. When you finish this part, you will have at least four feature classes in your LSN: edges, nodes, observations (called "STICs" in the example), and prediction points (called "Preds" in the example).

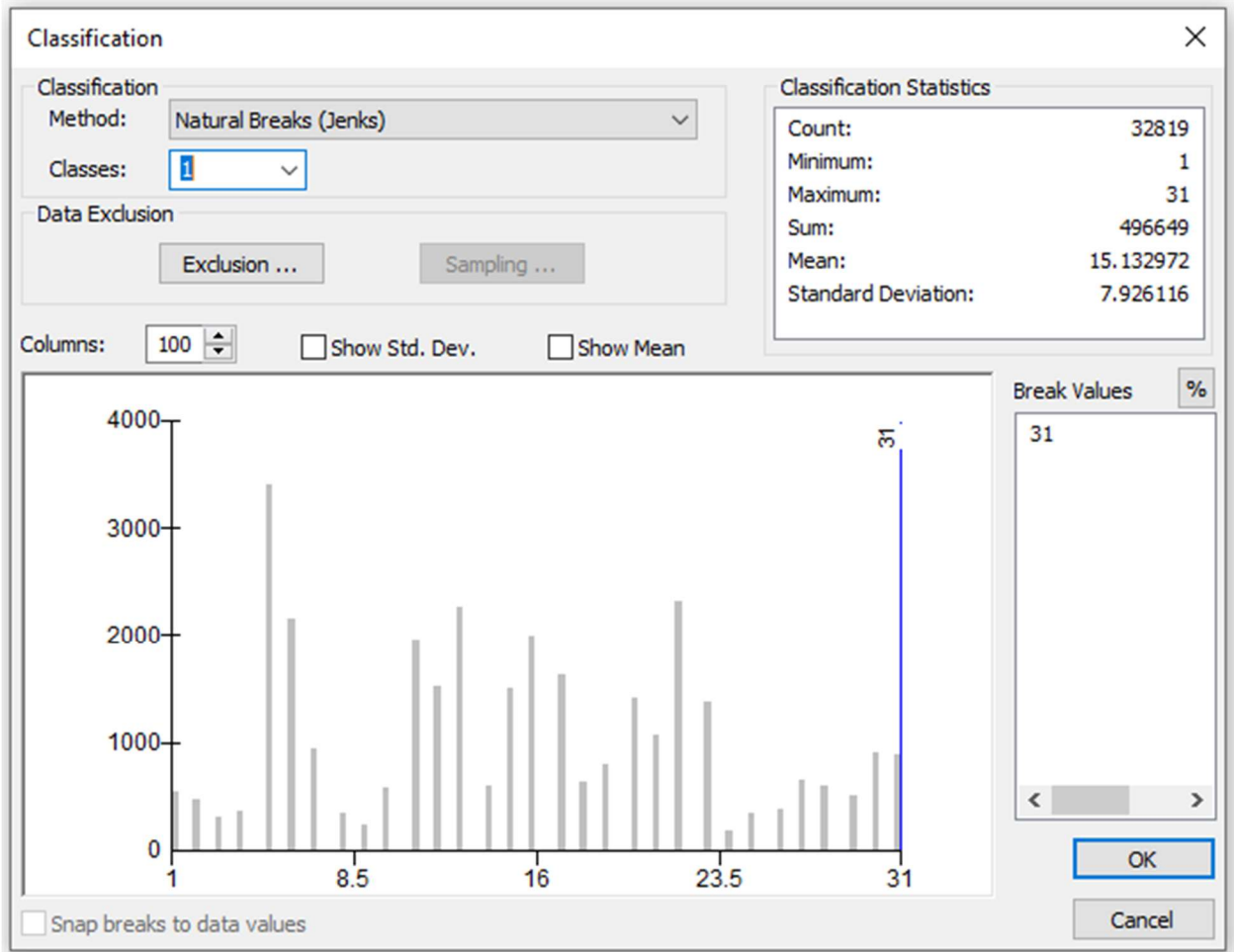
A3.6. Part 5: Creating Reach Contributing Areas

I think of the Reach Contributing Areas (RCAs) as a drainage area for each stream reach, or edge in the LSN. Each RCA corresponds to one edge and represents the area of the basin that contributes via overland flow directly to that edge ([Theobald et al., 2005](#)). We create the RCAs in a way that's similar to how you would create drainage areas using the **'Watershed'** tool in the 'Hydrology' subtoolbox in the Spatial Analyst Tools toolbox.

1. We need to relate the RCAs to the edges using one of the fields in the edges attribute table. The OBJECTID and the rid fields may change as you manipulate the LSN, so we will create another field called ReachID of type 'Short Integer'. Use the field calculator to make ReachID = OBJECTID.
2. Convert the edges feature class to a raster using the '**Polyline to Raster**' tool in the 'To Raster' subtoolbox in the Conversion Tools toolbox.

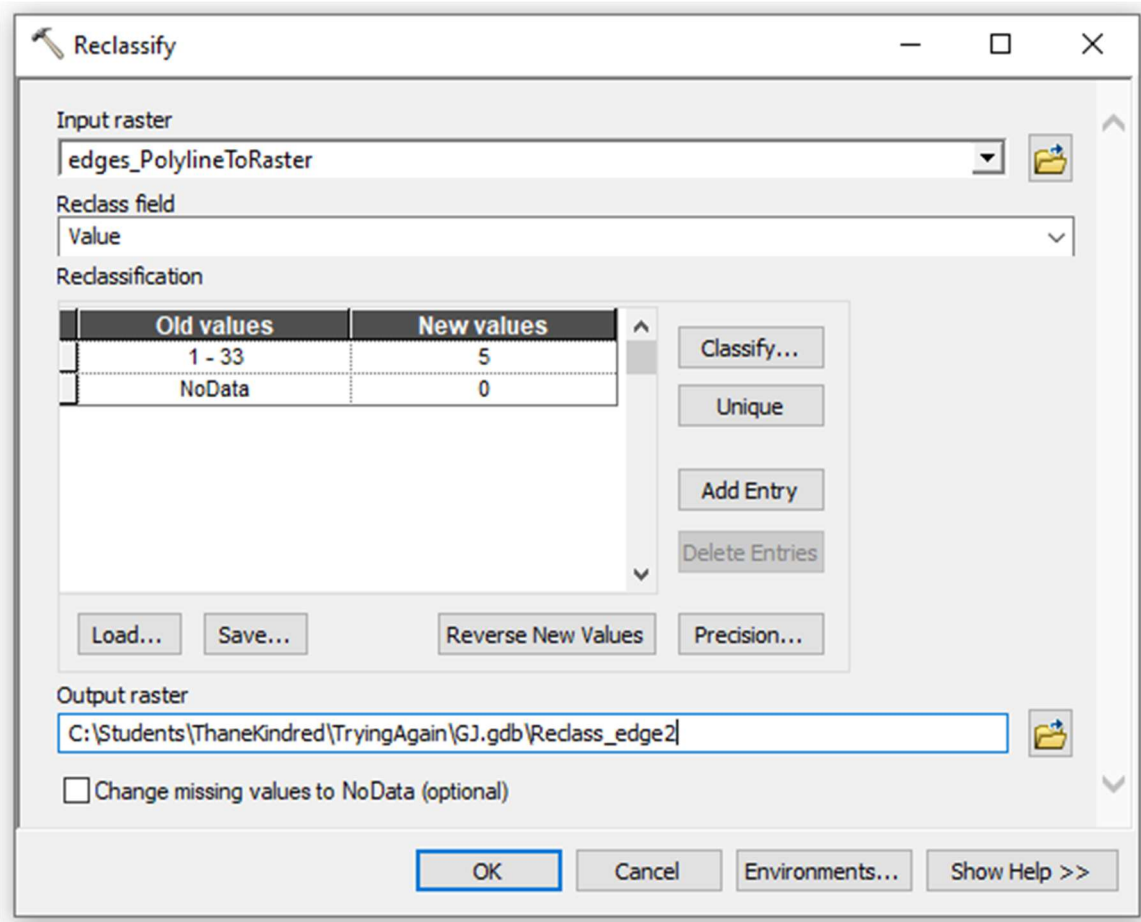


3. Now reclassify the newly created "edges_PolylineToRaster" raster using the '**Reclassify**' tool in the 'Reclass' subtoolbox in the Spatial Analyst Tools toolbox. Leave the reclass field as "Value" to identify between stream and not-stream. Start by clicking "classify" in the Reclassify Window: set the number of classes to 1 and then click OK.



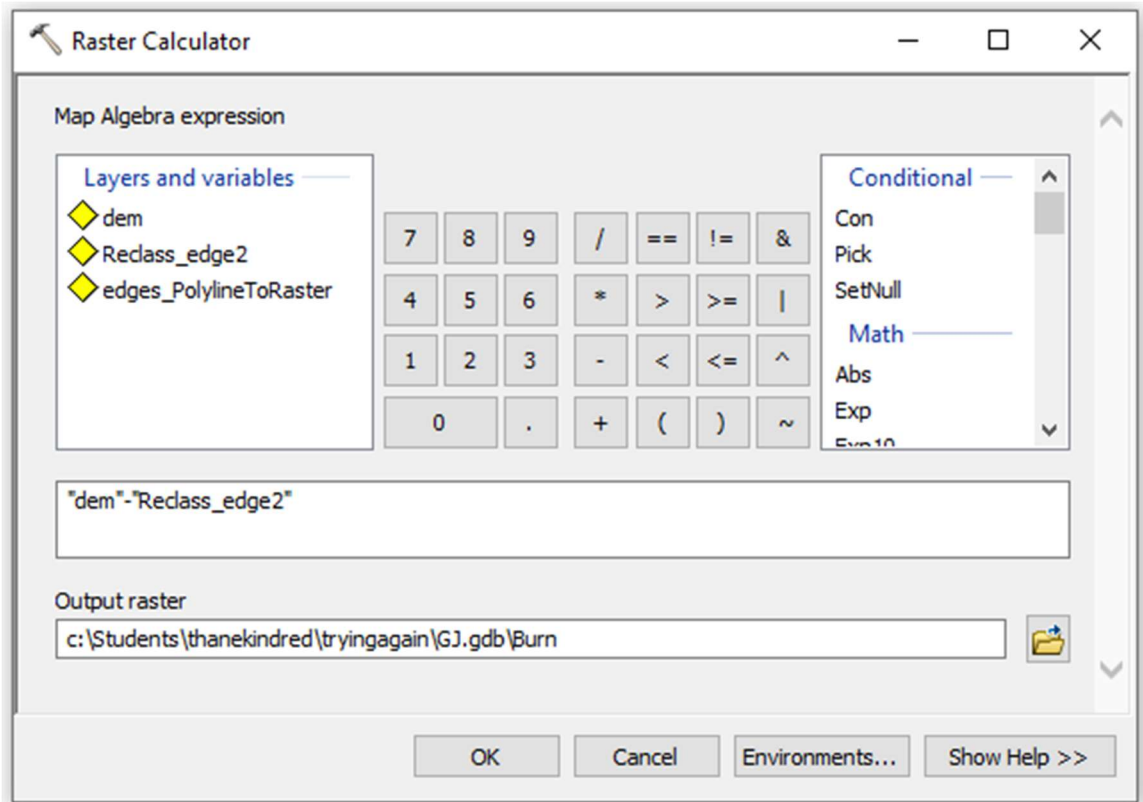
Then set new values to 5 for all edge values EXCEPT classify "No data" as 0 in

the window and click OK.



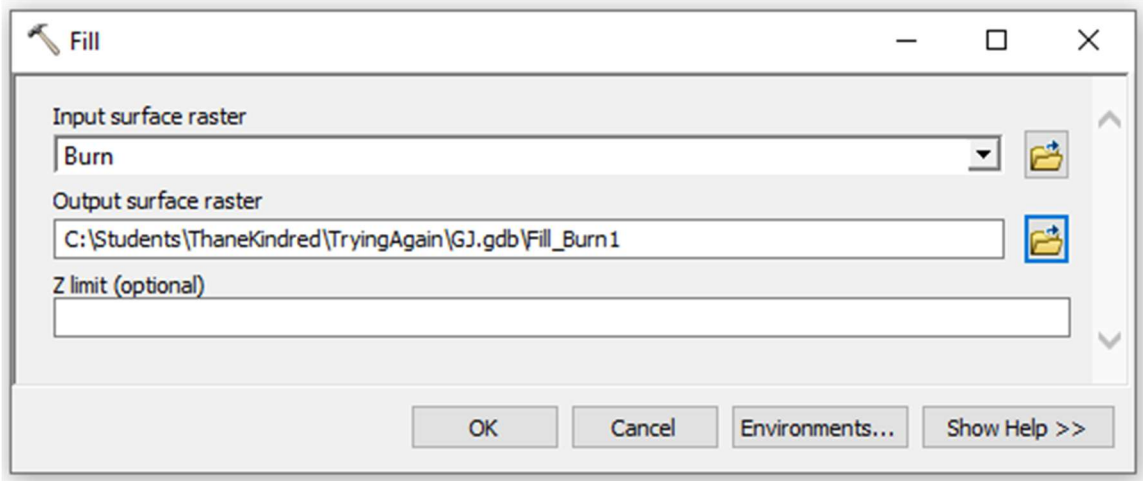
4. Convert any non-stream waterbodies (e.g., ponds, lakes, etc.) to a raster using the **'Polygon to Raster'** tool in the 'To Raster' subtoolbox in the Conversion Tools toolbox. It doesn't matter what value the waterbodies raster has as long as it is a numeric value because it will be overwritten in a later step. Note that in the example data, we can skip this step because we do not have major non-stream water bodies in Gibson Jack.
5. To ensure that our streams are recognized in future steps, we will "burn" the stream into our DEM. We do this using the **'Raster Calculator'** tool in the 'Map Algebra' subtoolbox in the Spatial Analyst Tools toolbox where we will type the

formula: "dem" - "Reclass_edge2"

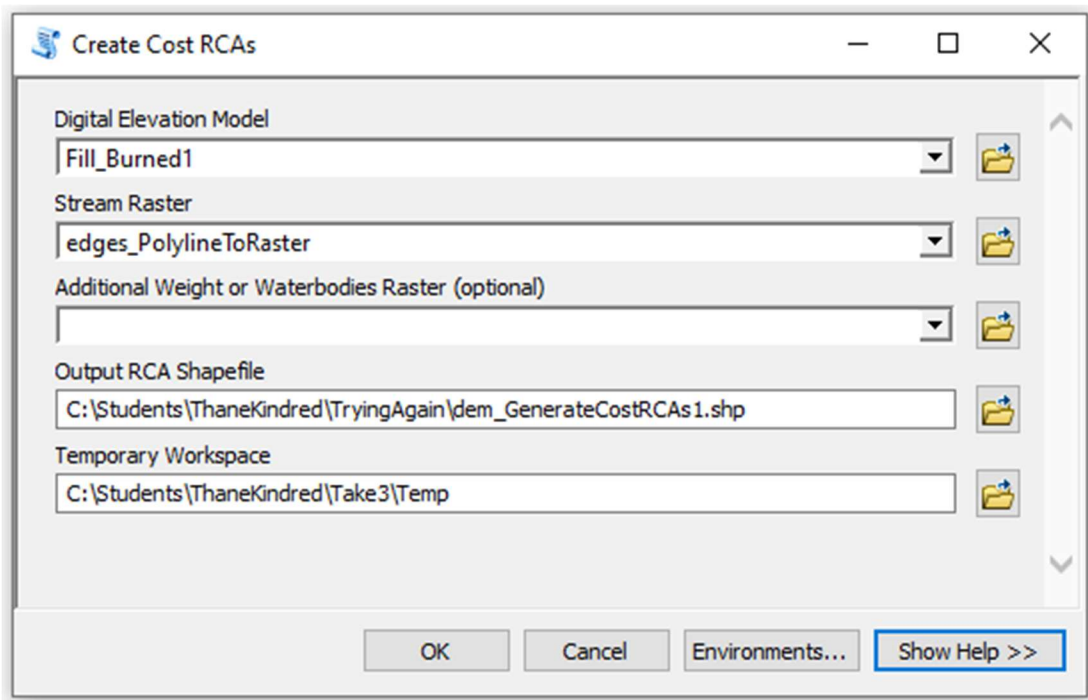


6. **Check your work:** At this point you should have a raster of only the stream network as defined by your edges feature class, a raster containing all non-stream waterbodies in the watershed if applicable, and a DEM of your watershed that has the stream network “burned” into it. Ensure that you have these rasters before moving on to step 7.
7. Next, we will “fill” our burned-in DEM to ensure all “water” flows out of our drainage area. To do this, use the ‘Fill’ tool in the ‘Hydrology’ subtoolbox in the Spatial Analyst Tools toolbox and ensure that the burned-in DEM is used as input

and the output raster is placed outside of the LSN folder.



8. Finally, we will create the RCAs using the **'Create Cost RCAs'** script in the 'Pre-processing' subtoolbox in the STARS toolbox.



Critically, the 'Digital Elevation Model' in this tool is the filled DEM that you created in step 7 and the 'Stream Raster' used in this tool is the original raster you made in step 2, not the reclassified raster you made in step 3. You will add

your waterbodies raster here if you have one. In the example, we do not, so we leave it blank. This tool will take a while to run, so now is a good time to take a break and give your significant other a kiss if they're nearby.

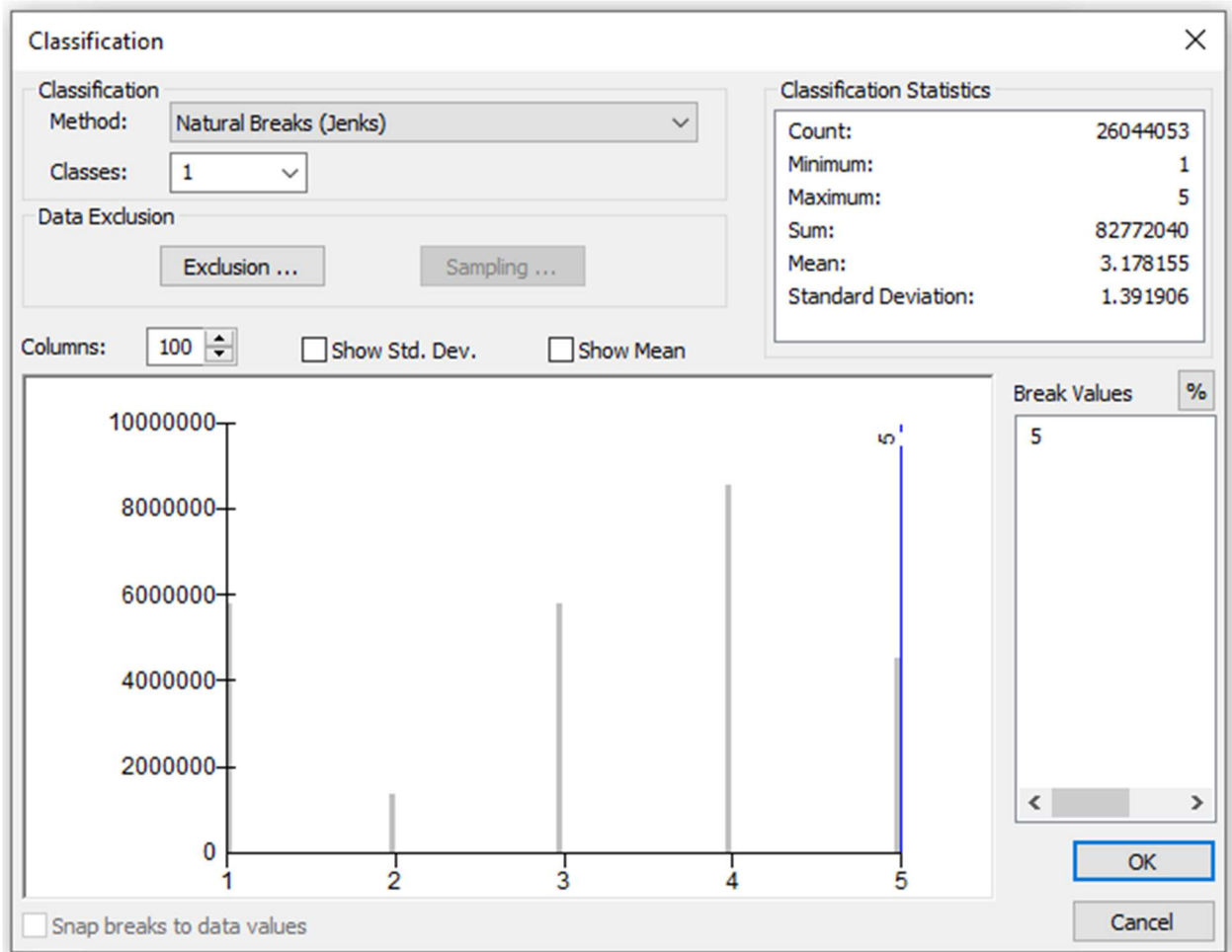
- a. If the script runs to completion, you will get a polygon shapefile of the RCAs. However, I found that sometimes this script struggles to finish running. If that happens, open your 'Temp' folder and look for a subfolder that starts with RCA. You should find a raster called rca_ras. This is a raster version of the shapefile that this script creates and you can often add it directly to the map even if the tool appears to fail. If you use this workaround, skip to step 11 as the polygon dissolution step is already completed.
9. If you open the attribute table for your newly created RCA shapefile, you will see that it has more rows than visible shapes. This is because the shapefile contains duplicates. Run the '**Dissolve**' tool in the 'Generalization' subtoolbox in the Data Management Tools toolbox to remove duplicate rows. Note that you will select 'gridcode' as the field to dissolve.
10. Convert the RCA shapefile to a raster using the '**Polygon to Raster**' tool in the 'To Raster' subtoolbox in the Conversion Tools toolbox.
11. **Check your work:** at this point you should have a raster containing all the RCAs in the basin. Ensure that the values of the raster visually align with the edges they correspond to (Figure A3.1). Specifically, look for edges that appear to have more than one RCA as this likely means that you missed a pseudonode in part 3.

A3.7. Part 6: Calculating Watershed Attributes

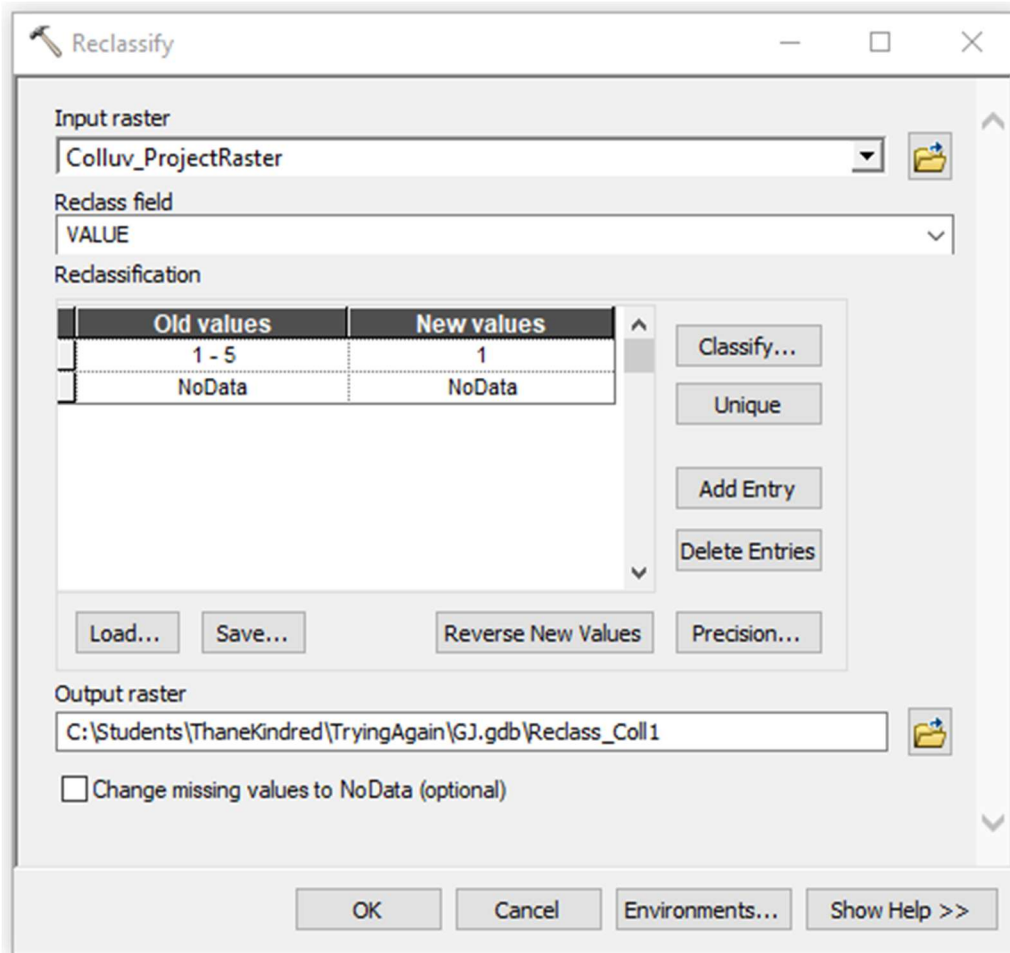
To create an accurate model, you may need to include explanatory variables to achieve stationarity before calculating the toregogram (Zimmerman and Ver Hoef, 2017). To do this, you need to have the explanatory variables in a column of the attribute table within your observation feature class. The easiest way to include these explanatory variables is to enter the correct corresponding value at each point. You can do this at least four ways, and the first three are fairly straightforward: 1) enter the data manually if it comes from your field notes, 2) use a **join** and the field calculator if the data is in another table, or 3) use the the **'Extract MultiValues to Points'** tool in the 'Extraction' subtoolbox in the Spatial Analyst Tools toolbox if the data is in a raster. In this SOP, I will explain the 4th way, which is to calculate the area-weighted value for each point and explanatory variable because that method requires the STARS toolbox and is more complicated than the other methods I've mentioned. This process starts by calculating attributes for the RCAs that we created in Part 5 and storing them in the edges feature class. Then we will calculate the attributes for each point in our observation and prediction feature classes.

1. Before we start, isolate the polygons with attributes of interest and export them as their own feature class. In the example, I took a shapefile containing all geologic units in Gibson Jack and exported only those that I classified as colluvium to a shapefile called 'colluvium'. Repeat this for each attribute you are interested in.
2. Next we will create a raster from a shapefile. In the example data provided with this SOP, you will find Colluv.shp. Use the **'Polygon to Raster'** tool in the 'To Raster' subtoolbox in the Conversion Tools toolbox.

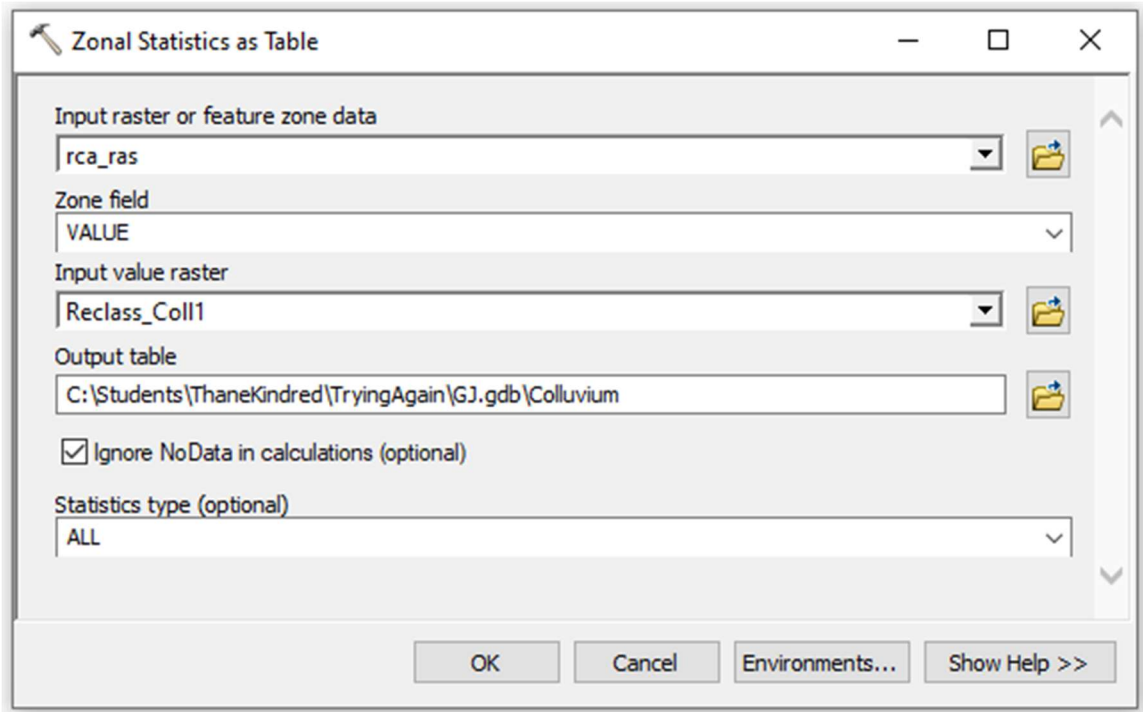
3. Reclass the newly created raster using the **'Reclassify'** tool in the 'Reclass' subtoolbox in the Spatial Analyst Tools toolbox. As above, start by clicking classify in the Reclassify Window and then set the number of classes to 1 then click OK.



Next, set new values to 1 in the Reclassification window and click OK.

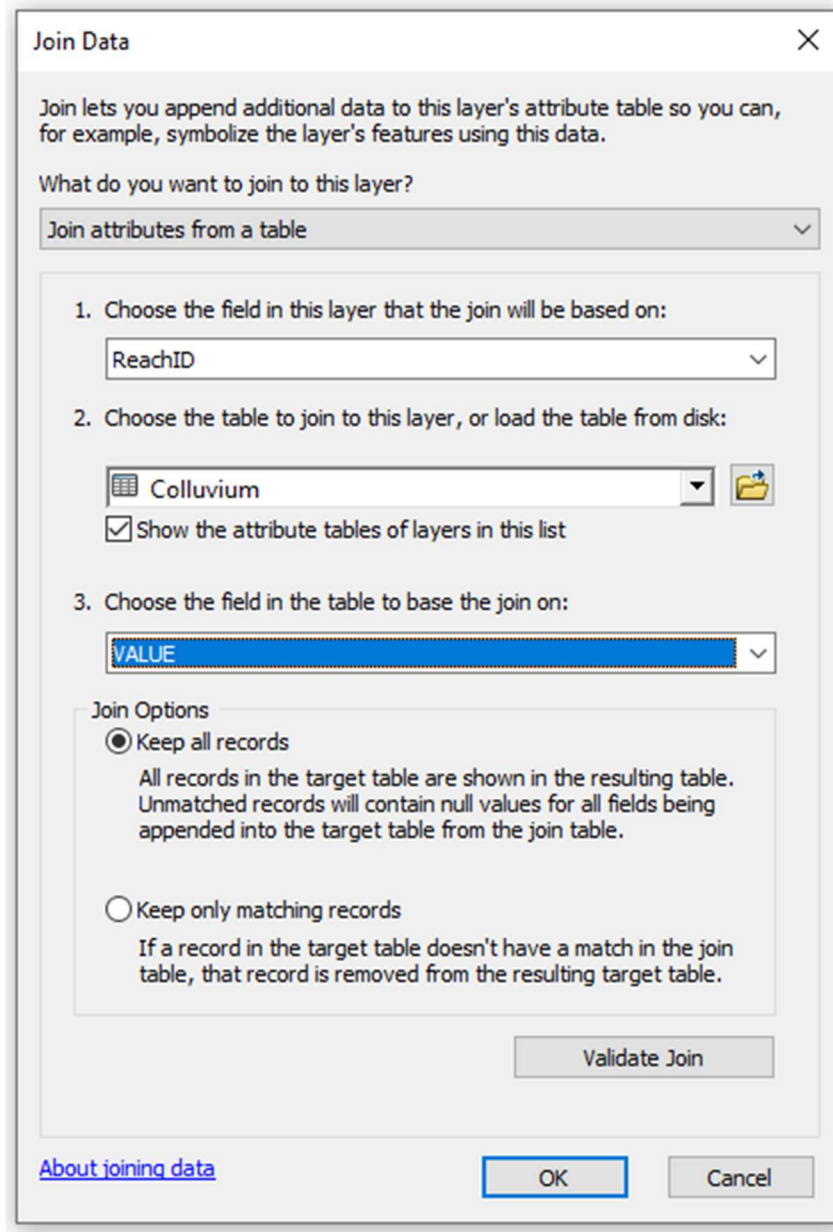


4. Then to help determine the area-weighted value, calculate the amount of area in the variable in each RCA using the **'Zonal Statistics as Table'** tool in the 'Zonal' subtoolbox in the Spatial Analysis Tools toolbox. This will create a dbf table.



Critically, the 'Input raster of feature zone data' asks for the RCA raster created in part 5 (above), not the attribute raster created in this part.

5. You can now add the RCA attribute to the edges attribute table using these steps:
 - a. Join the .dbf table created in step 3 to the edges attribute table. You will find **Join** by right-clicking on edges hovering over 'Joins and Relates', and selecting 'Join'.

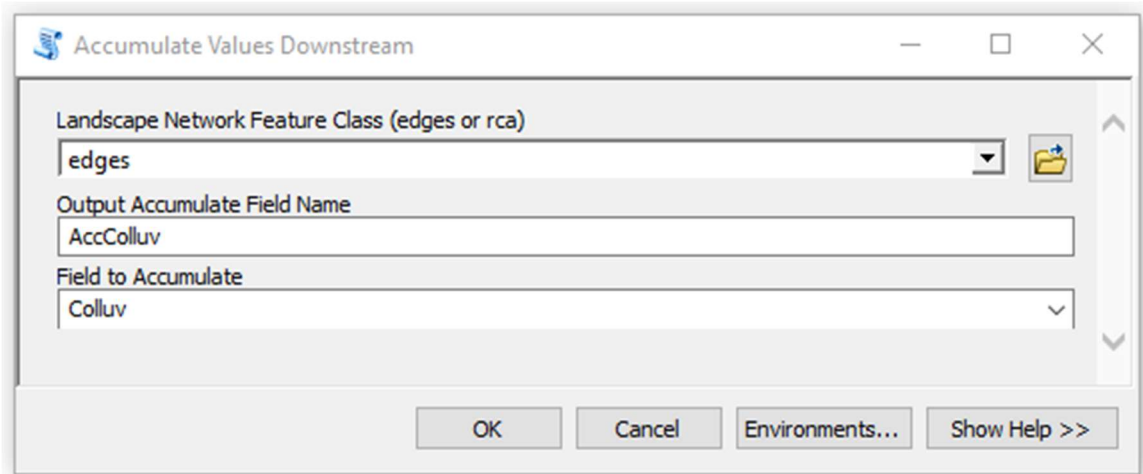


i.

- b. Create a new field in the edges attribute table. Give the field a short name that makes sense to you. For example, I chose to call the colluvium field Colluv. Short names are preferable because when we move feature classes to R all longer names will be shortened. This can be a problem if you have several names with similar starting characters. Be sure to change the type of field to double.

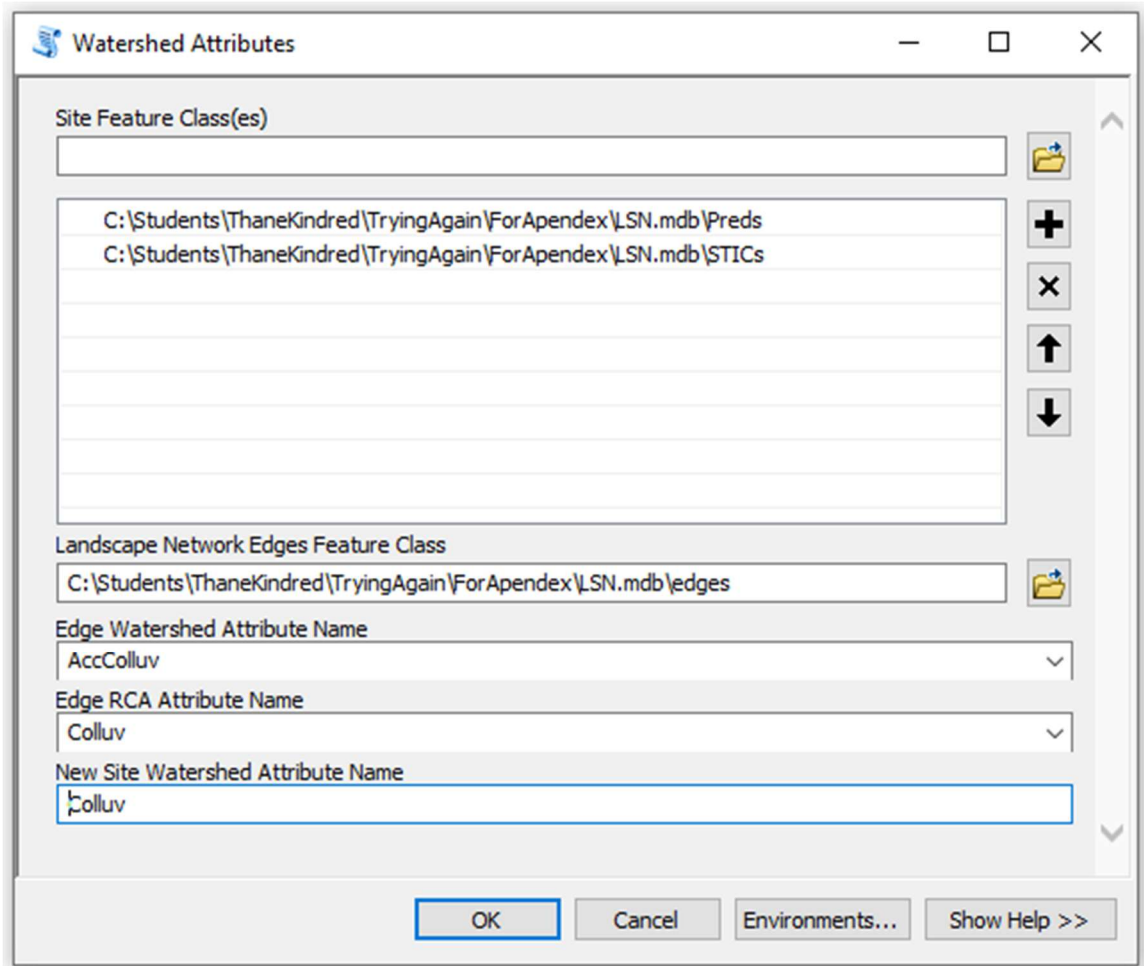
- c. Calculate the field you just made as equal to the dbf table's field 'Area'.
The formula will look something like this: `edges.Colluv = [Colluvium.Area]`.
Note the area units you are using. In this example, `Colluv.Area` is calculated in m^2 . (Check the projection early because this is calculated in terms of projected units, so projection decisions matter.) If you want km^2 , then add `"*0.000001"` to the end of the equation shown in this step.
 - d. Remove the join by right-clicking on edges, then hover over 'Joins and Relates', then hover over 'Remove Join(s)' and finally select 'Remove All Joins'.
6. Manually change all Null values in the newly created field to 0. Recall that in ArcMap you need to start an edit session before you can change values in the attribute table. Remember to end the edit session and save your edits when you are done.
 7. The values you calculated in step 4 show the area within each RCA. To account for the fact that downstream RCAs are affected by upstream RCAs we will use the '**Accumulate Values Downstream**' script in the 'Calculate' subtoolbox in the STARS toolbox. I like to give this field a name like 'AccColluv', but choose a short

name that makes sense to you.



8. **Check your work:** At this point, you should have two fields in the edges attribute table with the name of your variable. The first will indicate the area within the RCA underlain by that variable. The second will be a number equal to, or larger than the first indicating the area of interest in that edge plus the area of interest in every RCA above it.
9. Calculate the appropriate value for each point in the LSN using the **'Watershed Attributes'** script in the 'Calculate' subtoolbox in the STARS toolbox. It is best to do this for all point feature classes at once to ensure that they all call the variable by the same name. Note that the 'Edge Watershed Attribute Name' input asks for the accumulated value you calculated in step 6, while the 'Edge RCA Attribute Name' asks for the field you calculated in step 4. In the example below I used the same name for the 'New Site Watershed Attribute Name' and the 'Edge RCA Attribute Name'. You do not have to follow my example if different names make

more sense to you.



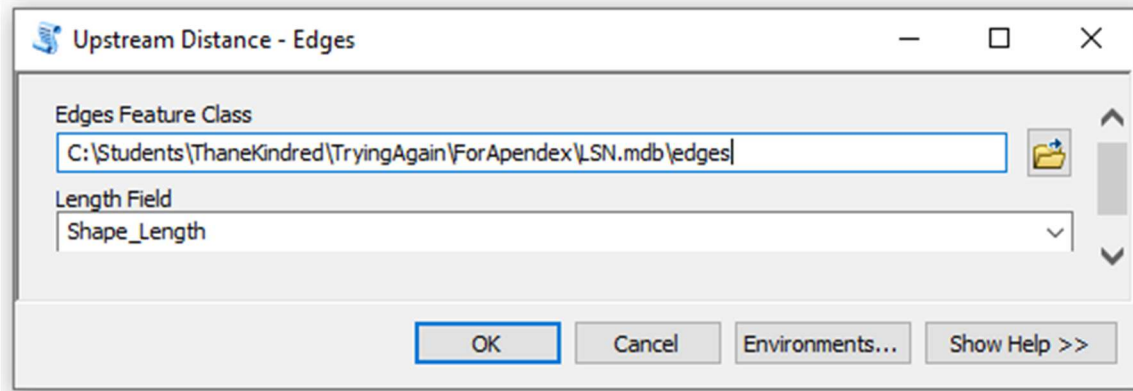
10. **Check your work:** Each of your point feature classes should have a field indicating the area of interest within the drainage area of that point.
11. Repeat this part (starting with step 4) to calculate RCA area, accumulate RCA area downstream, and then calculate RCA for each point. Note that when you run the **'Zonal Statistics as Table'** the 'Input Value Raster' input will match the 'Input raster or feature zone data'. This shouldn't give you problems. When you are done, you should have drainage area calculated for every point and both RCA area and drainage area calculated for every edge.

- a. Note: You may calculate Drainage Area using the Watershed tool in the 'Hydrology' subtoolbox in the Spatial Analyst Tools toolbox, but I did not. I used the above method to calculate the drainage area.
12. If you want to calculate the percent of the drainage area rather than the area within a drainage area, create a new field in each point feature class with a name that makes sense to you. I chose PerColluv as shorthand for 'percentage colluvium', but any name will work. Make the new field of type 'Double'. Then calculate the field as $[\text{Area of Interest}] / [\text{DrainageArea}]$. For example: $[\text{Colluv}] / [\text{DrainageArea}]$.
 13. You will repeat this part for each RCA attribute you want to add to your edges, observation, and prediction feature classes. For example, in Gibson Jack, I calculated attributes for colluvium, carbonates, and metasedimentary rocks. Each time I used these instructions for each attribute.

A3.8. Part 7: Calculating Spatial Variables

To finalize the feature classes that will go into our .ssn object, we need to calculate three more variables that are needed for the calculations in the SSN package: upstream distance (sometimes written as upDist for short), segment Proportional Influence (segment PI), and Additive Function Value (AFV).

Upstream distance is the distance upstream from the outlet. We first calculate this value for edge using the '**Upstream Distance - Edges**' script in the 'Calculate' subtoolbox in the STARS toolbox inputting these parameters.

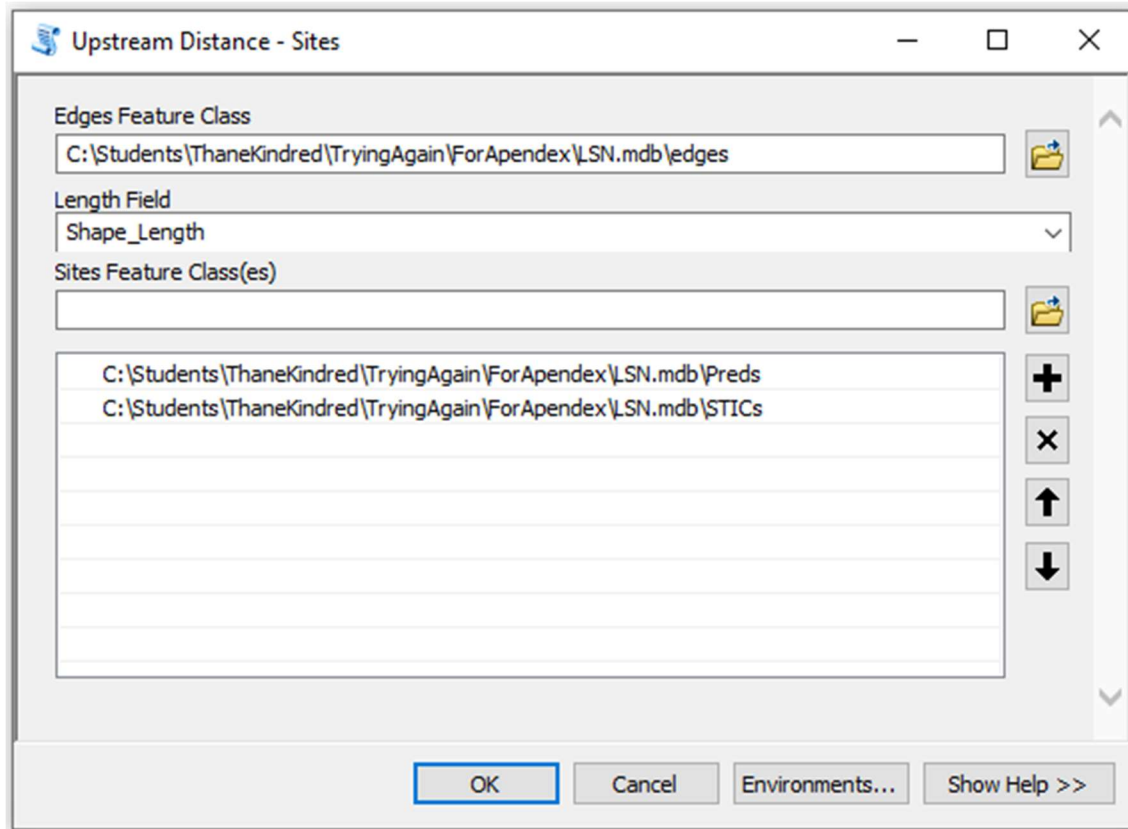


No

te that your edges attribute table probably has several fields labeled “Shape_Len”, “Shape_Le_1”, or “LengthKM”. I think these values were created when you created the LSN. To be safe, I always used the “Shape_Length” field as instructed by the STARS tutorial (Peterson, 2019).

Once we have calculated upstream distance for the edges, we can calculate upstream distance for the points. We will use the ‘**Upstream Distance - Sites**’ script in

the 'Calculate' subtoolbox in the STARS toolbox with the following parameters.

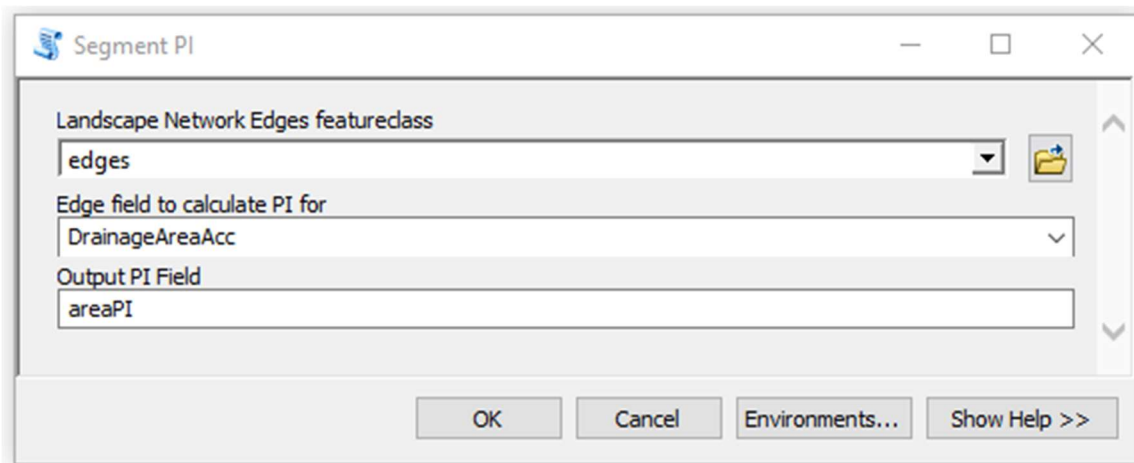


Check your work: After calculating upstream distance for both edges and sites, you should have a field in the edges, observation (STICs), and prediction (Preds) attribute tables called upDist. This number should be larger as you move to edges and points located further upstream.

Calculating segment PI is the first step in calculating the spatial weights needed in a spatial model. The segment PI indicates the relative weight that a tributary has on the stream it feeds into. Mathematically it is calculated as

$$1. \quad \Omega = \frac{W_A}{(W_A + W_B)}$$

Where Ω is the PI at a confluence node and W_A and W_B are accumulated RCAs from the two tributaries that feed into the confluence node (Figure A3.2). Note that we calculate segment PI at every confluence node for each edge that flows into the node. We will perform these calculations using the **'Segment PI'** script in the 'Calculate' subtoolbox in the STARS toolbox. Input the following parameters:

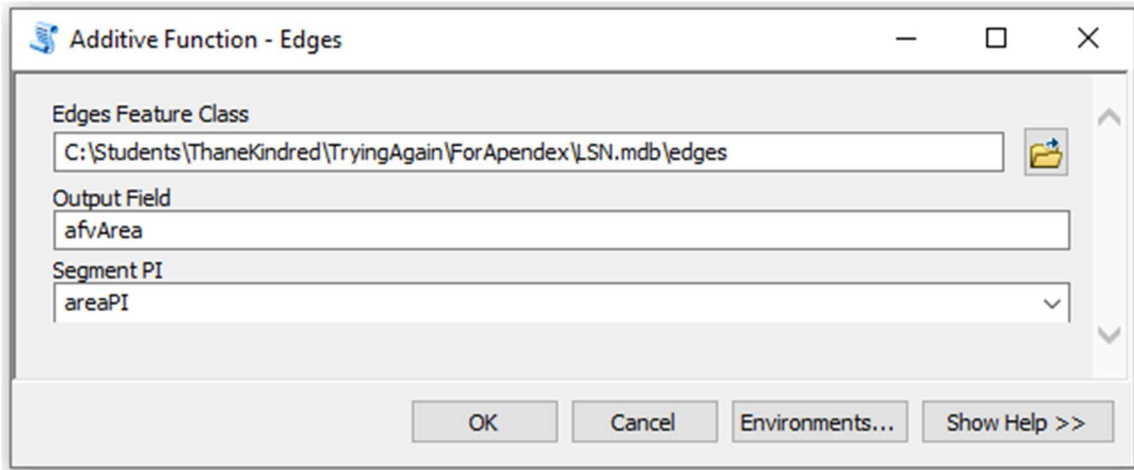


Note that the edge field required is the accumulated RCA area, which we labeled DrainageAreaAcc in Part 6.

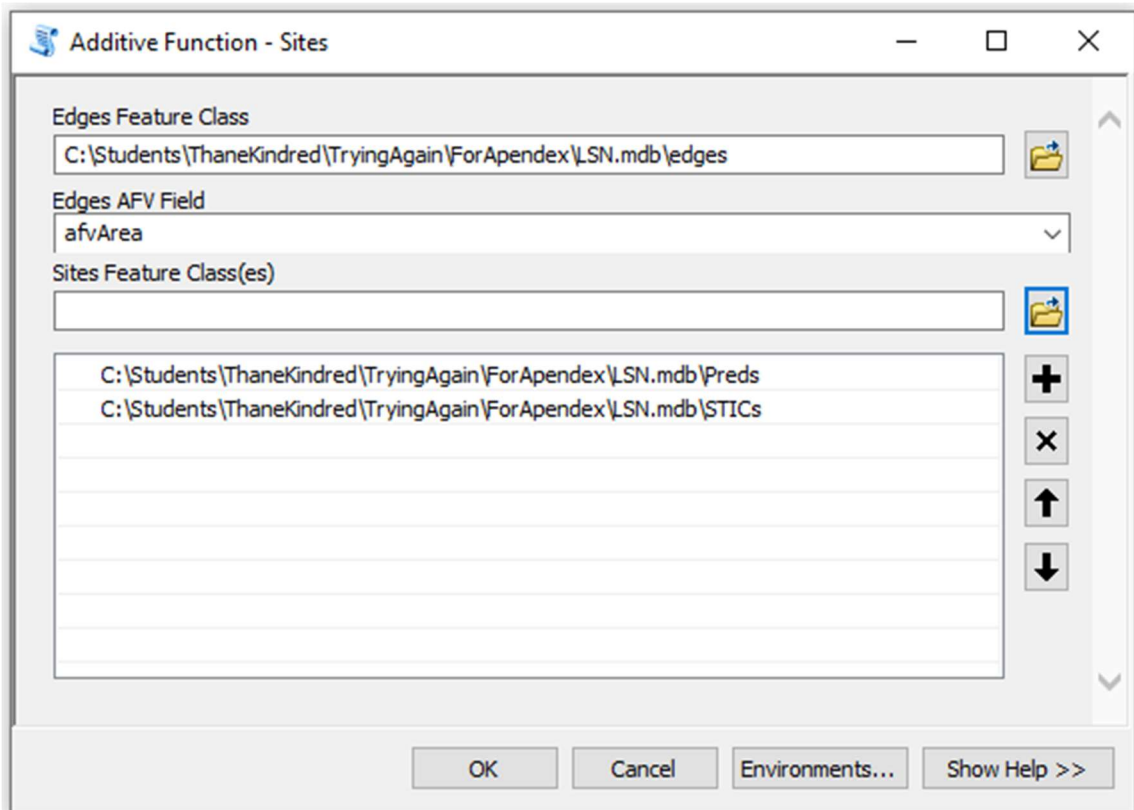
Check your work: After calculating segment PI, you should have a field in the edges attribute table labeled 'areaPI', or the name that you gave it. All values in this field should be less than 1 except for the outlet edge which should have a PI of 1.

Sadly, in this context, AFV is not America's Funniest Home Videos. Instead, it is the product (i.e. you have to do multiplication) of all PI's of downstream edges, including the edge of interest, and the edge it shares a confluence node with (Figure A3.3). We can calculate AFV for each edge using the **'Additive Function - Edges'** script in the

'Calculate' subtoolbox in the STARS toolbox.



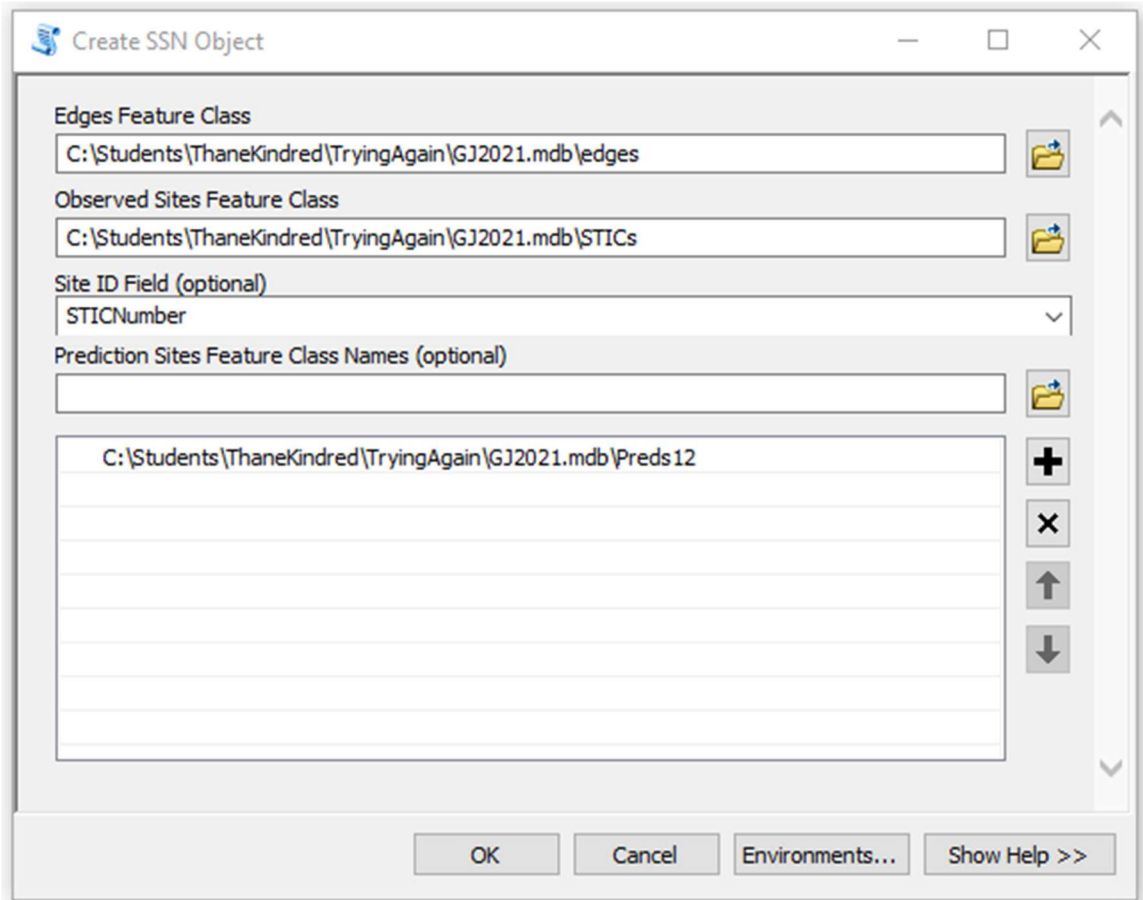
The AFV for each point is equal to the AFV of the edge it is located on. We can easily calculate this value using the '**Additive Function - Sites**' script in the 'Calculate' subtoolbox in the STARS toolbox.



Check your work: After calculating AFV for both edges and sites, you should have a field in the edges, observation (STICs), and prediction (Preds) attribute tables called afvArea, or whatever you named it.

Part 8: Creating the .ssn Object

Finally, we will create the .ssn object using the '**Create SSN Object**' script in the 'Export' subtoolbox in the STARS toolbox. Note that the 'Site ID' field is optional. I have tried running this tool with it filled in and left blank, and I can't figure out what good it does, or doesn't do. Also, you may enter multiple prediction sites if you wish. This may be helpful if you have multiple categories of sites where you need predictions. It may also be helpful if you need to krige at multiple resolutions.



Check your work: After running the **'Create SSN Object'** you should have a folder in your home directory with the same name as the LSN you created except that it is a .ssn object rather than a .mdb object. If you create multiple .ssn objects from the same LSN, make sure you manually rename older .ssn objects in the folder before rerunning the **'Create SSN Object'** script or it will overwrite the old object.

A3.9. Conclusion

Congratulations! You successfully created a .ssn object that you can use to perform spatial statistics using the SSN package in R! Your work is by no means complete. You will likely find that you need to make small changes in your .ssn as you correct data, calculate new watershed attributes, and generally torg it up! Good luck

with your future SSN adventures, and remember that this SOP is always here to guide you as you rework .ssn objects.

A.3.10 Figures

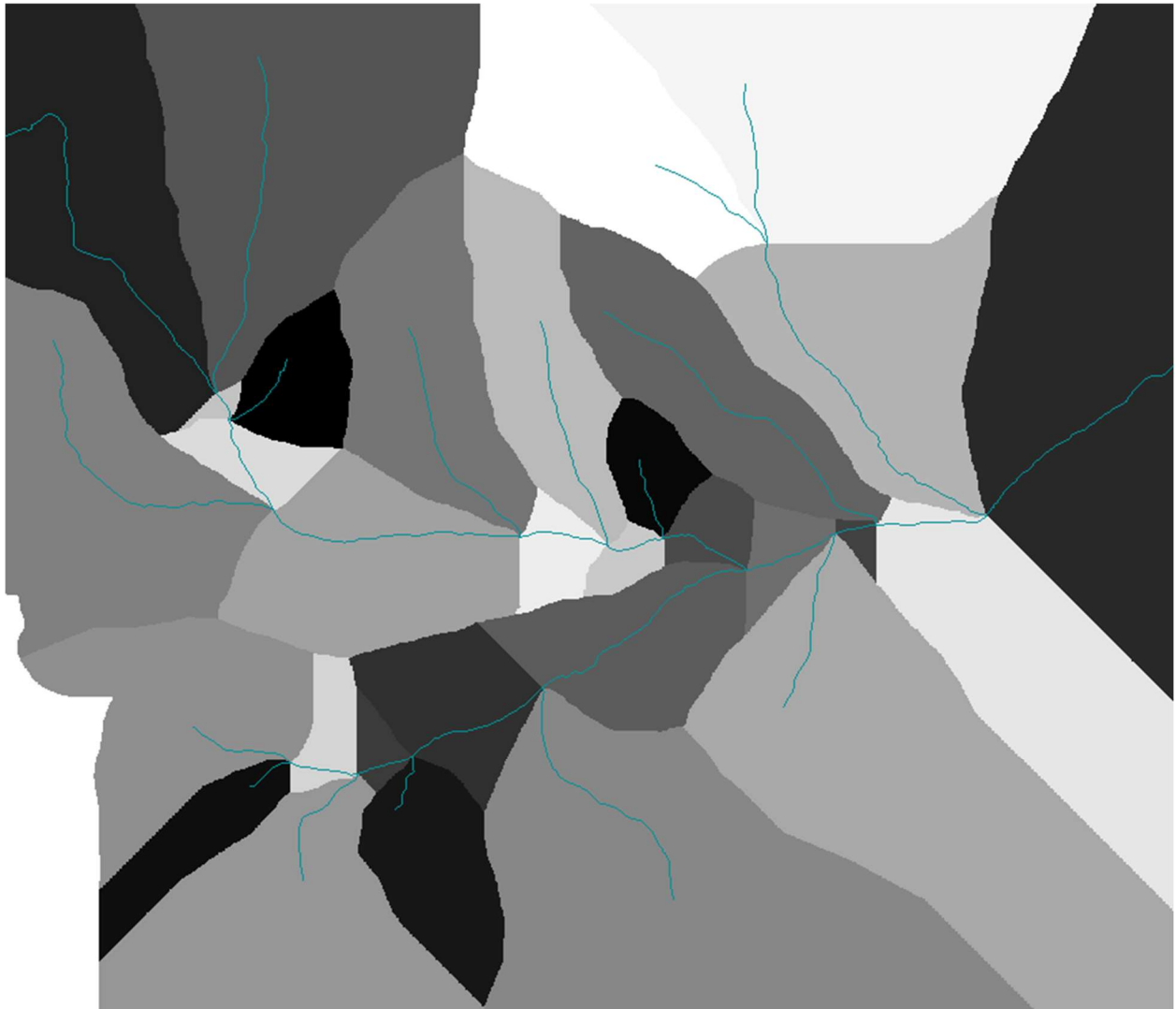


Figure A3. 1: Example of what a completed RCA raster should look like when the edges are displayed above them. Note that each RCA corresponds to one, and only one, edge.

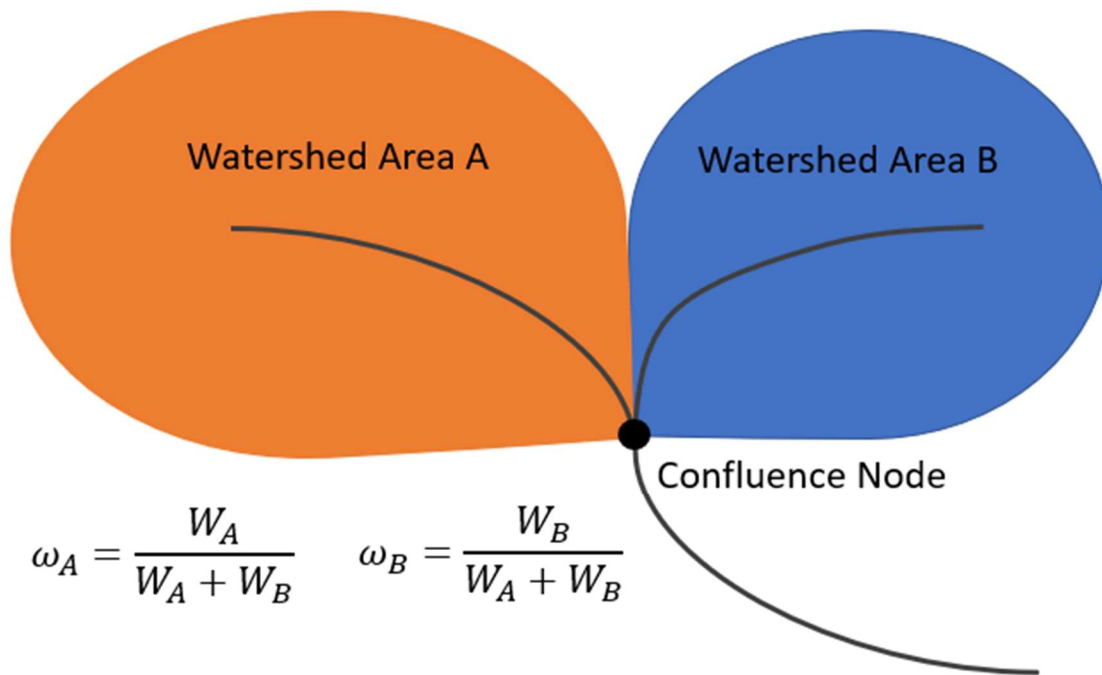
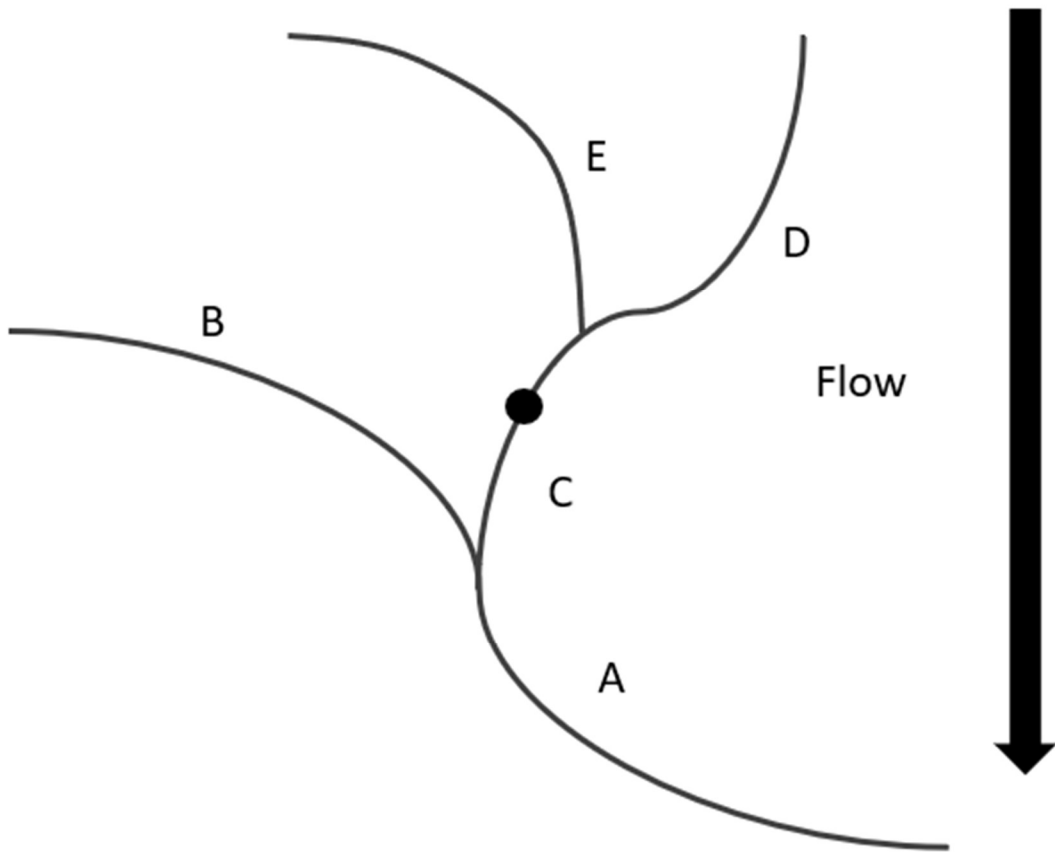


Figure A3. 2: Conceptual diagram of calculating segment proportional influence. Note that water flows from top to bottom in this diagram. The proportional influence is calculated for the bottom of each edge feature and included in the edges attribute table.



$$AFV_{edge\ C} = \omega_A * \omega_B * \omega_C = AFV_{point\ s}$$

Figure A3. 3: Conceptual diagram for calculating AFV. Once the value has been calculated for an edge, all points along that edge have the same AFV.

References

- Altman, D.G., and Bland, J.M., 1994, Statistics Notes: Diagnostic tests 3: receiver operating characteristic plots: *BMJ*, v. 309, p. 188–188, doi:[10.1136/bmj.309.6948.188](https://doi.org/10.1136/bmj.309.6948.188).
- Peterson, D.E.E. STARS: Spatial tools for the analysis of river systems - version 2.0.7 - A tutorial: , p. 48.
- Rodgers, D.W., and Othberg, K.L., 1999, Geologic map of the Pocatello south quadrangle, Bannock and Power counties, Idaho: Idaho Geologic Survey Geologic map.
- Theobald, D.M., Norman, J., Peterson, E., Ferraz, S., and Collins, F. Functional Linkage of Watersheds and Streams (FLoWS): Network-based ArcGIS tools to analyze freshwater ecosystems: , p. 15.
- Zimmerman, D.L., and Ver Hoef, J.M., 2017, The Torgegram for Fluvial Variography: Characterizing Spatial Dependence on Stream Networks: *Journal of Computational and Graphical Statistics*, v. 26, p. 253–264, doi:[10.1080/10618600.2016.1247006](https://doi.org/10.1080/10618600.2016.1247006).

Appendix 4: Advice for Future Grad Students

A4.1. Congratulations and Introduction

Congratulations on your acceptance to Idaho State University! I think that you will like it here. Pocatello is a wonderful place, with wonderful people, and you get to study in the shadow of the beautiful Gibson Jack watershed. I wish you the best while you are here. As I am finishing my time at ISU, I will give you a few words of advice: Make time for the things that you value most, don't forget about the small things in your research, and learn to look past the "bad days" toward better ones. As I share the things I have learned, I sincerely hope that you will find something to help you while you are here at ISU.

A4.2. Make Time for What You Value

A wise man once said, "Never let a problem to be solved become more important than a person to be loved." (Monson, 2008) In science, we have a lot of important problems that need solving. From a bug in your programming, to a lost sensor, to an uncompleted thesis, you can think of grad school as an endless list of problems. These problems are important, you should not ignore them, but you shouldn't allow them to consume your life because, believe it or not, some things are more important than science.

Namely, the people around you are more important than science. During my time at ISU, I made service in my family, church, and academic community my top priority. I

spent a lot of time serving in GeoClub, mentoring youth at church, and listening to friends who needed to vent. Though these activities took time away from my science, I don't regret a single minute of that time. In fact, the times that I regret most are when I let service slip out of my life so that I could focus on science. Don't make that mistake. Don't let your scientific problems become more important than the people around you.

Similarly, I had certain values that I held to while at ISU. Those values included family and church. For example, because it is important to me, I rarely worked on Sunday, and I always went to church, whatever form that took. Taking one day off a week encouraged me to get my work done before that day came. It also let me clear my head and start fresh on Monday. To be clear, you don't need to share my family or religious values, but you should identify values that are important to you and then make them a priority. Dr. Godsey was really good at respecting my values, allowing me to easily make them a priority. I hope your advisor is the same way.

Also, make sure you are safe in the field. I was lucky enough to perform all my fieldwork locally, so if something went wrong I could get help relatively easily. That isn't always true. Use the buddy system when you can and always let someone know where you plan on going. Also, keep a first aid kit handy and drink plenty of water. All this becomes more important when you have undergraduate assistants who look to you for guidance in the field.

Grad school is important. As are grades, field equipment, and data. But none of these things are worth compromising your safety, your integrity, or your friendships over. Because believe it or not, some things are more important than science.

A4.3. Make the small things count

Over the course of your time here you will learn lots of small tricks that help make life at ISU easier. Each of the tips I give you in this section are small, and may not drastically change your experience here, but they will help you avoid some of the mistakes that I made. Here is what I have learned in no particular order:

- Don't forget to record your field observations while you are in the field. This may be your only chance to record this observation.
- Double and triple check your field pack/equipment before you get in the car, and again before you start hiking. This will save you a lot of time.
- Clean the laboratory after you use it. This will help everyone in the lab as you move forward with different projects.
- Make time for writing in every stage of grad school. This will help keep you in the practice of writing. Additionally, it will help you get ahead so that you aren't as stressed in your final semester when you are desperately trying to finish your thesis.
- You are surrounded by amazing, successful people. Get to know them while you have the chance.
- When you get stuck on a coding project, leave it alone and go for a walk. Clearing your head does wonders for your ability to clear obstacles in your coding.

- Comment your code so that others (and your future self) can follow what you did.
- Save everything on a backup drive after EVERY work session. You don't want to lose hours of work because you dropped a storage device.
- Read papers on an exercise bike at the gym. You get a workout, and it's somehow easier to focus on a paper there.

Constantly doing these small things will help you make the most of your limited work time here at ISU. They will also help you maintain a positive attitude as you face challenges and they will keep Dr. Godsey happy, which is important.

A4. Move Forward to Better Days

In one of my favorite comic books, the villain reminds the protagonist of a mistake that he made and that “you are who you are on the worst day of your life”. The hero then responds by saying, “... [That's] true. [That's] 100% true. But [you] know who else [you] are? [You] are who [you] are on [the] **next** day. [The] day [you] wake up [and have to] decide: are [you] gonna make this [the] **new** worst day [of your] life, or [no]?” (Burlew, 2018; emphasis author's; character's fantasy dwarven accent removed)

Like the protagonist in this story, your experience at ISU won't always go the way you want it to. You won't get along with all of your teachers, you will get terrible assignments as a TA/RA, you may get a bad grade on a test or project, and your graduation date may get delayed.

When you have a bad day, decide that tomorrow won't be your "new worst day." Decide that you can be successful in a class despite your disagreements with the professor. Decide that you can grow by completing the TA/RA assignment you have. Decide that even though you failed one class project, you can do better on the next one. Decide that you can move on to "Better Days" after your worst ones.

Also realize that you are not alone. Your professor should be on your side, even when you mess up. Dr. Godsey did that for me. I found that being open with her about my frustrations has helped me move on to "Better Days" faster than if I tried to deal with them on my own. She was always there for me. Find someone who is always there for you.

A.5. Parting Words

Knowledge is a funny thing. The more you know, the more you know what you don't know. This is true in grad school. Concepts that you didn't understand as an undergrad will start to make more sense to you, but you will also realize that there is a lot that you don't yet understand. That is OK. You don't have to know everything now. Put important things first, make the small things count, and move forward to better days and you will be fine. Good luck, and remember that we are rooting for you.

Thanks,

Thane Kindred

A.6. References

Burlew, R., 2018, Order of the Stick; 1130 Better days: Giant in the Playground,

<https://www.giantitp.com/comics/oots1130.html>

Monsoon, T.S., 2008, Finding joy in the journey, Church of Jesus Christ of Latter-Day Saints,

<https://www.churchofjesuschrist.org/study/general-conference/2008/10/finding-joy-in-the-journey?lang=eng>